Developing a Synthetic Bone Marrow Niche for Testing Novel Leukaemia Therapies

William Sebastian Doherty-Boyd

BSc Hons

Submitted in fulfilment of the requirements for the Degree of Doctor of Philosophy (PhD)

Centre for the Cellular Microenvironment
School of Molecular Biosciences
College of Medical, Veterinary, and Life Sciences
University of Glasgow
Glasgow, United Kingdom
G12 8QQ

September 2024

Abstract

Haematopoietic stem cells (HSCs) are responsible for haematopoiesis, the continuous production of blood and immune cells within the bone marrow (BM) niche. The BM niche maintains the stem cell pool and haematopoietic activity with a variety of stimuli. Erroneous haematopoiesis can result in disorders and diseases such as acute myeloid leukaemia (AML). Chimeric antigen receptor (CAR) T-cell therapy has the potential to significantly improve AML patients' outlook. However, the efficacy of novel therapies is difficult to assess prior to clinical trials. A model BM niche was developed to provide insight into therapies' efficacies.

The model used mesenchymal stromal cells (MSCs), which support HSCs in the BM niche, as a feeder layer. The MSCs were cultured on a surface coated with poly(ethyl acrylate). This material caused fibronectin, which the surface was also coated with, to assemble in an open conformation. The fibronectin, which was loaded with the osteogenic growth factor bone morphogenic protein 2, directed the phenotype of MSCs cultured on top. A synthetic, peptide-based hydrogel was also layered on top of the MSCs, forming a barrier between MSCs under the gel and HSCs cultured on top of the gel, and acting as a culture interface between the different cell populations. This system promoted a niche-like phenotype in MSCs, which supported HSCs, mimicking the BM niche.

A CAR T-cell therapy which specifically eliminated AML cells was also developed. AML cells lack differentiable surface markers that can be used as CAR T-cell targets without harming healthy myeloid cells. To overcome this, CD33, a myeloid and AML cell surface marker, was disrupted in HSCs. This allowed CD33 to be targeted with CAR T-cells, theoretically eliminating all CD33 expressing cells, including AML cells, while a $CD33^{del}$ population of haematopoietic cells with the potential to repopulate the niche survived. This therapeutic approach was tested in the model BM niche and found to effectively eliminate AML cells, but also affect haematopoietic cells, warranting further research.

The successful modelling of a healthy, diseased, and treated BM niche demonstrated the usefulness of *in vitro* models for testing novel therapies for BM-associated disorders and diseases.

Table of contents

List of tables

List of figures

Publications

Publications authored by the candidate on research relating to this thesis.

Doherty-Boyd, W. S., Donnelly, H., Tsimbouri, P. M., and Dalby, M. J. (2024) 'Building bones for blood and beyond: the growing field of bone marrow niche model development', *Experimental Hematology*, 135, p. 104232. doi: 10.1016/j.exphem.2024.104232.

Donnelly, H., Ross, E., Xiao, Y., Hermantara, R., Taqi, A. F., **Doherty-Boyd, W. S.**, Cassels, J., Tsimbouri, P. M., Dunn, K. M., Hay, J., Cheng, A., Meek, R. M. D., Jain, N., West, C., Wheadon, H., Michie, A. M., Peault, B., West, A. G., Salmeron-Sanchez, M., and Dalby, M. J. (2024) 'Bioengineered niches that recreate physiological extracellular matrix organisation to support long-term haematopoietic stem cells', *Nature Communications*, 15(1). doi: 10.1038/s41467-024-50054-0.

Xiao, Y., McGuinness, C., **Doherty-Boyd, W. S.**, Salmeron-Sanchez, M., Donnelly, H., and Dalby, M. J. (2022) 'Current insights into the bone marrow niche: From biology in vivo to bioengineering ex vivo', *Biomaterials*, 286(April), p. 121568. doi: 10.1016/j.biomaterials.2022.121568.

Conference proceedings

United Kingdom Society for Biomaterials (UKSB) x Centres for Doctoral Training (CDT) conference 2021: Synthetic niches for haematopoietic stem cell maintenance (online flash talk presentation)

Nanoengineering for Mechanobiology (N4M) 2021: Synthetic niches for haematopoietic stem cell maintenance (online poster presentation)

N4M 2022: Developing an artificial BM niche for HSC maintenance (oral presentation)

Tissue and Cell Engineering Society (TCES) x CDT conference 2022: Developing an artificial bone marrow niche for HSC maintenance (flash talk)

Glasgow Orthopaedic Research Initiative (GLORI) conference 2023: Developing an artificial BM niche for HSC maintenance and genetic manipulation (oral presentation)

World Biomaterial Congress (WBC) 2024: A synthetic bone marrow niche for testing novel leukaemia therapies (poster presentation)

TCES x CDT conference 2024: A synthetic bone marrow niche for testing a novel leukaemia therapy (poster presentation)

Tissue Engineering and Regenerative Medicine International Society (TERMIS) World Congress 2024: A synthetic bone marrow niche for testing novel leukaemia therapies (oral presentation)

Awards

Best first year talk prize winner, Institute of Molecular, Cellular, and Systems Biology, University of Glasgow, 2021

Flash talk runner up, Joint UKSB CDT conference, online, 2021

Best flash talk abstract, Joint TCES CDT conference, Birmingham, 2022

Best talk, GLORI conference, Glasgow, 2023

TCES travel bursary, for TERMIS, USA, 2024

College of Medical, Veterinary and Life Sciences conference support funding, for WBC, Republic of Korea, 2024

Acknowledgements

Doing a PhD has been an exceptionally challenging experience. Battling failed experiments, administrative frustrations, and tight timelines has been a constant source of stress and at times had me questioning my decision to pursue a doctorate to begin with. However, the people I have surrounded myself with have paved the way to my success, enabled me to produce a thesis that I am proud of, and kept me going throughout the process.

First, I would like to thank my rather extensive supervisory team. Thank you to Adam West for grilling me on the mechanisms of CRISPR and nurturing my interest and abilities in genetic manipulation. Aline Miller and Alberto Saiani, thank you for the opportunity to experience everything your lab has to offer, and for putting up with all my questions about PeptiGels. Thank you, Manuel Salmeron-Sanchez for your sage advice and constant supply of PEA. I would also like to give a special thanks to Hannah Donnelly and Monica Tsimbouri. To Hannah, for tolerating me while I was still a fresh first year PhD student and giving me such excellent foundations upon which you have continued to help me build my knowledge and expertise. To Monica, for your continuous, unwavering support in all things, you are the greatest lab mum a PhD student could hope for. Last but not by any means least, thank you Matt Dalby for believing that a naïve undergraduate could bring this project to fruition; I wouldn't be where I am today without the endless opportunities, encouragement, and guidance you have given me over the last four years.

I am also exceedingly grateful to the innumerable people who guided me through the experimental challenges of my PhD. To name just a few: Vini, Al, Matt, Aqeel, Niall, and Manlio, thank you for drilling the necessary knowledge into me.

In addition, the friends I have made during my time at the Centre for the Cellular Microenvironment have made lab life a little less grey. From the Hector nook to the Quiche Quomrades, the weird lab chat, the lifETIME CDT, and beyond, I will cherish every moment we have spent together laughing, bonding, and killing brain cells with Guinness.

For my friends beyond academia, thank you for keeping me sane with nerdy games, deep chats, holidays, advice, and so much more. You have made Glasgow my home in more ways than I can say.

To my family, you are my rock. The love and support that we share is invaluable to me and has shaped me into who I am today. To my dad, thank you for always catching me when I fall, and for teaching me the meaning of compassion and diligence. Helen, thank you for bringing so much joy to our family. Ben and Jess, thank you for you for your goofs, antics, and thoughtfulness, it is a pleasure to watch you grow into such wonderful people. To my mum, thank you for your kindness and love. To the Boyd-Madsens, thank you for being my second family, and filling my life with so much colour and warmth. To my grandad, thank you for always taking an interest as I rattle off my research elevator pitch, and your encouragement in all things. To my grandma, thank you for your generosity. To the rest of my sizeable family, thank you for everything you have done for me, and for the connections we share.

I sometimes think on whether a PhD is worthwhile. But thanks to the people who have supported me, I know that I have had a brilliant, truly formative experience throughout the last four years. Thank you all.

Author's declaration

I hereby declare that the research reported within this thesis is my own work, unless otherwise stated, that the thesis has not been edited by a third party beyond what is permitted by the University's PGR Code of Practice, and at the time of submission is not being considered for any other academic qualification.

I acknowledge that if any issues are raised regarding good research practice based on review of the thesis, the examination may be postponed pending the outcome of any investigation of the issues.

William Sebastian Doherty-Boyd

2nd September 2024

Abbreviations

$\theta\delta$	Tan delta
AGM	Aorta-gonad-mesonephros
ALL	Acute lymphoblastic leukaemia
AML	Acute myeloid leukaemia
Angpt-1	Angiopoietin 1
BCL-2	B-cell leukaemia 2
BM	Bone marrow
BMP	Bone morphogenic protein
BMP2	Bone morphogenic protein 2
BMPR	Bone morphogenic protein receptor
BMPRI	Type I bone morphogenic protein receptor
BMPRII	Type II bone morphogenic protein receptor
CAR (MSC)	CXCL12-abundant reticular
CAR (T cell)	Chimeric antigen receptor
CAR T-cell	Chimeric antigen receptor T-cell
Cas	CRISPR associated protein
CD	Cluster of differentiation
CLL	Chronic lymphocytic leukaemia
CLP	Common lymphoid progenitor
CML	Chronic myeloid leukaemia
CMP	Common myeloid progenitor
CNS	Central nervous system
CRISPR	Clustered regularly interspaced short palindromic repeats
CTCF	Corrected total cell fluorescence
CTFR	Cell trace far red
CXCL12	CXC chemokine ligand 12
CXCL4	CXC chemokine ligand 4
CXCR4	CXC chemokine receptor 4
DLL1	Delta-like 1
DMEM	Dulbecco's modified eagle's medium
DNA	Deoxyribonucleic acid
DSB	Double strand break
E'	Young's moudulus

ECM	Extracellular matrix
EDTA	Ethylenediaminetetraacetic acid
FBS	Foetal bovine serum
FGF	Fibroblast growth factor
FGF1	Fibroblast growth factor 1
FL	Flt3 ligand
Flt3	FMS-like tyrosine kinase 3
FMS	Feline McDonough sarcoma
FN	Fibronectin
FSC-A	Forward scatter area
FSC-H	Forward scatter height
G’	Storage modulus
G”	Loss modulus
G-CSF	Granulocyte colony stimulating factor
GF	Growth factor
GFR	Growth factor receptor
GMP	Granulocyte-monocyte progenitor
GO	Gemtuzumab ozogamicin
GvL	Graft vs leukaemia
GvHD	Graft vs host disease
HDR	Homology-directed repair
HIF-1α	Hypoxia inducible factor 1a
HSC	Haematopoietic stem cell
HSCT	Haematopoietic stem cell transplant
HSPC	Haematopoietic stem and progenitor cell
IF	Immunofluorescent
Ig	Immunoglobulin
IMDM	Iscove Modified Dulbecco Media
INDEL	Insertion deletion [mutation]
KO	[Gene] knock-out
$LepR^{+}$	Leptin receptor positive
Lin	Lineage cocktail
LN	Laminin
LSC	Leukaemia stem cell
LT-HSC	Long-term haematopoietic stem cell
MEM NEAA	Minimum essential medium non-essential amino acids

MEP	Megakaryocyte-erythroid progenitor
MPL	Myeloproliferative leukaemia protein
MPP	Multipotent progenitors
MSC	Mesenchymal stromal cell
NG2	Neural glial antigen 2
NHEJ	Non-homologous end joining
NK cell	Natural killer cell
NPM1	Nucleophosmin
OPN	Osteopontin
PBS	Phosphate buffered saline
PCS	Polymer cover slip
PEA	Poly(ethyl acrylate)
PEA	Plasma polymerised poly(ethyl acrylate)
PVA	Polyvinyl acrylate
RF	Radio frequency
RNA	Ribonucleic acid
RNP	Ribonucleoprotein
ROI	Region of interest
ROS	Reactive oxygen species
RPMI	Roswell Park Memorial Institute
RPTP	Receptor protein tyrosine phosphatase
RT	Room temperature
RUNX2	Runt-related transcription factor 2
SAPH	Self-assembling peptide hydrogels
SCF	Stem cell factor
SD	Standard deviation
sgRNA	Single guide RNA
Siglec	Sialic acid-binding immunoglobulin-like lectin
SMAD	Suppressor of Mothers against Decapentaplegic
SSC-A	Side scatter area
ST-HSC	Short-term HSC
T:E	Target:effector
TCP	Tissue culture plastic
TGFβ	Transforming growth factor β
Tie-1	Tyrosine-protein kinase receptor
TPO	Thrombopoietin

v	Poisson’s ratio
VCAM-1	Vascular cell adhesion molecule-1
VLA-4	Very late antigen 4
VN	Vitronectin
WNT	Wingless-related integration site
XPS	X-ray photoelectron spectra

Chapter 1 Introduction

Haematopoietic stem cells (HSCs) natively reside within several niches, including the bone marrow (BM) niche which maintains the HSC population using a complex variety of stimuli and is found within trabecular bones (Morrison & Scadden, 2014; Xiao, McGuinness, et al., 2022). HSCs are responsible for the process of haematopoiesis, a specialised form of stem cell differentiation that continuously replenishes blood and immune cells, maintaining haematopoietic homeostasis (Seita & Weissman, 2010). When this process malfunctions, it can result in the development of various disorders and diseases, such as acute myeloid leukaemia (AML) (Döhner et al., 2015).

Recent efforts in the tissue engineering field have yielded a plethora of BM niche models which promise to deliver several key advances (Doherty-Boyd et al., 2024). These include establishing a robust model of haematopoiesis, allowing the manipulation of this process, and shedding light on how BM-associated disorders and diseases affect the niche and can be effectively treated (Méndez-Ferrer et al., 2020).

This chapter will explore the intricacies of both healthy and diseased haematopoiesis, the influence HSC niches have on this process with a particular focus on the BM niche, as well as recent advances in the development of *in vitro* models of the BM niche.

1.1 Stem cells

Stem cells have the capacity to produce various specialised cell types through a process known as differentiation (Dupuis & Oltra, 2021). In addition, stem cells self-renew, allowing a population of adult stem cells to be maintained *in vivo* throughout an organism's life (Fares et al., 2022; Seita & Weissman, 2010; Zon, 2008). To perform these processes stem cells can undergo two different forms of cell division; symmetrical cell division which produces two daughter cells which are either both stem cells or both more mature cell types, or asymmetrical cell division where two different cell types are generated (Jan & Jan, 1998; Zon,

2008). As a result, stem cells are the focus of several regenerative medicine applications.

Stem cells can be divided into two categories; immature pluripotent stem cells which can differentiate into any somatic cells in an organism, and less primitive multipotent stem cells which can only turn into a subset of somatic cells (Trounson & DeWitt, 2016). Embryonic stem cells derived from embryos (Shang et al., 2021; Young, 2011) and induced pluripotent stem cells (iPSCs) which are produced by genetically engineering terminally differentiated somatic cells (Takahashi et al., 2007) are generally considered pluripotent. Mature adult stem cells that replenish post-foetal cells and maintain homeostasis throughout an organism's life are multipotent (Pittenger et al., 1999; L. Rossi et al., 2011). The BM niche plays host to two clinically important adult stem cell types; HSCs and mesenchymal stromal cells (MSCs).

Recent efforts have been made to better understand and manipulate the process of differentiation for clinical purposes. This could allow the application of regenerative stem cell therapies to several candidate health problems such as cardiac disease (Segers & Lee, 2008) and strokes (G. L. Zhang et al., 2019) while also shedding light on stem cell-derived diseases such as sickle cell anaemia (Hulbert & Shenoy, 2018) and cancer (Ailles & Weissman, 2007; Locatelli, 2005; Willasch et al., 2020).

1.1.1 Haematopoietic stem and progenitor cells

Foetal establishment of the haematopoietic system is highly conserved among vertebrates (De La Garza et al., 2017). Initial "primitive" waves of haematopoiesis propagate within the yolk sac and only produce erythroid and myeloid cells that support the developing embryo. Subsequent "definitive" waves occur within the aorta-gonad-mesonephros (AGM) region of the embryo once it has developed, and produce erythromyeloid progenitors and naïve, long-term HSCs (LT-HSCs) (Jagannathan-Bogdan & Zon, 2013; Zhu et al., 2020). HSC precursors are then produced by the dorsal aorta, a major blood vessel which is part of the AGM, in a process termed endothelial-to-haematopoietic transition as organogenesis initiates (Bertrand et al., 2010; De La Garza et al., 2017; Y. Zeng et al., 2019).

These cells then localise to intermediate HSC niches such as the foetal liver, before colonising the BM niche (Ng & Alexander, 2017).

HSCs, a rare nonadherent population of BM stem cells (~0.01-0.04% of total BM mononuclear cells (Zon, 2008)), and lineage committed haematopoietic progenitor cells are collectively referred to as haematopoietic stem and progenitor cells (HSPCs). The traditional model of haematopoiesis was initially established in mice. Several key differences between mouse and human haematopoiesis have been identified, but the overall process is still assumed to be similar (Fares et al., 2022). This traditional model places HSPCs in a hierarchy at the top of which sits LT-HSCs, a self-renewing, multipotent subpopulation of HSCs (Fares et al., 2022; Wilson et al., 2008) responsible for the production of more proliferative progenitors (Cheshier et al., 1999; Yamamoto et al., 2013). LT-HSCs maintain long-term engraftment capacity, meaning they can reproduce an entire haematopoietic system when engrafted into an organism (Dykstra et al., 2007; Morrison & Weissman, 1994; Till & McCulloch, 2011). LT-HSCs are therefore critically important for the success of HSC transplants (HSCT), a curative treatment for BM malignancies and disorders (Hulbert & Shenoy, 2018; Locatelli, 2005; Schmitz et al., 2002; Willasch et al., 2020). LT-HSCs are typically quiescent and utilise a glycolytic metabolism that minimises oxidative stress and associated DNA damage (Guo et al., 2018; Kobayashi & Suda, 2012; Takubo et al., 2013). Occasionally LT-HSCs will produce short-term HSCs (ST-HSCs) via asymmetrical cell division (Busch et al., 2015). ST-HSCs are more metabolically and mitotically active than LT-HSCs, and possess reduced repopulation capacity (Wilson et al., 2008). Despite this, they have been shown to be capable of self-renewal and maintaining haematopoiesis after LT-HSC ablation (Schoedel et al., 2016), suggesting they are also capable of long-term engraftment. ST-HSCs differentiate into multipotent progenitors (MPPs), which in turn produce lineage restricted progeny via an oligopotent cell step (Pietras et al., 2015; Zon, 2008). Taken together, this view on haematopoiesis suggests a reserve pool of LT-HSCs that replenishes a much more active ST-HSC population that is the primary source of haematopoietic cells via intermediate cell types (see **Figure 1.1).**

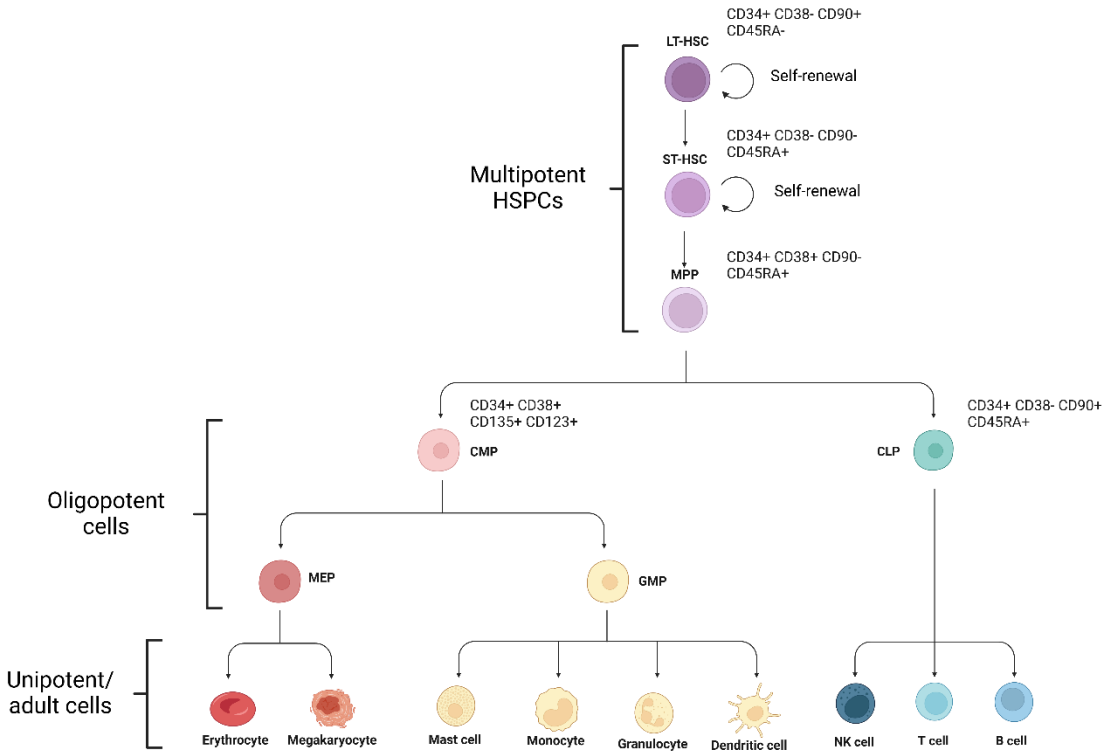

Figure 1.1 Schematic of stepwise model of haematopoiesis*. This model is based primarily off murine research. More naïve and potent stem cells differentiate into less potent, mature cell types, resulting in the proliferation of cells that make up the haematopoietic system. Markers used to distinguish between less mature cell types are shown. Note that this is only one interpretation of haematopoiesis. Abbreviations: LT-HSC, long-term HSC; ST-HSC, short-term HSC; MPP, multipotent progenitor; CMP, common myeloid progenitor; CLP, common lymphoid progenitor; MEP, megakaryocyte-erythroid progenitor; GMP, granulocyte-monocyte progenitor; NK cell, natural killer cell. Created with Biorender.com.*

Despite the exact pathway of human haematopoiesis remaining a contentious issue, until recently stepwise models based on murine studies like the one described above, in which cells became progressively more differentiated and transitioned through definitive intermediate cell stages, were considered dogma (Ceredig et al., 2009). However, recent advances in single cell analysis techniques have allowed previously indistinguishable differences within the putative subcategories of HSPCs to be investigated in humans and mice (Karamitros et al., 2018; P. Zhang et al., 2022). These findings suggest a highly heterogenous HSPC population with a fluid differentiation pathway. In this model, HSPCs are transcriptionally primed to produce a specific adult cell type, and differentiate through transient intermediate states before preferentially but not exclusively differentiating into the adult cell types they were primed for (Pietras et al., 2015;

Rodriguez-Fraticelli et al., 2018; Tusi et al., 2018; Watcham et al., 2019) (see **Figure 1.2**).

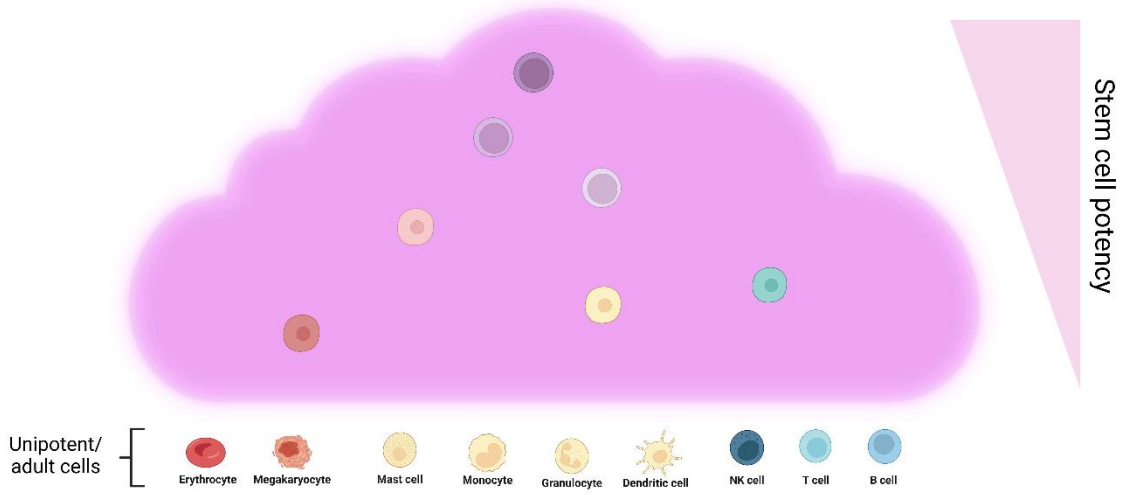

Figure 1.2. Schematic of fluid model of haematopoiesis. *All multipotent and oligopotent stem cells possess the ability to differentiate into any adult haematopoietic cell type. Intermediate cell states between HSCs and adult cells are transient and represent a heterogenous pool of HSC progeny that have been primed to preferentially differentiate into certain adult cell types. Created with Biorender.com.*

1.1.1.1 Clinical demand for HSCs

HSCT is the current standard treatment for Hodgkin's lymphoma, non-Hodgkin's lymphoma, multiple myeloma, sickle cell anaemia and autoimmune diseases such as multiple sclerosis (Mendelson & Frenette, 2014). It can either be administered directly or following elimination of haematopoietic cells, known as myeloablation (Hulbert & Shenoy, 2018; Schmitz et al., 2002; Willasch et al., 2020). When administered directly, the purpose of the treatment is to establish a parallel, non-infected haematopoietic system which has the potential to outcompete and replace the endogenous diseased system (Dickinson et al., 2017). When administered following myeloablation, a patient's haematopoietic system and ideally all diseased cells are eliminated and replaced with healthy donor cells that re-establish haematopoietic homeostasis.

These treatments are effective (Hulbert & Shenoy, 2018; Locatelli, 2005; Schmitz et al., 2002; Willasch et al., 2020). However, they are limited by the low availability of HSCs caused by their relative rarity as a cell type. This has driven

demand for increasing the supply of HSCs, leading to a focus on developing cell culture systems capable of expanding HSCs *in vitro*. A system which maintained HSCs numbers and engraftment capacity would also be beneficial as it could act as an HSC reservoir. This could allow excess HSCs to be stored and used at a later date or provide flexibility to patients and donors for when HSCs need to be collected (Chatterjee et al., 2021; Fares et al., 2022). Such a system would also be more biomimetic, as most LT-HSCs, which are typically considered essential for long-term engraftment, are quiescent in the native BM niche. This is discussed in greater detail in section **1.3**.

1.1.2 Mesenchymal stromal cells

Early attempts to culture BM HSCs *in vitro* resulted in the identification of a secondary, adherent cell type present in the BM niche without which the HSCs were unable to survive (Dexter et al., 1977). We now know that these cells are mesenchymal stromal cells (MSCs), which coexist with the HSCs and maintain haematopoietic homeostasis through secretion of soluble factors and juxtracrine signalling (Méndez-Ferrer et al., 2010; Pinho et al., 2013). MSCs are stem cells

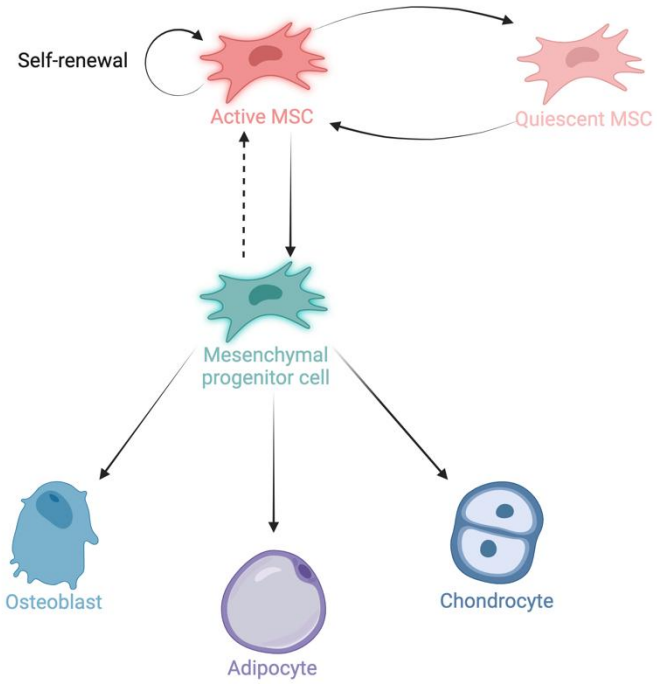

***Figure 1.3 MSC trilineage differentiation capacity**. MSCs, like all stem cells, possess the ability to self-renew. They also maintain a quiescent pool similar to HSCs that replenishes an actively dividing MSC pool. MSCs produce progenitor cells which in turn produce several adult cell types, including osteoblasts, adipocytes, and chondrocytes. Created with Biorender.com.*

that have tri-lineage differentiation capacity, referring to their ability to differentiate into mesenchymal lineage cells including adipocytes, osteoblasts and chondrocytes (Pittenger et al., 1999; Wheadon et al., 2024) (see **Figure 1.3**).

It has been suggested that MSCs and fibroblasts should be considered the same cell type since older MSCs adopt a fibroblastic phenotype, losing almost all differentiable markers (Denu et al., 2016; Ugurlu & Karaoz, 2020). However, this data could also be interpreted as demonstrating that fibroblasts are another adult cell type derived from MSCs. MSCs can be found in various tissues throughout the body, including the BM where they make up 0.001-0.01% of cells present (Banfi et al., 2000; Bhat et al., 2021), birth associated tissue (Shang et al., 2021), or adipose tissue (Tsuji, 2014). Wherever they are found, MSCs tend to be perivascular (Crisan et al., 2008).

1.1.2.1 MSC subpopulations

Like HSPCs, MSCs are highly heterogenous, with substantial differences in various proteins' expressions associated with different cell populations. Dissecting the different populations of MSCs has allowed various subcategories of these stem cells to be defined. These include nestin$^+$ MSCs which express high levels of the intermediate filament protein nestin and are frequently found co-localised with HSCs (Pinho et al., 2013). These cells also often express neural glial antigen 2 (NG2) (Pinho & Frenette, 2019). They have been shown to produce many of the soluble factors commonly associated with HSC maintenance, including CXC chemokine ligand 12 (CXCL12) and stem cell factor (SCF), which are essential for HSC maintenance and retention within the BM niche (Mendelson & Frenette, 2014), as well as vascular cell adhesion molecule-1 (VCAM1) (Kunisaki et al., 2013). Depletion of nestin$^+$ MSCs also results in a reduction of HSC numbers within the BM niche (Méndez-Ferrer et al., 2010).

CXCL12-abundant reticular (CAR) MSCs have also been posited to influence HSC maintenance due to their high levels of CXCL12 and SCF expression and secretion (Omatsu et al., 2010), which suggests these cells also play a role in regulating HSC self-renewal, proliferation, and trafficking (Sugiyama et al., 2006) (see **Section 1.2.2**). Further supporting this point, ablation of CAR MSCs has been shown to cause HSC depletion (Omatsu et al., 2010).

Other MSC phenotypes include leptin receptor positive ($LepR^+$) cells which have also been implicated in haematopoietic homeostasis (Asada et al., 2017). MSCs expressing cluster of differentiation (CD) 146, a putative adhesion and signalling molecule, have been proposed as more naïve MSCs and shown to express high levels of nestin, CXCL12 and LepR (Corselli et al., 2013).

These clear distinctions between MSC subtypes quickly breaks down when looking at other molecular markers, cell position and morphology. A high degree of overlap between $LepR^+$ cells and CAR cells has been observed (B. O. Zhou et al., 2014), and $LepR^+$ cells have been periodically classified as a subpopulation of $nestin^+$ cells (Kunisaki et al., 2013).

Adult stem cells hold vast therapeutic potential. However, their heterogenous nature, as well as an incomplete understanding of the factors which influence differentiation and self-renewal limit their usefulness.

1.2 The bone marrow niche

Haematopoietic homeostasis is essential to an organism's health and longevity. Adult humans generate approximately $4.5x10^{11}$ haematopoietic cells per day (Kaushansky, 2006). Dysregulation of this system can lead to unrestrained proliferation and associated diseases such as leukaemia, or depletion of haematopoietic cells and the stem cell pool (Bonnet, 2005). The BM niche, a highly complex organ comprising a variety of cellular and non-cellular components, regulates this process (Wei & Frenette, 2018) (see **Figure 1.4**).

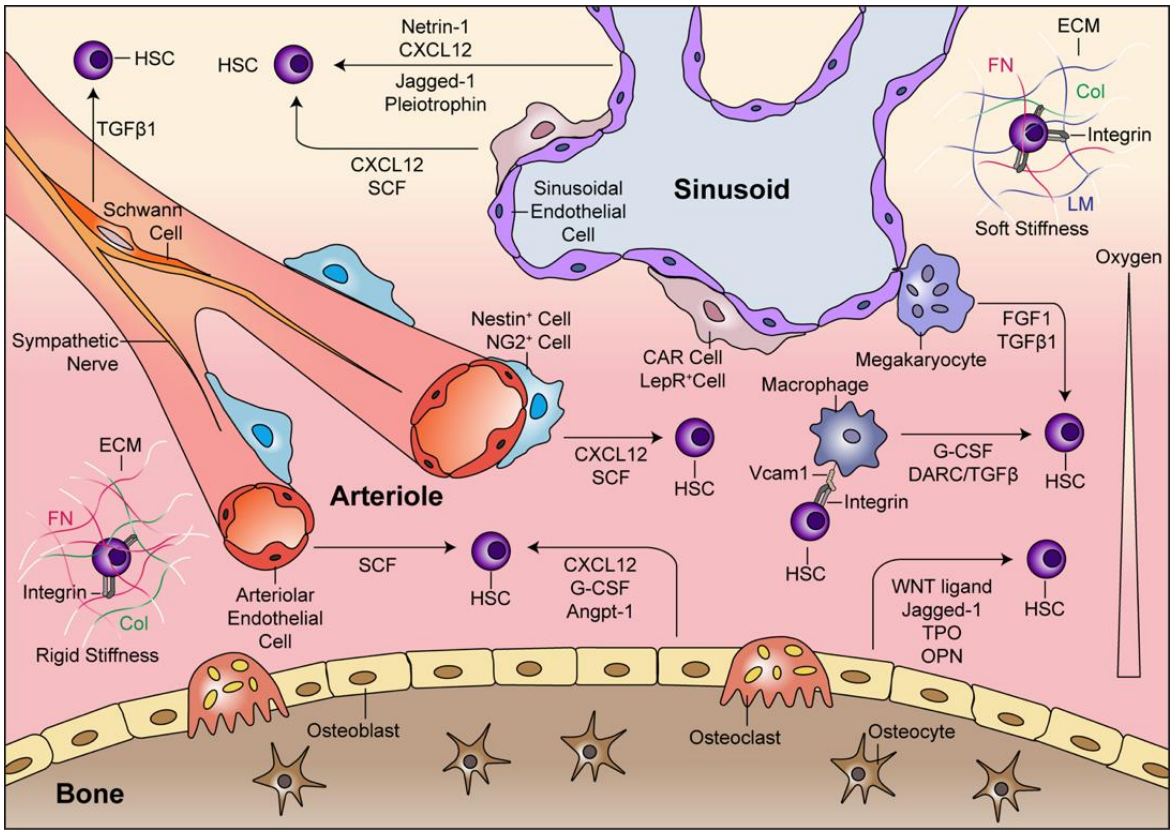

Figure 1.4 Schematic representation of the adult bone marrow niche's effect on HSCs. *The heterogeneous nature of the BM niche is illustrated with the stiff, oxygenated endosteum and adjacent arterioles shown in the lower half of the figure, and the deoxygenated, softer central cavity niche that is permeated with sinusoids shown in the upper half of the figure. The make-up of these environments' extracellular matrix (ECM) proteins is also illustrated in the top right and bottom left of the image. Mesenchymal stromal cells are shown in blue. Haematopoietic stem cells (HSCs) are purple. Endothelial cells are shown surrounding the arteriole and sinusoid blood vessels. Other cell types are labelled. Soluble factors involved in paracrine signalling to HSCs are represented by arrows from the producing cell type to the responding cell type. CXC chemokine ligand 12 (CXCL12) is involved in HSC localisation. Stem cell factor (SCF) is involved in HSC maintenance and recovery. Granulocyte colony stimulating factor (G-CSF) is involved in circulatory mobilisation and proliferation of HSCs. Angiopoietin 1 (Angpt-1) is involved in maintenance, quiescence, recovery and self-renewal of HSCs. Fibroblast growth factor 1 (FGF1) is involved in HSC self-renewal and recovery. Transforming growth factor β1 (TGFB1) (also shown as TGFB to encompass other isoforms) promotes HSC quiescence, maintenance and self-renewal. Wingless-related integration site (WNT) ligand promotes HSC quiescence, recovery, proliferation, inhibits self-renewal, and restricts the HSC pool. Jagged-1 is involved in self-renewal and proliferation of HSCs. Thrombopoietin (TPO) promotes HSC maintenance and quiescence. Osteopontin (OPN) is involved in HSC localisation, maintenance, restriction of HSC pool size, and quiescence. Juxtracrine signalling is also shown between a HSC and a macrophage, illustrated here using VCAM1 and integrins to interact, which induces retention and localisation in HSCs, as well as Duffy antigen receptor for chemokines (DARC), which interacts with CD82 and promotes HSC quiescence. From Xiao et al. (2022).*

1.2.1 Cellular cohort

The BM niche hosts several different cell types, including HSCs and MSCs, mesenchymal and haematopoietic progeny, as well as nerve cells, all of which have been shown to influence haematopoiesis (see **Table 1.1**).

Table 1.1 Cellular components of the BM niche.

BM niche cell type	Role of cell type in haematopoiesis	References
HSCs	HSCs are responsible for haematopoiesis. They also produce cells that regulate haematopoiesis.	(Cheshier et al., 1999; Dykstra et al., 2007; Fares et al., 2022; Morrison & Scadden, 2014; Morrison & Weissman, 1994; Seita & Weissman, 2010; Till & McCulloch, 2011; Wilson et al., 2008; Yamamoto et al., 2013; Zon, 2008)
MSCs	MSCs reside near HSCs in the BM niche. Some populations of MSCs produce high levels of soluble factors which maintain HSCs in the niche, as well as utilising juxtracrine signalling for the same purpose.	(Aleman et al., 2019; Bianco et al., 2019; Bourgine et al., 2018; Bray et al., 2017; Chou et al., 2020; De Barros et al., 2010; Donnelly et al., 2024; Futrega et al., 2017; Glaser et al., 2022; Goranov et al., 2020; Lai et al., 2013; Lima et al., 2013; Ma et al., 2020; Méndez-Ferrer et al., 2010; Nelson et al., 2021; Nichols et al., 2009; Rödling et al., 2017; Tiwari et al., 2012)
Megakaryocytes	Megakaryocytes are derived from HSC progenitors, produce platelets, regulate HSC fate, and interact with many cells within the BM niche contributing to its regulation.	(A. P. Stone et al., 2022)

BM niche cell type	Role of cell type in haematopoiesis	References
Osteoclasts	Osteoclasts influence MSCs, allowing them to attract HSCs for colonisation of the nascent BM niche during development. They also remodel the perinatal niche and aid with vascularisation.	(Mansour et al., 2012; Zeytin et al., 2022)
Macrophages	Macrophages produce several soluble factors and present surface antigens that influence haematopoiesis in a paracrine and juxtracrine manner, respectively.	(Hur et al., 2016; D. Li, Xue, et al., 2018)
Adipocytes	Adipocytes have potential suppressive effects on haematopoiesis within the bone-marrow niche.	(Naveiras et al., 2009)
Osteoblasts	Osteoblasts secrete soluble factors that influence HSC proliferation, localisation, and differentiation.	(Calvi et al., 2003; De Barros et al., 2010; Galán-Díez & Kousteni, 2017)
Endothelial cells	HSCs colocalise with vasculature in the in vivo BM niche, which is formed of endothelial cells. There is a possibility that these cells directly influence HSCs.	(Aleman et al., 2019; Braham et al., 2019; Bray et al., 2017; Chou et al., 2020; De Barros et al., 2010; Ding, Saunders, et al., 2012; Goranov et al., 2020; Heil et al., 2021; Kiel et al., 2005; Ma et al., 2020; Nelson et al., 2021; Perlin et al., 2017)
Fibroblasts	Fibroblasts provide mechanical/physical support to HSCs during proliferation and differentiation, through secreting and modulating the extracellular matrix (ECM)	(LeBleu & Neilson, 2020; Lee-Thedieck et al., 2022)
Nervous cells, e.g. Schwann cells and axons	Sympathetic nerves have been implicated in HSC mobilisation, maintenance and recovery following genotoxic insult	(Broome & Miyan, 2000; Katayama et al., 2006; Lucas et al., 2013; Maryanovich et al., 2018; Rameshwar & Gascon, 1995; C. Xu et al., 2018)

1.2.2 Soluble factors

Soluble factors, which include cytokines and growth factors (GFs), are produced by cells in the *in vivo* BM niche and are known to influence HSPC localisation, maintenance, quiescence, self-renewal, and expansion, as well as recovery of the haematopoietic system after depletion or ageing (Xiao, McGuinness, et al., 2022). The exact makeup of the soluble factor milieu and the impact of individual elements on HSPCs is contested, however several key factors' potential influences have been proposed (see **Table 1.2**).

Table 1.2 Soluble factors that influence HSPCs in the BM niche.

Soluble factor	HSC receptor	Source cells	Effect on HSCs	References
SCF	c-Kit	Endothelial cells, MSCs	Maintenance, recovery	(Asada et al., 2017; Ding, Saunders, et al., 2012; Kunisaki et al., 2013; Omatsu et al., 2010; B. O. Zhou et al., 2014)
CXCL12	CXC chemokine receptor 4 (CXCR4)	Endothelial cells, MSCs, osteoblasts	Localisation, retention, maintenance, self-renewal, quiescence	(Greenbaum et al., 2013; Omatsu et al., 2010; Sugiyama & Nagasawa, 2012)
CXCL4	Unknown	Megakaryocytes	Quiescence	(Bruns et al., 2014)
Thrombopoietin (TPO)	Myeloproliferative leukaemia protein (MPL)	Osteoblasts, hepatocytes	Maintenance, quiescence	(Decker et al., 2018; Qian et al., 2007; Yoshihara et al., 2007)
Osteopontin (OPN)	CD44	Osteoblasts	Localisation, maintenance, restriction of HSC pool size, quiescence	(Nilsson et al., 2005; Stier et al., 2005)

Soluble factor	HSC receptor	Source cells	Effect on HSCs	References
Angiopoietin 1 (Angpt-1)	Tyrosine-protein kinase receptor (Tie-2)	Osteoblasts, HSCs, MSCs	Maintenance, quiescence, recovery, self-renewal	(Arai et al., 2004; B. O. Zhou et al., 2015)
G-CSF	G-CSF receptor	Osteoblasts	Circulatory mobilisation, proliferation	(Schuettpelz et al., 2014; Taichman & Emerson, 1994)
Transforming growth factor β (TGF-ß) 1-3	Type I (Activin receptor-like kinase 5) and type II TGF-ß receptors	Megakaryocytes, schwann cells, macrophages	Maintenance, quiescence, self-renewal	(Blank & Karlsson, 2015; Hur et al., 2016; Yamazaki et al., 2011; M. Zhao et al., 2014)
Notch ligand/Jagged-1	Notch receptor	Osteoblasts, endothelial cells	Self-renewal and proliferation	(Butler et al., 2010; Calvi et al., 2003; Lampreia et al., 2017; Poulos et al., 2013)
Wingless-related integration site (WNT) ligand 5a and 3a	Fizzled receptors	Osteoblasts	Quiescence, recovery, proliferation, inhibit self-renewal, restrict HSC pool	(Reya et al., 2003; Richter et al., 2017; Sugimura et al., 2012)
Pleiotrophin	Receptor protein tyrosine phosphatase (RPTP)-ß/ζ	Endothelial cells	Expansion, recovery, self-renewal, retention	(Himburg et al., 2010, 2012)
Netrin-1	Neogenin-1	Endothelial cells	Quiescence, maintenance, self-renewal, rejuvenation	(Ramalingam et al., 2023; Renders et al., 2021)

Soluble factor	HSC receptor	Source cells	Effect on HSCs	References
TGFβ	CD82, type I and type II receptors	Macrophages	Quiescence, maintenance	(Blank & Karlsson, 2015; Hur et al., 2016)
Fibroblast growth factor 1 (FGF1)	Fibroblast growth factor (FGF) receptor	Megakaryocytes	Self-renewal, recovery	(de Haan et al., 2003; M. Zhao et al., 2012)
FL (Flt3 ligand)	Feline McDonough sarcoma (FMS)-like tyrosine kinase 3 (Flt3) (reportedly not expressed on LT-HSCs)	HSCs, CLPs and progeny	Differentiation into CLP, maintenance and expansion in combination with other factors	(Gabbianelli et al., 1995; Luens et al., 1998; Tsapogas et al., 2017; Yonemura et al., 1997)

1.2.3 Architecture

The niche itself is found in the lumen of trabecular long and axial bones (Morrison & Scadden, 2014). It consists of a central cavity surrounded by the endosteum and permeated by tiny blood vessels termed sinusoids and arterioles that connect with vasculature at the centre of the BM (Pinho & Frenette, 2019). Sinusoids carry deoxygenated blood to central veins, while arterioles distribute oxygenated blood from central arteries (Pinho & Frenette, 2019).

HSPCs primarily reside in “sub-niches” surrounding arterioles or sinusoids (Acar et al., 2015; Kunisaki et al., 2013; Nilsson et al., 1998). Despite conflicting claims regarding the exact position of HSPCs within the BM (Acar et al., 2015; Kunisaki et al., 2013), these sub-niches are strongly believed to influence the HSPCs that reside within them, with those found in the arteriolar niche believed to be more naive and quiescent than HSPCs in the sinusoidal niche, which hosts a greater overall number of HSPCs (Pinho & Frenette, 2019). Arterioles are primarily found close to the stiff endosteum’s surface, while sinusoids are distributed throughout the soft central BM cavity (Coutu et al., 2017). Other cells in these sub-niches react differently as well, lending credence to the multiple sub-niche hypothesis. Most notably, MSCs around arterioles express higher levels of nestin and NG2 than

those around sinusoids, which express increased levels of LepR instead (Asada et al., 2017; Kunisaki et al., 2013; B. O. Zhou et al., 2014). Arteriolar MSCs also express lower levels of SCF and CXCL12 (Morrison & Scadden, 2014; Xiao, McGuinness, et al., 2022). Complexly, the existence of a sinusoidal niche, as opposed to a BM cavity niche, is difficult to confirm due to the ubiquity of sinusoids throughout the central BM cavity (Acar et al., 2015; Kunisaki et al., 2013).

1.2.4 The extracellular matrix

Another influential aspect of the BM niche is the extracellular matrix (ECM) (Lee-Thedieck et al., 2022), which interacts with cells within the niche via non-uniform distribution of ECM proteins (Coutu et al., 2017), sequestration and display of GFs, and variable mechanical properties (Chaudhuri et al., 2020; X. Chen et al., 2020; Jansen et al., 2015; Wheadon et al., 2024).

1.2.4.1 Composition

The ECM of the BM niche is mostly composed of water, proteins, and polysaccharides. Most protein in the ECM is fibrous protein, predominately collagen type I, as well as some collagen type II-IX. Collagen X and XI are more associated with cartilage and primarily interact with BM at the chondro-osseus junction where cartilage and bone (Klamer & Voermans, 2014). Other proteins, including elastin and various glycoproteins such as laminin (LN), vitronectin (VN), and fibronectin (FN), constitute just 10-15% of the total ECM protein content (Clarke, 2008). These proteins are not evenly distributed; arterioles are enriched with FN and collagen I, while sinusoids are surrounded by high levels of LN (Lee-Thedieck et al., 2022; Nilsson et al., 1998). Proteoglycans are also found within the BM ECM (Bi et al., 2005; Sarrazin et al., 2011).

1.2.4.2 Growth factor distribution

GFs are a type of soluble factor which affects cellular behaviour by regulating signalling cascades (Xiao, McGuinness, et al., 2022). Proteoglycans and glycoproteins within the niche act as reservoirs for GFs, which they bind and

present in a tightly controlled manner, managing the distribution, activation and presentation of these GFs to BM niche cells (Hynes, 2009). Metalloproteinases secreted by BM cells can remodel the ECM, resulting in the release of soluble GFs (Wheadon et al., 2024). Alternatively, GFs can be presented to cells in a more potent "solid-phase" as part of a complex with ECM protein components (Martino et al., 2015; Salmerón-Sánchez & Dalby, 2016).

1.2.4.3 Mechanical properties

Various mechanical properties of the BM niche ECM influence the cells it houses, including stiffness and viscoelasticity. In terms of stiffness, the BM niche encompasses a wide range, with reported Young's moduli ranging from 1 to 10,000 Pa. The central marrow region is typically considered softest, while the endosteum, as well as the adjacent calcified region of bone, are much stiffer (X. Chen et al., 2020; Jansen et al., 2015). It is important to note that despite different average stiffnesses, all BM regions are highly heterogenous. Viscoelasticity refers to the dual properties of viscosity and elasticity, and how they interact in a substance when it is deformed. Viscosity refers to how a material resists shear forces, and elasticity refers to a material's ability to return to its original shape after deformation. For viscoelastic substances such as BM and other biological tissues, this results in deformable materials that lose the ability to return to their original shape when the deforming force is removed in response to increased frequency and duration of deformation (Chaudhuri et al., 2020).

Cells utilise actomyosin complexes linked to integrins to bind substrates and detect their mechanical properties. These interactions result in conformational changes in intracellular and membranal mechanosensitive proteins, including talin, vinculin, and piezo1, ultimately culminating in downstream cellular changes (Janmey et al., 2020; Kechagia et al., 2019) via signalling pathways such as Runt-related transcription factor 2 (RUNX2) and RhoA kinase signalling (Ross et al., 2023). The molecular clutch model, in which actin retrograde flow is reduced by integrin clustering and focal adhesion reinforcement, which is in turn modulated by substrate mechanics, further explains this process (Bennett et al., 2018; Elosegui-Artola et al., 2016, 2018). Effects on cells include short-term changes to motility and proliferation, and long-term changes affecting processes such as

differentiation and disease progression (Ayad et al., 2019; H. Lee et al., 2005; P. Zhang et al., 2019). BM cells' stiffness response is also influenced by the concentration of ECM proteins such as FN and laminin. These proteins contain RGD (Arg-Gly-Asp) domains which strongly interacts with some integrins (H. Lee et al., 2005).

Within the BM niche, lower stiffness microenvironments have been shown to promote adipogenesis in MSCs, while high stiffness environments are osteogenic (Vining & Mooney, 2017). The direct effect of these physical characteristics of the BM niche on HSPCs is less well understood. In spite of their putative non-adherence (P. Zhang et al., 2019), HSPCs are influenced by ECM content and stiffness (Choi & Harley, 2017; H. Lee et al., 2005), possibly due to a combination of indirect biochemical and mechanical signals (Vining & Mooney, 2017).

1.2.4.4 Structure

Topographical cues have been shown to influence cell fate decisions. These range from cell-sized microscale features that impact cell shape and movement in a process known as contact guidance (Curtis & Wilkinson, 1997), to nanoscale features, such as the lateral distance between adhesive ligands, which induce changes to adhesion size, number, and spacing (Ross et al., 2019; Tsimbouri et al., 2012), as well as lipid raft clustering (Lee-Thedieck et al., 2022). These cellular changes are adhesion-dependent (Ngandu Mpoyi et al., 2016) and have been shown to affect both MSCs and HSCs.

Nanoscale topography influences MSCs' survival, differentiation, and growth (C. S. Chen et al., 1997); structures which induce a rounded shape typically result in fewer mature adhesions and lower intracellular tension, while the opposite is true when MSCs can spread (Kilian et al., 2010). Similarly, microscale topography that encourages spreading due to dispersed or disordered adhesion ligands results in large adhesions associated with high intracellular tension (Tsimbouri et al., 2012), and vice versa (Kilian et al., 2010). The level of intracellular tension then dictates differentiation, with higher tension associated with osteogenesis, and lower tension yielding adipogenesis (Donnelly et al., 2018).

HSCs also interact with the topography of their microenvironment. The density of adhesive ligands has been shown to affect HSC behaviour (Lee-Thedieck et al.,

2022) and has been utilised to enhance HSC expansion *in vitro* (Ferreira & Mousavi, 2018). However, a direct link with HSC intracellular tension hasn't been established. In addition, some systems which showed increased expansion of HSCs with functionalised surfaces also used immobilised notch ligand delta-like 1 (DLL1), a juxtracrine signalling component found on MSCs (Winkler, Koenig, et al., 2017; Winkler, von Wulffen, et al., 2017), suggesting that the changes seen may have been due to simulated intracellular signalling rather than interactions with adhesive ligands.

The porosity of the ECM also directly affects diffusivity (Lee-Thedieck et al., 2022). This influences autocrine and paracrine signalling between cells in the BM (Gilchrist et al., 2019; Mahadik et al., 2017), as well as interactions with other soluble factors. HSCs have also been theorised to sense how physically restrained they are (Nelson & Roy, 2016), with more porous microenvironments resulting in greater HSC expansion (Kurth et al., 2009).

1.2.5 Oxygen saturation

Oxygen saturation also plays a role in the niche's interaction with HSCs. The niche itself is usually labelled as a hypoxic environment due to its low oxygen saturation (J. A. Spencer et al., 2014). This has been linked to the primarily glycolytic respiration of LT-HSCs, as well as their lack of mitotic activity, both of which are traits that have been observed in cells under hypoxia (Kierans & Taylor, 2021; Warburg Berlin-Dahlem, 1925). This glycolytic metabolism is also thought to protect LT-HSCs from DNA damage due to reduced levels of reactive oxygen species (ROS) and fewer mitosis-associated replication errors, therefore preserving a healthy LT-HSC pool (Jang & Sharkis, 2007).

However, this simple narrative breaks down when the oxygen saturation of the BM niche is measured reductively rather than holistically (J. A. Spencer et al., 2014). Notably, the perisinusoidal region was measured to have the lowest level of oxygen saturation in the niche, while the endosteal region which houses arterioles was determined to be less hypoxic. Furthermore, the mechanism of stabilisation for hypoxia inducible factor 1α (HIF-1α), elevated levels of which in HSCs have been used to justify the existence of a hypoxic niche (Takubo et al., 2010), has come under recent scrutiny. HIF-1α promotes expression of pyruvate

dehydrogenase kinase, which inhibits pyruvate conversion into acetyl CoA, preventing progression from glycolysis to the tricarboxylic acid cycle step of oxidative phosphorylation (Wang et al., 2021). Emerging evidence suggests regulation of HIF-1α in HSPCs is not entirely oxygen dependent (Nombela-Arrieta et al., 2013), and other aspects of the niche have been shown to regulate HIF-1α levels in MSCs as well (Donnelly et al., 2024; Ross et al., 2019).

The BM niche is a highly complex organ that maintains haematopoietic homeostasis with a wide range of cellular and non-cellular elements, many of which influence each other in a complicated crosstalk network. Despite an incomplete understanding of how these elements interact, there is a growing body of knowledge on the subject that has allowed researchers to begin tinkering with *in vitro* models of the BM niche organ.

1.3 Modelling the BM niche

Models of the BM niche promise to revolutionise our understanding of both physiological and pathological haematology and immunology, while also facilitating therapeutic advancements targeting BM-associated disorders and diseases. One of the primary goals of these niches is to manipulate HSPCs for HSCT. Many BM niche models seek to expand or maintain LT-HSCs to increase the availability of this treatment (Chatterjee et al., 2021; Fares et al., 2022). However, this ambition has met with mixed results, primarily due to expanded HSCs' heterogeneity and reduced differentiation capacity. The recent success of simple systems using media additives or gels rather than complex models for expansion demonstrated a more straight-forward method of achieving this goal (Meaker & Wilkinson, 2024). Other aims include expanding understanding of the BM niche and haematopoiesis and developing platforms for testing novel therapies for BM-associated disorders and diseases.

The current gold standard for BM models are animal models, which have been used successfully to achieve many of the goals stated (Haas et al., 2018; P. Zhang et al., 2022). However, these models present various challenges, including a lack of comparability with human biology, complexity obscuring specific mechanisms of the niche, and a lack of reproducibility (Ingber, 2020; Lee-Thedieck et al., 2022).

Attempts to replicate the BM niche *in vitro* have yielded increasing success in recent years. These systems aim to shed light on the haematopoietic process, harness it for clinical applications, and understand how it goes wrong in haematological diseases and disorders (Méndez-Ferrer et al., 2020). Foundational research combined with modern advances has galvanised the field and resulted in a wealth of new models, the current state of which will be discussed, as well as potential applications and the future of the field (see **Figure 1.5**).

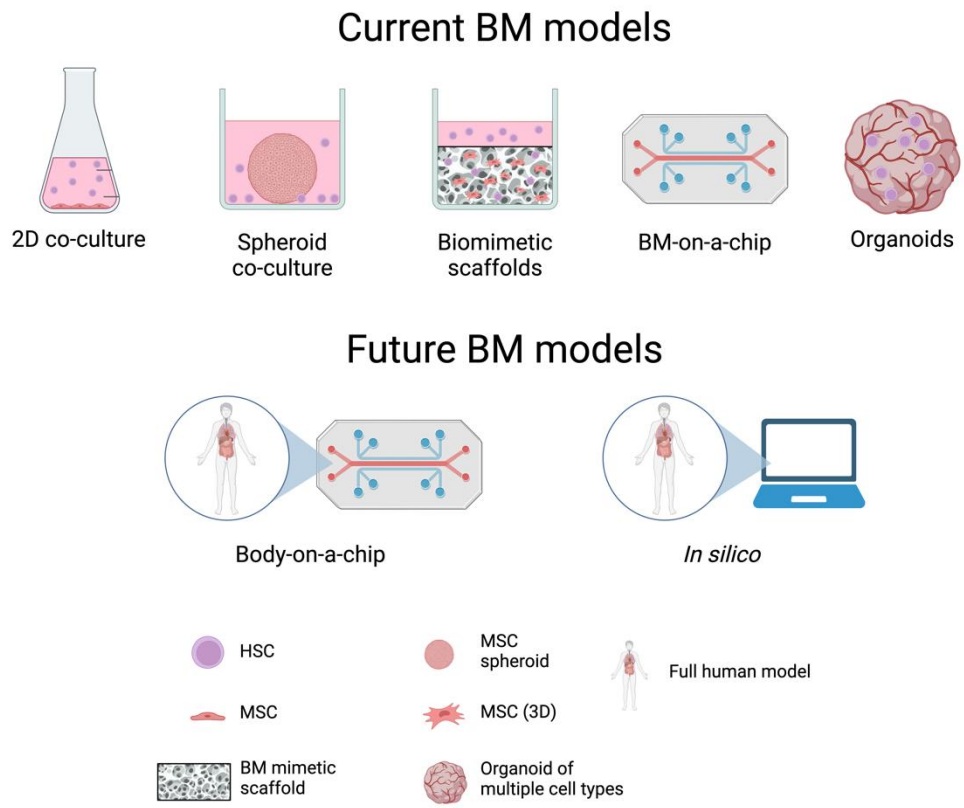

Figure 1.5 Illustrations of current and potential future bone marrow niche models. *Current models include 2D co-culture of HSCs and MSCs, spheroid co-culture, biomimetic scaffolds, bone marrow-on-a-chip, and organoids, among others. These models offer different levels of complexity and physiological relevance, which make them suitable for various applications when studying the bone marrow niche. Theoretical future models may include body-on-a-chip, which incorporate models of several or all human organs, and* in silico *models, which simulate biological processes computationally. Created with BioRender.com.*

1.3.1 Current state of BM niche models

Various elements of the *in vivo* BM niche have been incorporated into BM models, with a range of results (see **Table 1.3**).

Table 1.3 BM niche elements and their impact when included in BM models.

Model BM niche element	Element impact on HSCs	References
BM niche cells	Inclusion of BM resident cells simulates the complex cellular composition of the BM niche, with included cells interacting with HSCs via juxtracrine and/or paracrine signalling.	(Donnelly et al., 2024; Khan et al., 2023; Pinho & Frenette, 2019; Xiao, McGuinness, et al., 2022)
Soluble factors/cytokines	Soluble factors are typically used to improve HSC maintenance. The use of soluble factors has also been shown to improve HSC proliferation, however often the expanded cells are in the short-term HSC or progenitor compartment and lack long-term engraftment capacity.	(Boitano et al., 2010; Bray et al., 2017; Lai et al., 2013; Sánchez-Lanzas et al., 2022; Wilkinson et al., 2019)
ECM components	ECM components such as FN, VN, and LN have been shown to affect MSCs' and HSCs' phenotypes by sequestering and presenting signalling molecules and growth factors, as well as interacting with the cells mechanically	(Donnelly et al., 2024; Wilkinson et al., 2019; Xiao, McGuinness, et al., 2022)
Hydrogel	Hydrogels' 3D nature mimics the in vivo BM niche. Gels can also provide physical, mechanical, and chemical stimuli as well as hydrophobic and hydrophilic interactions to cells in a BM niche model.	(Aleman et al., 2019; Braham et al., 2019; Bray et al., 2017; Donnelly et al., 2024; Leisten et al., 2012; Nelson et al., 2021; Rödling et al., 2017)
Self-assembling peptide-based hydrogel (SAPH)	SAPHs such as PeptiGels are highly tuneable, offering precise control over the mechanical properties of cells' microenvironments. They can also be functionalised to further tailor their impact on cells.	(Clough et al., 2021; Scelsi et al., 2019)

Model BM niche element	Element impact on HSCs	References
Non-gel scaffold	Non-gel scaffolds possess many of the same benefits as hydrogels and afford the opportunity to add other elements as well, such as control over cellular localisation using magnetised cells and a magnetised scaffold. Examples of these scaffolds include ceramics, colloidal crystals, and hydroxyapatite.	(Bourgine et al., 2018; Goranov et al., 2020; Nichols et al., 2009)
Decellularised matrix	Using decellularised animal BM matrix to culture human BM cells has met with success due to the conserved BM architecture and physical properties.	(Bianco et al., 2019; Lai et al., 2013; Tiwari et al., 2012)
Blood flow/perfusion	Perfusion models replicate blood flow, which could impact HSCs that natively reside alongside blood vessels. HSCs may also enter the circulatory system, making this another important element of the BM niche to include in models.	(Bourgine et al., 2018; Chou et al., 2020; Glaser et al., 2022; Goranov et al., 2020; Lapidot & Petit, 2002; Ma et al., 2020; Nelson et al., 2021; Patra, 2021; Rödling et al., 2017; Wright et al., 2001)

1.3.1.1 MSCs and soluble factors

Developing a model BM niche for studying and manipulating normal and pathological haematopoiesis presents various challenges, not least of which being that HSCs rapidly differentiate when cultured under standard tissue culture conditions (Jaroscak et al., 2003). Soluble factors found within the niche have been shown to promote maintenance and expansion within the putative HSC compartment (Delaney et al., 2010; Horwitz et al., 2014; J. E. Wagner et al., 2016; Xiao, McGuinness, et al., 2022). Of note, SCF (Asada et al., 2017), fms-like tyrosine kinase 3 (Flt3) ligand (FL) (Sitnicka et al., 2002) and thrombopoietin (TPO) (Qian et al., 2007) have all been implicated in HSC maintenance and used for HSC culture *in vitro* (Donnelly et al., 2024). However, systems that solely utilised these factors and others like them showed limited success in growing HSCs with long

term-engraftment capacity for HSCT (Delaney et al., 2010; Horwitz et al., 2014; J. E. Wagner et al., 2016). Despite this, soluble factors are routinely used in model BM niche systems to promote HSC maintenance. MSCs maintain haematopoietic homeostasis by secreting soluble factors and utilising juxtracrine signalling (Méndez-Ferrer et al., 2010; Pinho et al., 2013). As a result, many modern BM niche models include MSCs.

The MSCs included in BM models have several sources; primary MSCs sourced directly from patients' BM (Bhat et al., 2021), extramedullary MSCs (Shang et al., 2021; Tsuji, 2014), iPSC-derived MSCs (Dupuis & Oltra, 2021), and immortalised MSC-like cell lines (Galarza Torre et al., 2018). MSCs sourced directly from donors' BM are considered gold standard but are difficult to acquire due to their relative rarity (Hass et al., 2011; H. Li et al., 2016; Pittenger et al., 1999). Other sources of MSCs from patients include adipose tissue (Tsuji, 2014) and birth-associated tissues (Shang et al., 2021). MSCs can be acquired easily from these sources following liposuction or birth, and MSCs are more abundant in these locations, making them a popular alternative to BM MSCs (Donnelly et al., 2024; Hass et al., 2011). MSCs derived from iPSCs also present various advantages, namely that they can be grown from patients' somatic cells and have the potential to self-organise and reproduce various cellular aspects of the BM niche simultaneously (Frenz-Wiessner et al., 2024; Khan et al., 2023). However, this technology is relatively new, and more research is required before iPSCs' pluripotency can be fully understood and readily manipulated to produce true MSCs (Dupuis & Oltra, 2021; Thanaskody et al., 2022). Immortalised MSCs, which are ergonomic due to their long-term maintenance of differentiation competency, have been used as a BM MSC alternative as well (James et al., 2015).

MSC feeder layers' microenvironments can be modified mechanically and chemically, indirectly influencing their effect on HSCs. A well-established example of this is the inclusion of ECM components such as FN or LN, alongside GFs such as BMP2 that influence MSCs' phenotype (Donnelly et al., 2024; Xiao, McGuinness, et al., 2022).

Attempts have also been made to identify media additives which can maintain HSCs without co-cultured MSCs. Recently, Wilkinson et al. (2019) created a defined culture system containing high levels of TPO, alongside low levels of SCF

and FN, which plates were coated with, and polyvinyl acrylate (PVA) as a substitute for serum albumin. This system was able to expand a population of mouse HSCs several hundred-fold. Produced cells, even from single-cell expansion cultures, were also demonstrated to have significant BM repopulation capacity, despite increased heterogeneity in self-renewal compared to freshly harvested HSCs. Sakurai et al. (2023) improved on this system further, developing a cytokine free system that included chemical agonists which directed cell fate, and a caprolactam-based polymer like PVA. This system expanded functional human HSCs, unlike the previous approach which was predominately shown to be effective in murine HSCs.

1.3.1.2 2D co-culture

Lima et al. (2013) attempted to expand HSCs from umbilical cord blood by co-culturing cord blood samples with BM-derived MSCs and various cytokines. They demonstrated remarkable expansion of putative HSCs using this method. However, when the expanded cells were transplanted in patients, long-term engraftment was significantly lower compared to transplantation with unmanipulated cord blood. These results suggested that a simple two-dimensional (2D) co-culture system was insufficient to either artificially expand HSCs for HSCT or as a model for LT-HSC maintenance in the *in vivo* BM niche (Seita & Weissman, 2010).

1.3.1.3 Spheroids

Later research attempted to improve upon simple co-culture models' ability to influence HSCs' maintenance and expansion by assembling MSCs into spherical masses, termed spheroids, prior to co-culture (Lewis et al., 2017; Méndez-Ferrer et al., 2010). The effect of spheroids appeared to be mixed, although MSCs within them reportedly adopted a more niche-like phenotype than those cultured in a monolayer (Isern et al., 2013). The number of putative HSCs after expansion was shown by one study to be comparable when MSC spheroids or monolayers were used for co-culture (Futrega et al., 2017). However, other studies reported a substantial increase in putative HSC count under similar conditions (Isern et al., 2013; Pinho et al., 2013). This was largely attributed to soluble factors produced by the MSCs, rather than juxtracrine signalling. The use of spheroids in BM niche

models was a big step forwards regardless of the mixed results obtained, as it demonstrated that three-dimensional (3D) culture systems were at least comparable to early 2D systems in terms of their ability to maintain and grow a population of LT-HSCs.

1.3.1.4 Physical properties of the cellular microenvironment

Various approaches have been utilised to manipulate the physical properties of the microenvironment experienced by cells in a model BM niche. These include using decellularized BM (Bianco et al., 2019; Lai et al., 2013; Tiwari et al., 2012) or 3D BM mimetic scaffolds to influence HSCs. An early example of this was Nichols et al. (2009), who used inverted colloidal crystals to mimic the porosity and stiffness of the *in vivo* BM niche, and demonstrated that this system was capable of expanding HSCs, albeit with the inclusion of MSCs. Raic et al. (2014) improved upon this approach using bio-functionalised macroporous hydrogels seeded with MSCs in cytokine-supplemented media, resulting in a system that was capable of transient maintenance of seeded HSCs' differentiation capacity, a big improvement on previous models. Collectively, these models illustrated the need to incorporate BM mimetic materials into future BM niche models, as well as the combinatorial effect of materials coupled with cellular components of the *in vivo* niche. Interestingly, Raic et al. (2014) discovered a population of HSCs which did not remain within the scaffold and instead settled underneath it. They found that this cell population had much higher levels of naivety and differentiation capacity than HSCs that remained within the niche, implying the simulation of multiple BM niche compartments which differentially influenced HSCs, akin to the sub-niches observed in the native BM niche.

1.3.1.5 The multifaceted nature of the BM niche

Bourgine et al. (2018) encapsulates some of the complexity of the BM niche using a porous hydroxyapatite scaffold functionalised with human MSCs. The MSCs were grown within the scaffold, causing them to deposit elements of the native BM ECM. This system was assembled in a perfusion bioreactor which mimicked the blood flow present within the *in vivo* BM niche. HSCs were added to this system, filling the scaffold and overflowing above it to form separate artificial ECM and

supernatant environments, similar to the static sub-niches observed by Raic et al. (2014). However, unlike Raic et al. (2014), Bourgine et al. (2018) demonstrated that a higher proportion of the HSCs found within the scaffold displayed surface markers typically associated with LT-HSCs. It's possible that the artificial ECM included in this model assumed the role of the arteriolar niche, with putative LT-HSCs preferentially localising within it, while more actively dividing HSCs localised to the supernatant, which may have taken on the role of the sinusoidal niche. However, without precisely characterising the HSCs within this system, a possibility remained that the supernatant component of these types of models simulates the vasculature around the in vivo BM niche, which is known to contain mobile, quiescent HSCs with high levels of engraftment capacity (Lapidot & Petit, 2002; Patra, 2021; Wright et al., 2001), as suggested by Raic et al. (2014). In spite of this, similar models favoured the former assessment (Leisten et al., 2012; Nelson et al., 2021), supporting the findings of Bourgine et al. (2018). These two-compartment models replicate the multifaceted nature of the BM niche and could help to elucidate some of its complexities. However, their application in a clinical setting is limited, as the naïve HSCs are trapped within the scaffold and co-cultured with MSCs without a barrier, making them difficult to isolate for investigation or clinical application (Bello et al., 2018).

1.3.1.6 Combinatorial niche models

In an attempt to encapsulate various other aspects of the BM niche, some researchers have attempted to create BM-on-a-chip models. Nelson et al. (2021) created a system using a complex co-culture of MSCs, osteoblasts, human umbilical vein endothelial cells and HSCs. These cells were cultured in separate wells connected via microfluidic channels, allowing nutrient exchange between them. Different combinations of cells and media with or without the inclusion of a hydrogel were applied to each well during the assembly of the model, resulting in an interconnected system of wells each of which simulated some aspect of the in vivo BM niche, including angiogenesis. A similar model developed by Glaser et al. (2022) even incorporated perfusion. These highly complex systems and others like them (Aleman et al., 2019; Chou et al., 2020) mimic many more aspects of the BM niche than the simpler models discussed. This makes them excellent

candidates for furthering our understanding of the BM niche in both a healthy and diseased state, and for screening treatments for BM-associated diseases and disorders.

1.3.1.7 Organoid models

Recently, efforts have been made to produce miniaturised, self-organising, multicellular, 3D versions of the BM niche, termed organoids (G. Rossi et al., 2018). Two parallel papers utilised similar multiphase pipelines to produce complex, vascularised organoids that mimic many aspects of the BM niche (Frenz-Wiessner et al., 2024; Khan et al., 2023). Each phase of organoid production utilised a different cocktail of media components. Initially, induced pluripotent stem cells (iPSCs) were encouraged to form embryoid body (EB) aggregates. Once established, the EB aggregates had a mesodermal phenotype induced, which was appropriate as BM niche cells are derived from the mesoderm over ontogeny (Mikkola & Orkin, 2006; Vodyanik et al., 2010). Next, the EBs were primed for vascular and haematopoietic differentiation, and subsequently embedded in a hydrogel. Within the gel, angiogenesis was observed as the EBs began to sprout (Wimmer et al., 2019). Finally, sprouting EBs were removed from the gel and cultured in ultra-low adhesion plates, resulting in the formation of vascularised organoids consisting of multiple cell types found within the native BM niche.

Organoid models present a unique opportunity to further our understanding of haematological development over ontogeny using a pluripotent *in vitro* system. In addition, they have shown potential for the maintenance of otherwise difficult to culture primary cancer cells (Khan et al., 2023), and as pathological models for diseases such as myelofibrosis and neutropenia (Frenz-Wiessner et al., 2024; Khan et al., 2023). While these models are impressive, they do not holistically mimic the *in vivo* BM niche due to limitations including a lack of a complete BM niche cellular cohort, and no recapitulation of the multiple sub niches present in the *in vivo* niche. Also, due to the immaturity of the cells produced, organoid models more closely resemble foetal rather than adult BM. However, organoids represent a significant advancement in the field; the ease with which iPSCs can be produced compared to other BM stem cell sources makes this an attractive model for HSC

expansion, and further optimisation of organoid production promises to yield even better in vitro BM models.

Similar results were produced using organoid-like constructs termed ossicles, which were assembled in vitro then transplanted into murine models (Reinisch et al., 2016, 2017). Although these constructs recapitulated some aspects of the BM niche and were subsequently invaded by murine hematopoietic tissue, they still possess many of the issues inherent to animal models compared to fully humanised models (Ingber, 2020).

1.3.2 Future of BM niche models

While the current crop of BM niche models is promising, none have managed to produce a system which can consistently expand a population of HSCs without sacrificing the cells' differentiation or engraftment potential. This is in part due to the highly heterogenous nature of HSCs (L. Rossi et al., 2011), which makes it difficult to identify LT-HSCs isolated from BM models (Futrega et al., 2017; Kiel et al., 2005; L. Rossi et al., 2011; Sonoda, 2021). Considering that LT-HSCs rarely multiply (P. Zhang et al., 2019), it is likely that any expansion observed occurs out with the LT-HSC compartment, resulting in a population of cells with reduced engraftment and differentiation capacity. Furthering our understanding of haematopoietic niches, especially foetal niches from which HSCs are initially derived (Mikkola & Orkin, 2006), could provide an avenue for the expansion of LT-HSCs in vitro which could in turn allow HSCT treatment to move away from the current one donor one recipient system towards a one donor multiple recipient system, greatly increasing its availability (Wilkinson et al., 2020).

However, simpler approaches to LT-HSC expansion have been employed with increasing success in recent years, including the addition of small molecules that prevent loss of the LT-HSC phenotype when expanding HSCs using cytokine cocktails (Cohen et al., 2023; Peled et al., 2012; Wilkinson et al., 2019), and the use of super-hydrophilic hydrogels for 3D HSC culture (Bai et al., 2019). This has led to a refocussing of BM niche models' purposes towards deepening our understanding of the niche, healthy and diseased haematopoiesis, and as platforms for developing treatments for BM-associated disorders and diseases.

In addition, reliance on extracellular stimuli such as perfusion or artificially separated cell populations is an adequate compromise but does not reproduce the complex interplay that occurs within a cellularly diverse, mechanically heterogenous organ such as the BM niche, not to mention interactions the BM has with other organs within an individual. Fully cellular organoid models could start to overcome this issue, but their development is still in its infancy.

Finally, recent advances have led to highly complex BM models. However, this complexity is itself a limitation, due to the inherent cost, time and level of expertise required to assemble these models.

1.3.2.1 Potential applications of BM niche models

A prospective application of BM models is their usefulness for studying and developing treatments for BM-associated disorders and diseases (Dozzo et al., 2023). Novel treatments such as chimeric antigen receptor T-cell (CAR T-cell) therapy show huge promise (Kim et al., 2018) but are often inaccurately assessed with animal studies due to differences in animal and human biology, preventing potential treatments from reaching the market, or allowing those which are unsafe or ineffective to do so (Akhtar, 2015; Ingber, 2020). Pathological *in vitro* models that more accurately replicate diseased human biology, reduce animal suffering and can be produced at scale have the potential to revolutionise our approach to drug testing, either as a screening step prior to animal testing or as a complete substitution (Haddrick & Simpson, 2019).

BM models have also been used to further our understanding of the BM niche and haematopoiesis, as previously discussed. They have shown that HSC maintenance is reliant on MSCs and the material properties of the HSCs' microenvironment, that soluble factors also play a part and are the main way in which MSCs interact with HSCs, and that the BM niche is formed of distinct, interconnected sub-niches. As BM niche models continue to evolve so will our understanding of the *in vivo* BM niche, haematopoiesis, and HSCs (see **Figure 1.6**).

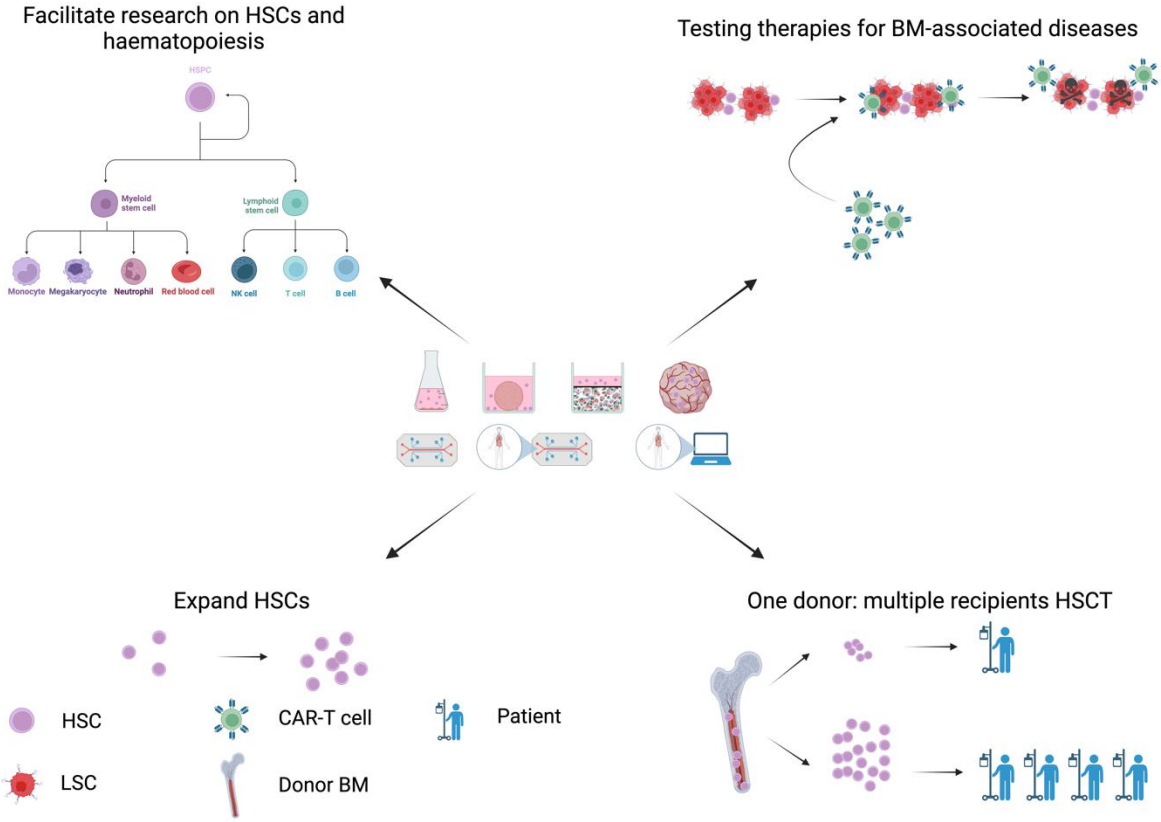

***Figure 1.6 Potential applications of a model BM niche**. By mimicking the native BM niche, BM models promise to facilitate* in vitro *investigation of haematopoiesis, providing new insights. They could also act as platforms for testing novel therapies, reducing the need for expensive and non-representative animal models. These systems could produce further benefits, such as expanding HSCs without sacrificing their repopulation capacity, addressing the unmet need for more of this clinically relevant cell type. Created with Biorender.com*

It is unlikely that a single BM niche model will emerge which can be utilised for all the applications stated. Rather, a range of niches is likely to develop, each specialised for a specific application, allowing the accomplishment of each using a different approach.

1.3.2.2 Future BM niche models

Future BM niche models could seek to replicate the *in vivo* niche more accurately by incorporating a complete BM cellular cohort or by precisely replicating the physical, mechanical, and chemical composition of the in vivo niche. If achieved this would result in BM niche models with high biomimicry, furthering our understanding of the *in vivo* niche's physiology, biochemistry, and biophysics. Other future models could include simplified niches specialised to accomplish a

specific goal, such as LT-HSC maintenance (Donnelly et al., 2024) and expansion, or as platforms to test novel therapies in which BM cells are easily accessible for treatment and evaluation. As our understanding of the BM niche continues to develop it may even become possible to eliminate the need for inherently complex co-cultures and replicate the effect of BM cellular components in HSC monoculture systems, simplifying artificial BM niches substantially.

Next generation models could also be developed. These may include whole body models which mimic several or all human organs (Novak et al., 2021). Whole body models could provide a platform for comprehensive assessment of treatments' efficacy and safety on an individual basis, and possibly lead to the development of a body-on-a-chip (Sung et al., 2019). *In silico* models of the BM or whole individuals may also emerge. These could take the form of a digital twin, mimicking the function of biological systems based on experimental datasets and/or biological principles (Geris et al., 2018). Simple *in silico* models are already in use, and have demonstrated the ability to assist with optimisation of experimental parameters (Baker et al., 2023), confirm hypotheses (Chang et al., 2010; Stratmann et al., 2014), and shed light on previously poorly understood biological systems (Edelman et al., 2010). Recent advances in artificial intelligence technology could facilitate further development of these revolutionary new models by helping with data compilation from diverse sources (Homeyer et al., 2022) and through utilisation of techniques such as deep learning and machine learning to collate and utilise large datasets for predicting the impact of stimuli such as novel drugs on biological processes (Sarker, 2022). As such, *in silico* models have the potential to exponentially accelerate research by identifying optimum parameters for experimentation, and, with further developments potentially leading to fully realised digital twins, may offer an alternative to animal and *in vitro* models for clinical trials.

One of the key benefits of whole body next generation models, both *in silico* and *in vitro*, is their use for predicting pharmacokinetics and off-target toxicity, which are not explorable using single organ models (Bender et al., 2007; Chang et al., 2010). These types of models require extensive knowledge of the simulated organs to develop, or large, reliable, and relevant datasets and systems which can interpret and utilise them. However, due to the rapidly evolving nature of the field they may be closer than they appear.

Within the last half century BM models have gone from simple liquid suspensions of HSCs to highly complex *in vitro* organ models specialised to achieve specific goals. This has greatly improved our understanding of the *in vivo* BM niche, allowing for the exponential pace of BM model development seen recently. As this field continues to develop it promises to deliver several benefits, namely a deeper understanding of haematopoiesis, an improvement over animal models to facilitate more efficacious and cheaper development of treatments for BM-associated disorders, and a potential method for the expansion of LT-HSCs for HSCT.

1.4 Acute myeloid leukaemia

Leukaemia is a common form of blood cancer which resulted in ~330,000 deaths globally in 2019 (Du et al., 2022). It is caused by aberrant haematopoiesis resulting in uncontrolled proliferation of malignant haematopoietic cells, and is characterised by clonal malignant haematopoietic cells (Ding, Ley, et al., 2012).

There are four broad types of leukaemia, categorized based on their acuteness and the type of cells that are malignant. These are chronic lymphocytic leukaemia (CLL), acute lymphocytic leukaemia (ALL), chronic myeloid leukaemia (CML) and acute myeloid leukaemia (AML) (Du et al., 2022; Ottensmeier, 2001). AML is the deadliest form of the disease, accounting for ~28% of all leukaemia-associated deaths (Du et al., 2022). It is caused by haematopoietic cells which acquire clonal mutations, over-proliferate, and rapidly become malignant while retaining an intermediate, poorly differentiated state (Ding, Ley, et al., 2012; Hope et al., 2004). AML cells are typically found in the circulatory system, but can metastasise to other parts of the body in later stages of the disease (Whiteley et al., 2021).

1.4.1 Leukaemic stem cells

The high probability of leukaemic relapse following traditional therapies is often attributed to the presence of leukaemic stem cells (LSCs) (Döhner et al., 2015). LSCs are highly heterogenous, quiescent, and typically maintain a glycolytic metabolism, similar to LT-HSCs (Hope et al., 2004). In addition, LSCs are thought

to be solely responsible for cancer initiation, as demonstrated by their ability to reconstitute the disease in xenograft assays (Batlle & Clevers, 2017). Due to their lack of mitotic activity, LSCs routinely evade most chemotherapy regimens, which work by targeting highly proliferative cancer cells (Batlle & Clevers, 2017; Gewirtz, 1999; Hamada et al., 2002). Following ablation of active cancer cells, cancer stem cells have been observed re-entering the cell cycle, resulting in recurrence in several cancer types (J. Chen et al., 2012; Kreso et al., 2013; Oshimori et al., 2015).

Conversely, the cancer stem cell hypothesis has been challenged by recent research showing that AML LSCs are not selectively resistant to chemotherapy regimens. Instead, a distinct, possibly therapy-induced population of leukaemia recursion cells (LRCs) reportedly appears following initial treatment and is responsible for recurrence (Boyd et al., 2018; Duy et al., 2021; Farge et al., 2017). To achieve long-term, curative treatments for AML, LSCs and/or LRCs need to be eliminated, or long-term protection from relapse accomplished by other means.

1.4.2 Causes of leukaemia

The cancer stem cell hypothesis dictates that cancer initiating cells are typically stem cells which acquire multiple damaging mutations to tumour suppressive genes and oncogenes (Hope et al., 2004). This suggests that the BM niche is the site of AML initiation (Passaro et al., 2017). Well understood causes of mutation, including exposure to radiation and mutagens such as cigarette smoke and some chemotherapy drugs, have been linked with higher risk of developing AML. However, due to accumulated random mutations acquired by individuals over time, the greatest risk factor for AML is age (Appelbaum et al., 2006; Buchner et al., 2008). AML also occurs in children, a conundrum explained by germ line mutations passed down from parents (Buijs et al., 2001; W. J. Song et al., 1999). Several common genetic mutations in AML cells have been identified. These are found in genes such as FLT3 (Daver et al., 2019), nucleophosmin (NPM1) (Heath et al., 2017), B-cell leukaemia 2 (BCL-2) (Adams & Cory, 2007) and TP53 (Rivlin et al., 2011; Stengel et al., 2017). 90% of AML patients' cells also express high levels of CD33, a myeloid cell surface marker and member of the sialic acid-binding immunoglobulin (Ig)-like lectin (siglec) family (Laszlo et al., 2014, 2016). In

addition, epigenetic changes are also associated with AML initiation and propagation, often as a result of a mutation in epigenetic regulators (Glass et al., 2017; D. H. Spencer et al., 2017).

Likewise, the cellular microenvironment plays a role in leukaemic initiation and progression. AML cells have been observed remodelling the BM niche by interfering in crosstalk with niche cells, altering the niche's vasculature, curating niche cells and changing the ECM's composition (Bernasconi & Borsani, 2019). Notably, MSCs and their progeny have markedly different expression profiles in the healthy niche and the AML niche (Kode et al., 2016; Kojima et al., 2011; Menendez et al., 2009; H. S. Zhou et al., 2016). This remodelling is potentially modulated by AML cells' secreted exosomes (Kumar et al., 2018). This results in a protective microenvironment that supports leukaemic cells' rapid proliferation and has been shown to shield them from damaging agents such as chemotherapy drugs (Ishikawa et al., 2007; Tabe & Konopleva, 2015).

1.4.3 Treatments of leukaemia

Despite being incurable sixty years ago, AML now has a curability of 35-40% (Döhner et al., 2015; Kantarjian, 2016). However, this statistic has remained virtually static since the advent of the "3+7" chemotherapy regimen in the 1970s, which is still widely considered the gold standard treatment for AML. Some other prominent treatment strategies are outlined below.

1.4.3.1 Chemotherapy

Intensive chemotherapy targets rapidly proliferating cells. Since cancer cells are highly proliferative, they are preferentially targeted (Batlle & Clevers, 2017; Gewirtz, 1999; Hamada et al., 2002). For AML, the most commonly used chemotherapy regimen is "3+7", which relies on administration of daunorubicin for three days and cytarabine for seven, typically followed by post-remission chemotherapy and HSCT (Kantarjian, 2016; Tefferi & Letendre, 2012; Yates et al., 1982). Unfortunately, a substantial proportion of patients eventually relapse following 3+7 and similar treatment regimens (Döhner et al., 2015; Schmid et al., 2012), possibly due to the presence of LSCs and a protective leukaemic BM niche.

Furthermore, intensive chemotherapy like 3+7 carries the risk of neutropenia and thrombocytopenia, resulting in side effects such as patients becoming immunocompromised, haemorrhaging or dying (Dombret & Itzykson, 2017). These factors have driven research into novel, safe, truly curative therapies for AML (Kantarjian et al., 2021).

1.4.3.2 Allogeneic HSCT

Allogeneic HSCT is a well-established treatment for AML. Its effectiveness relies on the graft-vs-leukaemia (GvL) effect, in which high numbers of donor CD34+ cells are thought to outcompete native diseased cells, including LSCs, by targeting them with immune cells and displacing them from the BM niche (Dickinson et al., 2017). Despite its success and wide use, allogeneic HSCT carries the risk of serious complications, such as graft vs host disease (GvHD) (Meaker & Wilkinson, 2024). Alternatively, autologous HSCT is often offered to low-risk patients, as it removes the issue of identifying compatible donors. Autologous HSCT is less potent due to a minimal GvL effect, which reduces the risk of GvHD but increases recurrence rate (Cornelissen & Blaise, 2016). Both forms of HSCT have a high recurrence rate, implying attenuation of AML, not elimination (Mardiana & Gill, 2020).

1.4.3.3 Oncoprotein inhibitor therapy

Inhibitors for AML-associated oncoproteins have demonstrated potential in recent years. Targets of these drugs include FLT3 (Konig & Levis, 2015; R. M. Stone et al., 2017), BCL-2 (Konopleva et al., 2016) and the hedgehog pathway (Wellbrock et al., 2015). These therapies dampen the AML phenotype, and have been shown in many cases to work well in combination with standard chemotherapy (Canaani, 2019). However, this type of therapy, like the chemotherapy it is frequently integrated with, is not curative.

1.4.3.4 Epigenetic therapy

Unlike genetic alterations which cause AML, epigenetic changes are often reversible. Several therapies seek to capitalise on this by reverting AML cells' epigenome from a malignant to a benign state (Issa et al., 2015; Klco et al., 2013;

Schuh et al., 2017). While these therapies produce fewer side-effects, allowing them to be used by patients who could not tolerate intensive chemotherapy, they also offer a lower remission rate (Dombret & Itzykson, 2017). Epigenetic therapies are used in clinic today, but are typically applied to patients on a case-by-case basis, with chemotherapy remaining the gold standard (Wouters & Delwel, 2016).

1.4.3.5 Antibody therapy

A landmark development was the creation of gemtuzumab ozogamicin (GO). Unlike chemotherapy treatments, which target cells based on their proliferative state, GO specifically targets AML cells by recognising their characteristically high level of CD33 expression (Laszlo et al., 2014). This allows GO to colocalise with AML cells before delivering a lethal payload of antibiotics (Van Der Velden et al., 2001). Initial results are encouraging (Jawad et al., 2010), however there have been concerns regarding the safety of GO, resulting in its voluntary withdrawal from the market in 2010 (Molica et al., 2021). This toxicity could be the result of other CD33 expressing cells also being targeted, resulting in the partial collapse of the haematopoietic system (Hebbar et al., 2022; Pinho & Frenette, 2019). Despite this, GO was recently reapproved for clinical use based on an improved understanding of its mode of action and potential side effects (Molica et al., 2021). The successes and failures of GO demonstrate the potential of targeted AML therapies, as well as the risks involved.

1.4.3.6 CAR T-cell therapy

CAR T-cell therapy has also been pursued as a targeted immunotherapy treatment (Kenderian et al., 2015; H. Qin et al., 2015; Yang et al., 2021). CAR T-cell therapy utilises autologous or allogeneic T-cells that are genetically modified to present a CAR that targets a predetermined antigen (Gross et al., 1989), referred to as (target antigen)-redirected CAR T-cells. This results in the CAR T-cells homing to target cells and eliminating them in the same manner as unedited T-cells (Fry & Mackall, 2013). CAR T-cell therapy has several advantages over other therapy types; it is highly specific, only attacking cells expressing the target antigen, and it provides long-term surveillance as the CAR T-cells remain active within the tissue they are transplanted into (Kim et al., 2018) (see **Figure 1.7**).

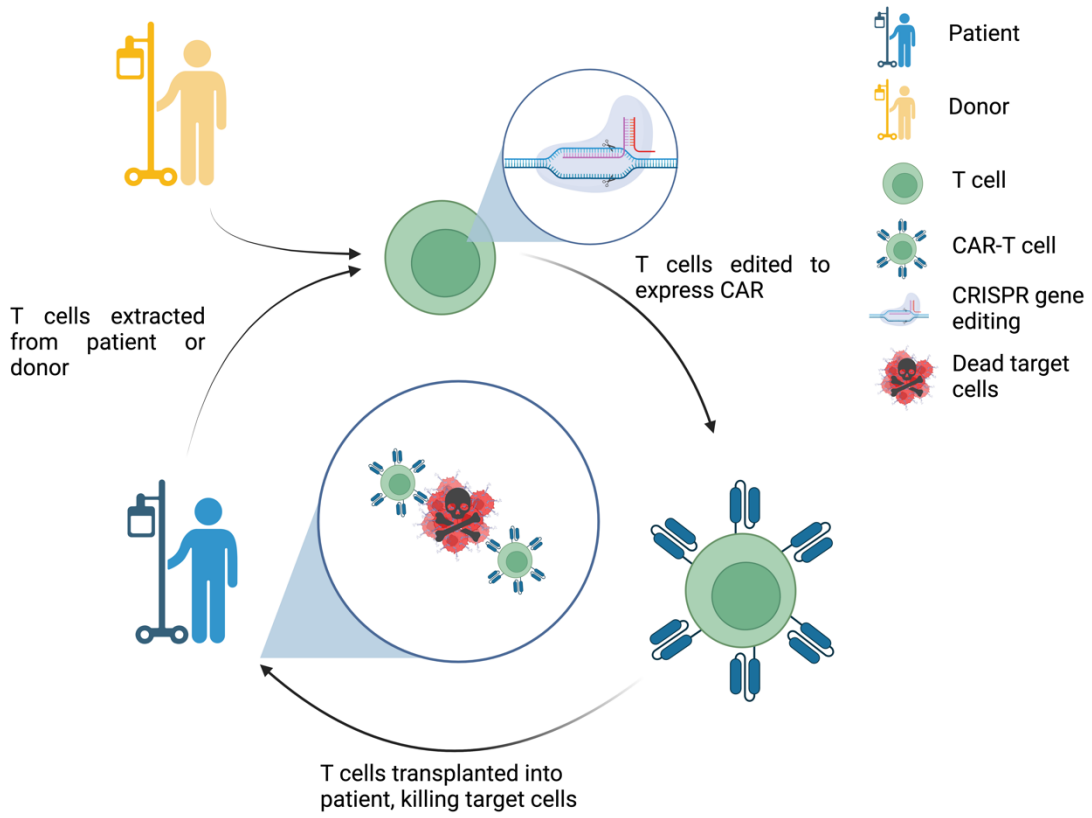

Figure 1.7 CAR T-cell therapy mode of action. *T-cells from a patient or suitable donor are genetically modified to express a chimeric antigen receptor (CAR). This allows these cells to target and eliminate diseased cells, which express a target protein that the CAR recognises, when transplanted into a patient. Created with BioRender.com.*

CAR T-cell therapy was recently shown to effectively eliminate ALL cancer cells from patients (H. Qin et al., 2015), inspiring the application of this technology to AML. However, unlike ALL no differentiable surface markers have been identified that can be used to selectively target AML cells without also eliminating healthy haematopoietic cells (Molica et al., 2021), raising the risk of side effects such as anaemia and immune compromisation.

A recently developed strategy used to overcome this obstacle was the use of clustered regularly interspaced short palindromic repeats (CRISPR)-CRISPR associated protein (Cas) 9 to create a population of haematopoietic cells that are unrecognized by CAR T-cells due to the elimination of the AML and haematopoietic cell surface marker CD33 (Borot et al., 2019; Kim, 2023; Kim et al., 2018). These cells were transplanted alongside CAR T-cells, repopulating the BM niche while diseased cells were eliminated (see **Figure 1.8**).

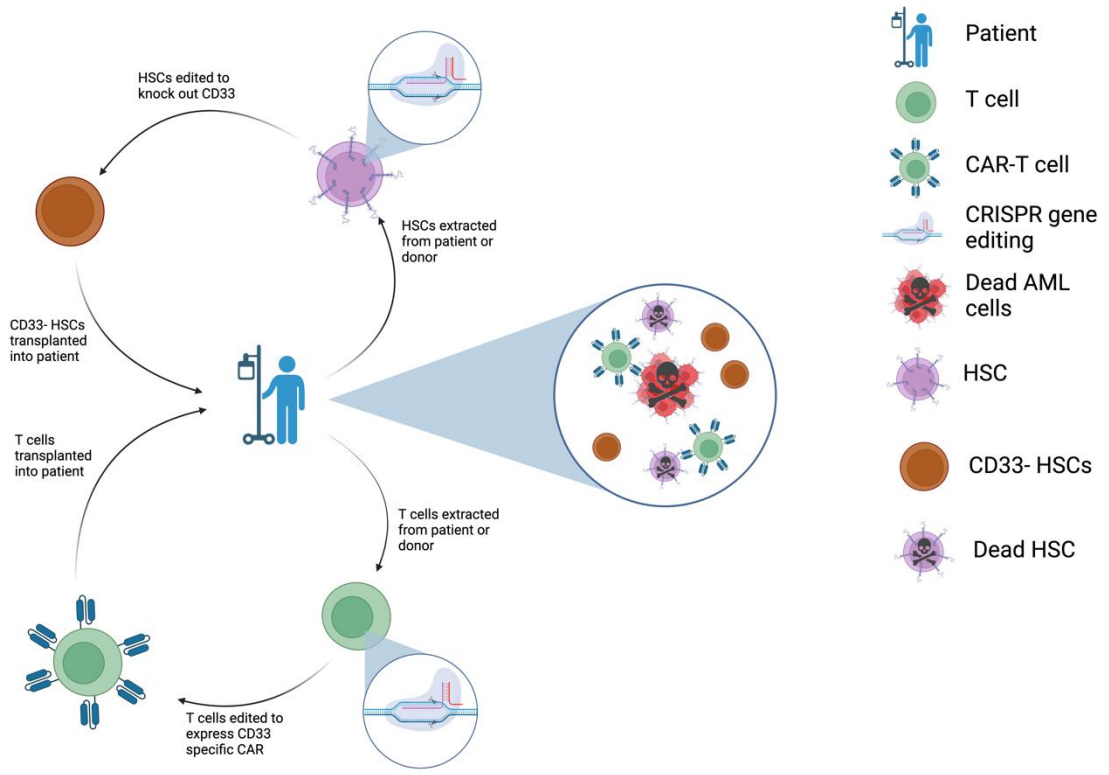

Figure 1.8 Schematic of theoretical CAR T-cell and HSC CRISPR combined therapy. *CD33-redirected CAR T-cells are used to target CD33+ AML cells without affecting edited, CD33- haematopoietic cells. This prevents collapse of the myeloid cell population, which natively expresses CD33. Note that this is a hypothetical pipeline as this system has only been tested in humans. Created with BioRender.com.*

The current understanding of AML is extensive thanks to decades of research, resulting in novel treatments that show much promise, with long-term curative approaches beginning to bear fruit. However, these treatments are constrained by the orthodox treatment validation pathway, which omits *in vitro* models in favour of animal models, as discussed previously in **section 1.3**.

1.4.4 Modelling AML

As with healthy BM, AML has traditionally been modelled using animals or simple suspension cultures. These models have contributed to the understanding of AML progression and initiation (Habbel et al., 2020; Yoshino et al., 2021), as well as effectiveness of AML therapies (B. Chen et al., 2018; Z. Zeng et al., 2017). However, these models share the same drawbacks as similar models of healthy BM

(see **1.3**). More biomimetic *in vitro* AML models are typically similar to *in vitro* BM models, since the BM is a well-established site of leukemogenesis and an AML cell reservoir (Ishikawa et al., 2007; Passaro et al., 2017; Tabe & Konopleva, 2015). These models allow investigation of AML cells' external stimuli (Abbott & Kaplan, 2015) and of novel treatments. This has resulted in an increased understanding of the leukaemic BM niche's role in drug resistance (Bray et al., 2017; Karimpoor et al., 2018; D. Li, Lin, et al., 2018).

1.5 Conclusion

The BM niche influences HSCs and haematopoiesis in a highly complex manner. When this equilibrium breaks down it can result in various BM-associated disorders and disease, including AML. *In vitro* BM models have helped elucidate some of the intricacies of these interactions and may prove useful for validating novel treatments for BM-associated disorders and diseases.

1.6 Aims and objectives

The aim of this thesis is to convey the successful realisation of a simple BM-mimetic *in vitro* niche for testing novel AML therapies. The model used MSCs as a feeder layer. The MSCs were cultured on a surface coated with poly(ethyl acrylate) (PEA), a monomer that caused fibronectin, which the surface was also coated with, to assemble in an open conformation (Llopis-Hernández et al., 2016). This allowed the fibronectin molecules' integrin binding and growth factor binding domains, the latter of which was loaded with the osteogenic growth factor bone morphogenic protein 2 (BMP2), to synergistically signal the MSCs cultured on top of them (Xiao, McGuinness, et al., 2022). A synthetic, peptide-based hydrogel (Gao et al., 2017) was also layered on top of the MSCs. HSCs were then cultured on top of the gel (see **Figure 1.9**).

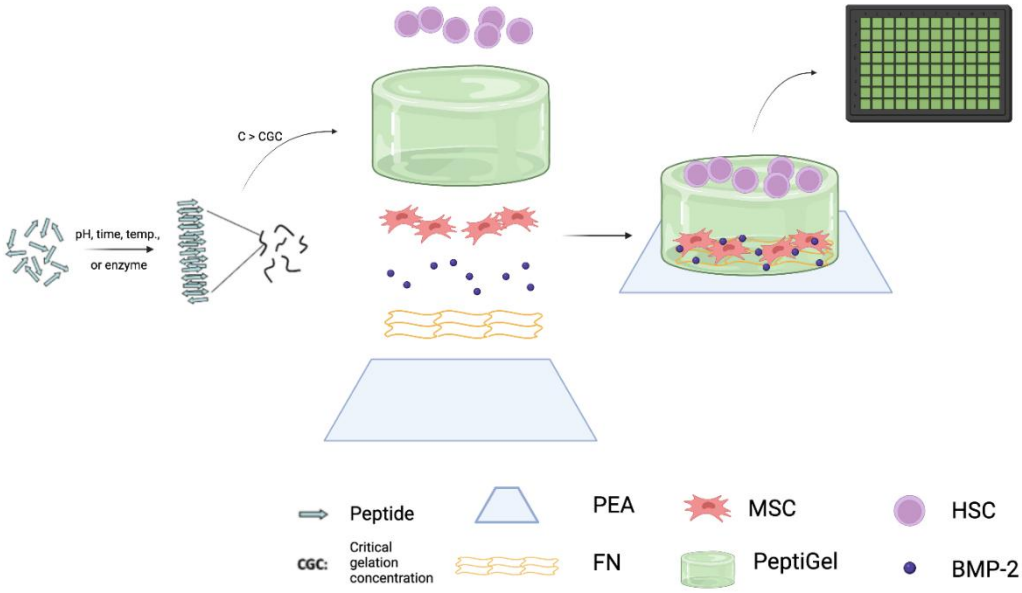

Figure 1.9 Schematic of in vitro BM niche model system. *MSCs were cultured in 96 well plates coated with PEA, FN, and BMP2. A synthetic, peptide-based hydrogel (PeptiGel) was layered on top of the MSCs. This gel consisted of short, amphipathic peptides which self-assembled into fibrils and formed a gel once they surpassed a critical gelation concentration. HSCs were cultured on top of the gel. Created with BioRender.com*

A novel leukaemia therapy was also developed that utilized CAR T-cells to specifically targets and eliminates AML cells expressing CD33, while sparing genetically modified CD33- HSCs. This therapy's efficacy was tested using the above BM niche model (see **Figure 1.10**).

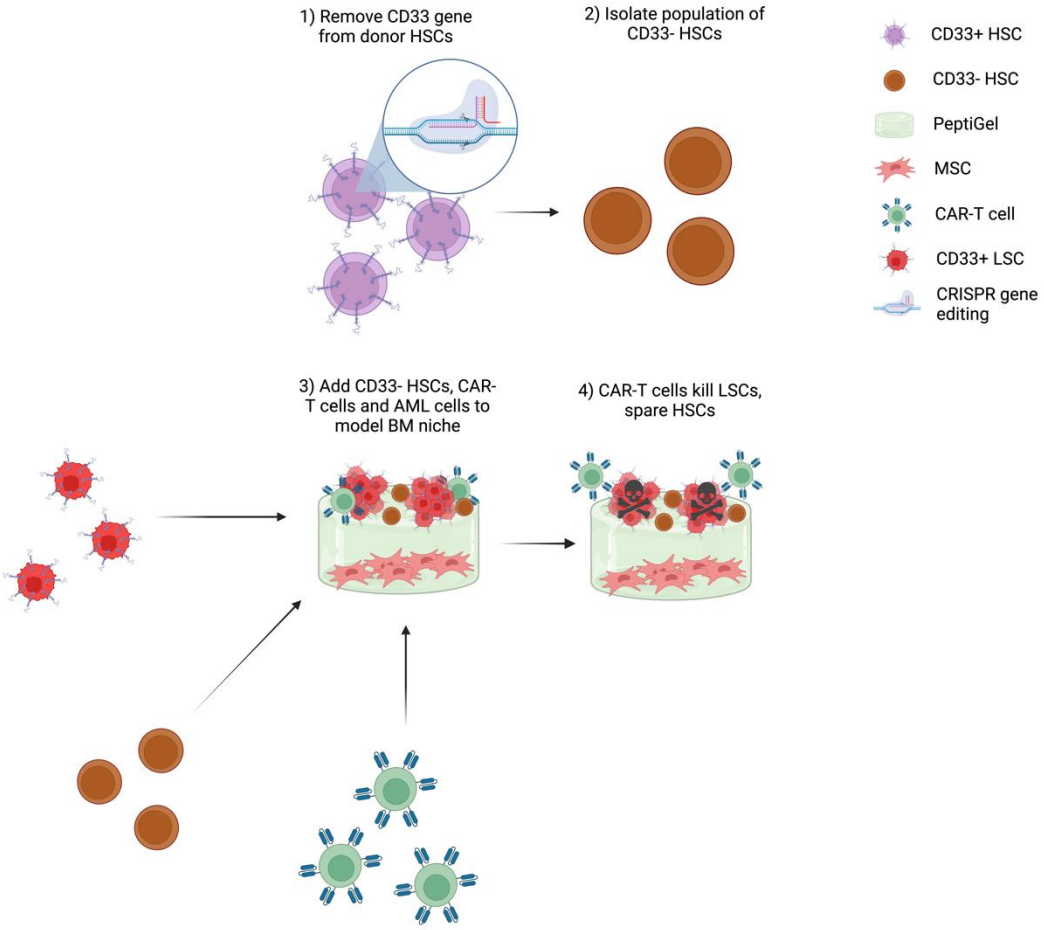

Figure 1.10 Testing combined CRISPR-CAR T-cell therapy in a model BM niche. *HSCs were genetically modified to be CD33-. They were then cultured in a model BM niche alongside AML cells and CD33-redirected CAR T-cells. The hypothesis was that the edited HSCs would be unaffected by the CAR T-cells, while the AML cells would be eliminated. Created with BioRender.com.*

Therefore, the aims of this thesis are:

- Characterise material properties of the model BM niche
- Assess the model's effect on resident cells
- Develop a method to knock out CD33 in HSCs
- Evaluate a combined CRISPR-CAR T-cell system on AML cells in the model BM niche

Chapter 2 Materials and methods

Details pertaining to the general materials and methods that were used to carry out the research described are included in this chapter. Methods that were developed as part of the research carried out are described in the relevant chapters.

2.1 Materials

2.1.1 Immunostaining reagents

Table 2.1 Generic antibodies.

Antibody	Dilution	Supplier
Biotinylated horse anti-mouse	1:50	Vector laboratories, BA-2000
Biotinylated horse anti-rabbit	1:50	Vector laboratories, BA-1100
Streptavidin fluorescein	1:50	Vector laboratories, SA-5001
Streptavidin texas red	1:50	Vector laboratories, SA-5006
NucBlue Live Cell Stain ReadyProbes Reagent	1 drop per mL	Invitrogen, R37605
Oregon green 488 phalloidin	1:200	Invitrogen, O7466
Rhodamine phalloidin	1:200	Invitrogen, R415

Table 2.2 Solutions and buffers used for immunostaining.

Reagent	Component	Amount	Supplier
Fixative solution	Sucrose	2 g (58.4 mM)	Fisher scientific, S/8600/60
	Formaldehyde	10 mL (10% v/v)	Fisher scientific, F/1501/PB17
	Phosphate buffered saline (PBS)	90 mL	Gibco, 14190-094
Permeabilisation buffer	Sucrose	10.3 g (301 mM)	Fisher scientific, S/8600/60
	Sodium chloride	0.292 g (5 mM)	VWR chemicals, 27810.295
	Magnesium chloride hexahydrate	0.06 g (2.95 mM)	VWR chemicals, 25108.260
	Hepes	0.476 g (20 mM)	VWR chemicals, 441485H
	Triton-X	0.5 mL (0.5% v/v)	Sigma-Aldrich, T9284-100ML
	PBS	100 mL	Gibco, 14190-094
	NaOH/HCl	As needed to make solution pH 7.2	NaOH (Fisher scientific, S/4920/53), HCl (Fisher scientific, H/1200/PB17)
Blocking buffer	PBS	100 mL	Gibco, 14190-094
	Bovine serum albumin (BSA)	1 g (1% w/v)	Sigma-Aldrich, A7906-100G
Wash buffer	PBS	100 mL	Gibco, 14190-094
	Tween20	0.5 mL (0.5% v/v)	Sigma-Aldrich, P1379-500ML

Reagent	Component	Amount	Supplier
Flow buffer	PBS	100 mL	Gibco, 14190-094
	BSA	0.5 g (0.5% w/v)	Sigma-Aldrich, A7906-100G
	Ethylenediaminetetraacetic acid (EDTA)	0.4 g (2 mM)	Invitrogen, 15575-038

2.1.2 Tissue culture solutions

Table 2.3 Media formulations and solutions used for tissue culture.

Reagent	Component	Amount	Supplier
Antibiotic mix	L-glutamine (200mM)	150 mL (57% v/v)	Gibco, 25030-024
	Penicillin-Streptomycin (10 mg mL^{-1}, 10,000 units mL^{-1})	100 mL (38% v/v)	Gibco, 15140-122
	Amphotericin (250 µg mL^{-1})	12.5 mL (5% v/v)	Gibco, 15290-026
Versene	Sodium Chloride	8 g (137.8 mM)	VWR chemicals, 27810.295
	Potassium chloride	0.4 g (5.4 mM)	VWR chemicals, 26764.260
	D-Glucose	1 g (5.6 mM)	Fisher scientific, G/0500/53
	Hepes	2.38 g (10 mM)	VWR chemicals, 441485H
	EDTA	0.2 g (0.7 mM)	Invitrogen, 15575-038
	0.5% Phenol red	2 mL (0.2% v/v, final concentration of $1x10^{-5}$ %)	Sigma Aldrich, P0290-100ML
	PBS	1 L	Gibco, 14190-094

Reagent	Component	Amount	Supplier
Versene (cont.)	NaOH/HCl	As needed to make solution pH 7.5	NaOH (Fisher scientific, S/4920/53), HCl (Fisher scientific, H/1200/PB17)
Trypsin/versine solution	Trypsin	0.5 mL (2.5% v/v)	Sigma, T4549-100ML
	Versene	20 mL	n/a
10% DMEM	Antibiotic mix	10 mL (1.75% v/v)	n/a
	Sodium pyruvate (100 mM)	5 mL (877 µM)	Sigma-Aldrich, S8636-100ML
	Minimal essential medium non-essential amino acids (MEM NEAA) (100X)	5 mL (0.877% v/v)	Gibco, 11140-035
	FBS (foetal bovine serum)	50 mL (8.77% v/v)	Sigma-Aldrich, F9665-500ML
	Dulbecco's modified eagle medium (DMEM) high glucose	500 mL	Sigma-Aldrich, D5671-500ML
2% DMEM	Antibiotic mix	10 mL (1.89% v/v)	n/a
	Sodium pyruvate (100 mM)	5 mL (943 µM)	Sigma-Aldrich, S8636-100ML
	MEM NEAA (100X)	5 mL (0.943% v/v)	Gibco, 11140-035
	FBS	10 mL (1.89% v/v)	Sigma-Aldrich, F9665-500ML
	DMEM high glucose	500 mL	Sigma-Aldrich, D5671-500ML

Reagent	Component	Amount	Supplier
10% RPMI	Antibiotic mix	10 mL (1.79% v/v)	n/a
	FBS	50 mL (8.93% v/v)	Sigma-Aldrich, F9665-500ML
	Roswell Park Memorial Institute (RPMI)	500 mL	Gibco, 21875-034
2% RPMI	Antibiotic mix	10 mL (1.92% v/v)	n/a
	FBS	10 mL (1.92% v/v)	Sigma-Aldrich, F9665-500ML
	RPMI	500 mL	Gibco, 21875-034
IMDM - cytokines	L-glutamine (200mM)	100 µL (1.96 mM)	Gibco, 25030-024
	Penicilin/Streptomycin (10mg mL^{-1})	100 µL (1% v/v)	Gibco, 15140-122
	Bovine insulin transferrin (BIT)	2 mL (19.6% v/v)	STEMCELL technologies, 09500
	Iscove Modified Dulbecco Media (IMDM)	8 mL	Merck, I3390-500ML
IMDM + cytokines	L-glutamine (200 mM)	100 µL (1.96 mM)	Gibco, 25030-024
	Penicilin/Streptomycin (10mg/mL)	100 µL (1% v/v)	Gibco, 15140-122
	BIT	2 mL (19.6% v/v)	STEMCELL technologies, 09500
	IMDM	8 mL	Merck, I3390-500ML
	Flt3L	10 µL (0.1% v/v)	Peprotech, 300-19

Reagent	Component	Amount	Supplier
IMDM + cytokines (cont.)	SCF	10 µL (0.1% v/v)	Peprotech, 300-07
	TPO	5 µL (0.05% v/v)	Peprotech, GMP300-18
Promo cell freezing media	Dimethylsulfoxide (DMSO)	1 mL (10% v/v)	Fisher scientific, D/4120/PB08
	FBS	6 mL (60% v/v)	Sigma-Aldrich, F9665-500ML
	10% DMEM	3 mL (30% v/v)	n/a
THP-1 freezing media	DMSO	1 mL (10% v/v)	Fisher scientific, D/4120/PB08
	FBS	6 mL (60% v/v)	Sigma-Aldrich, F9665-500ML
	10% RPMI	3 mL (30% v/v)	n/a
HSC freezing media	DMSO	1 mL (10% v/v)	Fisher scientific, D/4120/PB08
	Human serum albumin (HSA)	9 mL (90% v/v)	CSL Behring, B05AA01

Table 2.4 Coating reagents.

Reagent	Supplier
Fibronectin human plasma	Sigma-Aldrich, F2006-2MG
BMP2	Sigma-Aldrich, H4791-10UG
PEA	Sigma-Aldrich, E9706

2.1.3 CRISPR reagents

Table 2.5 sgRNAs used for CRISPR-Cas9 gene editing. Custom made by Synthego. *If a sgRNA was designed by another group, the source paper referenced. Note that the crRNA and tracrRNA scaffold sequences are proprietary.*

sgRNA genetic target	Target sequence
CD33 exon 2	GGGGAGUUCUUGUCGUAGUA
CD33 exon 3	CCUGUGGGUCAAGUCUAGUG (Borot et al., 2019)
CD33 upstream (+21) enhancer	GAUACAAGCAGACCACCAGA

Table 2.6 CRISPR reagents.

Reagent	Supplier
Alt-R EE	IDT, 1075916
Alt-R S.p. HiFi Cas9 Nuclease V3	IDT, 1081060
Glycerol	Fisher scientific, G/0650/17
Neon transfection kit 10 µL	ThermoFisher Scientific, MPK1096

Table 2.7 Primers used for PCR as part of TIDE analysis. Custom made by IDT. *If a primer was designed by another group, the source paper is referenced.*

Primer	Sequence
CD33 exon 2 F primer	AGCTGCTTCCTCAGACATGC (Kim et al., 2018)
CD33 exon 2 R primer	CAGGGATGAGGATTTTGGGC
CD33 exon 3 F primer	GGGAAGTTCATGGGTACTGC
CD33 exon 3 R primer	CATCCTGTCTCCCCTACACC
CD33 +21 enhancer F primer	TGAAAGGCATGCACTCAGAA
CD33 +21 enhancer R primer	TATCCAGCCCCAAATGCCA

Table 2.8 PCR reagents.

Reagent	Supplier
HF buffer	NEB, B0518S
dNTP mix	NEB, N0447S
HF Phusion DNA polymerase	NEB, M0530S
Nuclease free water	Synthego
DMSO	NEB, B0515A

2.1.4 Cells

Table 2.9 Cell lines used.

Cell line	Supplier
Promo cell MSCs	PromoCell, C-12974
THP-1s	DSMZ, ACC16
CAR T-cells	AMSbio, AMS.PMCAR1056-1M

In line with the ethical standards that were in place when this research was carried out, patient confidentiality was protected by blinding all investigators to details of individual samples' age and sex.

2.1.5 Gels

Table 2.10 PeptiGels used and their amino acid sequences.

PeptiGel	Amino acid sequence
Alpha 1	FEFKFEFK
Alpha 2	FEFKFEFKK
Alpha 2 RGD	80% FEFKFEFKK 20% KFEFKFEFKKGGRGD
Alpha 4	KFEFKFEFKK
Alpha 7	EFKFEFKFE
Delta 1	FEFKFEFK

Table 2.11 Collagen reagents.

Reagent	Supplier
Rat tail collagen type-I	First Link, 60-30-810
FBS	Sigma-Aldrich, F9665-500ML
10x DMEM	Sigma, D2429-100ML
Sodium hydroxide	J/7660/15
2% DMEM	n/a

2.2 Methods

2.2.1 Substrate preparation

2.2.1.1 Plasma polymerisation

48 and 96 well plates were placed in a plasma chamber perpendicular to the plasma flow. Samples were exposed to air plasma for 5 minutes at 50W of radio frequency (RF) incident power at 1.5-2.5X10^{-1} mbar pressure to ensure removal of any residual organic matter. Samples were then coated with PEA plasma using an RF power of 50W at 1.5-2.5X10^{-1} mbar pressure. The plasma treatment was carried out for 15 minutes.

2.2.1.2 Plate preparation

Well plates were sterilised in the tissue culture hood by irradiating them with UV light for 30 minutes. 96 well µ-plates with polymer cover slip bottoms (Ibidi, 89626) were typically used. Some plates or wells were coated with FN. The FN was diluted to 20 µg/mL in sterile phosphate buffered saline (PBS) and added to appropriate wells in the well plates. Plates were then incubated at room temperature (RT) for 1h before the FN solution was removed and the wells were washed twice with PBS. Some plates or wells were also coated with BMP2. The growth factors were diluted to 50 ng/mL in sterile phosphate buffered saline (PBS). The GF solution was then added to appropriate wells in the well plates. Plates were subsequently incubated at RT for 1h before the GF solution was removed and the wells were washed twice with PBS. The volume of FN or GF solution used is detailed in **Table 2.12**.

2.2.1.3 Collagen gel preparation

Collagen gel was made on ice by combining 2.5 mL type-1 rat tail collagen, 0.5 mL FBS, 0.5 mL 10X DMEM and 0.5 mL 10% DMEM, adjusted to pH 8.2 using sodium hydroxide.

2.2.1.4 PeptiGel dilution

PeptiGels were supplied pre-prepared and ready to use by Manchester Biogel. The method of gel preparation was proprietary. Gels were allowed to equilibrate to room temperature before being diluted to the desired concentration using ultrapure water, which was autoclaved when required for sterility. The gels were subsequently vortexed for roughly 1 minute. Six formulations of PeptiGels were used (see **Table 2.10**), with delta 1 used the most.

2.2.2 Tissue culture

2.2.2.1 General cell culture

Cells were grown in a humidified environment at 37°C with 5% CO_2. The same conditions were used for all incubations described unless otherwise stated. All media was heated for ~30 minutes in a 37°C water bath prior to use. All tissue culture procedures were performed under sterile conditions using a laminar flow cabinet. When counting cells, a haemocytometer was used. Alternatively, when large numbers of cells needed to be counted a Countess 3 automated cell counter from Invitrogen was used. When necessary, dead cells were excluded from cell counts by mixing trypan blue 1:1 with cell suspensions prior to counting.

2.2.2.2 Promo cell culture

Promo MSCs were seeded in flasks and fed twice a week using 10% DMEM. When cells reached confluency, they were passaged or seeded on a plate as required for an experiment. Cells between passages two and four were used for experiments. To passage the cells all the medium was removed, and the flask was washed with 10 mL of PBS. The MSCs were trypsinised by adding 5 mL trypsin/versene solution to the flask, which was subsequently placed in the incubator for ~3 minutes to allow the cells to detach. Once the cells had detached, as confirmed using a light microscope, 5 mL 10% DMEM was added to the flasks. The cell suspension was removed to a sterile plastic universal and centrifuged at 333 g for 4 minutes. The supernatant was discarded, and the cells resuspended in 10% DMEM for reseeding in a flask or 2% DMEM for seeding in a plate for an experiment. If seeded in an experiment, the cells were counted using a haemocytometer and the suspension

was subsequently made up to 12,000 cells/mL. An appropriate amount of this cell suspension (see **Table 2.12**) was then added to the plates, resulting in a seeding density of 3,000 cells/cm^2.

2.2.2.3 THP-1 culture

Non-adherent THP-1 cells, an AML cell line often used as an HSC model, were seeded in flasks at ~ $5x10^5$ cells/mL. 2-3 times per week when the cells reached confluency ~80% of cell suspension was removed and replaced with fresh 10% RPMI.

2.2.2.4 HSC isolation and culture

HSCs were isolated from the bone marrow aspirates of patients undergoing joint replacement surgery. Mononuclear cells were separated by density gradient centrifugation using Ficoll-Paque. Following nucleated cell isolation, CD34+ cells were isolated using a EasySep™ Human CD34 Positive Selection Kit II (STEMCELL technologies) according to the manufacturer's protocol. These cells were then counted using a haemocytometer before reseeding $5X10^4$ cells/mL in IMDM + cytokines in a 24 well plate and incubating overnight. Alternatively, the cells were frozen immediately after EasySep separation using HSC freezing media. In some cases, CD34+ HSCs were purchased (STEMCELL technologies, 70002), which is indicated in relevant figure legends.

2.2.2.5 Freezing cells

Adherent cells were trypsinised. Cell suspensions were then counted and centrifuged at 333 g for 4 minutes before the supernatant was removed. The cells were resuspended in appropriate freezing media (see **Table 2.3**) at a density of ~10^6 cells/mL. The cells were then transferred to cryovials purchased from Sigma-Alrdich, before being frozen at -80°C overnight in a Fisher Scientific Mr Frosty Freezing Container or appropriate substitute. The next day, cells were transferred to -150°C.

2.2.2.6 Thawing cells

Cryovials containing cells were thawed for ~3 minutes at 37ºC using a water bath. The cells were then added dropwise to 10 mL appropriate media. Next, the cells were spun at 333 g for 4 minutes. The cells were then resuspended in an appropriate volume of relevant media, counted, and used as needed.

2.2.2.7 Model assembly

Unless otherwise stated, 96 well black ibidi µ-plates were used. Following plate preparation, 140 µL of promo MSCs at a cell density of $1.2x10^4$ cells/mL were seeded in relevant wells and cultured overnight. The following day all media was removed from plates. 70 µL of PeptiGel was added using a positive displacement pipet before the plate was spun at 333 g for 1 minute. 140 µL of 2% DMEM was then added to the wells not containing collagen. Collagen was then made up and 70 µL added to the appropriate wells. The plates were then incubated overnight. Within the first hour of incubation half of the media in wells without collagen was replaced with fresh 2% DMEM twice. The following day half of the media was replaced again with fresh 2% DMEM. At this point collagen wells had 140 µL of media added. A half media change was then performed after a further 3 days. If the system was to be used for co-culture, 7 days after cell seeding, media was removed and 140 µL of cells for co-culture were added in appropriate media (10% RPMI for THP-1s, IMDM + cytokines for all other co-cultures). See **Table 2.12** for appropriate reagent volumes for other plate sizes.

Table 2.12 Reagent volumes for various plate types.

Plate	Volume of promo cell suspension (µL)	Volume of collagen gel and PeptiGel (µL)	Volume of media (µL)	Volume of FN and GF (µL)
96 well plate (ibidi)	140	70	150	100
48 well plate	275	138	300	196
24 well plate	475	238	500	339
12 well plate	875	437.5	1000	625

2.2.3 Immunocytochemistry

2.2.3.1 Brefeldin treating cells

If cells were being imaged for secreted proteins such as SCF or CXCL12, ~24 h before fixation the media in wells to be analysed was replaced with identical media containing 5 µg/mL of brefeldin A (Sigma Aldrich, B6542) to prevent protein secretion and allow translation to be quantified.

2.2.3.2 Immunofluorescent (IF) staining

Plates were processed 7 days after gel addition unless otherwise stated. Volumes of reagents for different plates are shown in **Table 2.13**. Media was removed from all wells. The wells were then washed with PBS. Prewarmed fixative was added for 30 minutes at 37°C. The fixative was then removed. In some cases, PeptiGel was then removed by two washes with ice cold PBS. In all experiments, permeabilisation buffer was then added to each well used before the plates were incubated at RT for 10 minutes. Blocking buffer was then added and the plates incubated at 37°C for 1h. The blocking buffer was removed and primary antibodies, diluted in blocking buffer, were added, as well as Rhodamine or Oregon Green Phalloidin. Plates were wrapped in foil then stored overnight at 4°C. The primary antibodies were removed, and the wells were washed 3 times for 5 min with wash buffer at RT. Secondary antibodies were then added and the plates wrapped in foil again and stored at 37°C for 1h or 4°C overnight. The secondary antibodies were removed, and the wells were washed 3 times as before. For biotinylated secondary antibodies, streptavidin fluorescein or streptavidin Texas red was then added, and the plates incubated in foil at 4°C for 30 minutes. Streptavidin was then removed, and the plates washed 3 times. To visualise cells nuclei, NucBlue Live Cell Stain was then added, and the plates incubated for 30 min at RT. Finally, the plates were washed twice with PBS before water was added. The plates were stored at 4°C in foil for up to a week before imaging.

Table 2.13 Volumes of reagents used for different plates.

Plate	Volume of fixative solution, permeabilisation buffer, NucBlue (µL)	Volume of blocking buffer, wash buffer, PBS, water (µL)	Volume of antibodies and streptavidin (µL)
96 well plate (ibidi)	200	300	50
48 well plate	400	590	70
24 well plate	680	1020	170
12 well plate	1250	1875	313

2.2.3.3 Microscopy

Stained samples were imaged in two or three (FITC, TRITC, and DAPI which was sometimes excluded) channels. An EVOS Cell Imaging System with Evos Cell Imaging System software, Nikon i800 with NX studios, or Zeiss LSM980 or LSM900 confocal microscopes with Zeiss ZEN software were used. Images were processed using FIJI, as described later.

2.2.4 Flow cytometry

Live cells were counted using a haemocytometer and trypan blue staining. $5x10^5$ cells or if there weren't enough cells, as high a number as possible, were aliquoted. 1 mL of flow buffer was added and the resultant suspension centrifuged at 387 g for 5 min. The supernatant was discarded, and the cells resuspended in 100 µL of staining master mix, which consisted of appropriate volumes of included antibodies and stains diluted in flow buffer (see **Table 2.14**). The cells were put on ice for 45 min, then 180 µL of flow buffer added and the samples centrifuged again at 387 g for 5 min before the supernatant was discarded. The cells were resuspended in 250 µL flow buffer and stored in the fridge for up to 6 h. An unstained control sample was also made up using 100 µL of flow buffer in place of the staining master mix. Compensation samples were also made for each experiment. Attune compensation beads (Invitrogen, 01-2222-42) were

predominately used. 1 drop of beads had an equivalent volume of antibody to that included in the staining master mix added before incubation on ice for 45 min. 180 µL of flow buffer was added and the samples centrifuged again at 387 g for 5 min before the supernatant was discarded. The samples were resuspended in 250 µL flow buffer and stored in the fridge for up to 6 h. A sytox blue viability stain (ThermoFisher scientific, S34857) was typically included. To compensate for this, two aliquots of cells of the same type used in an experiment were taken, termed the live and dead samples. The dead sample was centrifuged at 387 g for 5 min before being resuspended in 200 µL fixative solution and incubated at 37^{o}C for 30 min with no atmosphere control. Both samples then had 1 mL of flow buffer added before being centrifuged at 387 g for 5 min. The samples were resuspended in 100 µL flow buffer and an equivalent volume of sytox blue to that included in the staining master mix added. The samples were then incubated on ice for 45 min. 180 µL of flow buffer was added and the samples centrifuged again at 387 g for 5 min before the supernatant was discarded. The samples were resuspended in 250 µL flow buffer and stored in the fridge for up to 6 h if necessary. An attune NxT acoustic focusing cytometer was used to characterise cells' surface marker expression, viability, and number. Prior to running experimental samples, compensation samples were used to set the instrument's voltages to appropriate levels.

Table 2.14 Flow antibodies.

Antibody target	Channel	Volume (in 100 µL master mix) (µL)	Supplier, catalogue number
Lineage cocktail	FITC	6.25	ThermoFisher scientific, 22-7778-72
CD34	PE	1	ThermoFisher scientific, 12-0349-42
CD33	Cy5	1	Invitrogen, 15-0339-42
CD33	Brilliant violet	6.25	BioLegend, 303421
CD38	Cy7	0.5	ThermoFisher scientific, 25-0388-42
CD41/CD61	Alexa Fluor 488	1	ThermoFisher scientific, MA5-44123
CD7	PerCP-eFluor 710	1	ThermoFisher scientific, 46-0078-42
CD34	APC	1	Miltenyi Biotec, 130-113-176
CD90	Alexa fluor 700	1	Invitrogen, 56-0909-42
CD45RA	APC-eFluor 780	1	ThermoFisher scientific, 63-0458-42
CD16	eFluor506	1	ThermoFisher scientific, 69-0168-42
Viability	Sytox blue	2.5	ThermoFisher Scientific, S34857

2.2.5 CRISPR

2.2.5.1 Designing sgRNA and PCR primers

The sequence of sgRNA and PCR primers used for gene editing and analysis were either sourced from literature (cited in materials) or designed in collaboration with Dr. Adam West. Briefly, the UCSC genome browser was used to determine the suitability of CD33 for gene editing, determine transcriptional start sites, and check for confounding splice variants. Regulatory elements were identified using Roadmap Epigenomics Integrative Analysis track hub, CCTOP, and ENCODE. CCTOP was used to identify possible sgRNAs for target sites. Primer3 was used to design suitable primers. BLAST, UCSC and CCTOP were used to check sgRNAs and primers for off-target effects.

2.2.5.2 Editing THP-1s

For transfections, ~$2.4x10^5$ THP-1s in log phase were used. The Neon transfection system was used to carry out electroporation with various programmes, most commonly 1600 V/10 ms/3 pulses. Single guide RNAs (sgRNAs) were added at 2.25 µM (see Table 2.5), Cas9 was added at 1.5 µM, IDT electroporation enhancer was used at 3.85 µM, and glycerol was added at 2%. The cells were then cultured in a 24 well plate, or in a preprepared 96 well plate containing an artificial BM niche where appropriate, in appropriate media before the success of the transfection was determined using tracking or indels decomposition (TIDE) analysis or flow cytometry. Non-electroporated (NE) controls were typically included, in which cells were not electroporated and all reagents used for electroporation were substituted for R buffer. MOCK controls were also included, in which cells were electroporated and all reagents used for electroporation were substituted for R buffer.

2.2.5.3 Editing HSCs

HSCs were thawed the day before editing and rested overnight in a 24 well plate in IMDM media + cytokines at a cell density of $5x10^4$ cells/mL. They were then treated identically to THP-1s, except for cell number and electroporation protocol. Where possible ~$2.4x10^5$ HSCs were used per transfection, however this

number was lower as needed for samples with lower numbers of HSCs. In addition, two different protocols (1600 V/10 ms/3 pulses and 1700 V/20 ms/1 pulse) were tested on HSCs.

2.2.6 Statistics

All statistical analysis was performed with GraphPad Prism 8 or Microsoft Excel. Where appropriate, Prism 8 was used to statistically identify and remove outliers from datasets prior to analysis. Statistical significance levels are *$p < 0.05$, **$p < 0.01$, ***$p < 0.001$ and ****$p < 0.0001$. If no stars are shown, $p > 0.05$ unless otherwise stated. Where parametric tests were performed, data was first confirmed to be normal with a Shapiro-Wilk test or equivalent.

2.2.7 Graphs

All graphs show mean ± standard deviation (SD) unless otherwise stated. For super plots, each technical replicate is represented by a small dot, while the average of each biological replicate for a condition is represented by a large dot unless otherwise stated. Super plot statistical analysis was carried out on the averages of each biological replicate, unless otherwise stated. N denotes number of biological or experimental replicates, while n denotes number of technical replicates.

Chapter 3 Material characterisation

3.1 Introduction

Modern BM niche models primarily focus on the recapitulation of various aspects of the diseased of healthy niche *in vitro* by employing a variety of techniques. To produce a model which could mimic the BM niche's ability to modulate the phenotype of resident cells, the microenvironment that would be experienced by included cells in a simplified *in vitro* system was manipulated. ECM proteins, growth factors, and gels were utilised to stimulate cells chemically and mechanically. The model developed used a coating of PEA to promote FN assembly into fibrillar networks (Z. A. Cheng et al., 2019; Llopis-Hernández et al., 2016). The osteogenic growth factor BMP2 was also included, with the hope that it would be absorbed by the FN, as seen previously (Z. A. Cheng et al., 2019). In addition, a synthetic, peptide-based hydrogel was utilised. The efficiency of the various coatings, morphology of FN, efficacy of BMP2 absorption and mechanical properties of the gel will be discussed.

3.1.1 Fibronectin

FN is a glycoprotein that is found assembled in fibrillar networks throughout the ECM or dissolved in plasma. It is produced by a variety of cell types and consists of two similar subunits that are bound together via a couple of c-terminal disulphide bonds (Pankov & Yamada, 2002). The subunits themselves consist of three types of repeating motifs, termed FN repeats, that are assembled into functional domains (Singh et al., 2010). In the context of this thesis, the most important domains are the P5F3 domain ($FNIII_{12\text{-}14}$), which promiscuously binds and sequesters growth factors that contain heparin binding domains, likely via a bridging heparin or heparin sulphate proteoglycan molecule (Martino & Hubbell, 2010; Raitman et al., 2018), and the HFN7 RGD domain ($FNIII_{9\text{-}10}$), which interacts with cells mechanically by binding their focal adhesions (Keselowsky et al., 2005; Llopis-Hernández et al., 2016) (see **Figure 3.1A**). Various techniques have been employed to take advantage of FN's modular structure, including the use of FN

fragments for functionalising biomaterials, and altering surfaces' chemistries to influence FN morphology (Z. A. Cheng et al., 2019; Donnelly et al., 2018).

3.1.1.1 Material-driven fibronectin assembly

Cells are responsible for assembling FN into fibrillar networks, which exposes the functional domains of fibronectin. However, when absorbed onto most surfaces FN remains in its native globular structure (Salmerón-Sánchez et al., 2011). A robust system for promoting FN fibrillar network assembly has been developed. This approach involves an initial surface coating with PEA, either by spin or plasma coating, prior to addition of FN (Gugutkov et al., 2010; Llopis-Hernández et al., 2016). When absorbed FN is in an open conformation, cell signalling has been shown to be synergistically enhanced by simultaneous interactions with bound GFs and the RGD domain (Salmerón-Sánchez & Dalby, 2016; Xiao, McGuinness, et al., 2022) (see **Figure 3.1B**). In addition, this technique enables highly efficient solid-phase GF presentation and has been shown to significantly reduce the amount of GF required to induce clinically relevant responses, such as healing critical size defects in bone breaks in animals (Z. A. Cheng et al., 2019; Llopis-Hernández et al., 2016).

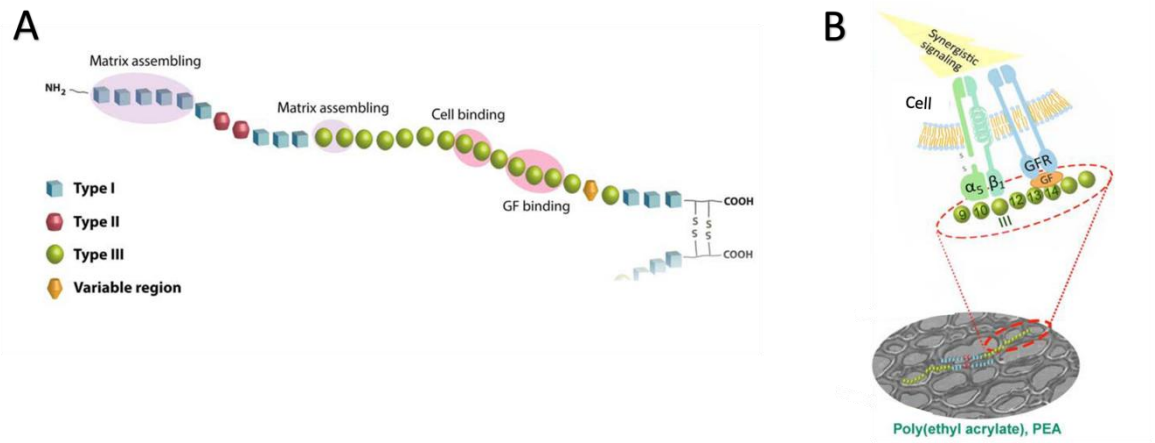

***Figure 3.1 Fibronectin structure**. (A) Schematic of FN domains with functional domains highlighted. (B) Illustration of synergistic signalling. The $\alpha_5\beta_1$ integrin receptor dimer, which is known to bind to the HFN7 RGD domain ($FNIII_{9-10}$), is shown, as well as a generic growth factor receptor (GFR) binding a generic GF attached to the P5F3 heparin-binding domain ($FNIII_{12-14}$). The open, network conformation FN adopts on PEA is illustrated below. Adapted from Llopis-Hernández et al. (2016).*

3.1.2 BMP2

Bone morphogenetic proteins (BMP) were first identified by (Urist, 1965). They are a subfamily of the TGFß superfamily (D. Chen et al., 2004). BMPs' role in bone formation is well established, with involvement in skeletal development, maintenance, and repair (Rosen, 2009). Since their discovery, a wide range of non-osteogenic physiological processes have been found that also involve BMP signalling (D. Chen et al., 2004; D. O. Wagner et al., 2010).

The mechanism of BMP2 signalling involves various serine/threonine receptors that form a complex upon interaction with a BMP GF. This BMP receptor complex (BMPR) consists of a type I receptor (BMPRI), which BMPs initially bind to, as well as a secondary (BMPRII) subunit which is recruited by the BMPRI receptor upon BMP binding and activates BMPRI via phosphorylation (Kaplan et al., 2009). Activated BMPRI then phosphorylates Suppressor of Mothers Against Decapentaplegic (SMAD) proteins, causing an intracellular signalling cascade, which regulates certain BMP-dependent genes' transcription (Brazil et al., 2015).

Various biomedical applications of BMP2 have been investigated, including stimulating bone repair following acute injury in animal models (Z. A. Cheng et al., 2019; Llopis-Hernández et al., 2016), and for spinal bone fusions in clinic (Sayama et al., 2015). Since previous research had demonstrated the usefulness of BMP2 inclusion for promoting a niche-like phenotype in MSCs when combined with PEA and FN coatings, the effect of BMP2 was investigated (Donnelly et al., 2024).

3.1.3 PeptiGel

A hydrogel is a three-dimensional matrix that can contain a large amount of water. Various hydrogels have been used in bioengineering applications, including attempts to replicate the BM niche (Donnelly et al., 2024; Lienemann et al., 2020; Raic et al., 2014). Synthetic, self-assembling, peptide-based hydrogels (SAPHs) are a promising candidate, due to their consistent, well understood contents (Clough, 2021), as well as a high degree of control over their mechanical properties and functionality, resulting in a substrate that can be finely tuned to stimulate mechanically sensitive cells' phenotypes (Scelsi et al., 2019). PeptiGels

fall into this category of gels. PeptiGels consist of short, amphipathic peptides with alternating polar and non-polar amino acids. These peptides self-assemble into β-sheet fibrils in a pH and temperature dependent manner. After surpassing a critical gelation concentration, these fibrils entangle, forming a mesh which holds water, causing gelation (Bowerman & Nilsson, 2012; Mohammed et al., 2007).

3.1.4 Aims

This chapter aimed to establish the chemical and mechanical properties of the surfaces and gels used in subsequent chapters for the assembly of a model BM niche.

3.2 Materials and methods

3.2.1 X-ray photoelectron spectroscopy

X-ray photoelectron spectra (XPS) were obtained by the team at the National EPSRC XPS Users' Service at Newcastle University, an EPSRC Mid-Range Facility. XPS was performed using a K-Alpha apparatus (Thermo Scientific), with a microfocused monochromatic Al Kα source (X-ray energy = 1486.6 eV) at a voltage of 12 kV, current of 3 mA, power of 36 W, and spot size of 400 μm × 800 μm. Spectra analysis and curve fitting were performed using CasaXPS software.

3.2.2 Atomic force microscopy

TCP or PCS plates were coated with PEA and FN, with certain steps skipped where necessary for different conditions. Individual wells were then cut out using a scalpel and/or wire cutters. If stored, surfaces were covered with PBS and kept at 4^{o}C for up to a week. Prior to imaging, surfaces were dried with high pressured nitrogen. They were then imaged with a Drive AFM apparatus from Nanosurf in collaboration with Dr Matthew Walker. The AFM was used in Dynamic Force mode using a conical cantilever holder, ceramic, grooveless (BT08891), and a 7.3 N/m pyramidal silicon cantilever from apex probes (USC-F1.2-K7.3-10); amplitudes

were driven at the resonance frequency of the cantilever (~1200 kHz). Height images were acquired from each scan using the following parameters: scan frequency of 1 Hz, 500 points per line, 1 μm^2 scan area, 30% amplitude reduction from the maximum free vibration amplitude. Gwyddion software was used to prepare and analyse AFM images. Image data was levelled by mean plane subtraction, then to make facets point upwards. Rows were then aligned using line medians, and horizontal scars were corrected. The processed image was then used to determine mean roughness (Sa).

3.2.3 Fibronectin in cell western

TCP or PCS plates were coated with PEA and/or FN, as per **2.2.1**. Plates were stained similarly to the protocol described in **2.2.3**, although no fixation or permeabilization steps were performed. The primary antibodies used were a rabbit polyclonal anti-FN antibody from Sigma-Aldrich (F3648) diluted 1:400, a mouse monoclonal anti-P5F3 antibody from Santa Cruz (sc-18827) diluted 1:100, and a mouse monoclonal anti-HFN7 antibody from abcam (ab212371) diluted 1:100. The secondary antibodies used were a goat anti-rabbit channel 800 antibody from Li-Cor (926-32211) at a 1:800 dilution, or a goat anti-mouse channel 680 antibody from Li-Cor (926-68070) at a 1:800 dilution. Plates were scanned with a Li-Cor Odyssey M.

3.2.4 BMP2 Enzyme-Linked Immunosorbent Assay (ELISA)

Plates were PEA treated and FN coated as needed. BMP2 was then added, and plates incubated overnight, as per **2.2.1**. Supernatant was harvested and stored in Protein LoBind Tubes (Eppendorf, 0030108094). ELISA was then carried out per manufacturer's instructions using a BMP-2 DuoSet ELISA kit (R&D systems, DY355), with standards of known BMP2 concentration also included. Briefly, samples were blocked with 1% BSA/PBS. Then, samples were incubated with primary antibodies for 2h at RT, followed by incubation with secondary antibodies (goat-anti-mouse-HRP) overnight at 4^{o}C. Next, substrate solution was added, and plates were incubated for 20 min at RT. The reaction was stopped by adding stop solution, and

the ELISA plate was read using a plate reader to measure absorbance at 450 nm with wavelength corrections at 570 nm.

3.2.5 Correlation coefficient IF microscopy and image analysis

Plates were coated with PEA, FN, and BMP2 per **2.2.1**, and cells were seeded identically to model preparation (**2.2.2.7**). 2 h after cell seeding, plates were fixed, and prepared for IF microscopy as described previously (**2.2.3**). The primary antibodies used were: BMPR 1α (Invitrogen PA5-11856) 1:50, integrin ß1 (R&D systems MAB17781) 1:100. Secondary antibodies: goat anti-rabbit Texas red (Vector labs TI-1000) 1:100, horse anti-mouse biotinylated (Vector labs BA-2000) 1:50. Fluorescein streptavidin was also used (Vector labs SA-5001) 1:50. Cells were imaged using confocal microscopy. Representative images were prepared using ImageJ and the below macro code:

```
//setup
channel1 = "C1-" + File.name;
channel2 = "C2-" + File.name;
channel3 = "C3-" + File.name;

run("Split Channels");
selectImage(channel2);
//run("Brightness/Contrast...");
run("Enhance Contrast", "saturated=0.35");
run("Apply LUT");
run("Subtract Background...", "rolling=200");
run("Despeckle");
selectImage(channel1);
//run("Brightness/Contrast...");
run("Enhance Contrast", "saturated=0.35");
run("Apply LUT");
run("Subtract Background...", "rolling=250");
run("Despeckle");
selectImage(channel3);
//run("Brightness/Contrast...");
run("Enhance Contrast", "saturated=0.35");
run("Apply LUT");
run("Subtract Background...", "rolling=200");
run("Despeckle");

//merge
run("Merge Channels...", "c1=[C1-"+File.name+"] c2=[C2-"+File.name+"] c3=[C3-"+File.name+"]
create keep");
run("RGB Color");
```

```
//[remove this and // if adding scale bar] run("Scale Bar...", "width=100 height=50 thickness=20
font=30 horizontal");
run("Images to Stack", "use");
run("Make Montage...", "columns=4 rows=1 scale=1");
waitForUser("Save”);
//save as .tif
close("*");
```

The Pearson’s R value was extracted from unprocessed images with ImageJ and the below macro:

```
//setup
channel1 = "C1-" + File.name;
channel2 = "C2-" + File.name;
channel3 = "C3-" + File.name;

//create mask
selectImage(File.name);
run("Duplicate...", "title=Copy duplicate");
selectImage("Copy");
run("Z Project...", "projection=[Max Intensity]");
selectImage("MAX_Copy");
run("Gaussian Blur...", "sigma=5");
run("Auto Threshold", "method=Huang2 white");
waitForUser("wand cells");

//tidy up
selectImage("MAX_Copy");
close();
selectImage("Copy");
close();
selectImage(File.name);
run("Split Channels");
selectImage(channel3);
close();

//measure PR
run("Coloc 2", "channel_1=C1-"+File.name+" channel_2=C2-"+File.name+" roi_or_mask=[ROI
Manager] threshold_regression=Costes show_save_pdf_dialog display_images_in_result
display_shuffled_images spearman's_rank_correlation manders'_correlation
kendall's_tau_rank_correlation 2d_intensity_histogram costes'_significance_test psf=3
costes_randomisations=10");
waitForUser("copy Pearson's R value");

//finish
close("*")
roiManager("deselect");
roiManager("delete");
```

3.2.6 Cell morphology analysis

Images of cells stained for BMPR 1α and integrin ß1 were used to discern cells' size and shape using the following macro code for ImageJ:

```
selectWindow(File.name);
//run("Brightness/Contrast...");
run("Enhance Contrast", "saturated=0.35");
run("Subtract Background...", "rolling=50");
run("Despeckle");
run("Set Measurements...", "area shape redirect=None decimal=3");
run("Analyze Particles...", "size=20-Infinity show=Overlay display exclude");
//prepare data
setOption("CopyHeaders", 0);
String.copyResults;
//Copy results to excel. Clear FIJI
waitForUser("Done");
close("*");
```

3.2.7 Rheology

A Discovery Hybrid 2 (DHR-2) rheometer (TA instruments) was used to measure the mechanical properties of delta 1. A 20 mm diameter parallel plate geometry rheometer head was used, with the geometry gap set to 500 µm and the trim gap set to 50 µm. All measurements were proceeded by a 3 min temperature soak at the desired temperature. Amplitude sweeps were carried out at 1.0 Hz, 0.05-40% strain. To test stress recovery, the gels were subjected to 0.2% strain at 1.0 Hz for 5 minutes. They were then placed under 100% strain at 1.0 Hz for a further 5 minutes. This process was repeated four times in total. Young's modulus was calculated using the below formula.

$$E' = 2(1 + v)G'$$

Where E' is the Young's modulus, G' is the storage modulus and v is Poisson's ratio, which was assumed to be 0.5.

Tan delta was calculated using the below formula:

$$\theta\delta = G'' \div G'$$

Where $\theta\delta$ is tan delta, G" is the loss modulus, and G' is the storage modulus.

3.3 Results and discussion

3.3.1 PEA coating validation

PEA was used to initially functionalise the surface of ibidi plates. PEA coatings were included to induce a more ECM-like, open network conformation in FN (Z. A. Cheng et al., 2019). To verify that PEA was being stably coated onto the plates used, XPS analysis was utilised. PEA coated ibidi plates were compared to uncoated ibidi plates (see **Figure 3.2**).

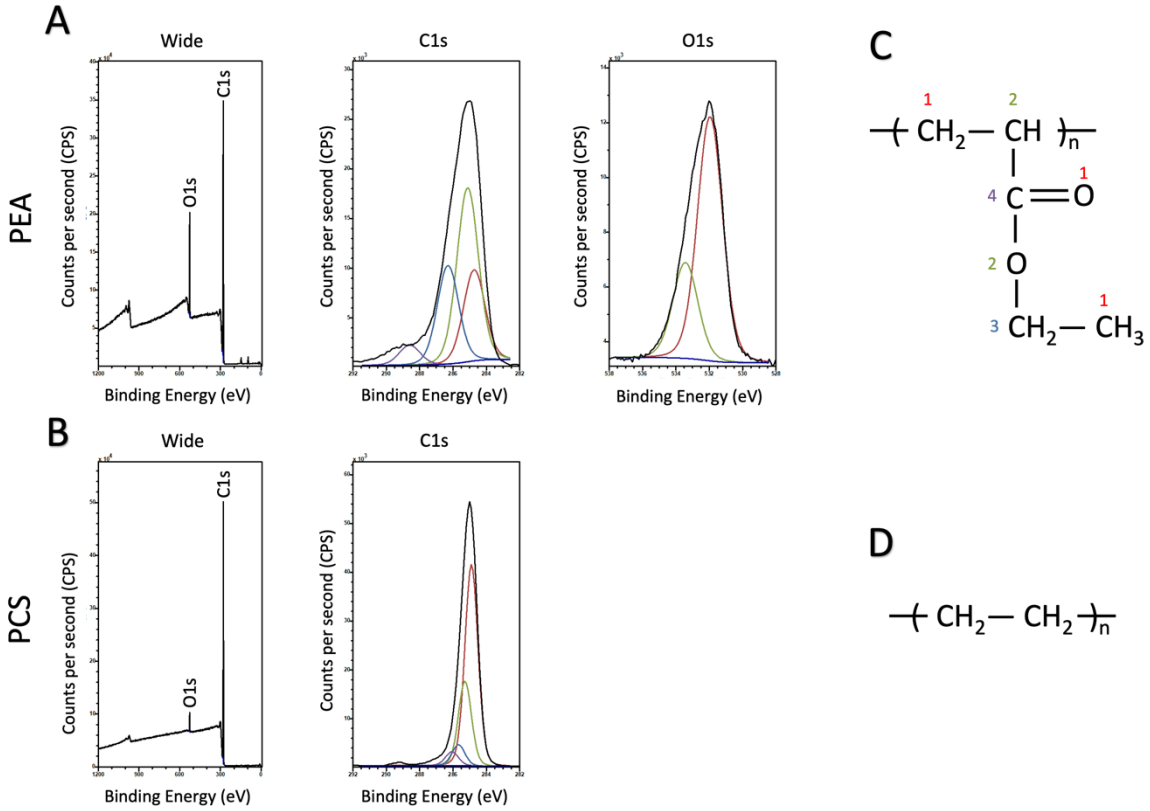

***Figure 3.2 XPS analysis of PEA coated and uncoated plates**. The surface chemistry of plates plasma coated with PEA or left as uncoated polymer cover slips (PCS) was assessed with XPS analysis. The wide field spectra of (**A**) PEA and (**B**) PCS conditions, as well as high resolution C1s and O1s spectra are shown where applicable from left to right. C1s and O1s include fitted components in coloured lines. The chemical structure of (**C**) PEA and (**D**) poly(ethylene) are also shown, with carbon and oxygen atoms numbered, and the numbers colour coded to match corresponding fitted lines in (**A**) and (**B**). Note that poly(ethylene) reportedly produces a four-carbon pattern due to vibrational fine structure caused by low level oxidation.*

The peaks observed in the PEA coated samples correlated roughly with the chemical structure of PEA (Z. A. Cheng et al., 2019). Previous research demonstrated that PEA fragments when plasma polymerised, causing some loss of

functional groups (Alba-Perez et al., 2020; Cantini et al., 2012). This explained the reduced peak heights seen for this sample, compared with the spectrum of unfragmented PEA, which typically includes more distinct peaks for both carbon and oxygen atoms (Beamson & Briggs, 1993). The uncoated polymer coverslip (PCS) samples had a spectrum like that of poly(ethylene) (Beamson & Briggs, 1993), a derivative of which the slips were reportedly made of. Significantly, the PCS spectrum also had a much smaller oxygen peak than the coated sample. This supported the hypothesis that the coated sample was successfully coated with PEA, which included oxygen atoms (Z. A. Cheng et al., 2019).

The presence of any oxygen on the uncoated sample was unexpected, as poly(ethylene) doesn't contain oxygen atoms (Beamson & Briggs, 1993). The small peak observed could have been part of the chemical structure of the plate or from oxygen atoms absorbed onto the surface, either from the air, or as part of the tissue culture-treating process. This process typically includes an oxygen polymerisation step (Lerman et al., 2018), so this was a logical conclusion. However, due to proprietary information surrounding the exact nature of the PCS material and the treatment process, other variables that could be influencing the observed spectra should not be ruled out.

3.3.2 Fibronectin conformation

The effect of the PEA coating on FN molecules' morphology was assessed using various methods.

3.3.2.1 AFM analysis of FN morphology

To further characterise the surface used, atomic force microscopy (AFM) was utilised to compare the conformation of FN molecules coated on bare PCS plates and PCS plates plasma coated with PEA. PEA coated tissue culture plastic (TCP) has previously been shown to encourage FN to adopt an open fibrillar network conformation (Alba-Perez et al., 2020), and was included as a control. In collaboration with Dr Mark Sprott and Dr Matthew Walker, FN morphology was investigated using AFM (see **Figure 3.3**).

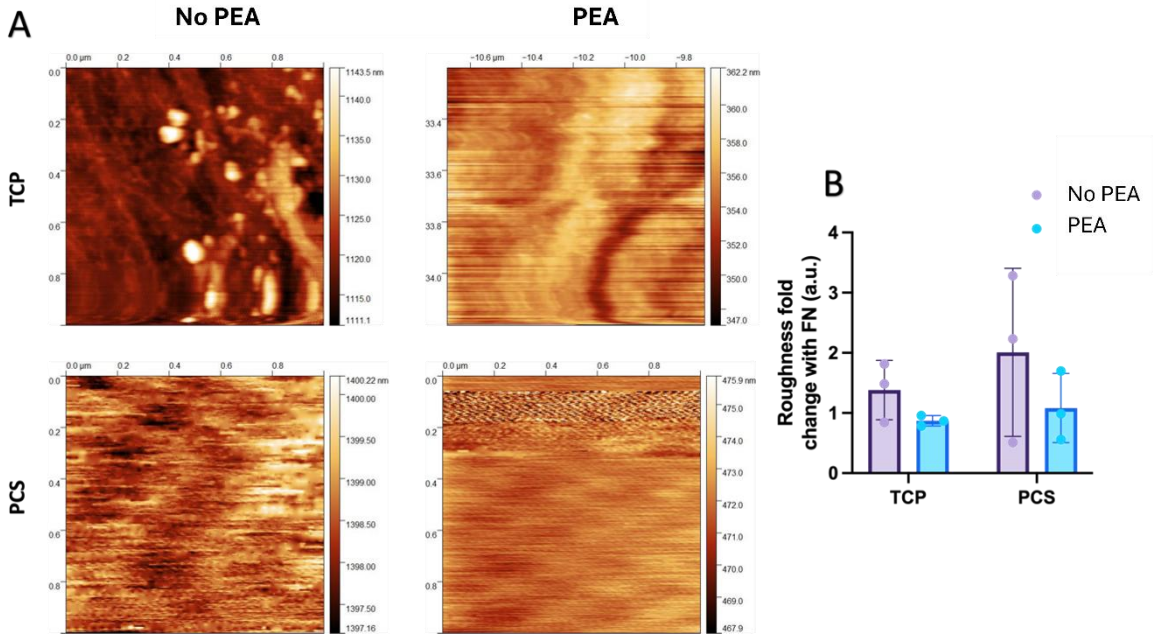

***Figure 3.3 AFM assessment of PEA and TCP surfaces' effects on FN morphology**. AFM was used to image FN on bare TCP and on TCP plasma coated with PEA. (**A**) Representative AFM images of conditions which included FN. Each image is 1 μm², with a scale shown on the top and left of the images. The bar to the right of each image illustrates the height measured by the AFM cantilever. Note that the scale used for height is different for each image to allow for clear visualisation. (**B**) Measured surface roughness (Sa) fold change when FN was included in each condition normalised against conditions without FN. Graphs show mean ± SD. n=3 technical replicates.*

While the representative images were poor, a trend emerged in the surface roughness data; inclusion of PEA on both PCS and TCP surfaces caused decreased roughness, suggesting that the FN in these conditions adopted a flatter conformation, indicative of network formation (Z. A. Cheng et al., 2019; Xiao, Donnelly, et al., 2022). This was despite the reported high affinity of the ibidi plates for ECM proteins. Future work could look to repeat these experiments and increase image resolution and data reliability. Subsequent experiments focussed on PCS surfaces with or without PEA, which were chosen as they improved IF microscopy image quality.

3.3.2.2 ICW analysis of FN absorption and domain availability

Next, the amount of FN absorbed on each surface was quantified using ICW with a polyclonal FN primary antibody. FN in an open network conformation has

previously been reported to have increased availability of its GF binding (P5F3) and RGD (HFN7) domains (Xiao, Donnelly, et al., 2022). Therefore, to further characterise FN morphology in the model system, ICW was also performed with specific monoclonal antibodies targeting each domain (see **Figure 3.4**).

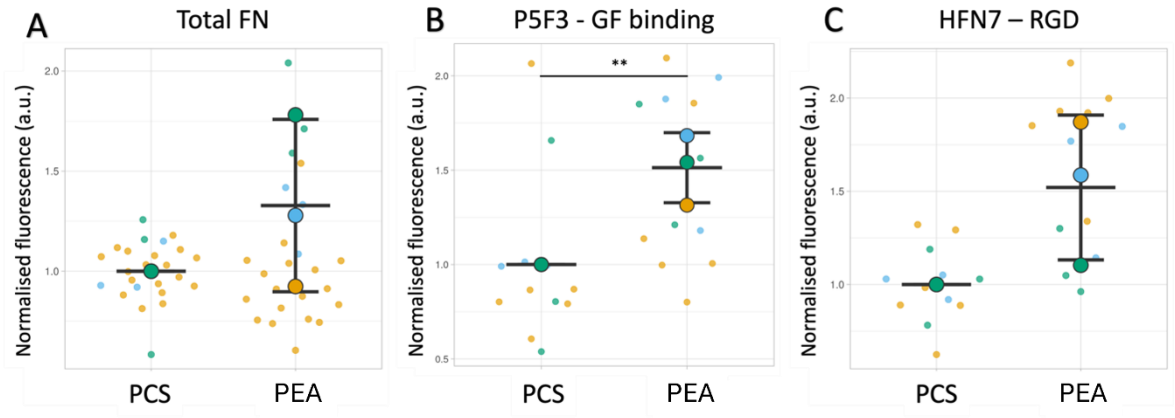

Figure 3.4 ICW assessment of PEA and TCP surfaces' effects on FN absorption and morphology. *ICW was used to determine (**A**) the amount of FN absorbed on bare ibidi plates (PCS) or PEA coated plates by utilising a polyclonal FN antibody. The availability of (**B**) the GF binding P5F3 domain and (**C**) the RGD HFN7 domain were assessed using corresponding monoclonal antibodies, with the fluorescence values measured normalised against corresponding total FN values in (**A**). Graphs show mean ± SD. Statistics by unpaired, two-tailed t-test**p < 0.01. Non-significant not shown. N=3 experimental replicates.*

When PEA coatings were included, a positive trend was observed in total FN absorption, as well as availability of both domains tested, though this difference was only statistically significant for the P5F3 GF binding domain. These data therefore suggest that, similarly to TCP (Z. A. Cheng et al., 2019), the PCS ibidi plates improved availability of FN domains when coated with PEA. This changed conformation made the FN more biomimetic and was hypothesised to allow cells to more readily interact with bound GFs and RGD domains (Llopis-Hernández et al., 2016; Salmerón-Sánchez & Dalby, 2016).

3.3.2.3 BMP2 absorption on various surfaces

As there was a trend towards an increase in heparin-binding domain availability seen in FN molecules absorbed onto PEA-coated surfaces, the absorption of heparin domain-containing growth factors was expected to follow a similar trend. This was tested using BMP2, which contains a heparin domain (Smith et al., 2018)

and was used in subsequent BM niche models. ELISA was used to assess absorbance (see **Figure 3.5**).

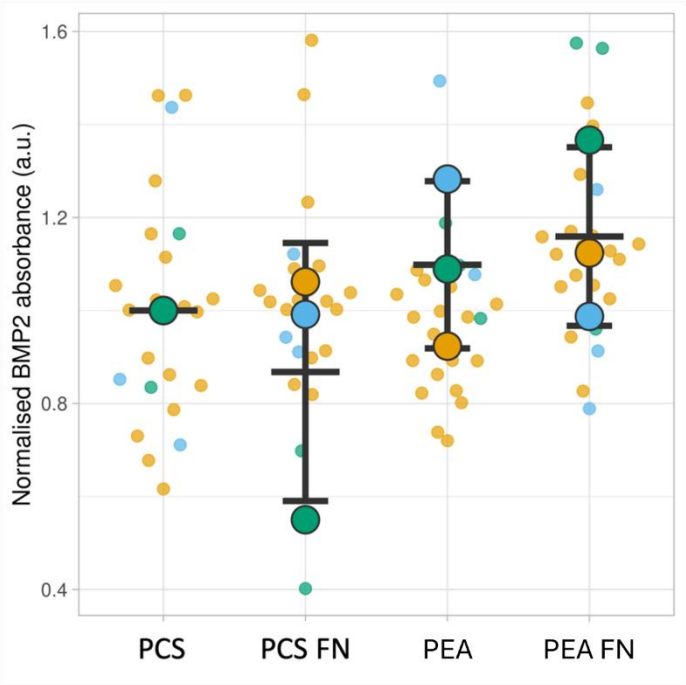

***Figure 3.5 BMP2 absorption on various surfaces**. ELISA was used to quantify the level of BMP2 absorption on various surfaces, normalised against PCS controls. Graphs show mean ± SD. N=3 experimental replicates.*

No statistically significant differences were observed in BMP2 absorption, and an inconsistent pattern was also present between repeats, suggesting that any differences were too marginal to be separated using the method employed. However, PEA FN surfaces more strongly absorbed the heparin-containing GF BMP2 than other surfaces on average, supporting the assertion that FN was absorbing BMP2 under these conditions due to the adoption of an open, ECM-like conformation (Xiao, Donnelly, et al., 2022). Future work could seek to assess BMP2 absorption more precisely to determine definitively if these differences represent a meaningful change in this metric. In addition, SMAD pathway activity in cells seeded on various surfaces could be investigated to determine the effect of these on BMP signalling (Brazil et al., 2015).

Overall, despite some trends emerging, little difference in FN morphology was seen between PEA coated and uncoated PCS surfaces. This was potentially due to FN being absorbed well on bare PCS, which is an assertion of the manufacturers.

3.3.3 Effect of surfaces on MSCs

To better understand the effect the coatings used would have on adherent cells, MSCs' morphologies on various surfaces were tested (see **Figure 3.6**).

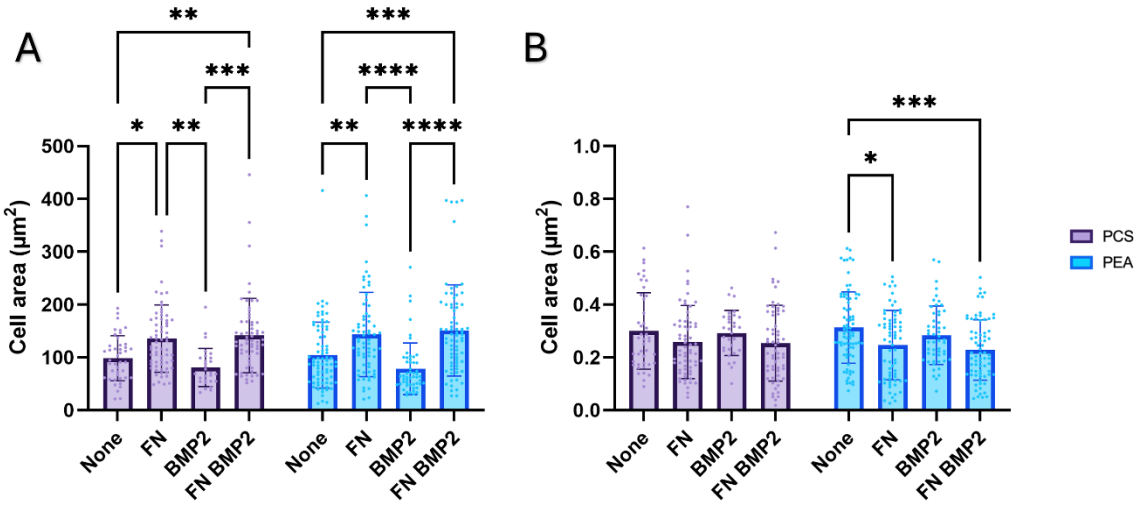

***Figure 3.6 Effect of surfaces on MSCs' morphology**. IF microscopy was used to measure the (**A**) area and (**B**) circularity of cells with stained integrin ß1 and BMPR 1a on surfaces with or without a PEA coating, in addition to FN, BMP2, both, or neither. Graphs show mean ± SD. Statistics by two-way ANOVA followed by Šidák multiple comparisons test. *p < 0.05, **p < 0.01, ***p < 0.001 and ****p < 0.0001. Non-significant not shown. n=3 technical replicates, with ~20 cells per replicate analysed. Representative images can be seen in **Figure 3.7A**.*

These results demonstrated that the inclusion of FN caused an increase in cell size due to cells binding to FN RGD domains more strongly than surfaces with no ECM proteins. An inverse relationship was observed with cell circularity, implying that the cells on surfaces without FN were forming fewer focal adhesions and interacting with the surface less (Keselowsky et al., 2005). However, no difference was visible when comparing PEA and PCS conditions, indicating that the supposed increase in availability of FN domains had a negligible impact on cell morphology. This, along with previous ICW data, suggested that FN was in a comparatively open conformation on both uncoated and PEA coated PCS surfaces, with any differences undetectable using this method.

To further assess the effect surfaces had on MSCs, the synergistic signalling effect of FN when coated on PEA and PCS surfaces was tested by assessing the colocalisation of integrin ß1, which forms part of the focal adhesion complex

(Hynes, 1992, 2009; Oria et al., 2017), and BMPR 1α, which is a subunit of the BMPR complex (Kaplan et al., 2009) (see **Figure 3.7**).

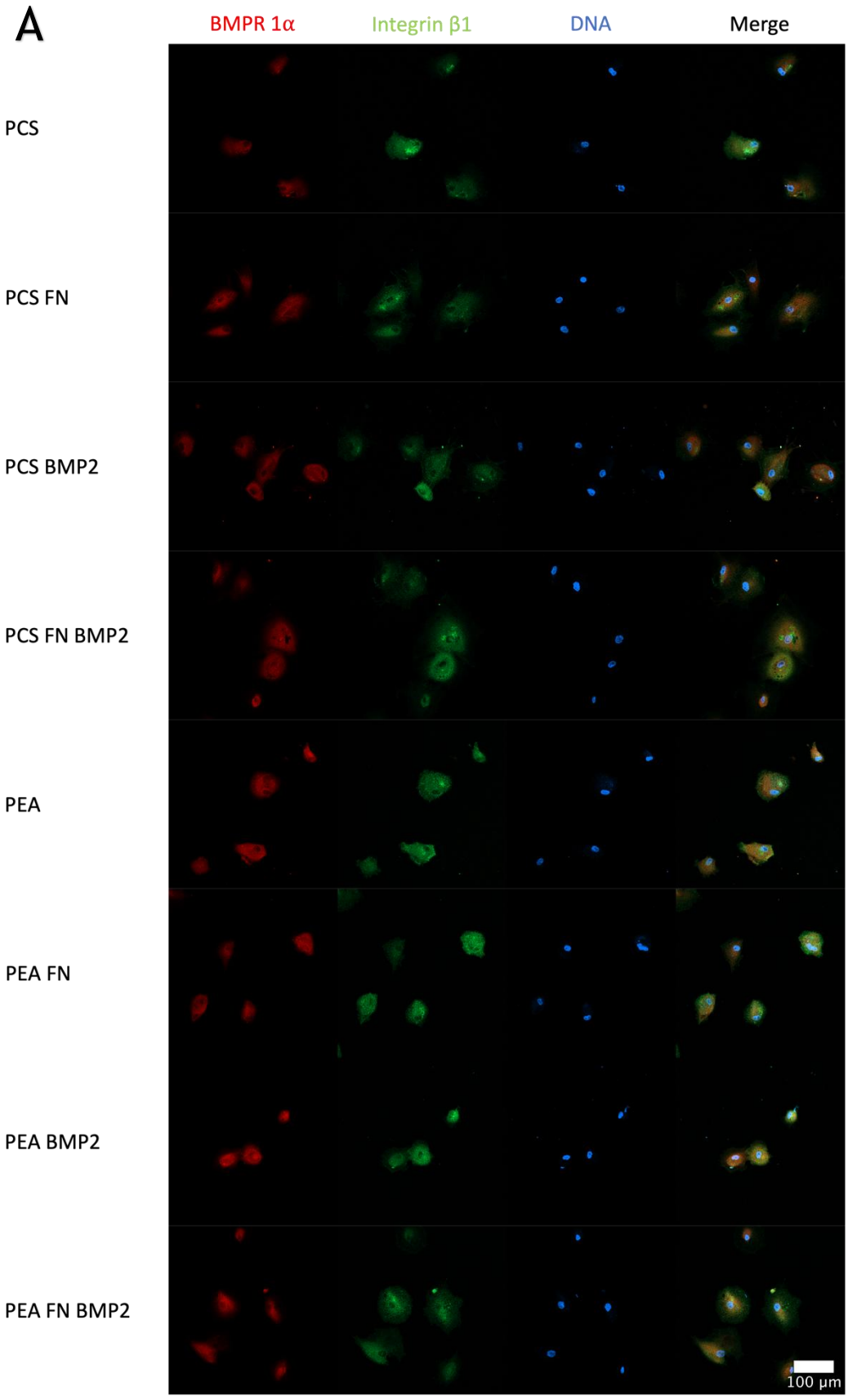

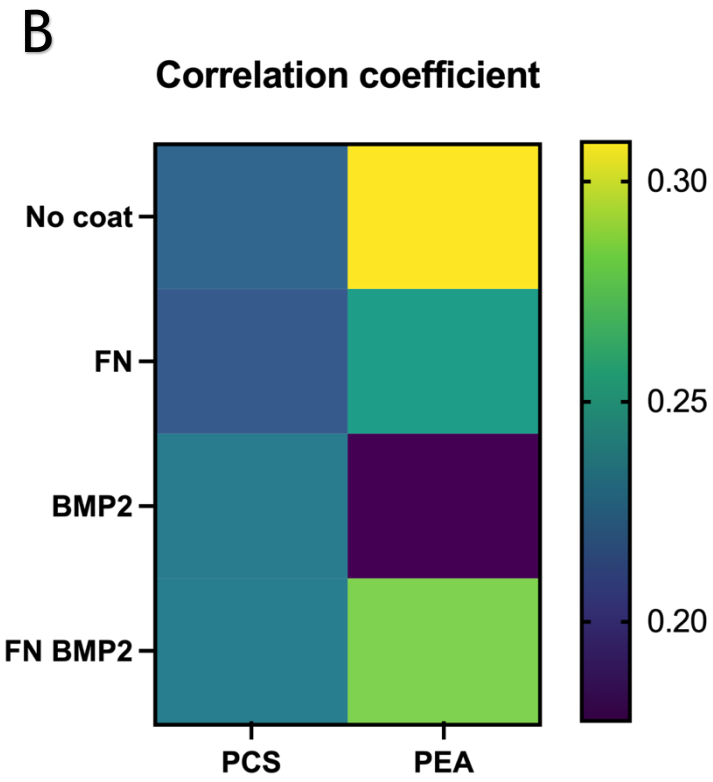

Figure 3.7 Colocalisation of integrin ß1 and BMPR 1a of MSCs on various surfaces. *IF microscopy was used to measure integrin ß1 and BMPR 1a colocalisation in cells cultured on various surfaces.* ***(A)*** *Representative images were prepared with FIJI.* ***(B)*** *The Pearson's R value (aka correlation coefficient), a measure of colocalisation, was calculated using FIJI. Heatmap shows mean. n=3 technical replicates with ~3 images taken per replicate.*

Colocalisation of these proteins implied that the focal adhesion and BMP receptor complexes were detecting adjacent domains on individual FN molecules (Llopis-Hernández et al., 2016), although notably these results are limited by image resolution (Dunn et al., 2011). The values gathered implied that the inclusion of FN and BMP2 caused increased colocalisation, but only on PEA surfaces. This was due to the adjacent domains on FN interacting with the complexes which had elements stained in this experiment, indicating that a PEA FN BMP2 system exhibited increased synergistic signalling compared to other conditions tested (Xiao, Donnelly, et al., 2022). This data also suggested a difference in FN openness between PCS and PEA surfaces, which was directly proportional to colocalisation of these proteins (Z. A. Cheng et al., 2019; Llopis-Hernández et al., 2016; Xiao, Donnelly, et al., 2022), though again this was just a trend and not statistically significant.

Surprisingly, the PEA only surface also caused high levels of colocalisation, suggesting some cellular interaction with the surface, though this was likely due to the small cell size observed in this condition, which may have resulted in the stained complexes being less spread out, yielding misleadingly high colocalisation.

However, this doesn't explain why a similar trend wasn't seen in other conditions which caused similarly reduced cell sizes.

3.3.4 Stiffness of gels

As well as the surface MSCs were to be cultured on, the mechanical properties of the gels included in the systems used throughout this project were assessed using rheology.

3.3.4.1 Delta 1 PeptiGel stiffness at various temperatures

Various concentrations of Delta 1 were used at this stage to assess dilution's effect on gels' properties. Since Delta 1 was warmed to room temperature prior to addition to wells, its stiffnesses were initially measured at 20°C (see **Figure 3.8**).

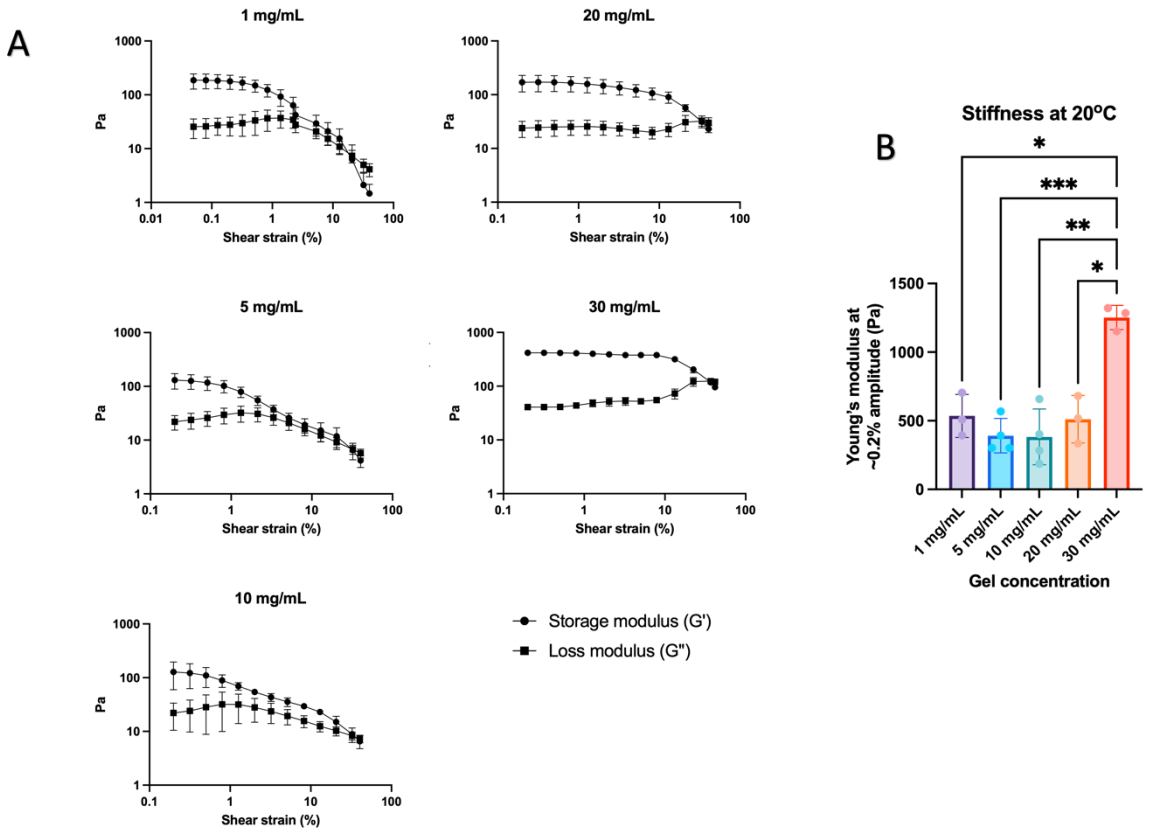

Figure 3.8 Stiffness of various concentrations of delta 1 PeptiGel at 20°C. *(A) Amplitude sweeps were used to measure the loss and storage moduli of several concentrations of dry delta 1 following a temperature soak at 20°C. Concentration of gels tested is shown above graphs. Circles represent G', squares are G". (B) The Young's modulus was also calculated using the*

*storage modulus at ~0.2% amplitude. Graphs show mean ± SD. Statistics by one-way Brown-Forsyth and Welch ANOVA followed by Dunnett T3 multiple comparison test. *p < 0.05, **p < 0.01 and ***p < 0.001. Non-significant not shown. N=3 or 4 experimental replicates.*

The stiffness was expected to be directly correlated to peptide concentration. While this was the case for undiluted, 30 mg/mL gel, the lower concentrations tested were all similarly low.

During model assembly, after warming to room temperature, the PeptiGels were added to wells during model assembly, then the plate was incubated at 37°C. Therefore, the gel's stiffnesses were also measured at 37°C (see **Figure 3.9**).

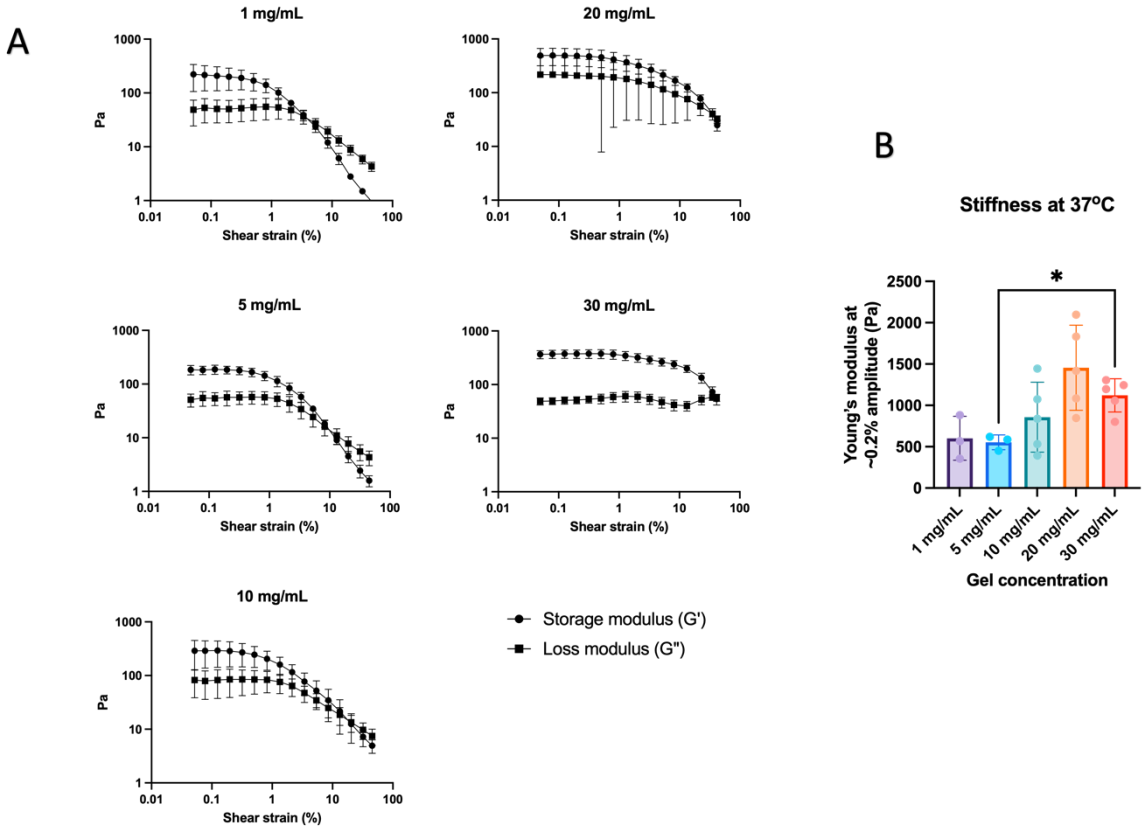

Figure 3.9 Stiffness of various concentrations of delta 1 PeptiGel at 37°C. *(**A**) Amplitude sweeps were used to measure the loss and storage moduli of several concentrations of dry delta 1 following a temperature soak at 37°C. Concentration of gels tested is shown above graphs. Circles represent G', squares are G". (**B**) The Young's modulus was also calculated using the storage modulus at ~0.2% amplitude. Graphs show mean ± SD. Statistics by one-way Brown-Forsyth and Welch ANOVA followed by Dunnett T3 multiple comparison test. *p < 0.05. Non-significant not shown. n=3 or 5 experimental replicates.*

The data at 37°C more closely matched the hypothesis than colder gels, with a general upward trend in stiffness associated with an increase in peptide

concentration. However, this trend was not uniform, with 30 mg/mL gel measured to be softer than 20 mg/mL.

The non-uniformity of the results at both temperatures could have been caused by the way in which the gels were diluted, as simply adding water and vortexing could have resulted in gels with non-uniform distribution of peptides, and therefore non-uniform stiffnesses. This method also resulted in bubbles forming in the gel, which were read by the rheometer as points of infinite pressure and could therefore also have affected the result. Sheer mixing could be used instead to produce a gel with more consistent stiffness in future (Vashisth et al., 2021). This however does not explain the discrepancy between the Young's moduli of undiluted delta 1 that were measured to be roughly 1.2 kPa at both temperatures tested, and the stiffness of the gel reported by the manufacturer to be 4.5 kPa.

3.3.4.2 Delta 1 PeptiGel stiffness with media

PeptiGels were not used dry; media was added following gel addition during model assembly. Therefore, the effect of various media on undiluted (30 mg/mL) delta 1's stiffness was assessed at 37°C (see **Figure 3.10**), since these were the most common conditions used in subsequent experiments.

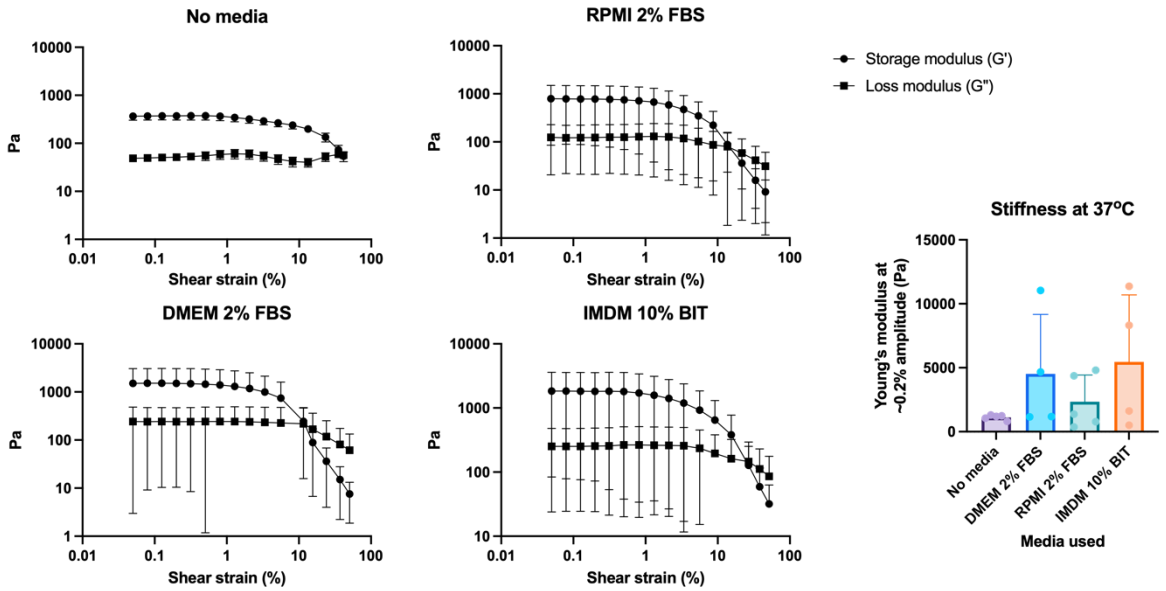

Figure 3.10 Effect of media on 30 mg/mL delta 1 PeptiGel stiffness. *(**A**) Amplitude sweeps were used to measure the loss and storage moduli of delta 1 treated overnight with media (shown above graphs). Circles represent G', squares are G". (**B**) The Young's modulus was also calculated*

using the storage modulus at ~0.2% amplitude. Graphs show mean ± SD. N=4 or 5 experimental replicates.

The stiffness of the gels when incubated overnight with media increased with all three media tested when compared to a dry control, however there was high variance in this data set and no statistical significance. Similar results have been reported for other PeptiGels (Ligorio et al., 2019). This could be attributed to the media used causing a change in the pH of the gel, therefore altering electrostatic interactions between peptides in the gel. This likely influenced the measured stiffness of the delta 1 gel, which was reported to have an initial pH of 9, compared to the media used, which had physiological pHs around 7. Another potential cause was charge screening; the addition of media may have caused an influx of ions to the gel, sequestering charged groups on the peptides, altering electrostatic interactions between peptides (Simonson & Brooks, 1996) and affecting the gel's stiffness. These factors could explain the increase in stiffness observed in delta 1 with the addition of media. Regardless of the cause, the addition of DMEM with 2% FBS, which was the predominate media used with the PeptiGels, resulted in the gel's average stiffness becoming ~4.5 kPa, the same as the value quoted by the supplier, although the variance in this data set was high.

3.3.4.3 Collagen stiffness

Collagen gel, which was used as a control throughout this project due to its proven ability to stimulate a niche-like phenotype in previous systems (Donnelly et al., 2024a) was also assessed (see **Figure 3.11**). Collagen was solidified at 37^{o}C then kept at this temperature during model assembly, so it was unnecessary to test different temperatures' effects on its stiffness. Note that only one concentration of collagen was used (see **2.2.1.3**).

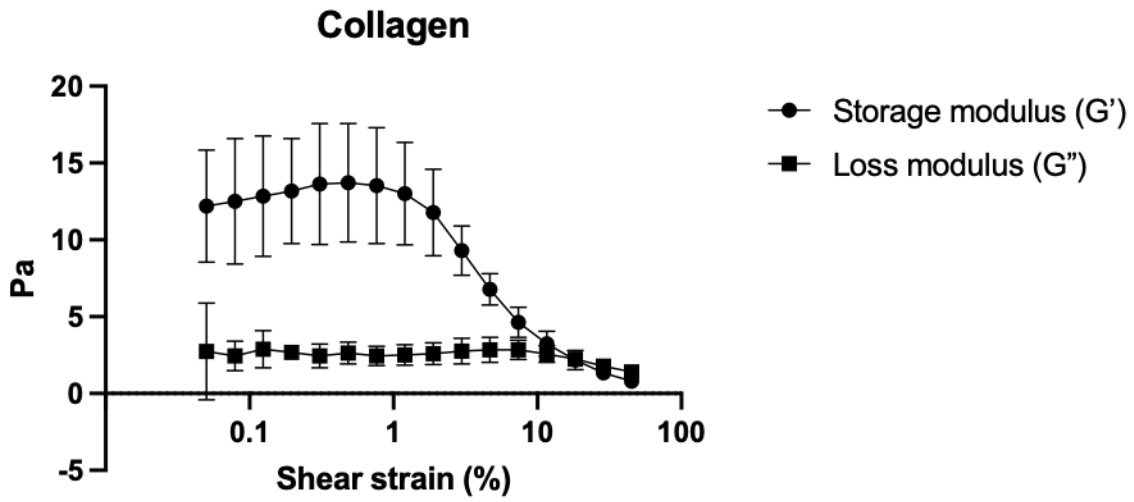

***Figure 3.11 Stiffness of collagen gel**. Amplitude sweeps were used to measure the loss and storage modulus of collagen gel. Circles represent G', squares are G". Graphs show mean ± SD. N=5 experimental replicates.*

Collagen's Young's modulus at ~0.2% amplitude strain was ~40 Pa. Collagen has previously been used to successfully replicate aspects of the BM niche (Donnelly et al., 2024), which implied that very soft gels were best for this. However, the BM niche is a highly heterogenous organ with a range of stiffnesses (X. Chen et al., 2020; Jansen et al., 2015). Collagen gel could imitate the soft, sinusoidal niche, while stiffer gels such as delta 1, layered on top of hard plastic, could replicate the endosteal interface typical of the arteriolar niche (Coutu et al., 2017). This could result in different, but still biomimetic interactions with cells, and have different applications, such as encouraging the maintenance of the quiescent HSCs that preferentially reside in the arteriolar niche (Pinho & Frenette, 2019).

3.3.5 Viscoelasticity of gels

Tan delta is the quotient of the loss and storage moduli and gives information on whether a material expresses more elastic, solid-like behaviours, resulting in a lower value, or more viscous, liquid-like behaviours, giving a higher value (Sharma et al., 2018). To quantify the viscoelastic properties of these gels, the effect of delta 1 concentration on tan delta was assessed (see **Figure 3.12**).

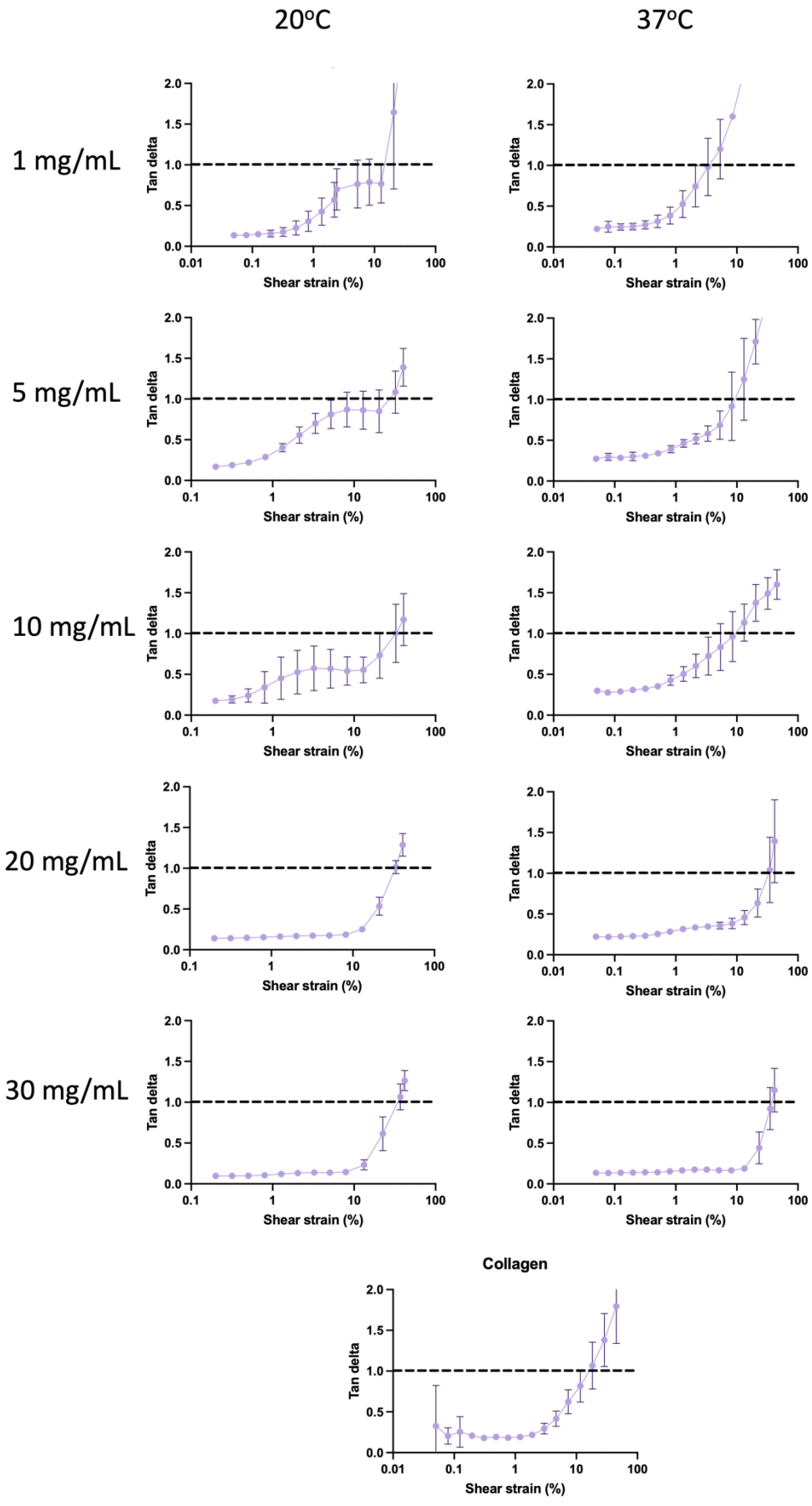
20°C
37°C
1 mg/mL
5 mg/mL
10 mg/mL
20 mg/mL
30 mg/mL
Tan delta
Shear strain (%)
Collagen

***Figure 3.12 Effect of concentration on viscoelasticity of gels**. Various concentrations of delta 1 PeptiGel were assessed at 20°C and 37°C to determine tan delta values over a range of shear strains using amplitude sweeps. Collagen was also assessed. Only values between 0 and 2 are shown. The transition point between elastic and viscous behaviour dominating is highlighted by a dashed line at a tan delta value of 1. Graphs show mean ± SD. N=3 or 5 experimental replicates.*

In more dilute gels, tan delta values increased at lower shear strain than in concentrated gels. This suggested that these gels more readily adopted viscous, liquid-like behaviours, which began to dominate as rheological manipulations outpaced material relaxation and tan delta increased above 1 (Sharma et al., 2018). The increased water to peptide ratio in these gels readily explains this occurrence. Interestingly, a common pattern emerged in PeptiGels assessed at 20°C; an increase in tan delta, followed by a plateau, then a rapid further increase beyond a value of 1. This indicated that these gels were more fragile, as the initial increase was likely caused by strain softening as the material began losing the ability to effectively distribute energy as it began to break down (Vignjevic et al., 2018), while the final rapid increase in tan delta indicated the gels were breaking. This may have been due to reduced peptide mobility within the colder gel, which reduced their molecular relaxation capabilities and made them more brittle than their counterparts measured at 37°C. Collagen gel was also assessed and found to have an intermediate tan delta profile, with a higher viscous component than undiluted PeptiGel observed.

The effect of media on tan delta was also assessed (see **Figure 3.13**).

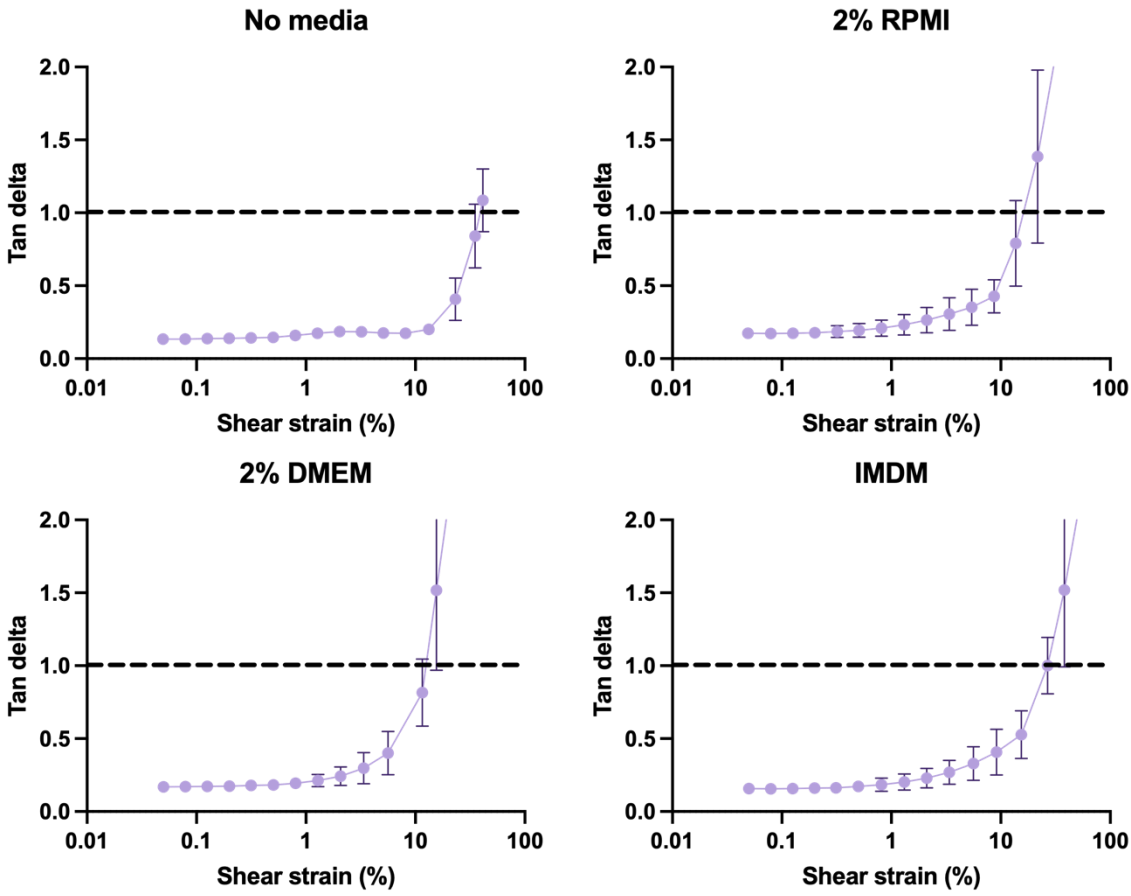

Figure 3.13 Effect of media on viscoelasticity of delta 1. *Undiluted delta 1 treated overnight with various media was analysed using an amplitude sweep to determine tan delta values. Only values between 0 and 2 are shown. The transition point between elastic and viscous behaviour dominating is highlighted by a dashed line. Graphs show mean ± SD. N=4 or 5 experimental replicates.*

When any of the media tested were used to treat delta 1, it increased its proclivity for adopting viscous properties, resulting in an earlier and more pronounced increase in tan delta. This was probably because of media interacting with the gel's pH and electrostatic properties, as previously discussed, as well as media being absorbed into the gel, decreasing its peptide concentration, though this was not reflected in the gel's stiffness.

Across all conditions tested, a tan delta greater than 0 and less than 1 was seen at lower amplitudes. This demonstrated the viscoelastic properties of the delta 1 and collagen gels used, which is essential due to the similarly viscoelastic nature of endogenous BM (Chaudhuri et al., 2020).

The ability of delta 1 to recover after experiencing stress was also measured by alternating low and high amplitude rotations of the rheometer head (see **Figure 3.14**).

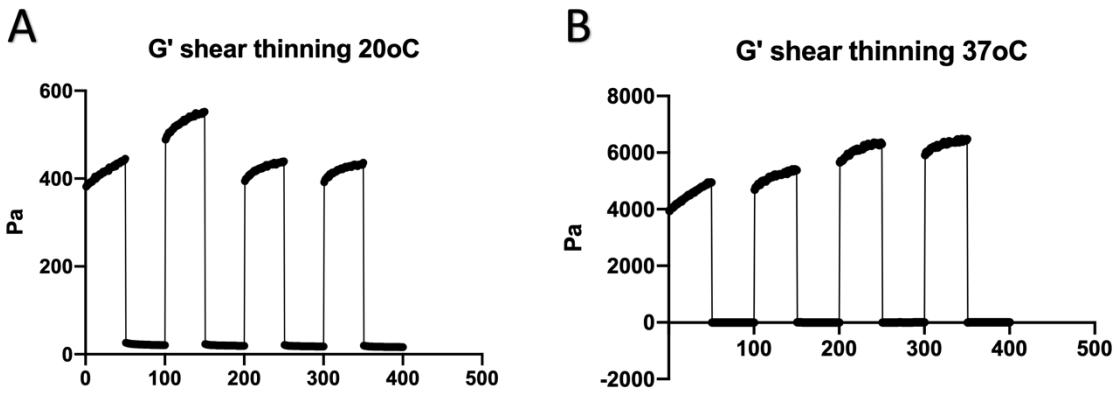

***Figure 3.14 Stress relaxation of delta 1 PeptiGel**. Alternating cycles of low and high amplitude rotations of a rheometer head were used to investigate the effect of stress on delta 1's stiffness at (A) 20°C and (B) 37°C. N=1 experimental replicate.*

When low amplitude rotations of the rheometer head were used, the storage modulus measured was consistently higher than when high amplitude rotations were used. These results suggested that the delta 1 gel exhibited shear thinning properties (Guvendiren et al., 2012), possibly due to the fibrils which made up the gel breaking and aligning when stress was applied, before entangling again when it was removed (Yan et al., 2010). Since the gel became increasingly stiff as it was exposed to repeated stress at 37°C, the gel was probably not fully recovering at this temperature after each run. However, at 20°C a less clear pattern was seen and the gel aPEAred more able to relax its stiffness following stress application. This may have been due to unbound peptides in the gel binding each other to form new fibrils when agitated, or binding existing fibrils, elongating them, and thereby increasing the PeptiGel's stiffness. This would explain the discrepancy between the two temperatures tested as at lower temperatures the peptides would be less mobile. Since the gels were only exposed to high levels of stress during model assembly, which was done at 20°C, it was safe to assume that the stiffness of the gel was consistent in the BM model.

3.4 Summary

Various chemical and physical properties of materials used in the final BM niche model were assessed. By investigating surface chemistry using XPS, PEA was shown to be efficiently coated onto PCS surfaces (see **Figure 3.2**). This coating was initially hypothesised to cause FN coated on top of it to unfold into a fibrillar network conformation (Gugutkov et al., 2010; Llopis-Hernández et al., 2016). The patterns that emerged through AFM (see **Figure 3.3**), ICW (see **Figure 3.4)** and BMP2 absorption (see **Figure 3.5**) analysis seemed to support this hypothesis, though minimal significance was observed. However, when investigating the effect of various coatings on MSCs, more robust conclusions could be drawn; the inclusion of FN caused MSCs to spread more (see **Figure 3.6**), suggesting that these cells were able to interact with the FN RGD domains similarly to native ECM (Chaudhuri et al., 2020; X. Chen et al., 2020; Jansen et al., 2015; Wheadon et al., 2024). This result was unexpectedly seen on both PEA and uncoated PCS surfaces, implying that the FN RGD domains were available in both conditions. But, when investigating colocalisation of focal adhesions and the BMPR complex, FN on PEA surfaces was shown to cause higher colocalisation (see **Figure 3.7**). This could indicate that the P5F3 and HFN7 domains were differentially exposed, with the latter exposed equally on all surfaces tested, while the former was preferentially exposed on PEA surfaces. This result would be different to previous data gathered (Z. A. Cheng et al., 2019; Xiao, Donnelly, et al., 2022), but could be explained by the different surfaces coated with PEA, with the PCS surface used here reportedly binding ECM proteins strongly, as opposed to TCP surfaces used in previous research. This hypothesis could have been further tested with techniques such as fluorescence energy transfer. Regardless, an increase in availability of both domains tested was desired, so PEA on PCS was selected as the optimal surface moving forwards.

Gels used in subsequent BM model experiments also had their mechanical properties robustly characterised. Delta 1 PeptiGel's stiffness was found to be associated with peptide concentration, though this relationship was complex and influenced by media addition (see **Figure 3.8** and **Figure 3.9**). The stiffness of the delta 1 PeptiGel was also shown to be increased by the addition of media (see **Figure 3.10).** In addition, undiluted delta 1 PeptiGel was shown to be stiffer than

collagen gel, but still within the range of native BM (see **Figure 3.11**) (X. Chen et al., 2020; Jansen et al., 2015). This difference was hypothesised to allow each gel to mimic different facets of the BM niche for different purposes, with the delta 1 niche potentially replicating the arteriolar niche where quiescent HSCs reside (Pinho & Frenette, 2019). Both collagen and delta 1 gels were shown to be viscoelastic under various conditions (see **Figure 3.12** and **Figure 3.13)**, and the delta 1 gel was determined to experience shear thinning (see **Figure 3.14**), with acceptable levels of stress relaxation at room temperature.

Additional experiments could have been carried out to further characterise the materials used in the BM niche model developed. For example, nanoindentation could have allowed the mechanical properties of gels to be further probed, and cryo-scanning electron microscopy could have allowed gels' pore sizes to be investigated. However, the characterisation experiments investigating the materials' mechanical properties were still robust and laid the foundations for a well-informed experimental approach in this project, allowing these parameters' influence in models to be understood and manipulated.

Chapter 4 The effect of a synthetic BM niche on resident cells

4.1 Introduction

As the model BM niche continued to be developed, MSCs were included to act as a feeder layer and support HSC maintenance within the artificial niche. The effect of the various niche components on MSCs was investigated, as well as the effect of various iterations of the model niche on HSCs and AML cells.

4.1.1 PeptiGel in a BM model

Previous BM models have made use of various scaffolds to simulate the BM niche microenvironment (Doherty-Boyd et al., 2024). These include inorganic materials such as crystals (Nichols et al., 2009) and ceramics (Bourgine et al., 2018), as well as animal-derived gels, such as collagen I gel (Donnelly et al., 2024) and Matrigel (Wimmer et al., 2019). However, these scaffolds are lacking in several areas; inorganic materials are readily available and easy to use but lack the mechanical and chemical properties of the *in vivo* BM niche. Organic materials on the other hand are typically animal-derived, resulting in niches which are impacted by inter-species heterogeneity (Clough et al., 2021; Ingber, 2020). These materials also usually have high batch-to-batch variability, and their contents aren't fully understood (Clough et al., 2021). Synthetic gels such as PeptiGels offer an alternative; their contents are fully defined, and they are highly consistent. They are also tuneable in terms of their mechanical properties and functionalisation (Scelsi et al., 2019). Furthermore, they have previously been shown to be compatible with MSCs (Castillo Diaz et al., 2016).

One potential pitfall when using purely synthetic gels is a lack of biocompatibility; without RGD and GF binding domains, the scaffold can fail to act sufficiently similarly to the ECM it is being used to replicate, preventing cells from adhering and GFs from being retained (Pinho & Frenette, 2019). This could be remedied by

incorporating elements of the ECM into PeptiGels. In some circumstances, it is also possible that some of the gel, which has been shown to be biodegradable (Castillo Diaz et al., 2016) could be replaced by ECM proteins produced by cells in a model system.

4.1.2 Surfaces' effects on MSCs

Solid-phase presentation of BMP-2 in a PEA and FN system has been utilised in the past primarily to stimulate osteogenesis for bone regeneration (Z. A. Cheng et al., 2019). However, recent work by Donnelly et al. (2024) adapted this system to mimic the BM niche, promoting a niche-like phenotype in MSCs. The exact mechanism behind this system's flexibility is unclear, though it is possible that in the case of (Donnelly et al., 2024a) the osteogenic nature of BMP-2 balanced the adipogenicity of the soft collagen gel used (Engler et al., 2006).

4.1.3 Mechanical properties of BM

Since the mechanical properties of the BM niche are known to influence resident cells (Chaudhuri et al., 2020), it is essential to take them into consideration when developing BM models in order to mimic the endogenous organ as much as possible. These properties encompass stiffness (X. Chen et al., 2020; Jansen et al., 2015), viscoelasticity (Cantini et al., 2020; Chaudhuri et al., 2020), topography (Dalby et al., 2007), adhesivity (Kilian et al., 2010), and pore size (P. Zhang et al., 2019). Systems with intermediate mechanical properties between stiff osteogenic microenvironments and soft adipogenic ones have been shown to retain MSC multipotency (Tsimbouri et al., 2012; D. Zhang & Kilian, 2013), i.e. the niche-like phenotype. Synthetic PeptiGels with tuneable mechanical properties offer a tempting avenue for optimisation of these properties to accurately replicate the BM niche and induce the desired phenotype.

4.1.4 MSCs as an HSC-supportive feeder layer

MSCs have been used as feeder layers to promote HSC maintenance and proliferation for decades (see **1.3**) (Dexter et al., 1977). Recent advances have

allowed more complex culturing techniques, including spheroids and 3D culture (Lewis et al., 2017; Méndez-Ferrer et al., 2010). These systems have several positive attributes, including higher biomimicry to the native 3D BM niche, and a putatively improved MSC phenotype (Isern et al., 2013; Pinho et al., 2013). However, 2D monolayer MSC systems, as well as 2.5D systems in which the MSC monolayers are cultured under gels they can migrate into, are routinely used (Donnelly et al., 2024; Lima et al., 2013), and hold several advantages. These include ease of use and fully separated cell types when MSC monolayers are separated from co-cultured non-adherent cells by a barrier like a hydrogel. Separated cell populations allow for straightforward isolation of different cell types, but also limit juxtracrine signalling (Pinho et al., 2013).

4.1.5 Markers of a niche-like phenotype

Several markers are associated with MSCs adopting a BM niche-like phenotype. These markers can be investigated to determine whether MSCs in *in vitro* systems are behaving similarly to how they would within the BM niche, indicating how well MSCs will support a population of HSCs. One such marker is nestin, which is highly expressed in MSCs that colocalise with HSCs (Pinho et al., 2013) and which cause HSC loss when ablated (Méndez-Ferrer et al., 2010). Despite previous research suggesting nestin is a neuroepithelial progenitor marker (Lendahl et al., 1990), recent evidence suggests that measuring nestin expression is an effective, simple method for estimating how well an MSC feeder monolayer will perform in terms of HSC maintenance (Donnelly et al., 2024). Nestin+ cells also typically express the HSC-supportive soluble factor SCF, as well as the HSC retention soluble factor CXCL12 (Mendelson & Frenette, 2014), expression of which can also be analysed to further characterise cells.

A more quiescent metabolic state in MSCs is also known to be linked to the niche-like phenotype (Ross et al., 2023). Metabolic state has been shown to be linked to cells' intracellular tension, which is regulated by bound substrates' mechanical properties via the molecular clutch (Elosegui-Artola et al., 2016, 2018; Ross et al., 2023). This potentially affects organelle distribution, as changes to intracellular tension may impact bound structures (Oria et al., 2017), although mitochondria are known to be primarily transported by microtubules (Melkov & Abdu, 2018).

Changes in mitochondrial distribution could in turn affect OXPHOS activity within cells. This was posited as a potential explanation for how cells sense their mechanical environment, which could complement established pathways, such as YAP/TAZ signalling (Janmey et al., 2020).

4.1.6 Haematopoietic cell hierarchy

As discussed previously (see **1.1.1**), HSCs and their progeny exist in a fluid hierarchy, with more naïve cells producing progressively more mature cells with decreasing differentiation capacity (Ceredig et al., 2009). Both healthy (Wisniewski et al., 2011) and cancerous (Boyd et al., 2018) haematopoietic cells can be sorted into rough categories based on their surface markers, providing information on the composition of a haematopoietic cell population. Mature cells are identified based on a series of established markers (see **Table 4.1**), but immature cells typically form a spectrum; CD34+ cells are usually described as HSCs or LSCs, though more stringent categorisation techniques often include the need for cells to be CD38-/low to be considered true stem cells (Dorrell et al., 2000). This population can be divided further, with LT-HSCs typically expressing high levels of CD90 and low levels of CD45RA, while ST-HSCs have the opposite phenotype (Wisniewski et al., 2011).

Table 4.1 Markers for mature haematopoietic lineage cell types.

Marker	Population
CD45+	Haematopoietic
CD45+ CD41/CD61+	Megakaryocyte
CD45+ CD16+	Monocytes, B cells, and lymphocytes
CD45+ CD7+	T cells
CD45+ CD41/CD61- CD16- CD7-	Progenitor cells

4.1.7 Aims

This chapter aimed to determine the effect of various iterations of a model BM niche on resident MSCs, HSCs, and AML cells.

4.2 Materials and methods

4.2.1 IF microscopy characterisation of MSCs

MSCs were stained and imaged as described previously (see **2.2.3**). The primary antibodies used were Nestin (abcam ab155090) diluted 1:100, SCF (abcam ab64677) diluted 1:200, SDF1 (aka CXCL12) (Proteintech 19483-1-AP) diluted 1:100, TOMM20 (Proteintech 66777-1-Ig) diluted 1:200.

4.2.1.1 Corrected total cell fluorescence (CTCF) analysis

Cells' expression of fluorescently labelled proteins was directly proportional to their mean grey value when imaged using a microscope channel with an appropriate wavelength. Integrated density, as well as the mean grey value of an area of each image which contained no cells, was determined using the following FIJI macro, or a similar derivative:

```
//setup
channel1 = "C1-" + File.name;
channel2 = "C2-" + File.name;
channel3 = "C3-" + File.name;

//open file

selectWindow(File.name);
run("Split Channels");

selectWindow(channel2);
run("Duplicate...", "title=C2copy");
selectWindow(channel2);
run("Enhance Contrast", "saturated=0.35");
run("Subtract Background...", "rolling=1000");
run("Gaussian Blur...", "sigma=2.50");

selectWindow(channel1);
run("Enhance Contrast", "saturated=0.35");
run("Subtract Background...", "rolling=500");
run("Gaussian Blur...", "sigma=2.50");
```

```
//make and adjust composite image for masking
run("Merge Channels...", "c1=[C1-"+File.name+"] c2=[C2-"+File.name+"] c3=[C3-
"+File.name+"]create");
run("Auto Threshold", "method=Mean white");

waitForUser("Threshold and wand cells. Remember background ROI!");
//select cell ROIs then move on to macro part 2
//don't select doublets etc or cells not wholly in frame
//REMEMBER BKG ROI!

run("Set Measurements...", "area mean integrated redirect=None decimal=3");
selectWindow("C2copy");

//measure cells
n = roiManager('count');
for (i = 0; i < n; i++) {
roiManager("Select", i);
run("Measure");
}

//prepare data
setOption("CopyHeaders", 0);
String.copyResults;

//clear FIJI
waitForUser("Paste results in excel");
close("*");
roiManager("deselect");
roiManager("delete");
run("Clear Results");

//paste data into excel for CTCF processing
```

The resultant values were then used to determine each cell's level of stained protein expression using the below CTCF formula:

$$CTCF = I - A \times G$$

Where CTCF is the level of protein expression, I is the cell's integrated density value, A is the cell's area, and G is the mean grey value of the background measurement.

4.2.1.2 Viability assay

An ethidium homodimer-1 and calcein AM kit from Invitrogen (L3224) was used to stain adherent cells for viability. A master mix containing 4 µM ethidium homodimer-1 and 2 µM calcein AM was made up in PBS. The media was removed

from wells in well plates containing cells and an equivalent volume of master mix was added. The plate was then incubated at room temperature for 30 minutes before the staining master mix was removed and the wells were washed twice with PBS. The plates were then imaged using a Zeiss LSM980 microscope, or a Zeiss axio observer microscope. Cells were determined to be alive or dead using the following FIJI macro:

```
// Set the path to the folder containing the .czi files
inputFolder = getDirectory("Choose input directory");

// Get a list of all .czi files in the input folder
list = getFileList(inputFolder);

// No need to initialize FileName, greenCount, and redCount arrays at this point

// Ensure the Results table is reset/cleared before adding new data
if (isOpen("Results")) {
    selectWindow("Results");
    run("Close");
}

// Loop over all .czi files in the input folder
for (i = 0; i < list.length; i++) {
    // Open the current file
    open(inputFolder + list[i]);

    // File.name might not directly work; ensure you have the correct file name
    // Assuming list[i] gives you the file name
    fileName = list[i];

    // Perform the image processing operations on the green and red channels
    // It's important to correctly name your channels according to your specific files
   run("Split Channels");
    // Assuming the split results in windows named "C1-<filename>" and "C2-<filename>"
    green = "C2-" + File.name;
    red = "C1-" + File.name;

    // Process the green channel
    selectWindow(green);
    run("Remove Outliers...", "radius=10 threshold=50 which=Bright");
    run("Gaussian Blur...", "sigma=2");
    run("Find Maxima...", "prominence=60 exclude output=Count");

    // Process the red channel
    selectWindow(red);
    run("Enhance Contrast", "saturated=0.35");
    run("Apply LUT");
    run("Despeckle");
    run("Gaussian Blur...", "sigma=3");
    run("Find Maxima...", "prominence=50 output=Count");
```

```
    // Close the current file windows
    close("*"); // This closes all open image windows; adjust if you need more granularity
}
String.copyResults;
// Paste results in excel; first value for each photo is number of live cells, second is number of dead cells
```

For non-adherent cells, an aliquot of homogenously suspended cells was mixed 1:1 with Gibco Trypan Blue solution (0.4%) (15250-061). The number of cells in 10 µL of the resultant mix was then counted using a Countess 3 automated cell counter, and the cell density and viability calculated.

4.2.1.3 Mitochondrial distribution analysis

Cells' mitochondrial positioning was also measured using imageJ to visualise mitochondria stained with an anti-TOMM20 antibody, staining the mitochondrial surface marker. The distance of each block of TOMM20 stain to a cell's nucleus was determined by first measuring the centroid of the mitochondria and the nucleus using the following FIJI macro:

```
Phalloidin = "C1-" + File.name
TOMM20 = "C2-" + File.name
DAPI = "C3-" + File.name

if (roiManager("count")>0) {
roiManager("deselect");
roiManager("delete");
}
run("Split Channels");
selectWindow(Phalloidin);
run("Duplicate...", "title=Pcopy");
//run("Brightness/Contrast...");
run("Enhance Contrast", "saturated=0.35");
run("Apply LUT");
run("Subtract Background...", "rolling=1000");

selectWindow(TOMM20);
run("Duplicate...", "title=T20copy");
selectWindow("T20copy");
//run("Brightness/Contrast...");
run("Enhance Contrast", "saturated=0.35");
run("Apply LUT");
run("Subtract Background...", "rolling=500");

selectWindow(DAPI);
```

```
run("Duplicate...", "title=DAPIcopy");
//run("Brightness/Contrast...");
run("Enhance Contrast", "saturated=0.35");
run("Apply LUT");
run("Subtract Background...", "rolling=500");

//make composite image for ROI selection
run("Merge Channels...", "c1=Pcopy c2=T20copy c3=DAPIcopy");
run("8-bit");
run("Gaussian Blur...", "sigma=2");
run("Auto Threshold", "method=Triangle");
waitForUser("Select ROIs");
//Select ROIs with wand tool or draw them if image quality is poor

//Prep DAPI image
selectWindow(DAPI);
//run("Brightness/Contrast...");
run("Enhance Contrast", "saturated=0.35");
run("Apply LUT");
run("Subtract Background...", "rolling=100");
run("Despeckle");
run("Gaussian Blur...", "sigma=2");

for (i = 0; i < roiManager("count"); i++) {

//Cell area
selectWindow(DAPI);
roiManager("select", i);
run("Set Measurements...", "area redirect=None decimal=3");
run("Measure");
run("Duplicate...", "title=[DAPIcopy]");
selectWindow("DAPIcopy");
run("Auto Threshold", "method=RenyiEntropy white");
run("Set Measurements...", "area centroid redirect=None decimal=3");
run("Analyze Particles...", "size=200-Infinity display exclude overlay");
close("DAPIcopy");

//T20
selectWindow(TOMM20);
roiManager("select", i);
run("Duplicate...", "title=[TOMM20copy]");
//run("Brightness/Contrast...");
run("Enhance Contrast", "saturated=0.35");
run("Apply LUT");
run("Subtract Background...", "rolling=10");
setAutoThreshold("Default");
//run("Threshold...");
setOption("BlackBackground", false);
run("Convert to Mask");
run("Invert LUT");
run("Analyze Particles...", "size=0.3-Infinity display exclude overlay");
close("TOMM20copy");
```

```
//Data transfer
setOption("CopyHeaders", 0);
String.copyResults;
waitForUser("Paste data");
Table_name = "Cell " + i;
Table.rename("Results", Table_name);
}
close("*");
```

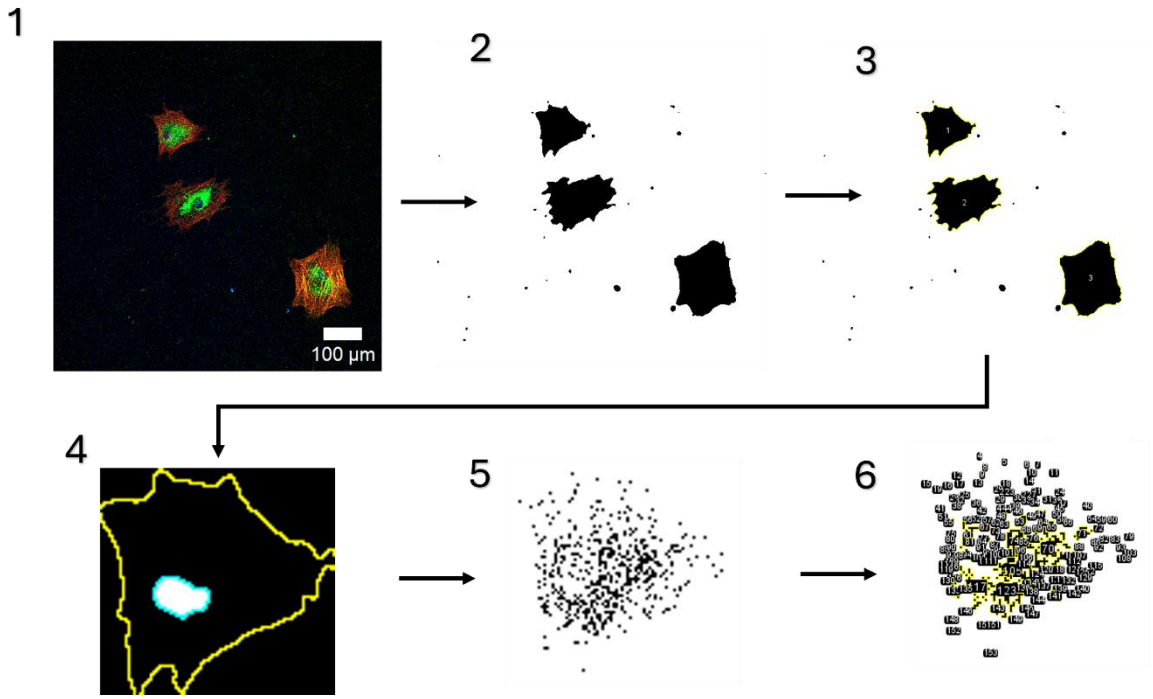

***Figure 4.1 Mitochondrial distribution analysis**. Cells were stained and imaged in three channels: DAPI (DNA), FITC (mitochondria), TRITC (actin). FIJI was used to assess distribution of stained mitochondria relative to a cell's nucleus. This process can be broken down into six steps, shown here. In step 1 the raw image was brightness enhanced, and had its channels merged. A 100 µm scale bar is shown here for clarity but was not added during analysis. In step 2, the composite image incorporating all channels had a threshold applied to produce a mask of the cells. In step 3 the mask was used to add each cell as a region of interest (ROI), shown here with a yellow outline and numbered cells. Cells were then individually analysed; in step 4 the ROI for a cell was used to create a duplicate image of the cell in the DAPI channel, which had a threshold applied. The ROI was also used to measure the cell's size. To identify a cell's nucleus, particles with >200 µm^2 area were measured. The identified particles were later manually checked to ensure only a single object was found, which was assumed to be the nucleus. The coordinates of the nucleus' centroid were extracted. In step 5 the same cell's ROI was used to create a duplicate image of the cell in the TRITC channel. In step 6, to identify the position of mitochondria, particles with area >0.3 µm^2 had their area and centroid coordinates recorded. It was assumed that mitochondrial size remained roughly consistent, and that therefore a contiguous block of positively stained pixels in step 6 represented a number of mitochondria proportional to its area. Steps 4-6 were then repeated for each other cell.*

The distance between the nucleus' centre and the centre of each block of mitochondria was hypothesised to change in response to intracellular tension. To calculate this, where x_{nuc} is the x coordinate of the centroid of the nucleus, x_{mito} is the x coordinate of the centroid of the TOMM20 stain particle, y_{nuc} is the y coordinate of the centroid of the nucleus and y_{mito} is the y coordinate of the centroid of the TOMM20 stain particle, the below formula was used.

$$d = \sqrt{(x_{nuc} - x_{mito})^2 + (y_{nuc} - y_{mito})^2}$$

As each TOMM20 stain particle likely contained several mitochondria, the size of the mitochondria was assumed to remain roughly consistent, and d was normalised with the corresponding TOMM20 particle's area a_{mito} and the total area of all TOMM20 stains in a cell to give a normalised distance D of the TOMM20 stain in each cell.

$$D = \frac{\sum(d * a_{mito})}{\sum a_{mito}}$$

Cells under identical conditions were assumed to have evenly distributed mitochondria, regardless of cell size. Therefore, D was normalised with cell area a_{cell} to give a final value f.

$$f = \frac{D}{a_{cell}}$$

4.2.1.4 Representative image preparation

High quality images were selected and processed using the following FIJI macro:

```
//setup
channel1 = "C1-" + File.name;
channel2 = "C2-" + File.name;
channel3 = "C3-" + File.name;

run("Split Channels");
selectImage(channel2);
//run("Brightness/Contrast...");
run("Enhance Contrast", "saturated=0.35");
run("Apply LUT");
run("Subtract Background...", "rolling=200");
selectImage(channel1);
//run("Brightness/Contrast...");
run("Enhance Contrast", "saturated=0.35");
run("Apply LUT");
```

```
run("Subtract Background...", "rolling=250");

//merge
run("Merge Channels...", "c1=[C1-"+File.name+"] c2=[C2-"+File.name+"] c3=[C3-"+File.name+"]
create keep");
run("RGB Color");
//[remove this and // if adding scale bar] run("Scale Bar...", "width=100 height=50 thickness=20
font=30 horizontal");
run("Images to Stack", "use");
run("Make Montage...", "columns=4 rows=1 scale=1");
waitForUser("done");
close("*");
```

4.2.2 PeptiGel charge calculation

The charge of each gel was calculated using benchling.com, which uses the pKa of the amino acid residues that make up a peptide to accurately determine the average charge of a peptide. The charge of each gel was also reported by the supplier, cell guidance systems, and was calculated as follows:

$$Charge = K - E$$

Where K is the number of lysine residues, and E is the number of glutamic acid residues (see **Table 4.2**).

Table 4.2 PeptiGel charge reported by Cell guidance systems and calculated using benchling.

PeptiGel	Reported charge	Calculated charge
Alpha 1	0	-0.24
Alpha 2	+1	0.76
Alpha 2 RGD	+1	0.96
Alpha 4	+2	1.76
Alpha 7	-1	-1.15
Delta 1	0	-0.24

4.2.3 Model assembly with HSCs or THP-1s

Models were assembled as described (see **2.2.2**). If HSCs were included, 6 days after MSC seeding HSCs were thawed and incubated overnight at $5x10^4$ cells/mL in IMDM + cytokines in a 24 well plate. The next day HSCs were counted and resuspended at $5x10^4$ cells/mL to account for any cell loss. All 2% DMEM was removed from the model niche and replaced with 150 µL HSC suspension. If THP-1s were used instead, the process was identical, except young (passage <20) THP-1s were used instead and were often in culture in 10% RPMI for over a week prior to addition to the model.

4.2.4 Nestin qPCR

4.2.4.1 Isolating cell lysate from PeptiGels

Cells were seeded in coated 24 well TCP plates prepared as per model preparation. 6 or 9 days after cell seeding, pronase (Merck, 10165921001) was diluted in sterile water to 2 mg/mL. If not used immediately, pronase solution was stored at 4°C for up to two weeks. Prior to use, an aliquot of pronase was warmed to 37°C. 800 µL of pronase was added to each well, and the plate incubated for 20 min. The resultant solution was then aspirated and added to 400 µL trizol (Invitrogen, 15596026) in a 2 mL eppendorf tube in a fume hood. 400 µL RLT buffer (part of RNeasy Micro Kit from Invitrogen, 74004) was then added to each well. The wells were thoroughly scraped with pipette tips to break up any remaining gel and cells. The resultant mixture was then added to the trizol mixture. The samples were stored at -80°C for up to two weeks before processing.

4.2.4.2 RNA extraction

All steps were performed in a fume hood. Samples were thawed if frozen. 320 µL of chloroform was added to each sample. Samples were incubated for 2-3 minutes, then centrifuged at 12000 g at 4°C for 15 min. The aqueous phase was isolated. 800 µL isopropanol (ThermoFisher scientific, 149320025) was added to each sample. Samples were incubated for 10 min at 4°C, then centrifuged for 10 min at 12000 g at 4°C. The supernatant was discarded and the pellet resuspended in 1600

µL 75% ethanol. The samples were vortexed then centrifuged at 7500 g 4°C for 5 min. The supernatant was discarded and 20 µL RNAse-free water used to resuspend the pellet. The samples were then further purified by following the RNeasy Micro Kit (Invitrogen, 74004) manufacturer's protocols, with 350 µL buffer RLT added to the resuspended RNA in step 1. After processing, a NanoDrop 2000c (ThermoFisher scientific, ND-2000) was used to determine samples' RNA concentrations, and the samples diluted to ~2.5 ng/µL using RNAse-free water.

4.2.4.3 RNA quantification

The QuantiNova SYBR Green PCR Kit (Qiagen, 208052) was used according to manufacturer's protocols with a 7500 Fast Real-Time PCR System (ThermoFisher Scientific, 4351106) to determine RNA levels. The primers used were: GAPDH (TCAAGGCTGAGAACGGGAA) and nestin (TCAAGATGTCCCTCAGCCTGGA). The GAPDH housekeeping gene's expression was used to normalise nestin expression.

4.2.5 Western blot

Cells were seeded in coated 24 well TCP plates prepared as per model preparation (see **2.2.2**). RIPA buffer was made up the day before protein extraction (see **Table 4.3**). 7 days after cell seeding, media and as much gel as possible was removed before the wells were washed with ice cold PBS. 100 µL RIPA buffer was added to each well. The wells were scraped with pipette tips. The RIPA buffer and cell lysate was then transferred to a 1.5 mL Eppendorf tube and left on ice for 30 min, while being vortexed every 5-10 min.

Table 4.3 RIPA buffer components.

Reagent	Supplier
50 mM Tris pH 8.0	Sigma-Aldrich, T3253
150 mM NaCl	VWR chemicals, 27810.295
1% Triton-X	Sigma-Aldrich, T9284-100ML
0.5% Sodium deoxycholate	Sigma-Aldrich, 30970-25G
0.1% SDS	Sigma-Aldrich, L-4509
Protease and phosphotase inhibitor tablets	ThermoFisher scientific, A32959

The mixture was then lysed in Laemmli buffer (ThermoFisher scientific, 84788) (Laemmli, 1970), separated by 3-8% Tris acetate (ThermoFisher scientific, EA0375BOX), and transferred to a PVDF membrane (ThermoFisher scientific, LC2002) using a mini gel tank system (ThermoFisher scientific, A25977), alongside SeeBlue Plus 2 Prestained Standard protein ladder (Invitrogen, LC5925). Membranes were blocked in 5% milk for 1 h at RT before staining. Membranes were cut into strips for each antibody used and stained separately. Primary antibodies against SCF (abcam, ab64677) and GAPDH (abcam, ab128915) were used, as well as anti-rabbit HRP-linked secondary (Cell Signalling technology, 93702). Protein bands were visualised using chemiluminescent western blot reagents (ThermoFisher scientific, 32106) with a Li-Cor Odyssey M. Images were prepared with FIJI.

4.2.6 HSC in niche flow cytometry

When seeding HSCs in a model niche, any leftover cells were used for a day 0 control and analysed immediately with flow cytometry (see **2.2.4**). After 5 days in the model niche, HSCs were removed and analysed by flow cytometry. The antibodies and stains used for basic HSC characterisation were: sytox blue (ThermoFisher scientific, S34857), CD45 (Miltenyi Biotec, 130-110-635), Lineage cocktail (Lin) (ThermoFisher scientific, 22-7778-72), CD34 (Miltenyi Biotec, 130-113-176). For LT-HSC characterisation: sytox blue (ThermoFisher scientific,

S34857), CD45 (Miltenyi Biotec, 130-110-635), Lin (ThermoFisher scientific, 22-7778-72), CD34 (Miltenyi Biotec, 130-113-176), CD38 (ThermoFisher scientific, 25-0388-42), CD90 (Invitrogen, 56-0909-42), CD45RA (ThermoFisher scientific, 63-0458-42). For extended haematopoietic cell characterisation: sytox blue (ThermoFisher scientific, S34857), CD45 (Miltenyi Biotec, 130-110-635), CD16 (ThermoFisher scientific, 69-0168-42), CD41/61 (ThermoFisher scientific, MA5-44123), CD7 (ThermoFisher scientific, 46-0078-42), CD34 (Miltenyi Biotec, 130-113-176), CD38 (ThermoFisher scientific, 25-0388-42), CD90 (Invitrogen, 56-0909-42), CD45RA (ThermoFisher scientific, 63-0458-42).

4.2.7 THP-1 in niche flow cytometry

THP-1s were analysed by flow cytometry identically to HSCs. The antibodies used were: sytox blue (ThermoFisher scientific, S34857), CD34 (Miltenyi Biotec, 130-113-176), CD38 (ThermoFisher scientific, 25-0388-42).

4.3 Results and discussion

4.3.1 The effect of PeptiGels on MSCs

Various factors were investigated to determine the optimum PeptiGel formulation for promoting a niche-like phenotype in MSCs (see **Figure 4.2**)

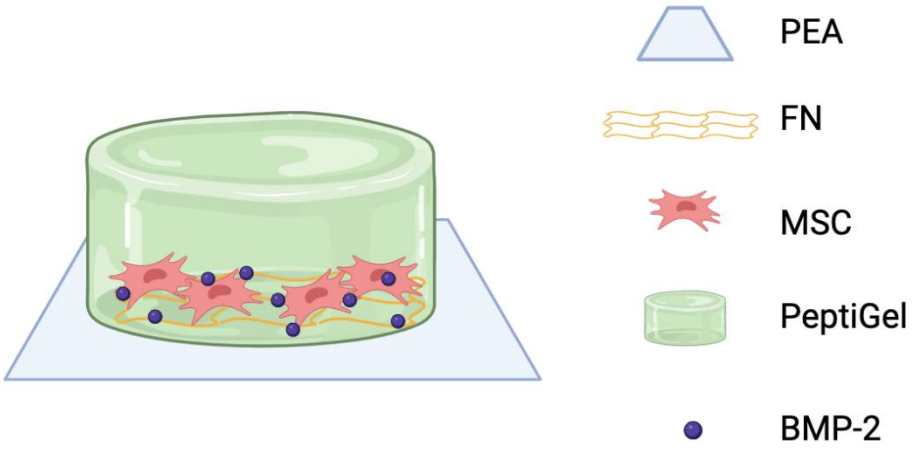

Figure 4.2 Schematic of model BM niche used for optimisation to produce desired MSC phenotype*. Collagen and no gel conditions in which the PeptiGel was replaced with collagen gel or no gel was used respectively were also used. Created with BioRender.com.*

4.3.1.1 Nestin expression

Nestin expression was quantified using confocal IF microscopy and CTCF analysis. Various PeptiGels conditions, as well as no gel and collagen controls, were included. No gel and collagen controls were included as the former tested if the gels were necessary for any observed effect, and the latter was a well-established system known to promote a niche-like phenotype (Donnelly et al., 2024) (see **Figure 4.3**).

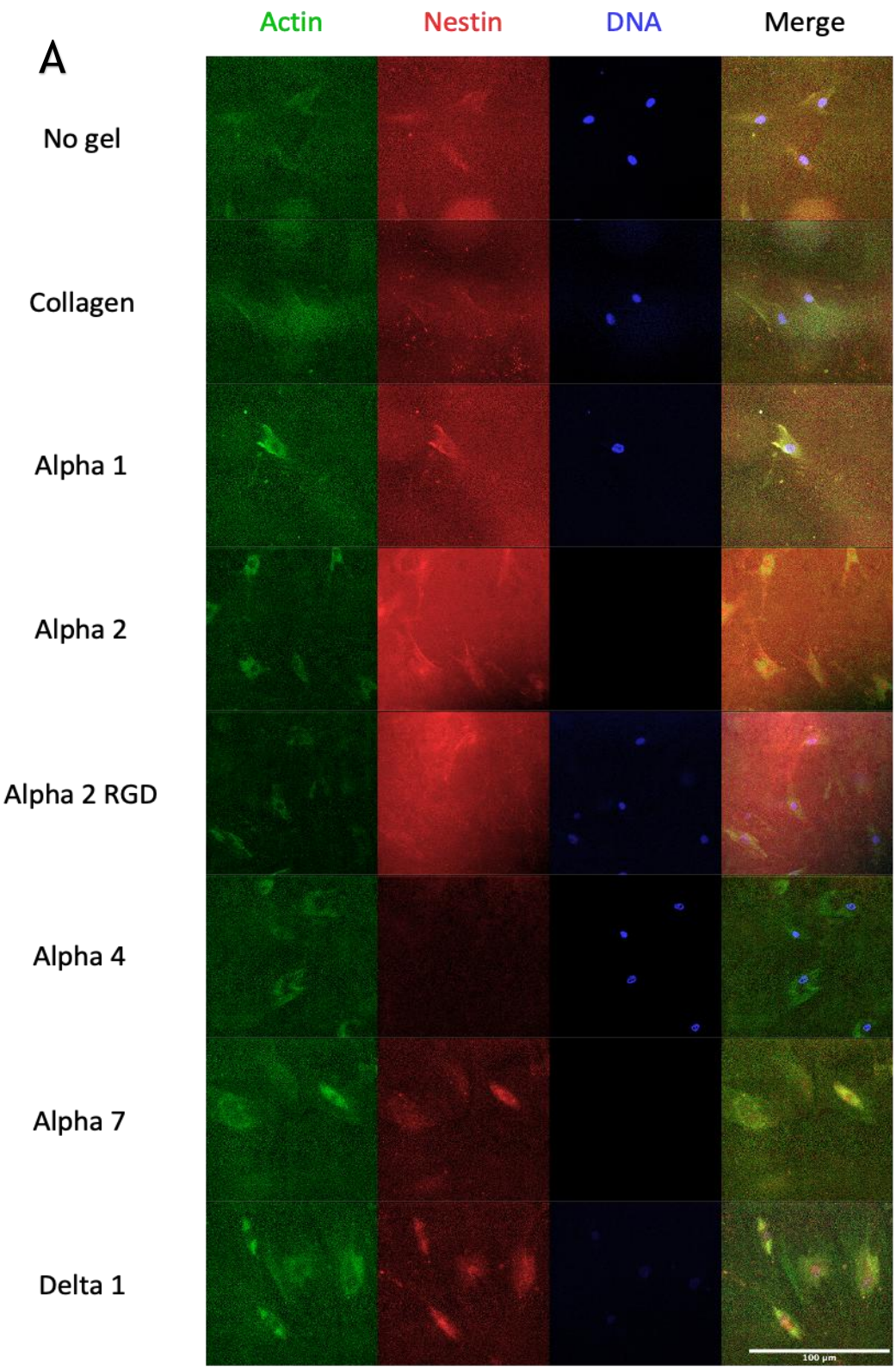
A
Actin
Nestin
DNA
Merge
No gel
Collagen
Alpha 1
Alpha 2
Alpha 2 RGD
Alpha 4
Alpha 7
Delta 1
100 µm

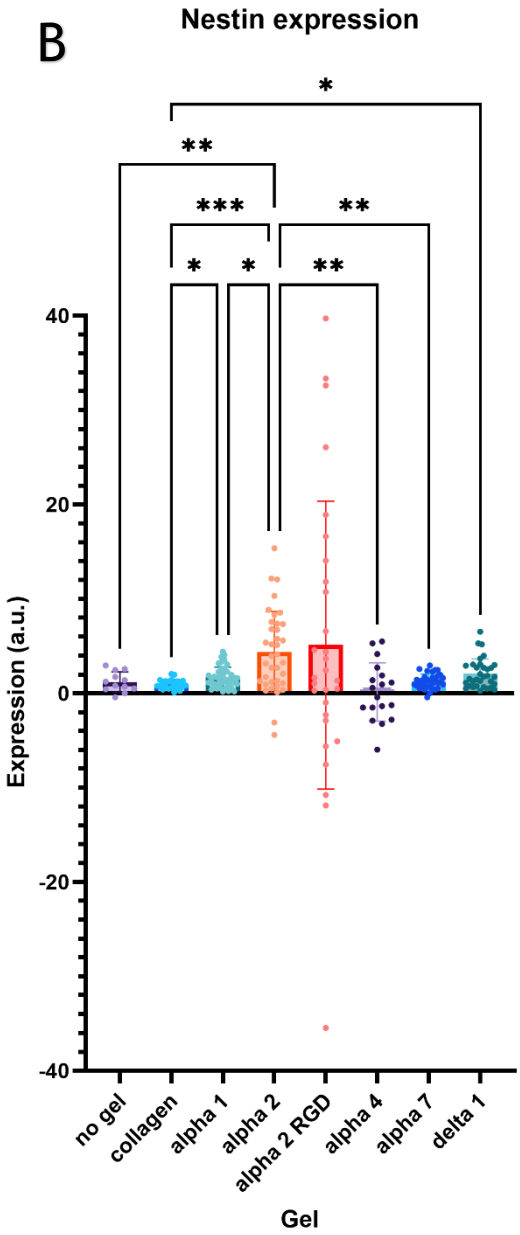

Figure 4.3 Various PeptiGels' effects on MSC nestin expression quantified by IF microscopy. *Confocal IF microscopy was used to image promo MSCs grown under various PeptiGels, as well as controls in which collagen gel and no gel were used. (**A**) Representative confocal IF microscopy images of stained MSCs. Scale bar is 100 µm. FIJI was used for image preparation. (**B**) FIJI and CTCF analysis were utilised to analyse the expression level of nestin. Graphs show mean ± SD. Statistics by one-way Brown-Forsyth and Welch ANOVA followed by Dunnett T3 multiple comparison test. *p < 0.05, **p < 0.01 and ***p < 0.001. Non-significant not shown. n=3 technical replicates, with ~10 cells per replicate analysed.*

This data suggested that the alpha 1, alpha 2, and delta 1 gels strongly promoted nestin expression, with significant differences observed between these conditions and the collagen condition, though only the alpha 2 gel produced a significant increase compared to the no gel control. The alpha 2 RGD condition also strongly promoted nestin expression, but this effect was highly variable so yielded an insignificant result. The increase observed in alpha 2 and alpha 2 RGD were also dubious due to the high level of background seen when imaging cells in these conditions, though this should have been accounted for when performing CTCF analysis. Unexpectedly, the collagen gel condition did not promote nestin expression more strongly than the no gel condition, contrary to previous results (Donnelly et al., 2024).

4.3.1.2 SCF expression

The effect of the PeptiGels on SCF expression was also quantified using confocal IF microscopy following brefeldin treatment (see **Figure 4.4**).

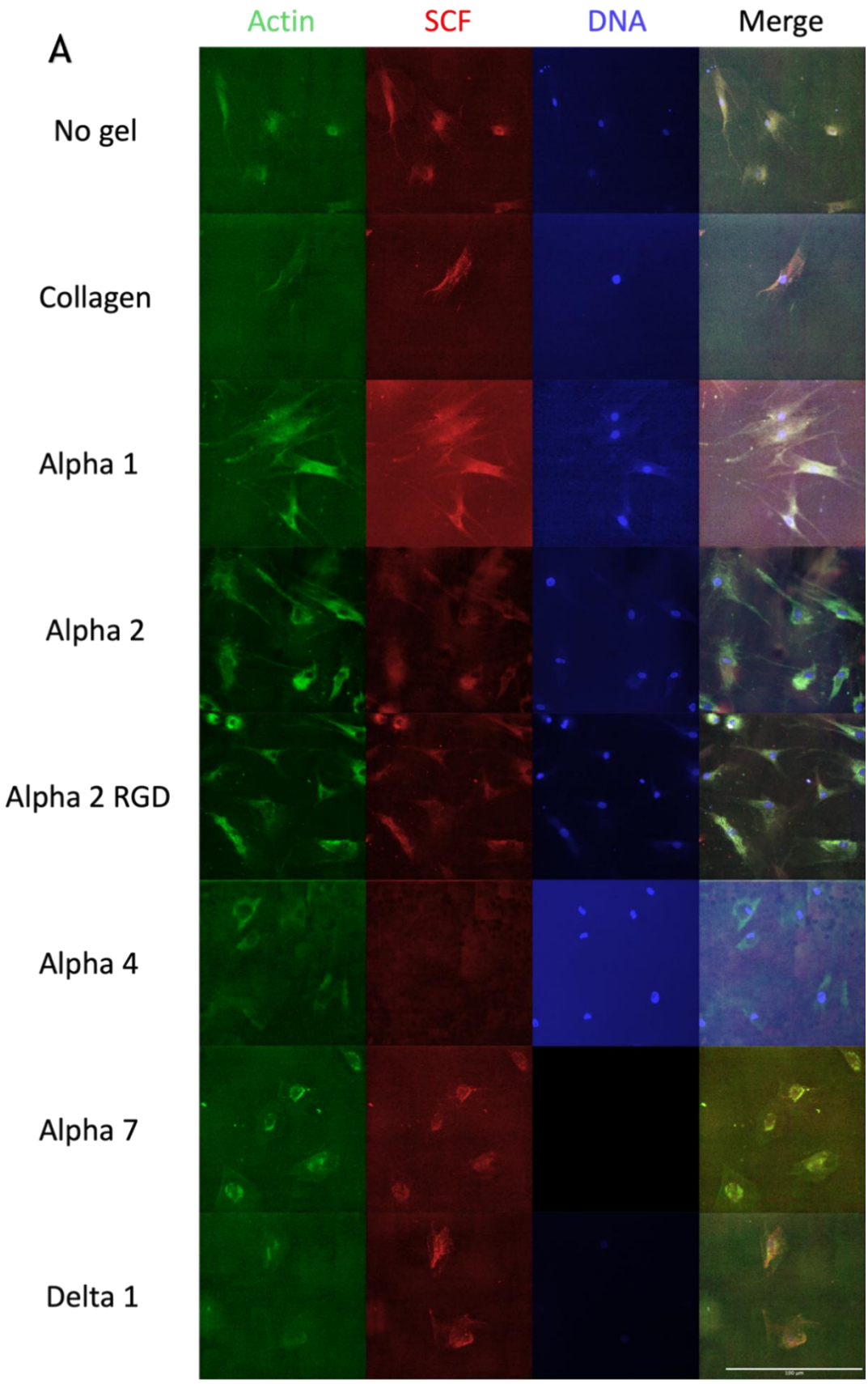

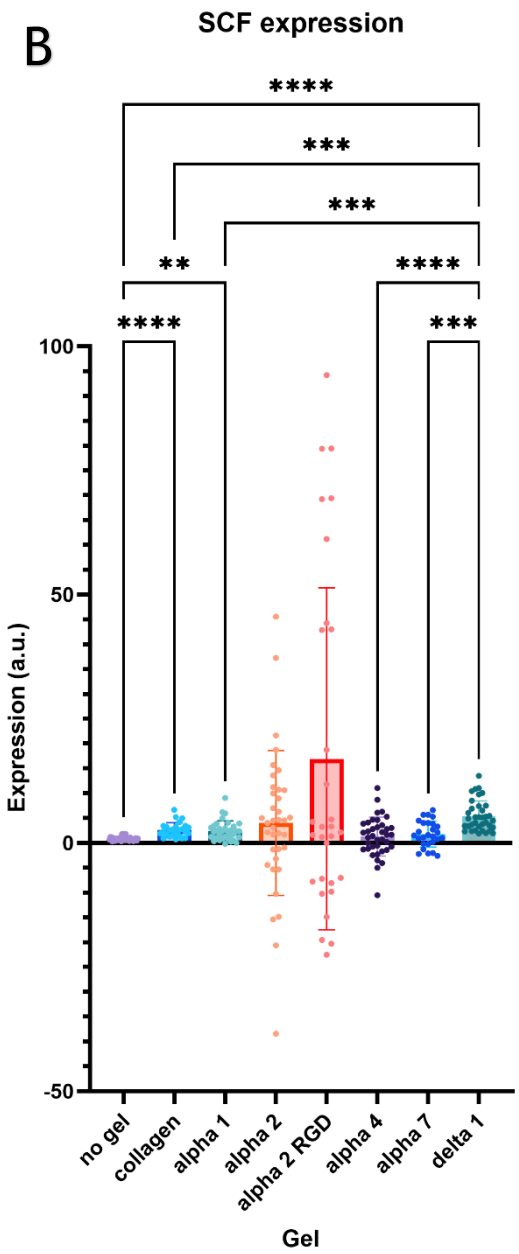

Figure 4.4 Various PeptiGels' effect on MSC SCF expression quantified by IF microscopy. *Confocal IF microscopy was used to image promo MSCs grown for 7 days under various PeptiGels, as well as controls in which collagen gel and no gel were used. (**A**) Representative confocal IF microscopy images of stained MSCs. Scale bar is 100 µm. FIJI was used for image preparation. (**B**) FIJI and CTCF analysis were utilised to analyse the expression level of SCF. Graphs show mean ± SD. Statistics by Kruskal-Wallis followed by Dunn's multiple comparison test. **p < 0.01, ***p < 0.001 and ****p < 0.0001. Non-significant not shown. n=3 technical replicates, with ~10 cells analysed per replicate.*

A similar expression pattern in SCF and nestin was observed in most conditions, with SCF expression significantly enhanced by the alpha 2, alpha 2 RGD and delta 1 conditions, as well as the collagen control. Alpha 1 also increased expression, though this change was not statistically significant. Furthermore, the delta 1 condition promoted SCF expression significantly more than the collagen and alpha 1 conditions, highlighting this gel's potential for promoting the desired phenotype.

MSCs grown under the alpha 2 RGD gel had the highest mean expression of both nestin and SCF expression of all conditions tested. However, a very high level of variability prevented this gel from being selected. Despite this, the alpha 2 RGD gel outperformed base alpha 2 on average. These gels were identical, other than 20% of peptides in the RGD version, which incorporated an RGD tail. This implied

that functionalising PeptiGels with endogenous ECM components has the potential to promote the niche-like phenotype in MSCs, likely due to the increased binding and interaction of MSCs with functionalised gels, which increases biomimicry (Romani et al., 2021). Previous research has also shown that other forms of functionalisation can replicate ECM GF capture and release mechanisms (Lienemann et al., 2020).

The difference between delta 1 and alpha 1 is also interesting, as these gels have identical amino acid sequences, but different pH values; alpha 1 is pH 3-4, delta 1 is pH 9. These pHs were only experienced by the MSCs briefly, as the gel conditioning step of model assembly should have reverted both gels' pHs closer to the physiological pH of BM (Yeh et al., 2022). The improved phenotype of delta 1 implies that a more alkaline microenvironment is beneficial for stimulating the desired phenotype, though the difference between these gels is marginal. Since the pH of mesenchymal cells' microenvironment has been shown to affect MSC proliferation, self-renewal and gene expression (Fliefel et al., 2016), the effect of pH in model BM niches may warrant further investigation.

4.3.1.3 Viability

The delta 1 and alpha 2 conditions were selected as the two most promising candidates. The viability of MSCs in these systems, as well as no gel and collagen control systems, was tested (see **Figure 4.5**).

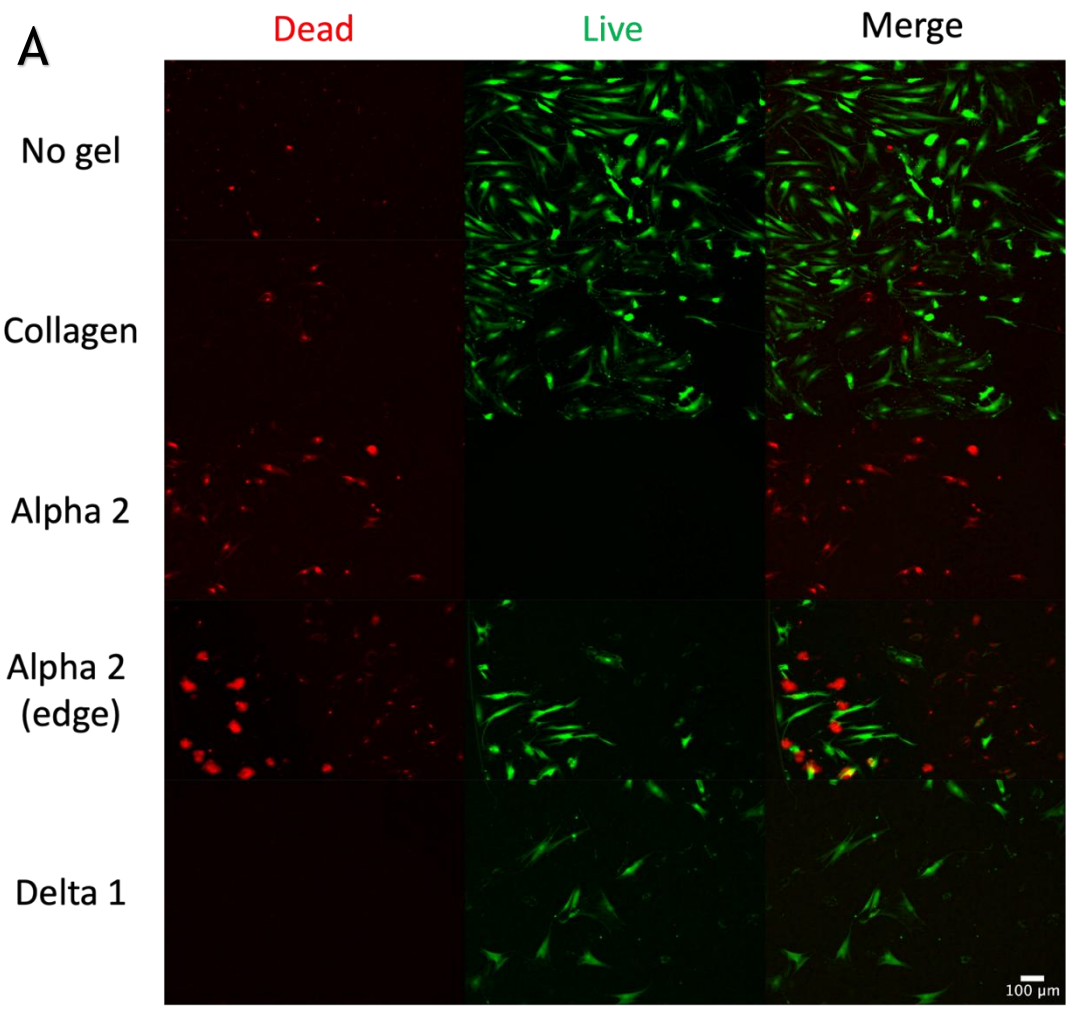

Figure 4.5 Viability of MSCs in various systems. *IF microscopy was used to image promo MSCs grown for 7 days in various conditions following ethidium homodimer and calcein AM staining. (**A**) Representative images of stained MSCs. Scale bar is 100 µm. FIJI was used for image preparation. (**B**) The percentage of live cells in each image was determined using FIJI, with each image represented by a data point. Graphs show mean ± SD. Statistics by Kruskal-Wallis followed by Dunn's multiple comparison test. **p < 0.01, ***p < 0.001 and ****p < 0.0001. Non-significant not shown. n=3 technical replicates with 4 or 5 images analysed per replicate.*

The no gel and collagen control systems both had very high viability. However, despite reports that similar cell types cultured with these gels have comparable viability to cells cultured with collagen (Castillo Diaz et al., 2016; Faroni et al., 2019), the PeptiGel systems tested both exhibited a significant drop in viability, though this was less pronounced in the delta 1 system. This was presumed to be due to the electrostatic charge of the peptides within the gel, which have been shown to affect mesenchymal cells' proliferation, viability, and differentiation (He et al., 2022). Although the mechanism for this phenomenon has not been determined, possibilities include interactions with cells' membranes, and localised pH. The reduced impact of the more neutral (-0.27 net charge at pH 7) delta 1 gel compared to the more strongly and oppositely charged alpha 2 (+0.76 net charge at pH 7) supported this hypothesis. Another explanation could be limited nutrient transfer to cells due to differences in the gels' structure, such as pore size, which would explain the higher level of viability seen in MSCs seeded under alpha 2 that resided around the edge of wells. Interestingly, this edge effect was not seen in delta 1 conditions, suggesting charge also played a role, possibly influencing ionic nutrients' localisation. Future work could elucidate the cause of the observed viability changes by investigating the effect of material charge and pore size on MSC viability more thoroughly.

The death observed in the models' MSCs could present an issue, as it likely caused reduced production of soluble factors, potentially lowering the usefulness of these cells as an HSC feeder layer. Therefore, the delta 1 gel was selected as the best PeptiGel candidate to carry forwards due to its promotion of the desired phenotype and relatively low MSC mortality. Ongoing research strives to improve the biocompatibility of these gels by incorporating elements of the *in vivo* microenvironment (King et al., 2016).

4.3.1.4 Gel stiffness

The exact reason for delta 1's effect on MSCs is unknown, however the gel's mechanical properties likely played a role. To investigate this, various concentrations of delta 1 had their effect on MSCs' phenotypes investigated using IF microscopy (see **Figure 4.6**).

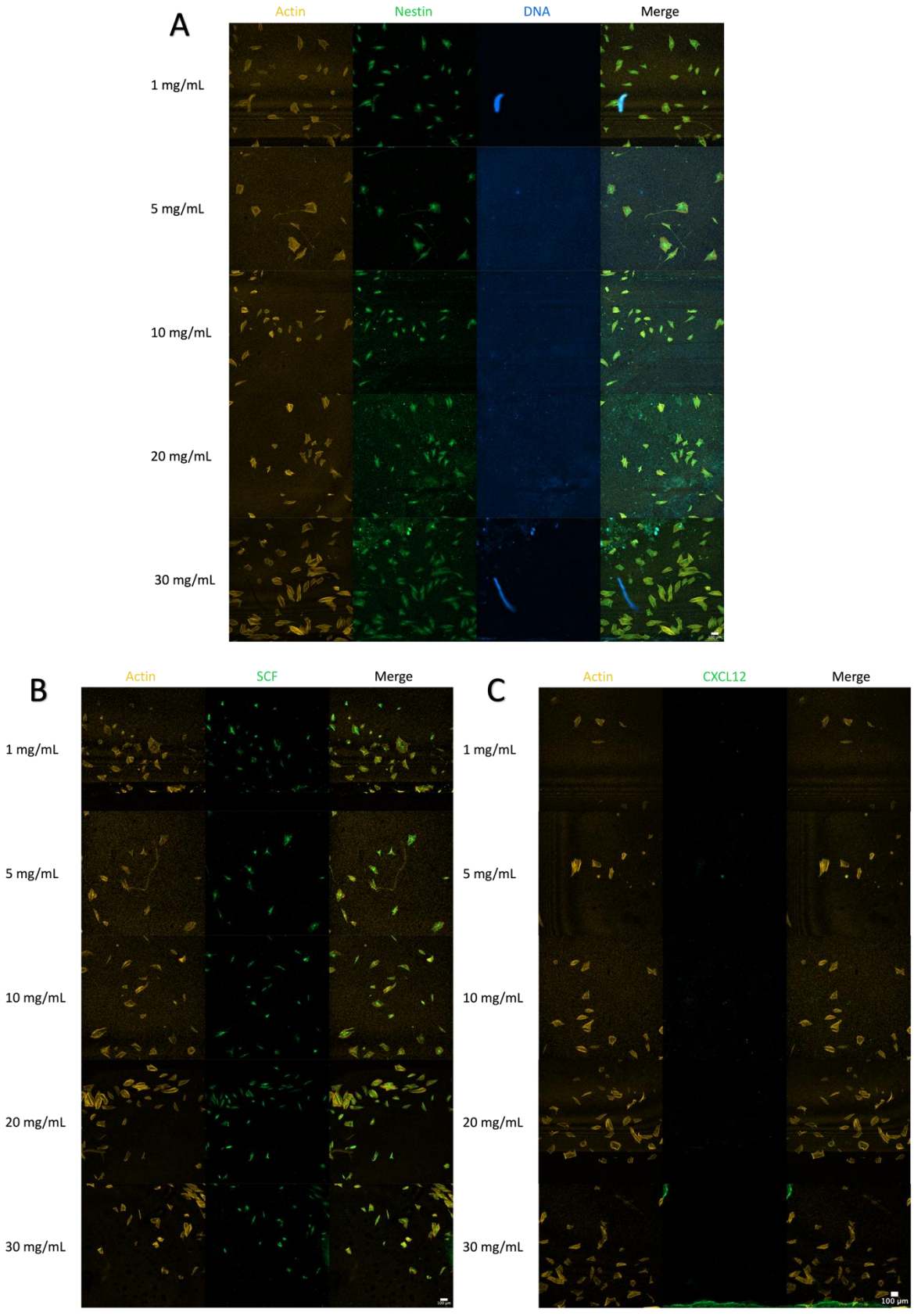
A
Actin
Nestin
DNA
Merge
1 mg/mL
5 mg/mL
10 mg/mL
20 mg/mL
30 mg/mL
B
Actin
SCF
Merge
1 mg/mL
5 mg/mL
10 mg/mL
20 mg/mL
30 mg/mL
C
Actin
CXCL12
Merge
1 mg/mL
5 mg/mL
10 mg/mL
20 mg/mL
30 mg/mL
100 µm

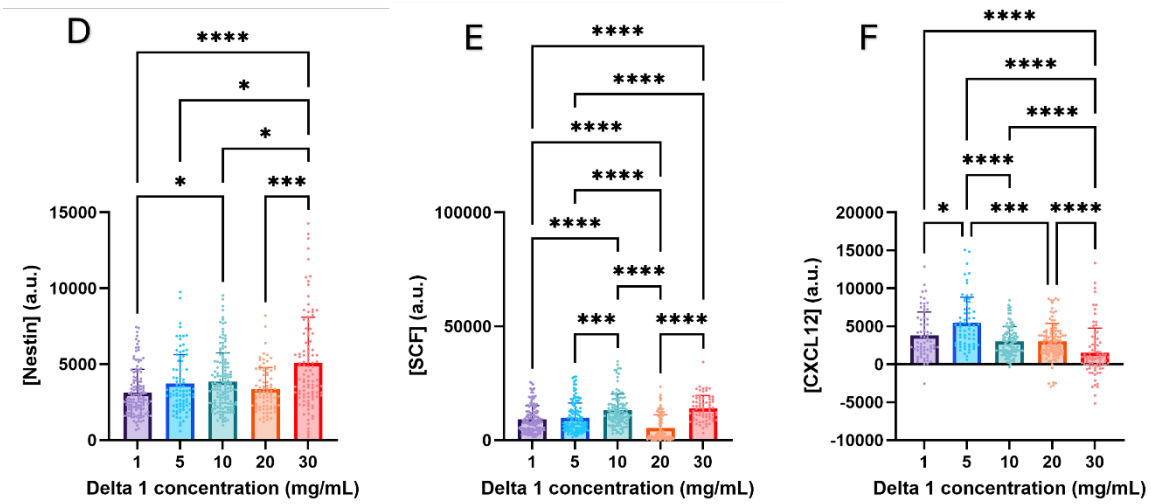

***Figure 4.6 Effect of Delta 1 concentration on MSC phenotype**. Confocal IF microscopy was used to test (**D**) nestin, (**E**) SCF, and (**F**) CXCL12 expression in MSCs after culture for 7 days under PeptiGels diluted to various concentrations. Representative images of MSCs with stained (**A**) nestin, (**B**) SCF, and (**C**) CXCL12 are also shown. Scale bars are 100 µm. Graphs show mean + SD. Statistics by Kruskal-Wallis followed by Dunn's multiple comparison test. *p < 0.05, ***p < 0.001 and ****p < 0.0001. Non-significant not shown. n=3 technical replicates, ~10 cells analysed per replicate.*

The undiluted (30mg/mL) delta 1 caused the biggest increase in nestin and SCF expression, and a high level of CXCL12 expression. This was likely due to the mechanical and physical properties of the cellular microenvironment, which are known to affect cells' phenotype (Chaudhuri et al., 2020; X. Chen et al., 2020; Jansen et al., 2015) and were altered by dilution, as discussed earlier. Interestingly, the undiluted gel, which was shown to be generally stiffer and more elastic than diluted gel, most strongly promoted the desired phenotype. The MSCs likely perceived the stiffer gel, as well as the stiff, FN coated polymer coverslip they were initially seeded on, as an arteriolar niche, which natively resides near the stiff endosteum (Coutu et al., 2017) and is enriched in FN (Lee-Thedieck et al., 2022; Nilsson et al., 1998). This would explain the increased expression of nestin (Asada et al., 2017; Kunisaki et al., 2013; B. O. Zhou et al., 2014), as well as SCF and CXCL12 (Mendelson & Frenette, 2014). Adoption of an arteriolar niche phenotype by MSCs in the model system boded well for maintenance of HSCs, as this niche is known to act as a quiescent reservoir of naïve LT-HSCs (Pinho & Frenette, 2019).

However, there was not a direct correlation between concentration and phenotype, with a similar increase at 5 and 10 mg/mL compared to 1mg/mL,

followed by a decrease at 20 mg/mL, and a subsequent dramatic increase at 30 mg/mL seen across all markers. The inconsistent peptide distribution caused by the dilution technique used may have played a role, however these results suggest a more complex interaction between peptide concentration, the mechanical properties this affects, and MSC phenotype, and possibly suggest that an intermediate stiffness mimicked the sinusoidal niche (Coutu et al., 2017). Future work could seek further characterisation of PeptiGels' mechanical properties, tweaking them by introducing different peptide sequences, using large side chains to disrupt fibril alignment and formation, or using alternative suspension fluid of the dried peptides, then measuring these changes' effects on cells. However, this was beyond the scope of this project, and therefore undiluted (30 mg/mL) delta 1 PeptiGel was selected as the most optimum dilution.

4.3.2 Various iterations of the model BM niche and their effects on MSCs

To identify the optimum conditions for stimulating the desired niche-like phenotype in MSCs, various iterations of the model BM niche were tested.

4.3.2.1 Coatings and gels

All possible combinations of coatings and gel combinations (from amongst the selected delta 1 PeptiGel, collagen, and no gel controls) were tested by confocal IF microscopy to determine their effects on nestin expression (see **Figure 4.7**).

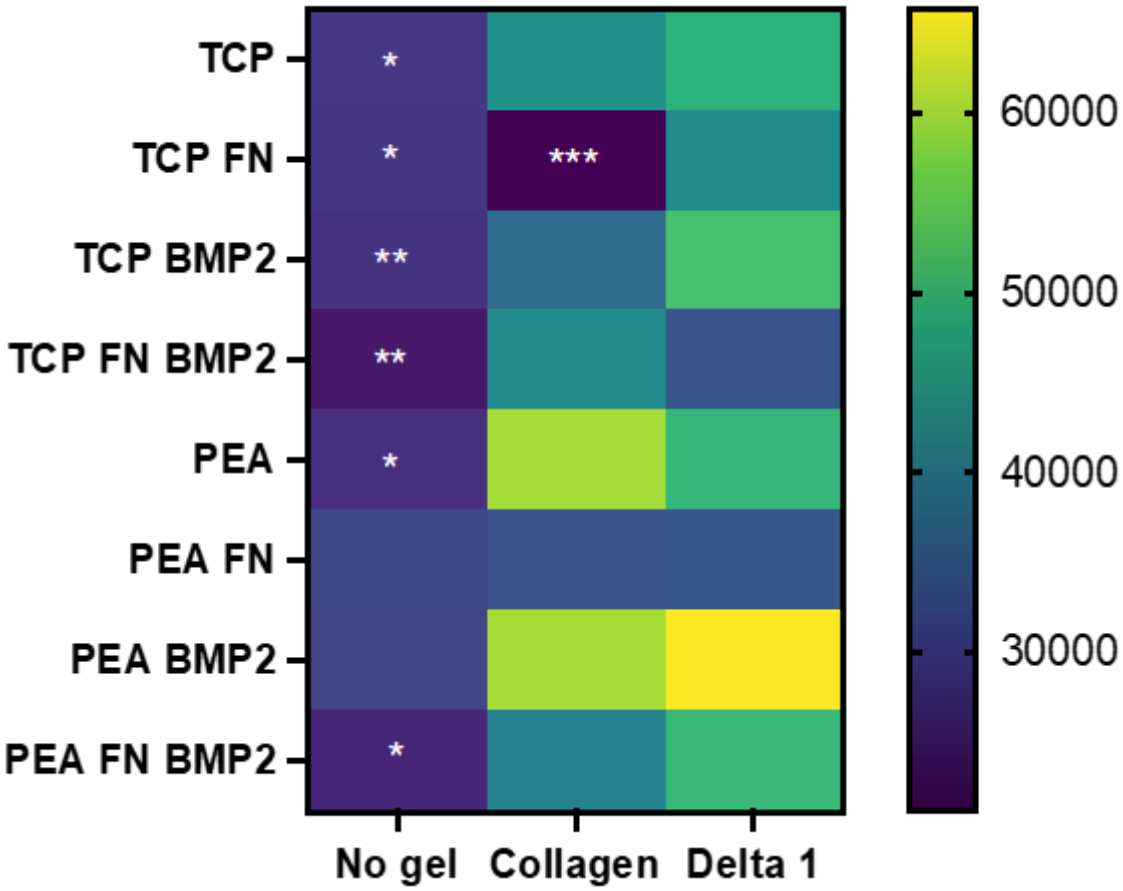

Figure 4.7 Various model BM niche iterations' effect on MSC nestin expression. *Confocal IF microscopy was used to determine nestin expression in MSCs cultured in various conditions for 7 days. See* ***Supplementary Figures 1-3*** *for representative images. Statistics by two-way ANOVA followed by Tukey multiple comparison test. *p < 0.05, **p < 0.01 and ***p < 0.001. Non-significant not shown. *s indicate significance compared to the delta 1 PEA FN BMP2 condition (bottom right). Heatmap shows mean. n=3 technical replicates with ~10 cells per repeat analysed.*

The gel and coating variables were both found to impact nestin expression significantly, and to interact significantly as well (Column factor (gel) p-value ****, row factor (coating) p-value ****, interaction p-value ***). In addition, the delta 1 PEA FN BMP2 condition promoted nestin expression more than most conditions tested, with no statistical difference detected when comparing this system with those that had higher mean nestin expression. Taken together, these results imply that the PEA FN BMP2 system was compatible with delta 1 gel, and was an appropriate choice for stimulating the desired phenotype in MSCs, corroborating previous results (Donnelly et al., 2024; Sweeten, 2019). Interestingly, the PEA BMP2 and PEA systems with collagen or delta 1 also increased nestin expression. This may have been part of a stress response, which nestin expression has

previously been linked to (Donnelly et al., 2024a; Sahlgren et al., 2006), and which could be associated with the decreased cell spreading seen in these systems.

4.3.2.2 Media types

Various media types were tested to determine their effect on MSCs' nestin expression and viability in a model BM niche using IF microscopy (see **Figure 4.8**).

Media had a marginal effect on cells' nestin expression, with 10% RPMI found to encourage increased expression compared to 2% DMEM. This was in spite of 2% DMEM being used previously to promote a niche-like phenotype (Donnelly et al., 2024). As the change was small, and 2% DMEM was an established media for model niche systems, it was used in some subsequent experiments, though the use of different media formulations could be explored in future work. 2% DMEM and IMDM + cytokines had indistinguishable effects on MSCs' nestin expression. This was important as both these media types were used in subsequent model niche experiments.

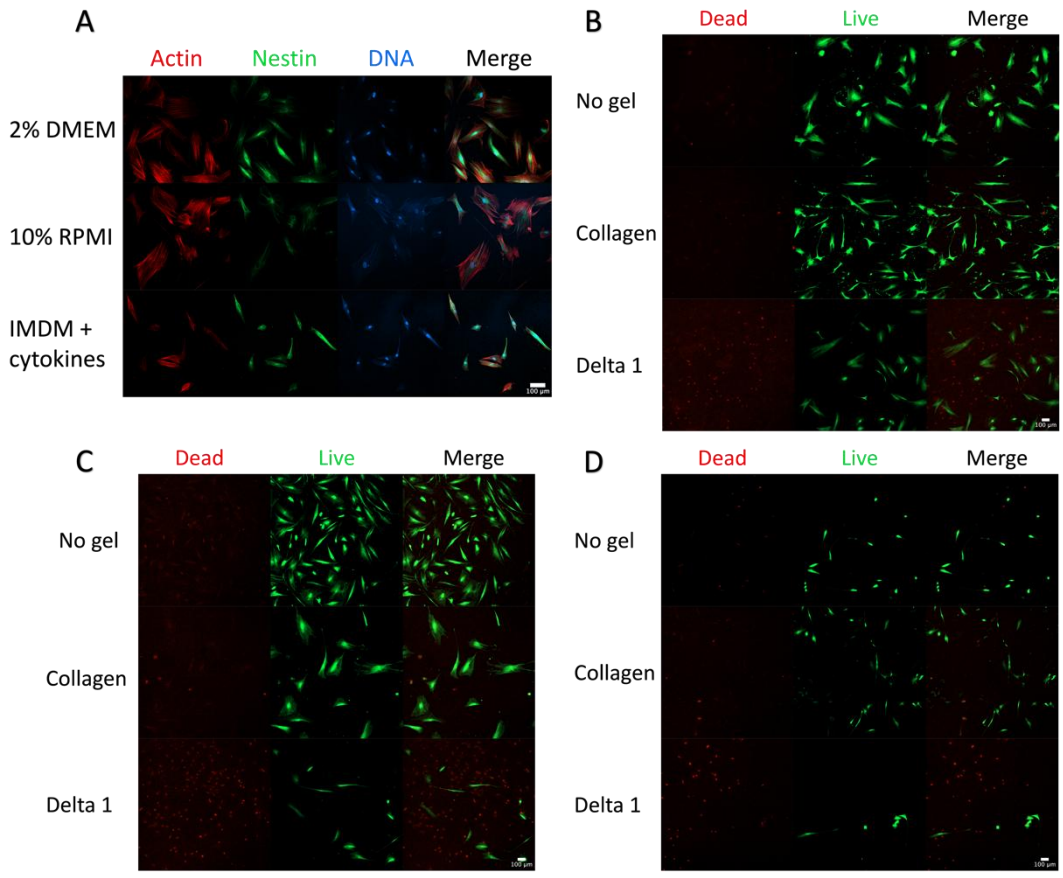

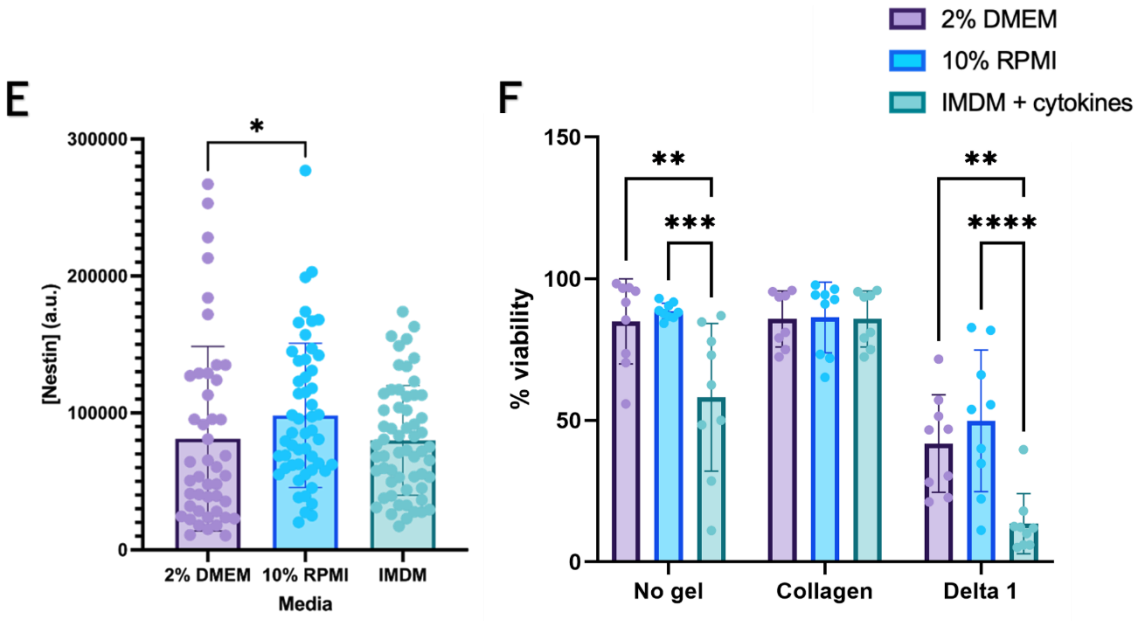

***Figure 4.8 Media effects on MSCs**. MSCs were seeded in various systems and cultured for 7 days with 2% DMEM, before this media was replaced with appropriate media for each condition. The effect of these media on MSC (**E**) nestin expression and (**F**) viability was tested using confocal IF microscopy. Note that all conditions in (**E**) were with no gel. Representative images for (**E**) are shown in (**A**). Representative images for (**F**) are shown in (**B**) (2% DMEM), (**C**) (10% RPMI), and (**D**) (IMDM + cytokines). All scale bars are 100 µm. Graphs show mean ± SD. Statistics for (**E**) by Kruskal-Wallis followed by Dunn's multiple comparison test. n=3 technical replicates, with ~10 cells analysed per replicate. Statistics for (**F**) by two-way ANOVA followed by Tukey multiple comparison test. n=3 technical replicates with ~3 photos taken per repeat. *p < 0.05, **p < 0.01, ***p < 0.001 and ****p < 0.0001. Non-significant not shown.*

Viability was much more complex; as previously shown, delta 1 caused decreased viability compared to no gel and collagen controls (row factor (gel) p-value ****). However, the media used also impacted viability significantly in no gel and delta 1 conditions (column factor (media) p-value ****); IMDM + cytokines reduced it significantly. The inclusion of delta 1 and IMDM + cytokines also appeared to have a mild cumulative effect (interaction p-value *). As IMDM + cytokines was used in subsequent HSC/MSC co-culture experiments, this may have resulted in poorer MSC viability, and worse HSC maintenance. However, the IMDM + cytokine media is the gold standard for HSC culture (Donnelly et al., 2024) and was assumed to be essential. Therefore, it was deemed to still be appropriate. Future work could investigate alternative media formulae to maximise MSC and HSC viability, maintenance, and promotion of desired phenotype.

4.3.3 Finalised model's effect on MSCs

Following the discussed optimisation experiments, a model system using PEA FN BMP2 coatings, undiluted delta 1 PeptiGel, and 2% DMEM, referred to as the delta 1 niche, was selected, and rigorously tested to determine its effect on included MSCs. A similar collagen system, which used collagen in place of delta 1, and a no gel system which didn't use gels, were included as controls.

4.3.3.1 Marker expression

The stains used for confocal IF microscopy to assess marker expression in initial experiments were inconsistent in PeptiGel conditions, and a high level of background was observed. This was not seen in no antibody controls (data not shown), suggesting that the gels were being stained when the wells were prepared for imaging. Gels were removed in later experiments after fixation and before blocking by addition of cold PBS to avoid this (see **Figure 4.9**).

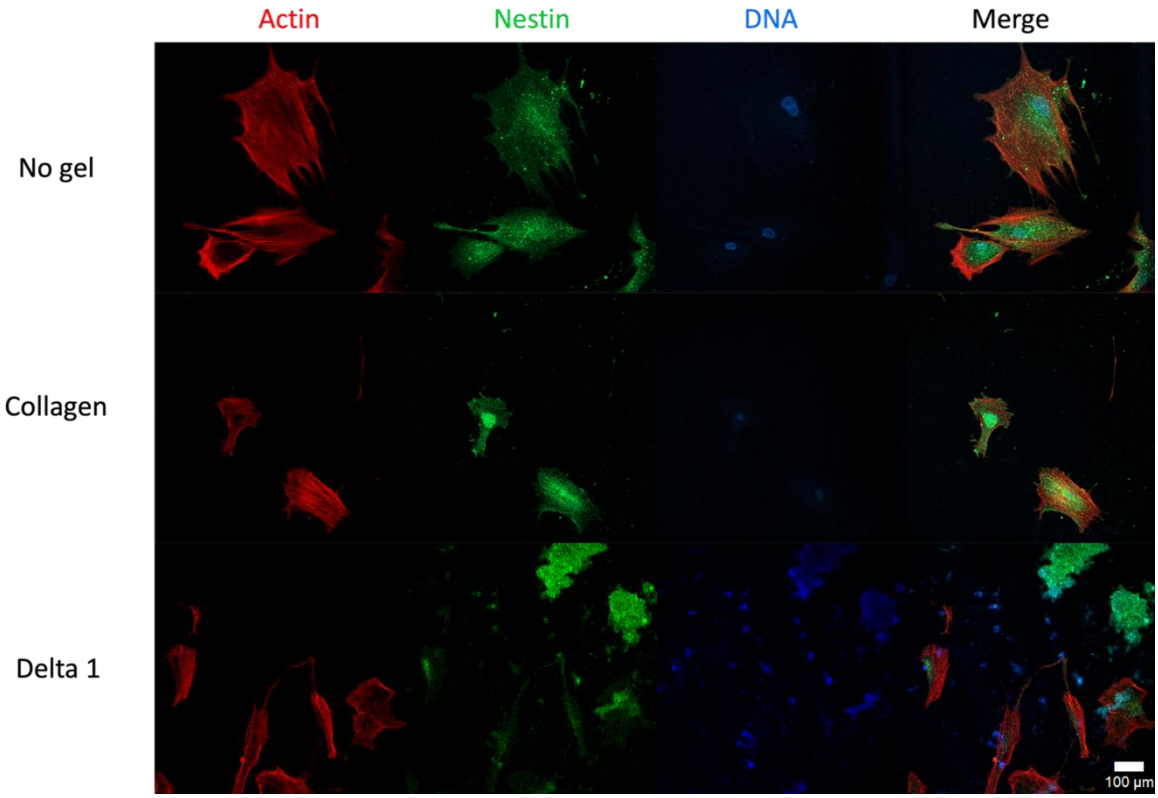

Figure 4.9 Representative confocal IF microscopy images of MSCs with nestin stained after optimisation. *The model systems were assembled, then on day 7 the cells were fixed and prepared for imaging using an optimised protocol. Scale bar is 500 µm. FIJI was used for image preparation.*

These adjustments visibly improved image quality, although some issues persisted, such as fragments of gel which remained and were stained in PeptiGel conditions, and non-specific HOESCHT staining in all gel conditions. To minimise the impact of these variables, only cells with negligible non-specific staining and gel remnant coverage were analysed, and possible overlapping cells which could not be separated without a nuclear stain were ignored.

The optimised delta 1 system was investigated rigorously with further IF microscopy experiments, alongside no gel and collagen controls, to confirm its effect on nestin expression in MSCs (see **Figure 4.10**).

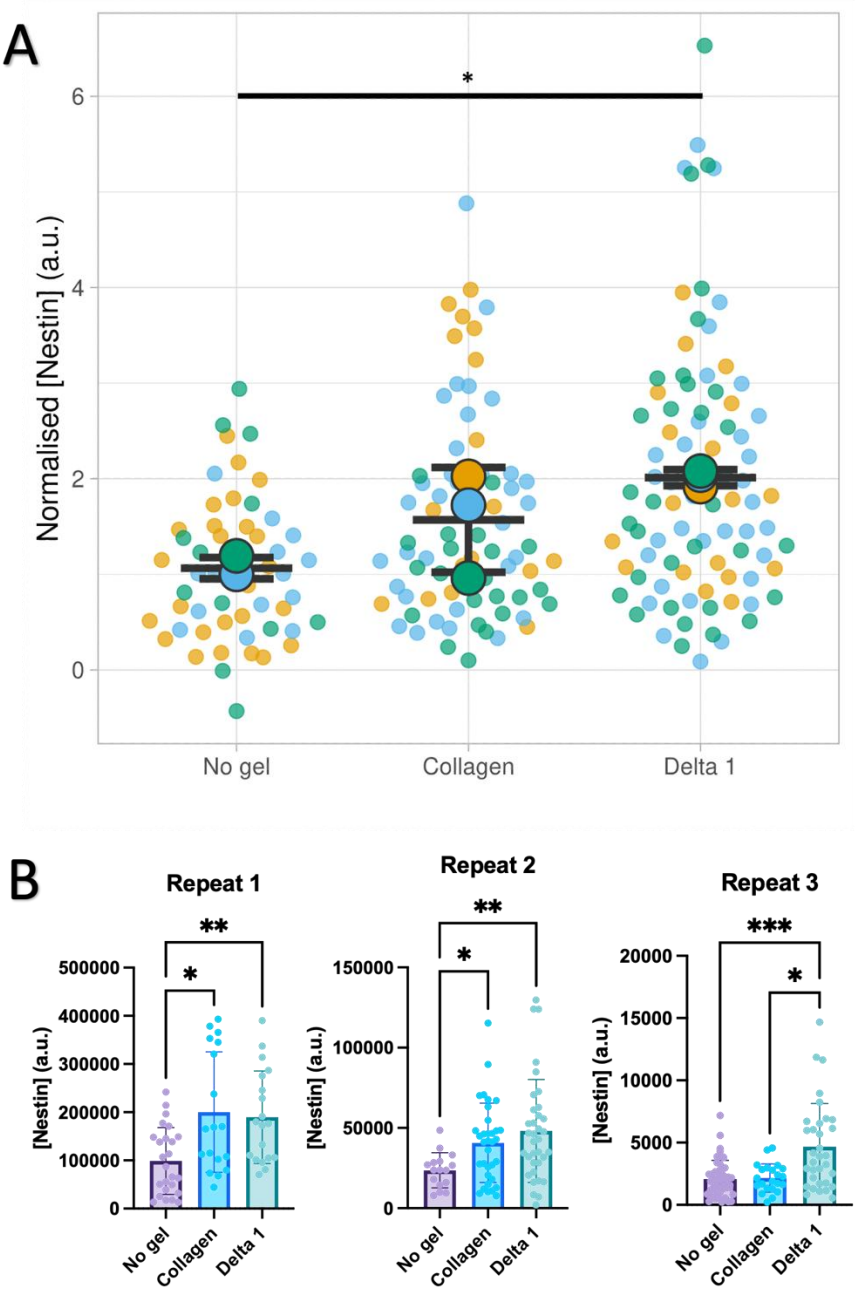

Figure 4.10 Nestin expression in select conditions tested with IF microscopy. *MSCs grown in model systems with no gel, collagen gel, or delta 1 gel had their expression of nestin investigated by IF microscopy. (**A**) Superplot of all biological repeats. Statistics by one-way ANOVA followed by Tukey multiple comparison test. (**B**) Individual repeats. Statistics by Kruskal-Wallis followed by Dunn's multiple comparison test. *p < 0.05, **p < 0.01 and ***p < 0.001. Non-significant not shown. In the superplot, orange data points represent repeat 1, blue represents repeat 2, green represents repeat 3. Graphs show mean ± SD. N=3 biological replicates, each consisting of n=3 or 4 technical replicates with ~10 cells per technical replicate analysed.*

In addition, SCF expression was tested by the same method (see **Figure 4.11**).

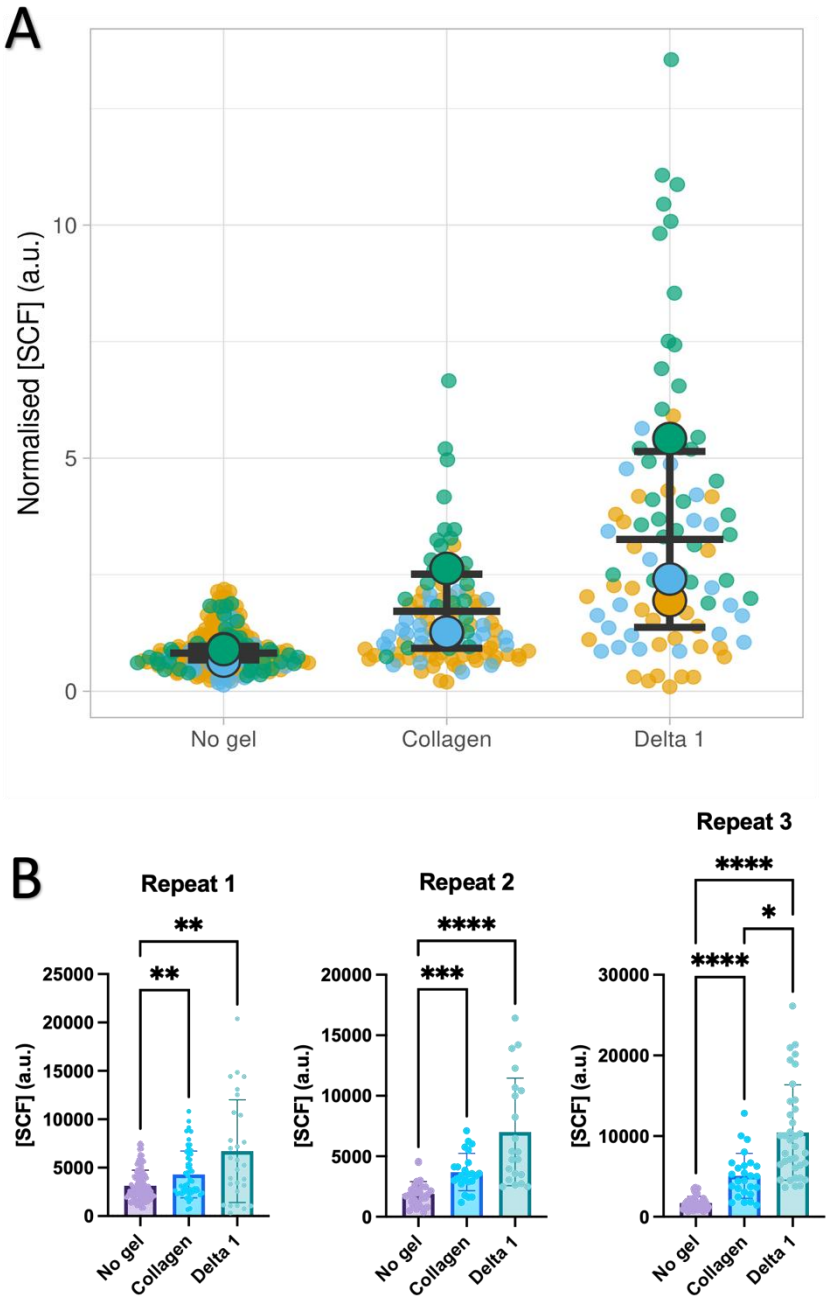

Figure 4.11 SCF expression in select conditions tested with IF microscopy. *MSCs grown in model systems with no gel, collagen gel, or delta 1 gel had their expression of SCF investigated by IF microscopy. (**A**) Superplot of all biological repeats. Statistics by one-way ANOVA followed by Tukey multiple comparison test. (**B**) Individual repeats. Statistics by Kruskal-Wallis followed by Dunn's multiple comparison test. *p < 0.05, **p < 0.01, ***p < 0.001 and ****p < 0.0001. Non-significant not shown. In the superplot, orange data points represent repeat 1, blue represents repeat 2, green represents repeat 3. Graphs show mean ± SD. N=3 biological replicates, each consisting of n=3 or 4 technical replicates with ~10 cells per technical replicate analysed.*

There was some patient-specific variation in the degree of nestin and SCF expression change when MSCs were placed in delta 1 or collagen niches. However, over multiple patient samples, a consistent pattern emerged; the delta 1 niche

strongly promoted both nestin and SCF expression compared to no gel controls, outcompeting, or equalling collagen in all tests. Collagen also performed well, consistently promoting nestin and SCF expression more than no gel controls in all but one patient sample.

To provide redundancy and improve the reliability of these results, nestin and SCF expression was also investigated using western blot and qPCR (see **Figure 4.12**).

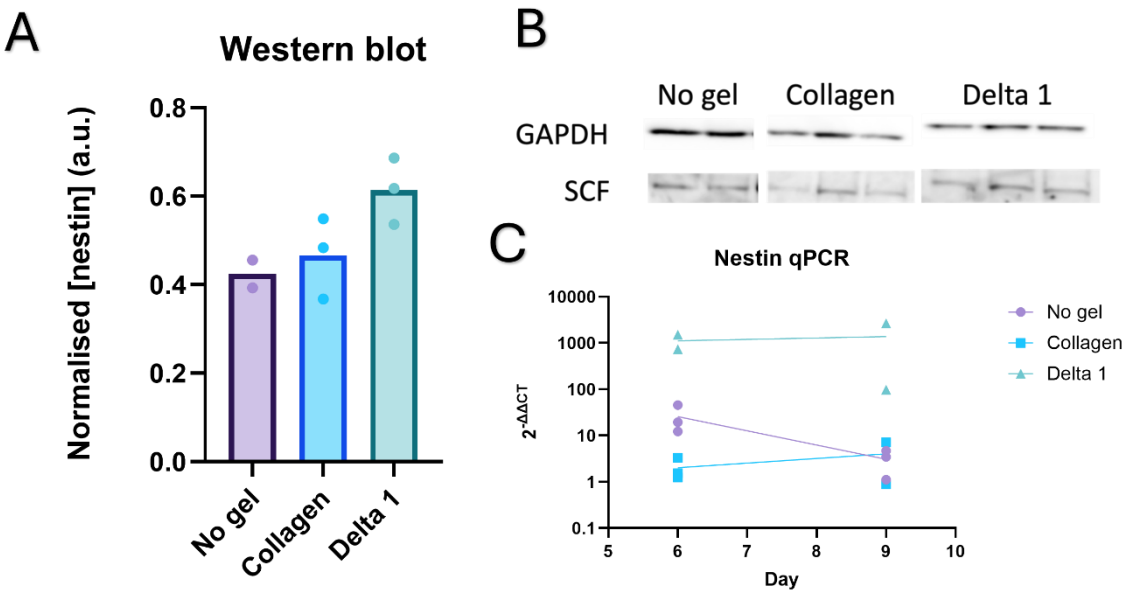

Figure 4.12 Nestin and SCF expression in select conditions western blot and qPCR. *MSCs grown in model systems with no gel, collagen gel, or delta 1 gel had their expression of SCF and nestin investigated by (**A** and **B**) western blot, or (**C**) qPCR, respectively. Graph (**A**) shows mean, graph (**B**) line passes through mean. For graph (**A**), n=2 technical replicates for no gel condition, and n=3 technical replicates for collagen and delta 1 conditions. Images of blots shown in (**B**). For graph (**C**), n=2 technical replicates for collagen day 9 and for delta 1 days 6 and 9, n=3 technical replicates for other conditions and timepoints.*

PeptiGels and collagen gels hindered data acquisition by these methods, as the amount of protein and RNA extracted was significantly reduced in these conditions. For collagen, this was due to fewer cells being present after gel removal, with many cells possibly removed with the gel. For the PeptiGel conditions, the gel was removed alongside the cell extracts, contaminating the associated samples (Burgess et al., 2017, 2018). In addition, the reduced MSC viability observed in PeptiGel conditions was a contributing factor. Nevertheless, these results agreed with the IF microscopy data, and together these datasets showed that the delta 1 PeptiGel and collagen promoted nestin and SCF

expression. CXCL12 expression, which was also linked with a niche-like phenotype and HSC maintenance (Greenbaum et al., 2013), was tested by IF microscopy as well (see **Figure 4.13** and **Figure 4.14**).

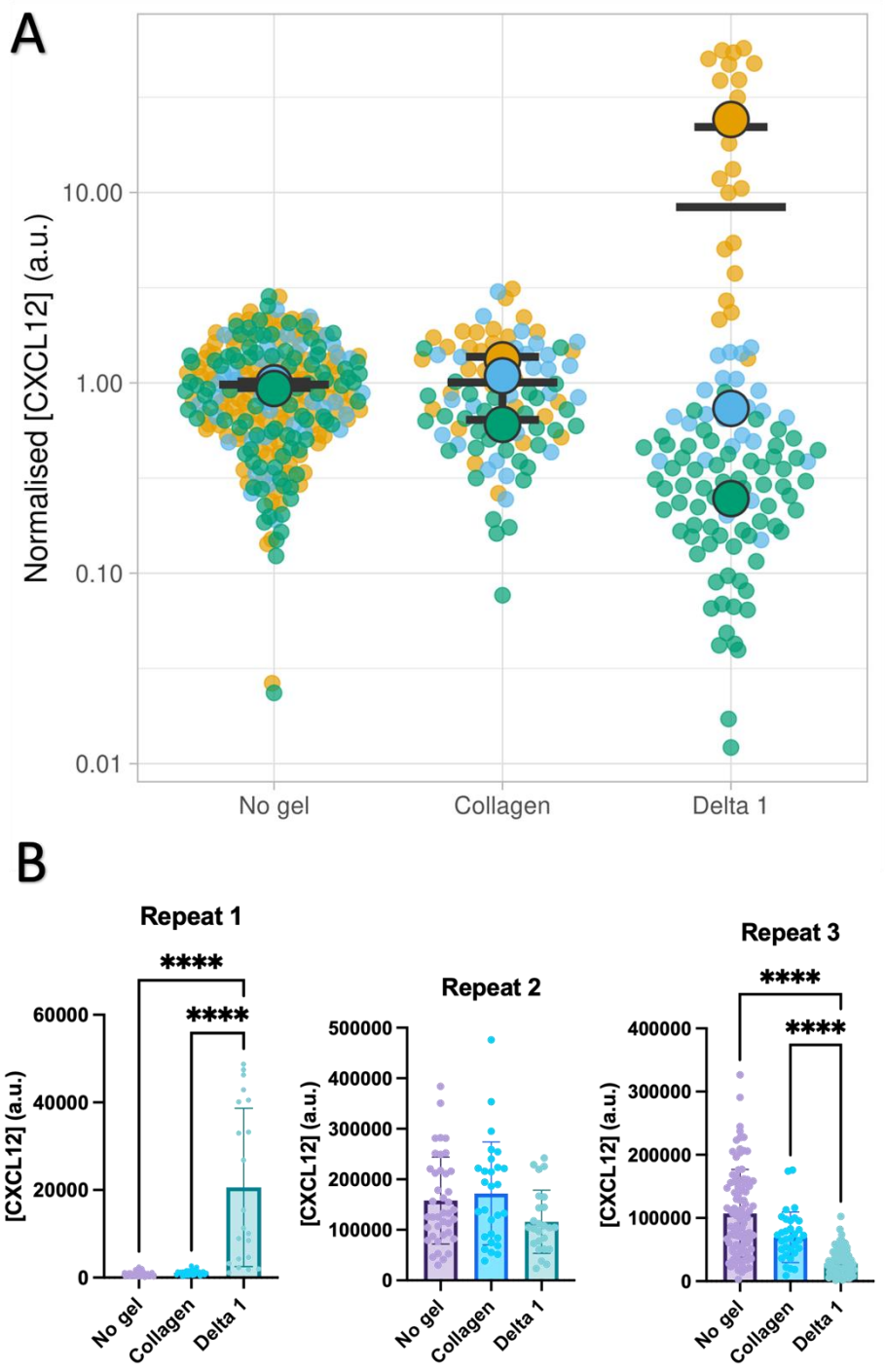

Figure 4.13 CXCL12 expression in select conditions tested with IF microscopy. *MSCs grown in model systems with no gel, collagen gel, or delta 1 gel had their expression of CXCL12 investigated by IF microscopy. (**A**) Superplot of all biological repeats. Statistics by one-way ANOVA followed by Tukey multiple comparison test. (**B**) Individual repeats. Statistics by Kruskal-Wallis followed by Dunn's multiple comparison test. ****p < 0.0001. Non-significant not shown. In the superplot, orange data points represent repeat 1, blue represents repeat 2, green represents repeat 3.*

Graphs show mean ± SD. N=3 biological replicates, each consisting of n=3 or 4 technical replicates with ~10 cells per technical replicate analysed.

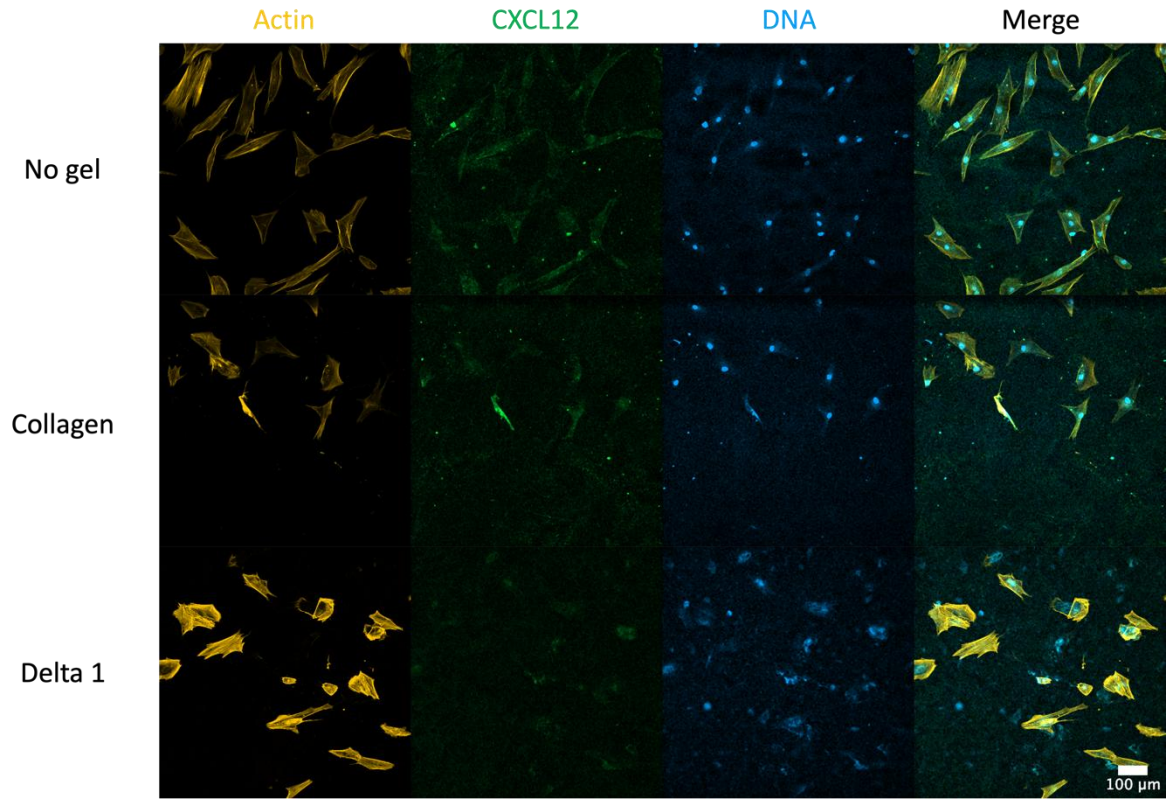

Figure 4.14 Representative confocal IF microscopy images of MSCs with CXCL12 stained. *The model systems were assembled, then on day 7 the cells were fixed and prepared for imaging. Scale bar is 100 µm. FIJI was used for image preparation. A z-stack of 8 images spaced 4.05 µm apart in the z axis was z projected with maximum intensity.*

There was a high degree of patient variability in CXCL12 expression in MSCs exposed to various systems, with two out of three patients showing a decrease in CXCL12 expression in delta 1 compared to no gel and collagen conditions, while one patient's cells experienced a massive increase in expression. While this may have been due to outlier patients, future work could investigate the cause of this difference by investigating genetic differences between CXCL12-responsive and CXCL12-unresponsive patients. Rather than assume that a decrease in CXCL12 expression in delta 1 conditions is indicative of a CXCL12- phenotype, it is possible that the no gel conditions mimicked the soft sinusoidal niche (Coutu et al., 2017), the delta 1 condition mimicked the arteriolar niche, and the collagen conditions created an intermediate niche. If this was the case, MSCs in the control conditions may have adopted a phenotype similar to CAR cells, resulting in high levels of CXCL12 expression (Sugiyama & Nagasawa, 2012), though as previously discussed

MSCs form a spectrum of phenotypes. This would have masked a comparatively small increase in CXCL12 expression in MSCs cultured in the delta 1 system. This hypothesis could be tested by analysing CXCL12 expression over time via other assays, such as western blot or qPCR. However, without this data, it cannot be assumed that CXCL12 expression increased in delta 1.

4.3.3.2 Mitochondrial distribution

Mitochondrial distribution was hypothesised to be influenced by MSCs' intracellular tension and actin retrograde flow (Bennett et al., 2018), and to affect cells' metabolic state, changes in which are known to be closely tied to the niche-like phenotype (Guo et al., 2018; Kobayashi & Suda, 2012; Takubo et al., 2013). Therefore, the distribution of mitochondria in different conditions was investigated (see **Figure 4.15**).

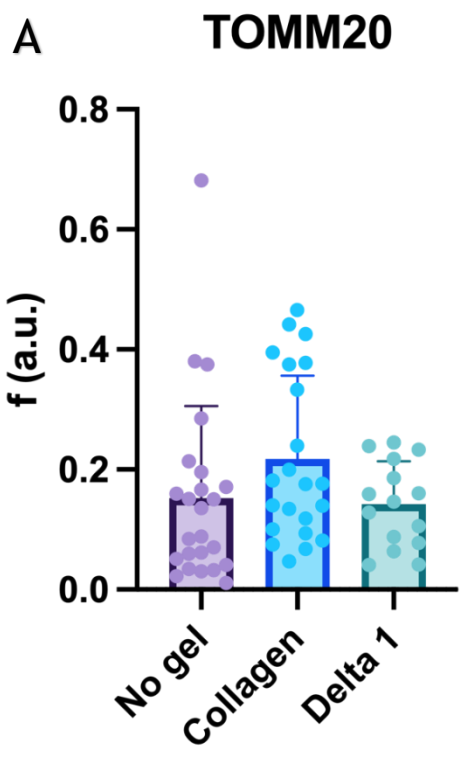

***Figure 4.15 Mitochondrial distribution of MSCs in select conditions**. MSCs grown in model systems with no gel, collagen gel, or delta 1 gel were grown for 7 days then fixed and prepared for imaging. (**A**) Average distance of a μm² of TOMM20 stain from the centre of the nucleus of a cell measured using FIJI, weighted appropriately, and averaged, giving each data point shown. (**B**) Representative confocal IF microscopy images of MSCs' mitochondria in various conditions. Scale bar is 100 μm. FIJI was used for image preparation. Graphs show mean ± SD. n=3 twchnical replicates with ~7 cells per replicate analysed.*

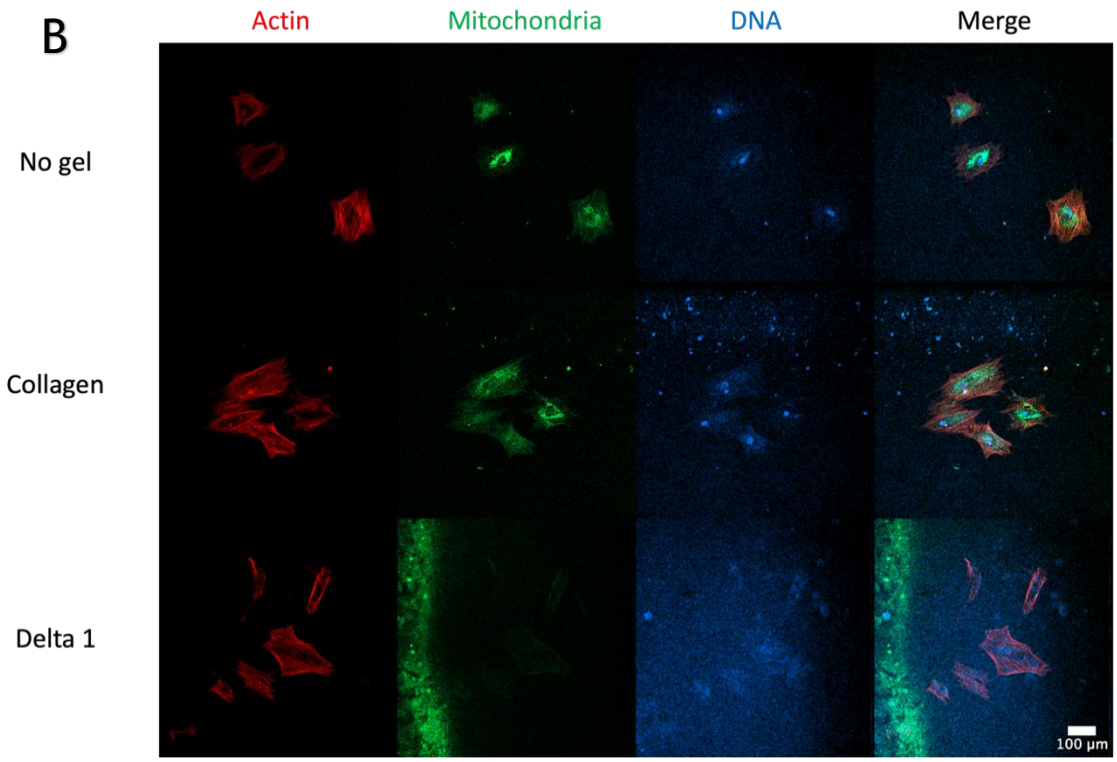

No significant trends in mitochondrial distribution were observed between conditions tested, despite the collagen and delta 1 conditions being shown to produce a niche-like phenotype in MSCs (see **Figure 4.10**, **Figure 4.11**, and **Figure 4.12)**. This suggested that mitochondrial distribution was not affected by the phenotypic alterations induced in MSCs in these systems. Future work could investigate the metabolic state of MSCs in the conditions tested using alternative methods, such as C^{13}-glucose tracing. While mitochondrial distribution was not appropriate in this situation, inhibition of actin retrograde flow and induction of different metabolic states could be used to test the effects of these variables and more thoroughly examine whether the suspected changes in distribution arise.

Defining the MSCs in the delta 1 system as adopting a niche-like phenotype is overly simplistic due to the multi-faceted nature of the BM niche and the cells within (Doherty-Boyd et al., 2024). While MSC populations within the BM niche are heterogenous and overlap significantly, the cells within the delta 1 system, and to a lesser extent the collagen system, are most like nestin+ MSCs that colocalise with HSCs, and are essential for their maintenance (Méndez-Ferrer et al., 2020; Pinho et al., 2013). The increased nestin expression and decreased CXCL12 expression could also have implied that the MSCs adopted an arteriolar niche

phenotype in delta 1 conditions, while a more sinusoidal phenotype was stimulated by the collagen and no gel conditions (Asada et al., 2017; Kunisaki et al., 2013; B. O. Zhou et al., 2014). However, this did not explain the increased SCF expression observed, which is associated with a sinusoidal phenotype. Alternatively, a nestin+ SCF+ CXCL12- phenotype not yet identified in the BM niche may have been induced. Investigation of other markers, such as LepR, NG2, and (Asada et al., 2017; Kunisaki et al., 2013; Pinho & Frenette, 2019) could reveal more information on the specific phenotype produced by the systems trialled.

4.3.4 Model's effect on HSCs

After creating and optimising the model BM niche for MSC phenotype, the next step was to see how the model niche affected other BM-resident cells. First, the effect on HSCs was investigated (see **Figure 4.16**).

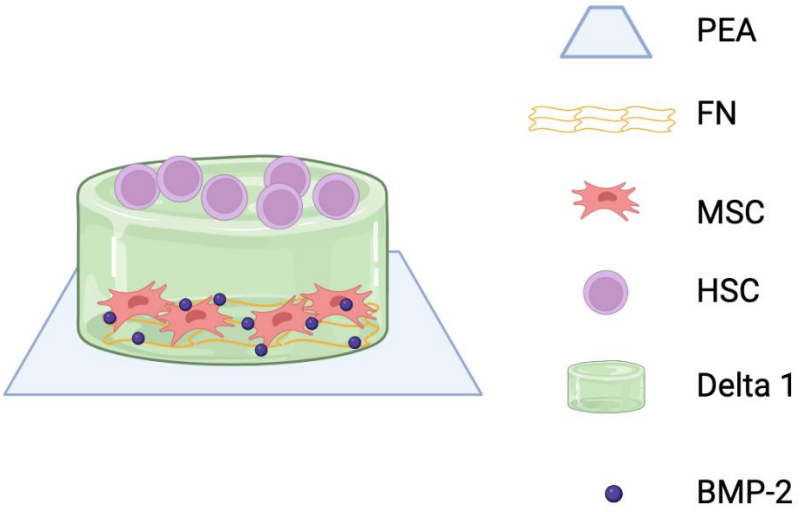

Figure 4.16 Schematic of model BM niche which had its effect on HSCs tested. *Collagen and no gel conditions in which the delta 1 PeptiGel was replaced with collagen gel or no gel was used respectively were also used. Created with BioRender.com.*

4.3.4.1 Effect of cytokines on HSC retention

One of the initial goals of this project was to devise a synthetic system that could facilitate HSC maintenance *in vitro* by mimicking aspects of the BM niche (Chatterjee et al., 2021; Fares et al., 2022). The MSCs in the model niche were

shown to produce some of the soluble factors associated with HSC maintenance, (Xiao, McGuinness, et al., 2022). However, inclusion of exogenous cytokines such as SCF, FL, and TPO in other models designed for HSC maintenance is routine (Donnelly et al., 2024; J. Li et al., 2022). Therefore, the need for exogenous cytokines to maintain HSCs in the delta 1 niche was examined (see **Figure 4.17**).

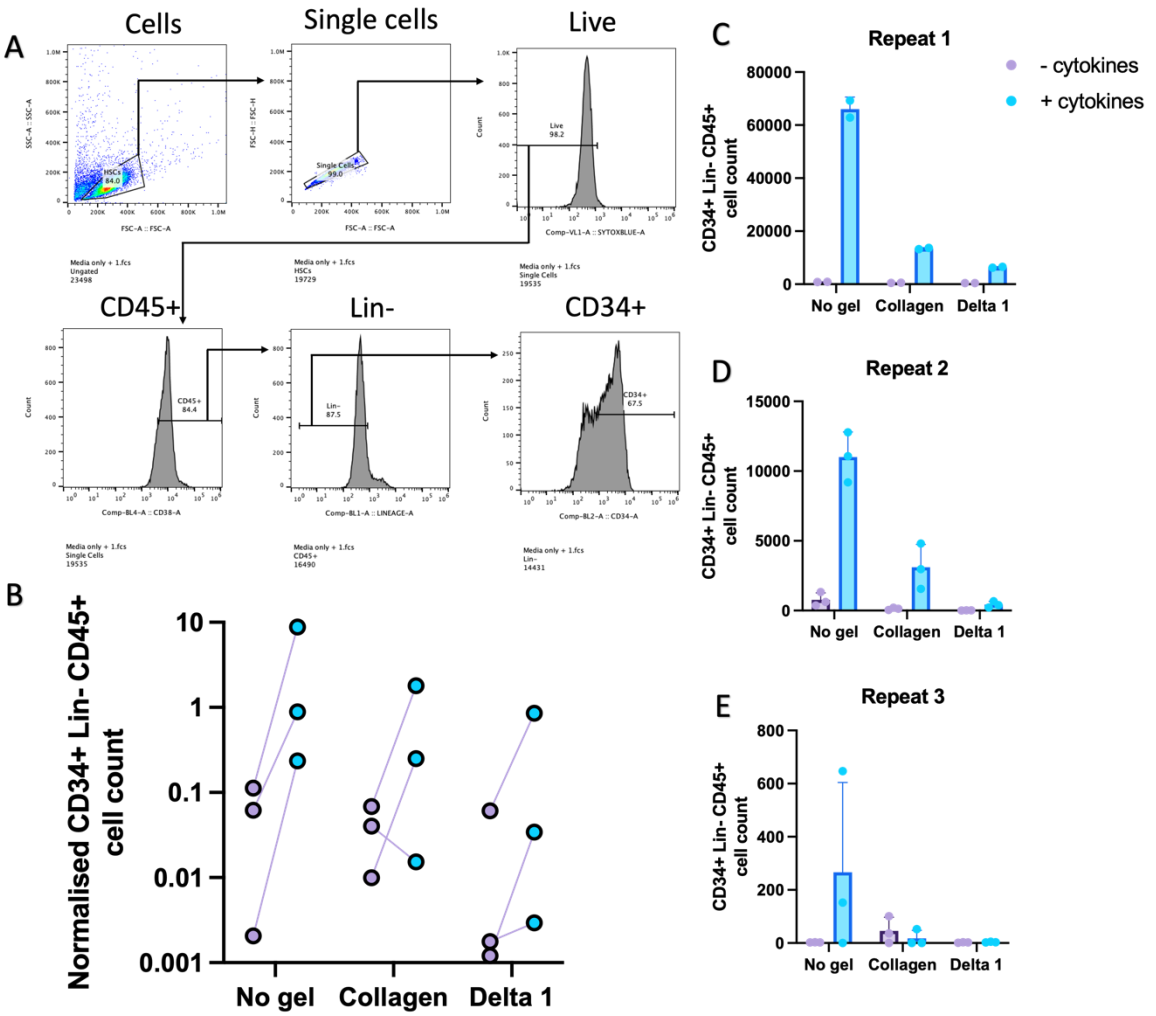

Figure 4.17 Effect of cytokines on HSC retention in BM niche models. *Patient-derived HSCs were cultured in no gel, collagen, and delta 1 systems, then analysed by flow cytometry. (**A**) Flow gating strategy. Forward scatter area (FSC-A) and side scatter area (SSC-A) were used to identify cells. FSC-A and forward scatter height (FSC-H) were used to identify single cells. A sytox blue gate was used to omit dead cells. A CD45+ gate identified haematopoietic cells, a Lin- gate omitted differentiated cells, and a CD34+ gate identified HSCs. (**B**) Gated (CD34+ Lin- CD45+) cell counts in model systems normalised against the number of HSCs added. Each point represents the average of a biological repeat for a condition. Conditions without cytokines (purple) are connected to identical conditions with cytokines (cyan) from the same biological repeat. (**C-E**) Gated cell counts for individual biological repeats. Graphs (**C-E**) show mean + SD. N=3 biological replicates, each consisting of n=2 or 3 technical replicates.*

Gated cell counts, which reflected the number of HSCs in the model systems, predominately decreased in all conditions over the course of the experiment. The delta 1 niche retained the fewest HSCs of all the conditions tested, likely due to poor biocompatibility and the synthetic nature of the PeptiGel, as seen in MSCs. The inclusion of cytokines caused a positive trend in HSC count across conditions. This implied that HSC retention was dependent on cytokine inclusion, as seen in other models (Doherty-Boyd et al., 2024).

Previous research demonstrated that a no gel system with cytokines caused increased HSC proliferation, while a collagen based system maintained HSCs with a more naïve phenotype, regardless of cytokines' presence (Donnelly et al., 2024). The data presented generally follows this trend, with no gel, cytokine inclusive conditions yielding the best HSC retention/proliferation. However, a large amount of patient-specific variation was also observed, with two out of three patient samples demonstrating increased HSC retention in collagen systems when cytokines were included. The delta 1 niche was also reliant on cytokine inclusion to improve HSC retention. Therefore, cytokines were included in subsequent experiments.

The positive effect of the cytokines was likely due to the inclusion of FL and TPO, which are not produced by MSCs (Decker et al., 2018; Tsapogas et al., 2017), rather than SCF, which the MSCs in the delta 1 and collagen systems strongly produced. This could be tested by removal of SCF from the cytokine cocktail added when making IMDM + cytokines. However, this was not attempted due to the limited availability and high cost of HSCs. Several other cytokines not produced by MSCs, such as TGF-β1 (Yamazaki et al., 2011; M. Zhao et al., 2014), notch ligand (Lampreia et al., 2017) and WNT ligand (Richter et al., 2017), are known to influence HSC retention, proliferation, and phenotype, and could have a positive impact on HSC number if included in future models. Other models have used a diverse population of BM cells, such as osteoblasts and endothelial cells, to complement MSCs and create a more physiologically relevant feeder layer that could produce a full complement of BM cytokines (Doherty-Boyd et al., 2024). However, these complex systems often still require exogenous cytokines, are difficult to assemble, and are ultimately challenging to analyse due to their complexity.

4.3.4.2 Effect of MSCs on HSC retention

The MSCs in the model BM niche systems had a niche-like phenotype. This was hypothesised to improve their potency as a feeder layer for HSC maintenance. To assess this, the number of haematopoietic cells, HSCs, and LT-HSCs in systems with or without MSCs in various conditions were tested with flow cytometry (see **Figure 4.18**).

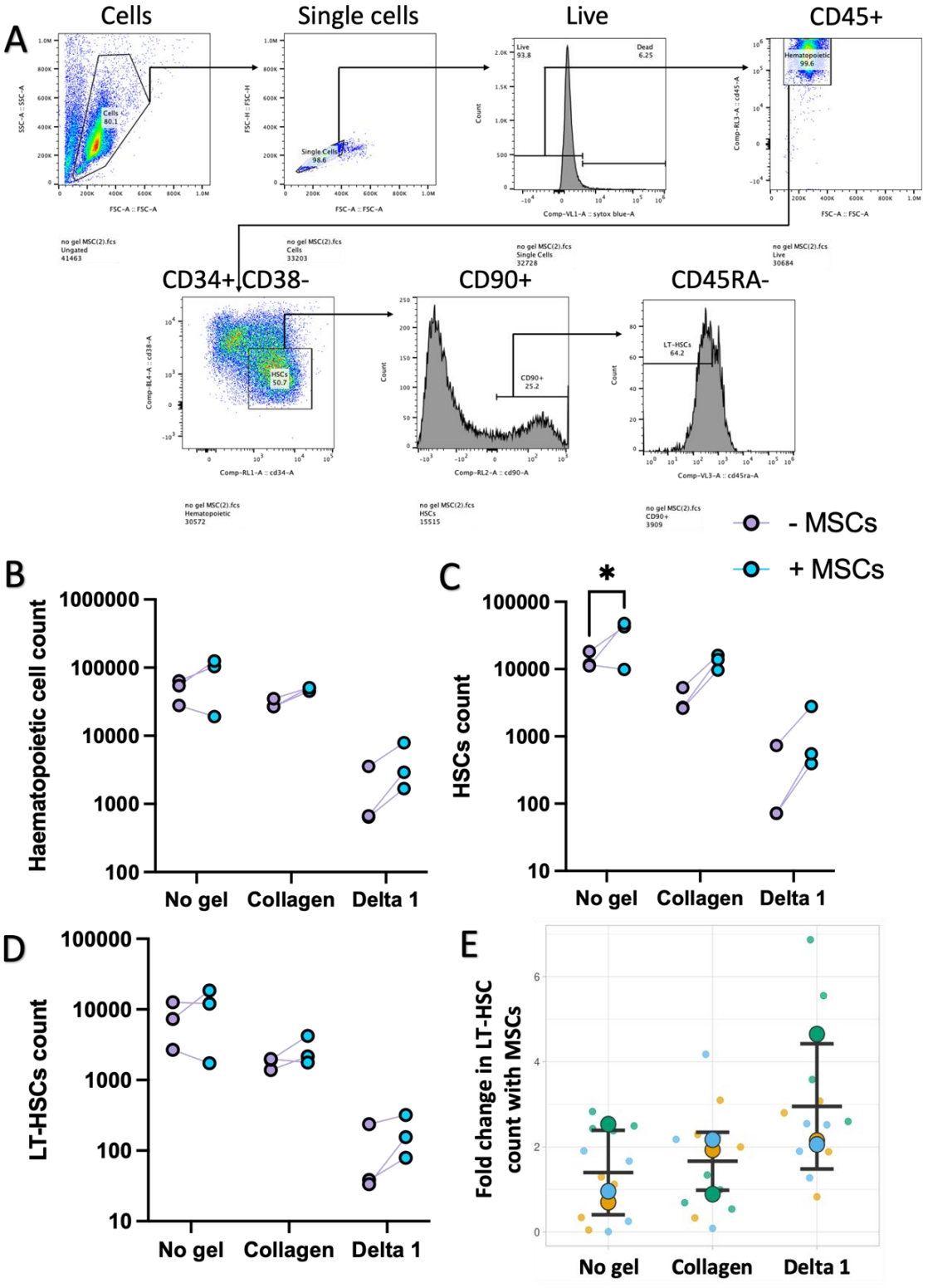

***Figure 4.18 The effect of MSCs on HSC retention in BM niche models**. One STEMCELL technologies HSC sample per biological repeat was cultured in no gel, collagen, and delta 1 systems, then analysed by flow cytometry. (**A**) Flow gating strategy. FSC-A and SSC-A were used to identify cells. FSC-A and FSC-H were used to identify single cells. A sytox blue gate was used to omit dead cells. A CD45+ gate identified haematopoietic cells. A CD34+ CD38- gate identified HSCs. Two gates for CD90+ and CD45RA- cells identified LT-HSCs. The number of (**B**) haematopoietic cells, (**C**) HSCs, and (**D**) LT-HSCs was quantified. Each point represents the average of a biological repeat for a condition. Conditions without MSCs (purple) are connected to equivalent conditions with MSCs (cyan) from the same biological repeat. (**E**) Fold change in LT-HSC count when MScs are included. (**E**) shows mean ± SD. Statistics for (**B-D**) by two-way ANOVA followed by Šídák multiple comparison test. *p < 0.05. Non-significant not shown. N=3 biological replicates, each consisting of n=4 technical replicates.*

In all models tested, the inclusion of MSCs caused an increase in haematopoietic cell, HSC, and LT-HSC retention/proliferation. This demonstrated the supportive role MSCs played in the niche models, which mimicked their behaviour in the endogenous niche (Méndez-Ferrer et al., 2010; Pinho et al., 2013). LT-HSC retention was increased the most by the inclusion of MSCs in the delta 1 system. This aligned well with the original hypothesis that niche-like MSCs, such as those created by the delta 1 niche, act as a superior feeder layer, adopting a similar role to their *in vivo* counterparts and aiding in the maintenance of the most naïve haematopoietic cell types. Interestingly, the addition of MSCs caused a statistically significant increase in no gel HSC count, despite a decrease in LT-HSC count in the same conditions being observed in two thirds of repeats. This implied that the HSC increase was non-uniform, preferentially encouraging expansion/retention out with the LT-HSC compartment. This was not unexpected, as LT-HSCs are known to proliferate rarely (Guo et al., 2018; Kobayashi & Suda, 2012; Takubo et al., 2013). The fact that this difference was not seen in collagen and delta 1 conditions is indicative of these systems retaining rather than expanding HSCs (Donnelly et al., 2024).

Due to these results, the optimum form of the delta 1 niche was determined to include both cytokines and MSCs. However, even with these optimisations, the delta 1 niche still retained fewer haematopoietic cells, HSCs, and LT-HSCs than collagen conditions, which in turn maintained fewer of these cell types than no gel conditions which likely encouraging HSC proliferation (Donnelly et al., 2024). This could have been due to the gel systems limiting differentiation, or it could have been the result of cell death.

Changes in the make-up of the haematopoietic cell cohort over time within the model niches tested were investigated further (see **Figure 4.19**).

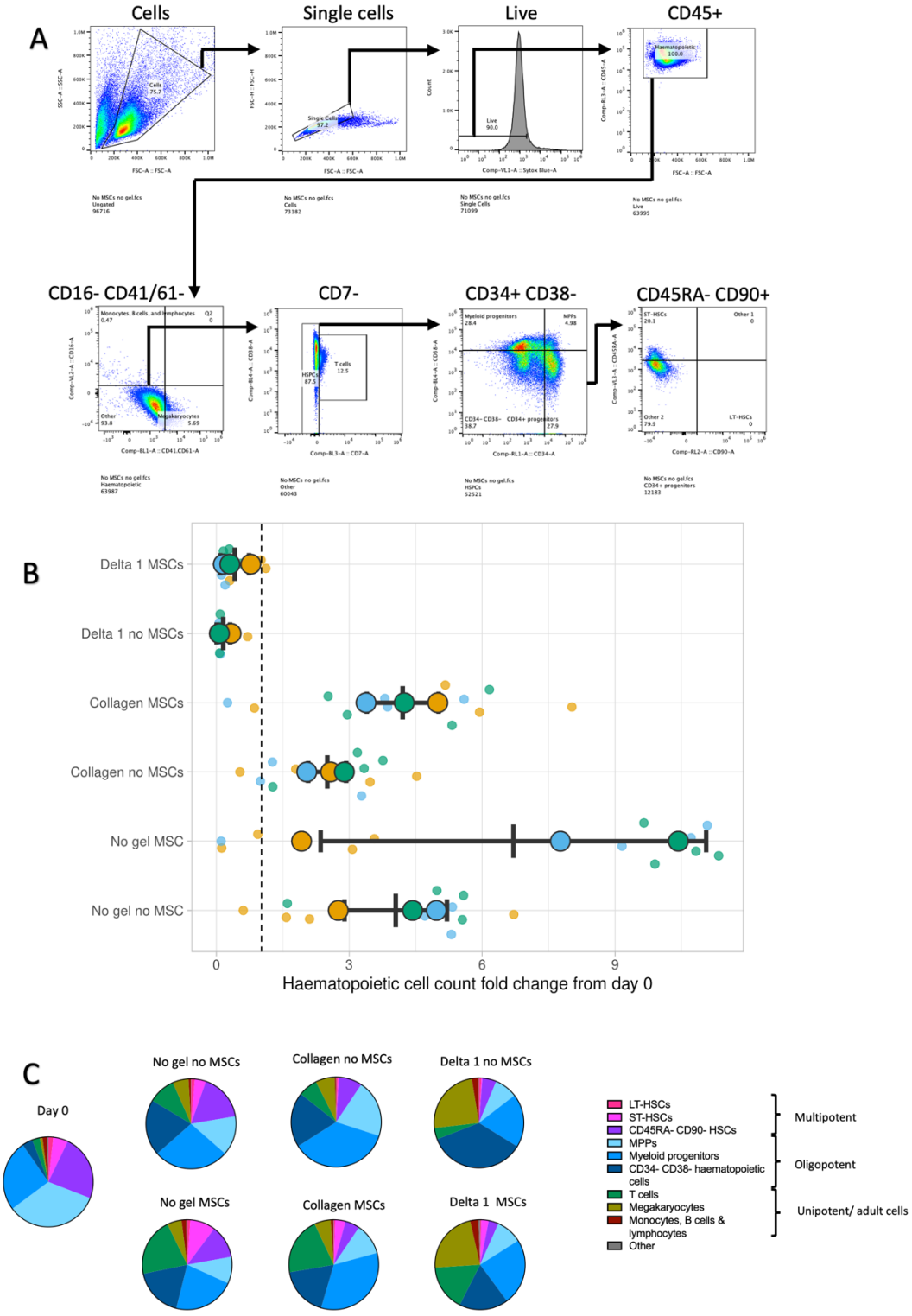

Figure 4.19 The effect of BM niche models on haematopoietic cells' phenotype, retention, and differentiation. *One STEMCELL technologies HSC sample per biological repeat was cultured in no gel, collagen, and delta 1 systems, then analysed by flow cytometry. (**A**) Flow gating strategy. FSC-A and SSC-A were used to identify cells. FSC-A and FSC-H were used to identify single cells. A sytox blue gate was used to omit dead cells. A CD45+ gate identified haematopoietic*

*cells. A series of gates were then used to identify and exclude different cell populations from subsequent characterisations. Gates were used for a CD16 and CD41/61 scatter plot to identify two populations: megakaryocytes (CD16- CD41/61+); monocytes, B cells and lymphocytes (CD16+ CD41/61-). CD16- CD41/61- cells were then assessed for CD7 expression, with CD7+ cells determined to be T cells. CD7- cells were separated based on a CD34 and CD38 scatter plot. Three populations were identified: myeloid progenitors (CD34- CD38+), multipotent progenitors (CD34+ CD38+), and an anomalous population of CD34- CD38- cells. CD34+CD38- cells were then assessed with a CD45RA and CD90 scatter plot to identify several final populations: ST-HSCs (CD45RA+ CD90-); LT-HSCs (CD45RA- CD90+); intermediate HSCs (CD45RA- CD90-). (**B**) Fold change in haematopoietic cell count over 5 days in a model system. Dashed line represents a fold change of 0. (**C**) Make-up of haematopoietic cell population after 5 days in the models tested. Graphs show mean ± SD. N=3 biological replicates, each consisting of n=4 technical replicates (n=3 for day 0).*

While the adult cell populations were readily defined by surface markers, several intermediate, naïve HSC populations also emerged, including CD45RA- CD90- HSCs and CD34- CD38- HSPCs. These cells were difficult to categorise using the traditional gating strategy employed (Donnelly et al., 2024; Wisniewski et al., 2011), and exemplify the spectrum of haematopoietic differentiation discussed previously (see **1.1.1**) (Karamitros et al., 2018; P. Zhang et al., 2022). Therefore, it was important to not only consider distinct cell populations, but also cells with similar levels of potency.

The delta 1 niche was shown to cause a reduction in haematopoietic cell count, implying that it caused cell death, as opposed to the collagen system which seemed to merely dampened proliferation and differentiation compared to no gel systems. This was again likely due to the poor biocompatibility of synthetic PeptiGels.

For the haematopoietic cells' phenotypic changes, a few common trends emerged. Firstly, across all conditions, incubation for 5 days caused a dramatic increase in mature cell types, resulting from differentiation of the initially naïve HSC population (Cheshier et al., 1999; Yamamoto et al., 2013). Next, the inclusion of MSCs caused increased retention of multipotent HSCs, particularly ST-HSCs, in all systems. This increased naïve cell retention was probably due to the supportive, maintaining role MSCs play in the *in vivo* niche (Pinho & Frenette, 2019). Previous research sought to uncover the impact of BM niche models on clinically important LT-HSCs (Doherty-Boyd et al., 2024; Donnelly et al., 2024). Across model iterations tested, the LT-HSC count remained proportionately low, and in two out of three

patient samples tested, very few LT-HSCs were identified using the stringent gating strategy shown, primarily due to low levels of CD90 expression (Wisniewski et al., 2011), even when analysed a day after thawing. This was not overly surprising considering the exceptionally low number of LT-HSCs present in each individual (Abkowitz et al., 2002). While this data does provide some information on LT-HSCs, the heterogenous nature of these cells (P. Zhang et al., 2022) prevents thorough investigation by flow cytometry. Other approaches, such as *in vivo* serial engraftment assays or LTC-IC and CFU analysis (Donnelly et al., 2024; Wilkinson et al., 2019), could provide greater insight by interrogating how cells' ability to reconstitute a haematopoietic system is affected by incubation in the niche models tested.

A larger T-cell population was also observed in conditions with MSCs compared to their no MSC counterparts. This was unexpected, as MSCs are generally considered to dampen the immune response by inhibiting T cell proliferation (Negi & Griffin, 2020). A possible explanation for this was that the gels prevented juxtracrine interactions, which are known to play a part in MSCs' immunomodulatory effect (N. Song et al., 2020). This raises questions about the impact MSCs have on other haematopoietic cells without juxtracrine signals and could be an avenue for future research. However, the fact that an increase in T cell number was still seen in no gel conditions suggests otherwise. A more plausible explanation is that the HSCs were mounting an immune response to the MSCs themselves, in a similar manner to GvHD (Meaker & Wilkinson, 2024). The fact that this occurred despite the repressive effects of the MSCs, as well as the lack of similar reports in the literature, warrants further investigation.

In addition, Delta 1 systems caused an increased megakaryocyte population relative to the total haematopoietic cell cohort in these niches. The low number of haematopoietic cells in the delta 1 systems and low PeptiGel biocompatibility suggest that this was likely a stress response, which is known to induce megakaryopoiesis (Noetzli et al., 2019). Another explanation is that the delta 1 system prevented a transplantation phenotype; transplanted HSCs are known to produce large numbers of other cell types, while unperturbed, native haematopoiesis has been shown to favour megakaryocyte differentiation (Rodriguez-Fraticelli et al., 2018). However, due to the drop in haematopoietic

cell count, it is difficult to determine whether prevalent cell types are the result of differentiation or preferential retention within the delta 1 niche.

4.3.5 Model's effect on THP-1 cells

Finally, the effect of the model niche on AML cells was assessed. THP-1, an AML cell line (Chanput et al., 2014), was used as an AML model (see **Figure 4.20**).

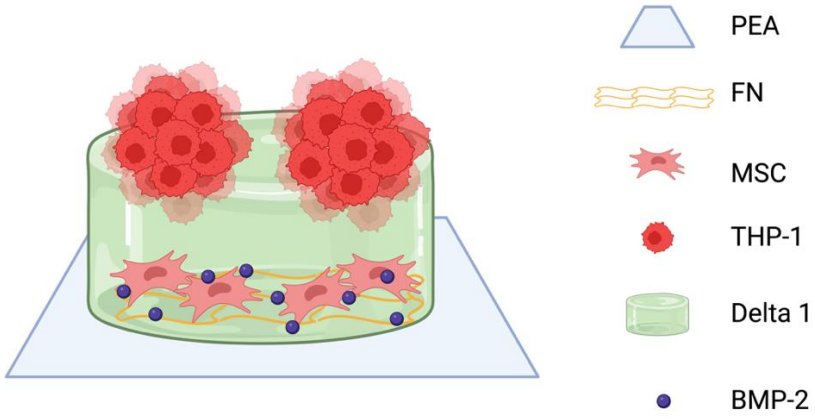

Figure 4.20 Schematic of model BM niche which had its effect on THP-1s tested. *Alpha 2, collagen, no gel, and PCS conditions were also used. In these conditions delta 1 PeptiGel was replaced with alpha 2 PeptiGel, collagen gel, no gel, or no gel and no PEA, FN, or BMP2 coats, respectively. Created with BioRender.com.*

The effect of various gels and inclusion or exclusion of MSCs on THP-1 cells in model niche systems in terms of proliferation and viability was assessed using an automated cell counter and trypan blue staining (see **Figure 4.21**).

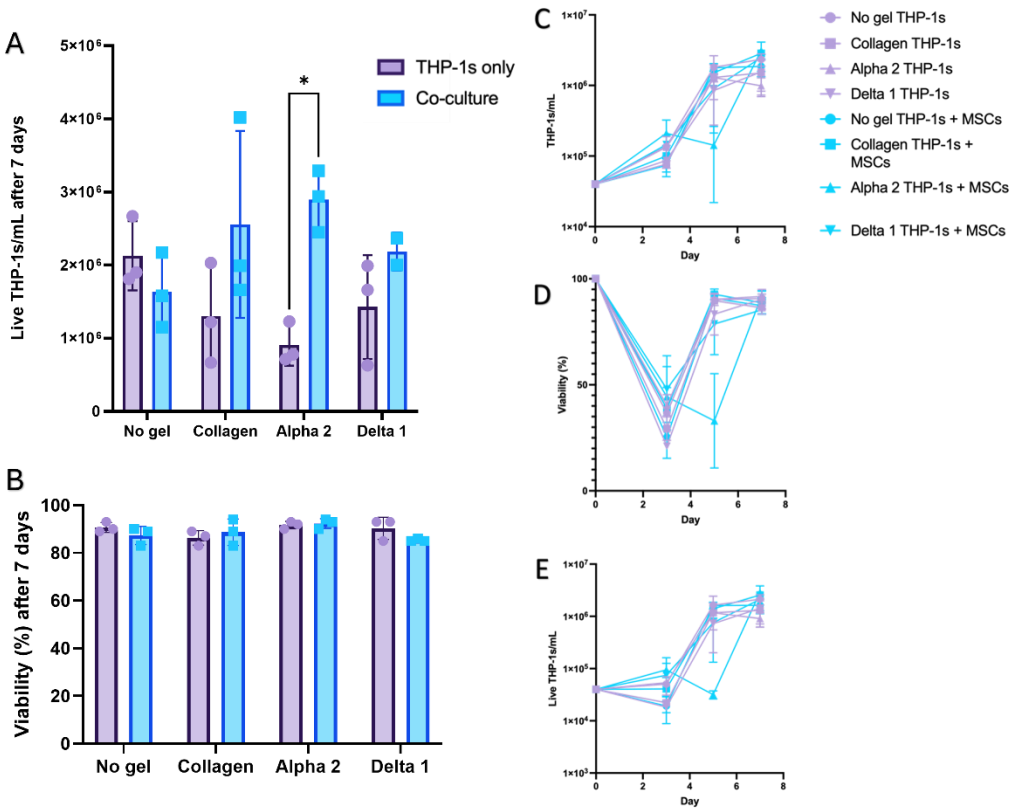

Figure 4.21 Effect of various models' on THP-1 viability and proliferation. *THP-1s cultured with (blue) or without (purple) MSCs in no gel, collagen, alpha 2 or delta 1 systems for 0, 3, 5, or 7 days were counted and assessed for viability. After 7 days (**A**) the number of live THP-1s per mL after and (**B**) their viability was tested. Over 7 days the change in (**C**) the total number of THP-1s per mL, (**D**) THP-1 viability, and (**E**) Live THP-1s per mL was also tracked. Graphs show mean ± SD. Statistics for (**A**) and (**B**) by two-way ANOVA followed by Šídák multiple comparison test. *p < 0.05. Non-significant not shown. N=3 biological replicates, each with a unique MSC donor and THP-1 sample.*

This data demonstrated proliferation of THP-1 cells in all conditions tested, as well as high (>85%) viability after 7 days. This was despite initial low viability, likely caused by the change in media from 10% RPMI in culture to IMDM + cytokines in the model niches. This indicated that the THP-1s either remodelled their microenvironment (Kumar et al., 2018) or adjusted to it themselves.

The inclusion of MSCs in the model systems caused a positive trend across all conditions bar no gel in terms of live THP-1 count on day 7. This was likely due to the supportive effect of the MSC feeder layer, which was previously shown to adopt a niche-like phenotype more strongly in the gel conditions tested compared to the no gel control. This follows, as the BM niche, which nestin+ MSCs are a key

aspect of, is known to act as a supportive reservoir of AML cells (Ishikawa et al., 2007; Tabe & Konopleva, 2015).

The effect of a delta 1 niche system on THP-1 cells was subsequently investigated using flow cytometry (see **Figure 4.22**).

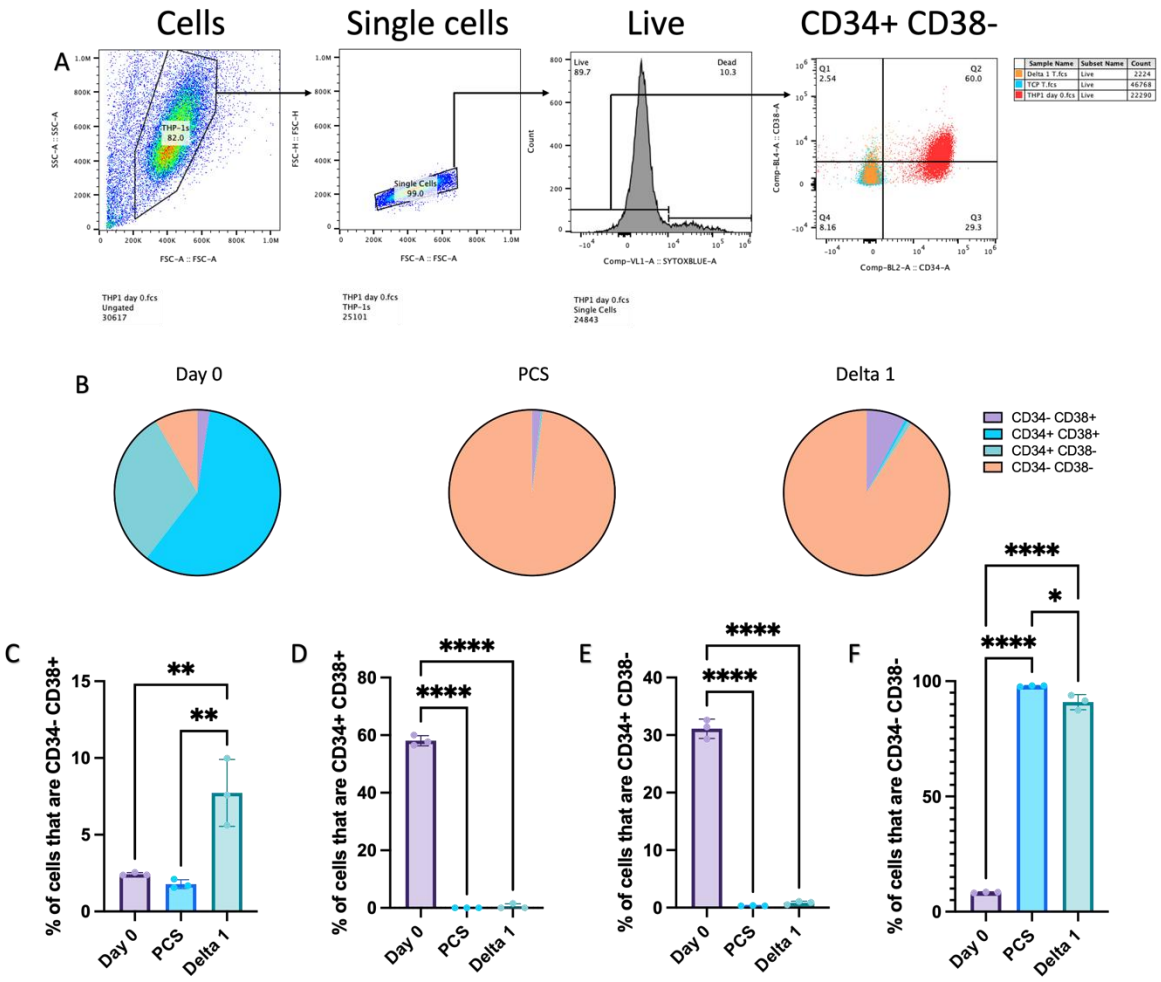

***Figure 4.22 Effect of various models' on THP-1 phenotype**. THP-1s were cultured in bare PCS (no coatings) or delta 1 systems for 7 days before being analysed by flow cytometry. (**A**) Flow gating strategy. FSC-A and SSC-A were used to identify cells. FSC-A and FSC-H were used to identify single cells. A sytox blue gate was used to omit dead cells. A final gate was used to separate cells based on CD34 and CD38 staining. The final panel shows distribution of cells from day 0 (red), PCS (blue), and delta 1 (orange) conditions in terms of CD34 and CD38 expression. Gated cells were also all found to be CD45+ (not shown). (**B**) Population distribution of THP-1s in terms of CD34 and CD38 expression after 7 days in the model systems. (**C-F**) Percentage of the total THP-1 population that consists of specific CD34 and CD38 subpopulations. Graphs show mean ± SD. Statistics by one-way ANOVA followed by Tukey multiple comparison test. *p < 0.05, **p < 0.01 and ****p < 0.0001. Non-significant not shown. n=3 technical replicates.*

THP-1 cells underwent extensive phenotypic changes when incubated in the delta 1 niche, rapidly losing expression of both CD34 and CD38 over 7 days. Surprisingly,

a similar response was also seen in PCS, despite its similarities to standard THP-1 culture conditions. The niches caused an increase in CD34-CD38- cells' % of total cells compared to day 0, while delta 1 alone caused a shift to the CD34-CD38+ phenotype. This indicated that these niches were accelerating complete differentiation of immature CD34+ CD38- THP-1 cells into adult cells, which are typically CD34- CD38+ (Duy et al., 2021; Hope et al., 2004). Alternatively, since the delta 1 niche was shown to cause a high level of initial THP-1 death, it's possible that it was eliminating cells from the decreased subpopulations preferentially, though this does not explain the changes seen in the PCS control niche. These changes were likely caused by the change in media (IMDM + cytokines rather than 10% RPMI).

The precise reason for the observed changes, as well as any related impact media could have on other haematopoietic cells such as HSCs, could be investigated further. Ultimately, these results showed that THP-1s were able to survive in the model BM niches developed, allowing them to be used in subsequent experiments.

4.4 Summary

By testing various parameters related to PeptiGels used in the model niches developed, undiluted delta 1 PeptiGel was found to promote a niche-like phenotype in MSCs without compromising their viability (see **Figures 4.3-Figure 4.6)**. Plate coatings and media used were also optimised (see **Figure 4.7** and **Figure 4.8)**. FN coated on PEA and loaded with BMP2 was shown to induce the desired phenotype (Donnelly et al., 2024). Furthermore, different media formulations didn't adversely affect this phenotype, though viability was affected. The optimised system was then further assessed and found to strongly induce a niche-like phenotype in MSCs (see **Figure 4.9**-**Figure** 4.12**)**, which were hypothesised to act as a superior feeder layer for HSCs (Mendelson & Frenette, 2014).

This model's effect on included HSCs was then tested. HSCs were found to react more favourably to this system and others when cytokines and MSCs were included (see **Figure 4.17** and **Figure 4.18)**. The effect of MSCs was more pronounced in the delta 1 system, implying that the improved MSC phenotype was having a

positive effect (Donnelly et al., 2024). The phenotypic composition of haematopoietic cells in the niche was also determined (see **Figure 4.19)**, with some specific differentiation preferences and their possible implications noted. Interestingly, the delta 1 niche appeared to promote megakaryocyte differentiation, implying that HSCs in this niche avoided the typical transplantation phenotype and instead acted similarly to how they would *in situ* (Rodriguez-Fraticelli et al., 2018). T cell differentiation was also seen in all conditions which included MSCs, the cause of which was speculated to be an immune response from the HSCs to the foreign MSCs.

Finally, the effect of the model on THP-1 AML cells was analysed (see **Figure 4.21** and **Figure 4.22**). THP-1s experienced an initial shock phase when introduced to the niche, before recovering. The THP-1s also rapidly lost naïve cell surface markers in the niches tested.

The delta 1 niche replicated several aspects of the endogenous BM niche, and supported populations of BM resident cells, including MSCs, haematopoietic cells, and AML cells. Therefore, this model was appropriate for testing novel therapies for BM-associated diseases and disorders.

Chapter 5 Targeted gene disruption of an AML surface marker in HSCs

5.1 Introduction

To demonstrate the usefulness of the developed BM niche model for testing novel therapies, an approach to CAR T-cell therapy for AML was developed. This system's efficacy was subsequently modelled in the synthetic niche and will be discussed in the next chapter. Similar to the CAR T-cell approach developed by (Kim et al., 2018), the method described here involved the targeting of the CD33 AML surface marker via CAR T-cells. Unfortunately, CD33 is expressed on myeloid cells as well as AML cells (Laszlo et al., 2014), which would also be eliminated by any CAR T-cell treatment targeting CD33+ cells. To overcome this, a method for knocking out CD33 in HSCs, preventing them from producing CD33+ progeny, was developed. CD33- HSCs could be implanted alongside CD33-redirected CAR T-cells, preventing myeloid collapse by creating a parallel, CD33-, CAR T-cell resistant haematopoietic system while the CAR T-cells eliminate CD33+ cells, including AML cells (Borot et al., 2019; Kim et al., 2018).

5.1.1 CRISPR

CRISPR-Cas9 technology has emerged as a powerful tool for precise genetic modification of cells (Doudna & Charpentier, 2014). It makes use of the bacterial viral response. In bacteria, invading viruses that are fended off have their genetic information incorporated into the genome of the infected host cell in an array of palindromic repeats. When the bacterial cell is reinfected with the same pathogen, it produces a form of RNA from this array that is complementary to the virus' invading genetic information. This RNA complexes with other components, including a Cas protein molecule, forming a ribonucleoprotein (RNP) complex that recognises the viral DNA via complementary base pairing and cleaves it, causing double strand breaks (DSBs). This technology has been leveraged by researchers to produce breaks in DNA with a high degree of specificity and efficiency (Barrangou & Doudna, 2016). To do this, RNPs are assembled either *in vitro* then

inserted into cells, or *in situ* by inserting genetic information encoding RNP components into cells. Typically, a modified form of RNA, termed single guide RNA (sgRNA) is used, alongside Cas9, though other types of Cas and guide RNAs are used as well (Doudna & Charpentier, 2014).

The DSBs caused by CRISPR-Cas9 are repaired by the cell's intrinsic DNA repair pathways. If non-homologous end joining (NHEJ) is active, it occasionally results in insertion or deletion mutations (INDELs) as DSBs are directly ligated back together without requiring much homology. This results in either frame-shift mutations and the gene producing erroneous protein, referred to as gene knock out (KO), or tolerated mutations that don't prevent functional protein production, termed missense mutations (Doench et al., 2014). Alternatively, the homology-directed repair (HDR) pathway can be active. This pathway revolves around the use of a homologous piece of DNA, typically on an organism's homologous chromosomes, that is used as a template to repair damaged DNA in its image. This system has been manipulated to allow researchers to introduce DNA into a cell's genome by providing exogenous template DNA (Gaj et al., 2017). In quiescent cells like HSCs NHEJ is the dominant mechanism, as it does not require cells to be in an active cell cycle to operate (Shin et al., 2020). This is an ideal state for knocking out target genes (Mohrin et al., 2010).

The CRISPR-Cas9 system has been used previously to edit HSCs, despite the difficulties associated with editing such a rare and fragile cell population (Bak et al., 2018; Frangoul et al., 2021; Kim et al., 2018). Applications for this include Frangoul et al. (2021)'s work, in which they successfully reactivated foetal haemoglobin production in sickle cell anaemia patients' HSCs, leading to significant improvements in their conditions.

5.1.2 CD33

The myeloid cell surface marker CD33 is expressed in 85-90% of AML patients' cancer cells (Molica et al., 2021). This makes it an ideal target for AML therapies such as CAR T-cell therapy or the antibody drug gentuzumab ozogamicin (GO) (Van Der Velden et al., 2001), as discussed previously. However, targeting CD33 also risks myeloid toxicity and associated side-effects (Gill et al., 2014), as illustrated by the temporary withdrawal of GO from the market due to safety concerns in

2010 (Borot et al., 2019; Laszlo et al., 2014). Knocking out CD33 in healthy cells to establish a CAR T-cell therapy-resistant haematopoietic system could side-step this issue (Kim, 2023).

CD33 is a sialic acid-binding immunoglobulin-related lectin (siglec), a subset of the immunoglobulin superfamily, and is also known as siglec 3 (Laszlo et al., 2014). It is a transmembrane receptor comprising N-terminal, extracellular IgV and IgC immunoglobulin domains, a transmembrane domain and a C-terminal intracellular tail with two tyrosine-based inhibitory signalling motifs (ITIM) (Molica et al., 2021). The CD33 gene contains seven exons, each of which encodes a separate domain, except for exons 3 and 4, which jointly encode the IgC domain (see **Figure 5.1**).

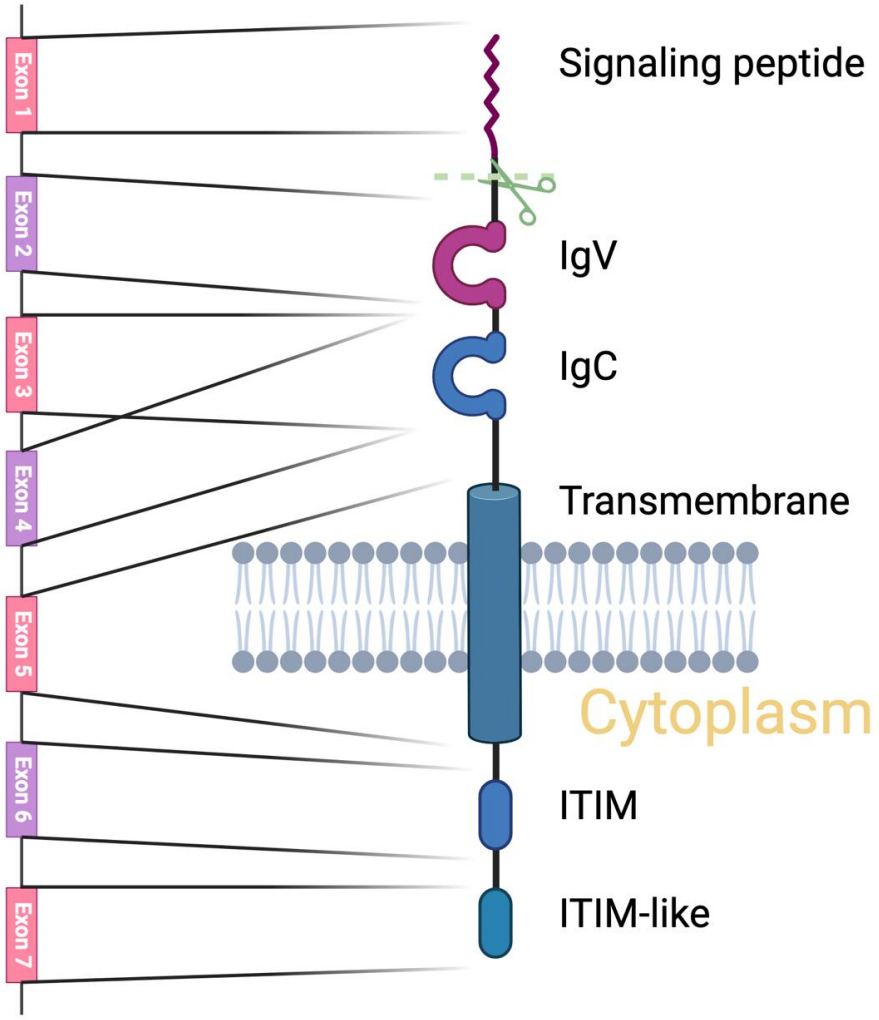

***Figure 5.1 CD33 protein and gene structure**. The exons that constitute the CD33 gene are shown on the left and are each linked to the domain of CD33 that they encode. Note that the IgC domain is encoded by two exons. The signalling peptide encoded by exon 1 is removed in the mature*

protein, illustrated by the dashed line and scissors. The phospholipid bilayer is shown, with the cytosolic side labelled. Created with BioRender.com.

The role of CD33 in wild-type cells is an area of debate, however it is believed to dampen the inflammatory response when activated by sialic acid-containing proteins. It has also been shown to inhibit phagocytosis (Bhattacherjee et al., 2019; Molica et al., 2021; L. Zhao, 2019) and autophagy (Eshraghi et al., 2021) when active, though these attributes have been predominately observed in microglia (Bhattacherjee et al., 2019).

Despite CD33 typically being described as a myeloid marker, lymphoid cells have also been shown to express a form of CD33. However, unlike myeloid CD33, also known as CD33M, lymphoid cells have been shown to express a splice variant, CD33m. CD33m lacks the IgV domain of CD33M (Hernández-Caselles et al., 2006; Pérez-Oliva et al., 2011). In spite of this, the CAR T-cells used in the next chapter used the P67.6 mAb to target the IgV domain, so should have only affected myeloid cells (Pérez-Oliva et al., 2011).

CD33 has been knocked out in HSCs previously, either by targeting a site in exon 2 (Kim et al., 2018), or one in exon 3 (Borot et al., 2019; Humbert et al., 2019). The resultant CD33- HSCs repopulated the BM niche of animal models and maintained haematopoiesis following CD33+ cell ablation by CAR T-cells. However, the effect on human cells in a similar context has yet to be established. *In vitro* models offer an experimental method for testing this system on human cells while mitigating the implicit high risk and ethical concerns of human trials.

5.1.3 Aims

The aim of this chapter was to develop a method for efficiently knocking out CD33 in HSCs. To accomplish this, a protocol for knocking out CD33 in THP-1s, a human AML-derived cell type often used to model haematopoietic cells (Chanput et al., 2014), was first optimised. This system was then applied to HSCs.

5.2 Materials and methods

5.2.1 Flow cytometry

Flow cytometry was carried out as previously described (see **2.2.4**). For assessing CD33 expression, the following gating strategy was used (see **Figure 5.2**).

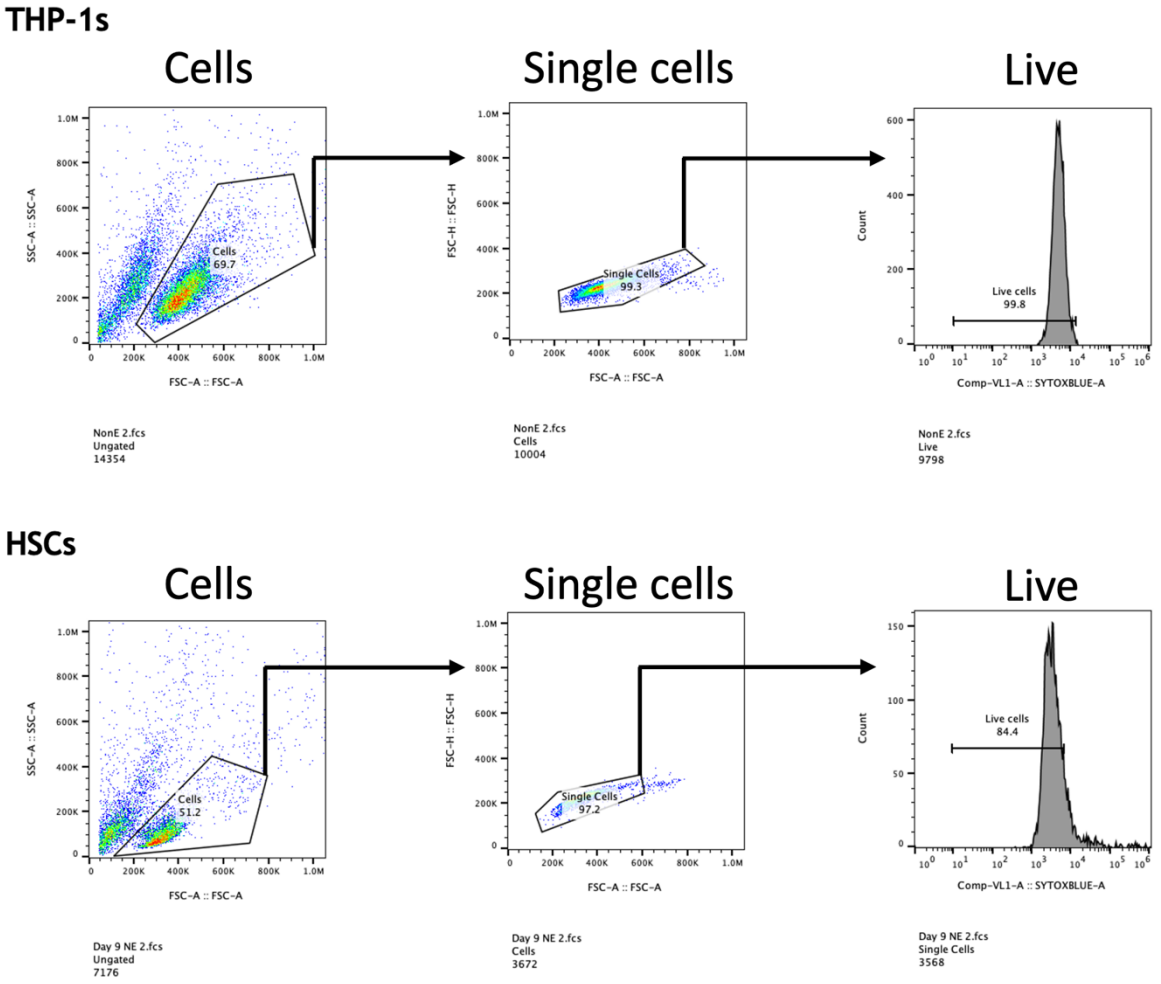

Figure 5.2 Representative gating strategies for live THP-1s and HSCs. *FSC-A and SSC-A were used to identify cells. FSC-A and FSC-H were used to identify single cells. A sytox blue gate was used to omit dead cells.*

The viability stain sytox blue (ThermoFisher Scientific, S34857) was used. Gated cell populations were then analysed by measuring the median fluorescence intensity (MFI) of the populations in specific channels. To assess levels of the surface protein CD33 two antibodies were used in parallel (see **Table 5.1**).

Table 5.1 CD33 flow antibodies.

Flow channel	Clone	Target CD33 domain	Catalogue #	Manufacturer
B3	HIM3-4	IgC	15-0339-42	Invitrogen
V2	WM53	IgV	303421	BioLegend

These were selected as they target different CD33 domains, increasing redundancy without risking competitive binding (Pérez-Oliva et al., 2011). Notably, the B3 antibody's reactivity has been shown to be affected by cell sialylation, potentially leading to erroneous measurements (Pérez-Oliva et al., 2011). However, similar trends were seen with both antibodies, which were used interchangeably.

5.2.2 Fluorescent-activated cell sorting (FACS)

A BD FACSAria III cell sorter from BD biosciences was used to isolate a population of CD33- THP-1s following CRISPR gene editing (see **Figure 5.3**).

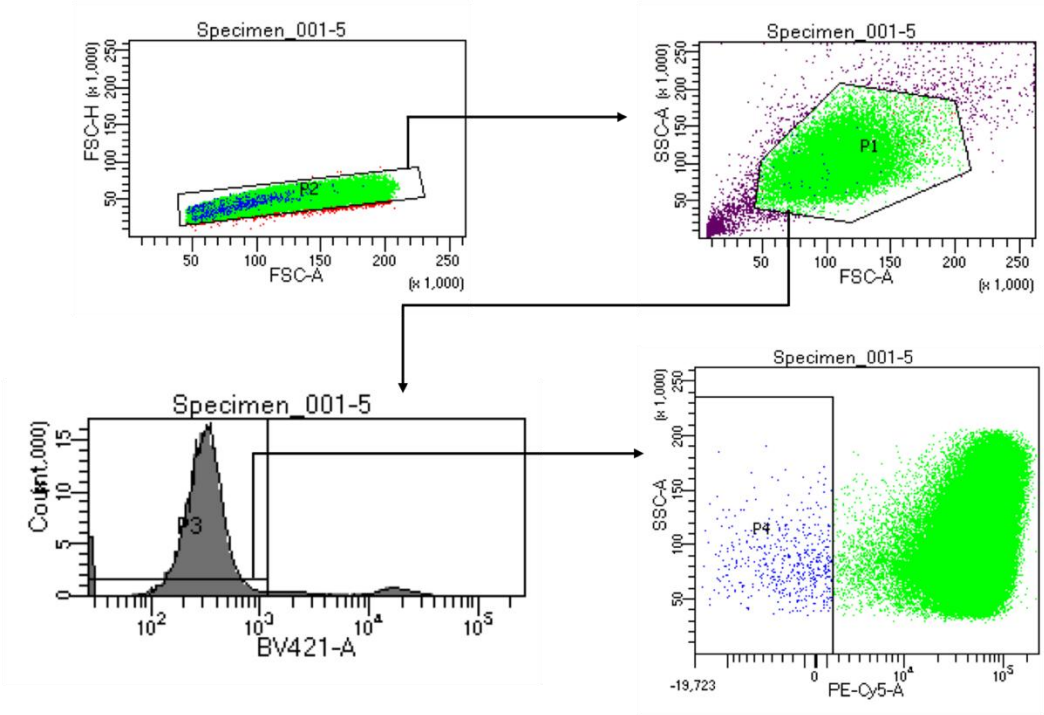

Figure 5.3 Gating strategy used for FACS sorting CD33- THP-1s. *FSC-A and SSC-A were used to identify cells. FSC-A and FSC-H were used to identify single cells. A sytox blue gate was used to omit dead cells. THP-1 cells which had been successfully edited and expressed low levels of CD33 were then identified, and this population isolated.*

The viability stain sytox blue (ThermoFisher Scientific, S34857) was used, as well as the anti-HIM3-4 CD33 antibody (Invitrogen, 15-0339-42).

5.2.3 DNA isolation

Genomic DNA was extracted from cells using a Qiagen DNeasy blood & tissue kit and the corresponding protocol. To create and expand the desired PCR product, primers for sites 5' and 3' of sgRNA target sites were designed in collaboration with Dr Adam West. 45 µL of a master mix of PCR reagents (see **Table 5.2**) was added to 5 µL of genomic DNA.

Table 5.2 PCR master mix reagents.

Reagent	**Volume used per sample (µL)**	**Product code**	**Manufacturer**
5X Phusion HF buffer	10	EO553S	New England Biolabs (NEB)
10 mM dNTP mix	1	EO553S	NEB
10 µM forward primer	2.5	-	Integrated DNA technologies (IDT)
10 µM reverse primer	2.5	-	IDT
100% Dimethylsulfoxide	1.5	EO553S	NEB
2000 U/mL Phusion HF polymerase	0.5	EO553S	NEB
Nuclease-free water	27	-	NEB

The primers used are listed in **Table 2.7**. The resultant solution was then run through the following PCR programme:

1. 98°C for 30 s for initial denaturation
2. 98°C for 10 s for denaturation
3. *°C for 20 s for annealing
4. 72°C for *s for extension
5. Repeat steps 2-4 30 times
6. 72°C for 2 min for final extension
7. Hold at 4°C

*The annealing temperature for each primer pair was determined using the NEB calculator. The elongation time was determined based on the length of the desired PCR product (30s per kb). Both are shown in **Table 5.3.**

Table 5.3 Annealing temperature and extension time for each sgRNA target.

sgRNA target	Annealing temperature	Extension time
Exon 2	64°C	22 s
Exon 3	63°C	15 s
+21 enhancer	63°C	15 s

The PCR product produced was either frozen at -80°C or immediately processed as described below.

5.2.4 Sanger sequencing and analysis

10 µL of PCR product was added to 2 µL of purple loading dye and loaded into a 1.2% agarose gel made with 1% SYBR safe. This was run alongside 1 µL of 1kb plus ladder mixed with 2 µL purple loading dye and 9 µL nuclease free water. Following loading, the gels were run at 110V for ~60 min. The gels were then visualised on a UV visualiser to confirm the presence of a band PCR product of the appropriate length. PCR product was then cleaned up using a Qiagen QIAquick PCR Purification Kit. Next, the concentration of PCR product was calculated using a NanoDrop 2000c spectrophotometer (Thermo scientific). Finally, PCR products were diluted to 5 ng/µL and Sanger sequenced using the eurofins SupremeRun Tube Sequencing Service with the relevant forward primer. TIDE analysis was subsequently used to determine the efficiency and nature of the edit.

5.2.5 Trypan blue staining and automated cell counting

An aliquot of homogenously suspended cells was mixed 1:1 with Gibco Trypan Blue solution (0.4%) (15250-061). The number of cells in 10 µL of the resultant mix was then counted using a Countess 3 automated cell counter, and the cell density calculated.

5.3 Results and discussion

5.3.1 Optimising CD33 knock-out in THP-1s

To efficiently knock out CD33 in haematopoietic cells, a protocol was first optimised using the THP-1 AML cell line. The majority of THP-1 cells, like many other AML cell types, express CD33 (Laszlo et al., 2014). This was ideal as it made changes in CD33 expression more quantifiable. In addition, AML cells are cancerous haematopoietic cells (Chanput et al., 2014), and are often used as a haematopoietic cell model (Z. Qin, 2012), so it was theorised that an optimised protocol for THP-1s would also work well on HSCs.

Three different sgRNAs were used to knockout (KO) CD33. These each targeted a different site. These sites were in exon 2 of the CD33 gene, exon 3 of the CD33 gene, and a putative upstream enhancer of CD33 expression (denoted as +21 enhancer) (see **Figure 5.4**). A well-established electroporation protocol for human haematopoietic cell transfection (1600 V/10 ms/3 pulses) was used initially (Shiroshita et al., 2022).

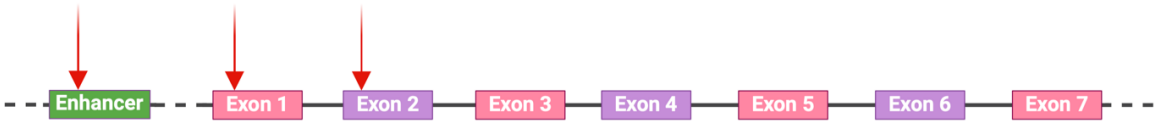

***Figure 5.4 Target sgRNA sites for CRISPR induced DSBs**. Red arrows denote target sites.*

5.3.1.1 TIDE analysis of mutagenesis caused by sgRNAs in THP-1s

The efficiency of KO, as well as the type of mutations caused by each of the sgRNAs, was assessed. Cells were edited, incubated for three days, then their genomic DNA was isolated, and PCR amplified. The resultant PCR product was Sanger sequenced and compared to PCR product from unedited control cells using

tracking of indels by decomposition (TIDE) analysis. TIDE analysis investigates genetic changes caused by gene editing and is a reliable method for characterising mutations around a target site caused by CRISPR, and assessing the efficiency of gene editing on a genetic level (Brinkman et al., 2014) (see **Figure 5.5**).

These results indicated that all three sgRNAs tested caused mutagenesis at their target sites within a range of high efficiencies, with the exon 3 sgRNA associated with the highest level of efficiency, followed by the exon 2 sgRNA and finally the +21 enhancer sgRNA. These results also shed light on the nature of the mutations caused by each sgRNA. The exon 2 sgRNA edit primarily resulted in thymine insertions, as well as some adenine insertions and some deletions. The exon 3 sgRNA edit was more heterogenous, with a mix of insertions and deletions observed. The insertions were mostly cytosine, with some guanine and rarely adenine. The sgRNA targeting the +21 enhancer exclusively caused deletions.

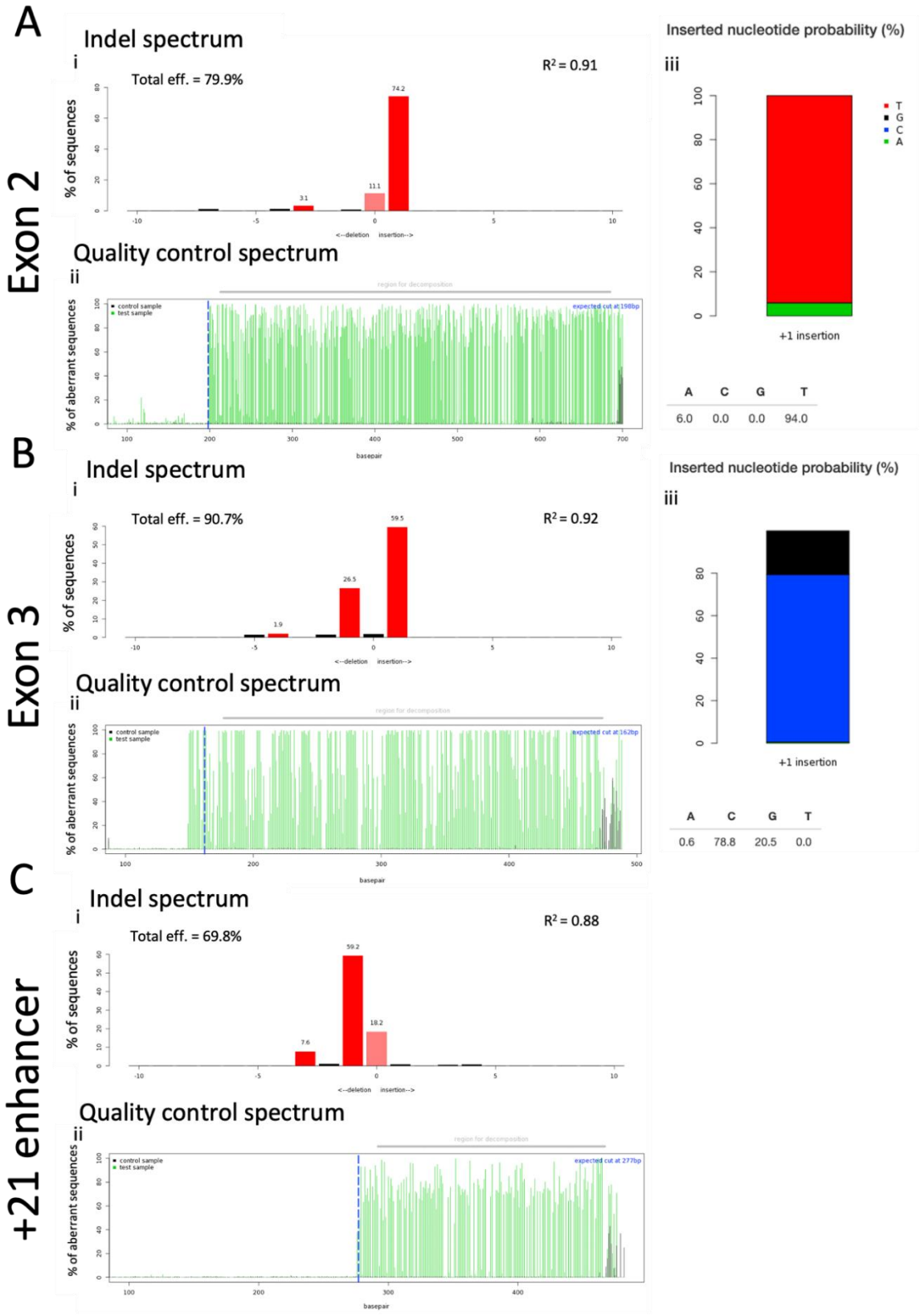

Figure 5.5 Editing efficiency of individual sgRNAs assessed by TIDE analysis*. Three different sgRNA targets, namely (**A**) a site in exon 2 of CD33, (**B**) a site in exon 3 of CD33, and (**C**) a site in a putative upstream enhancer, were edited with individual sgRNAs. Three days after electroporation, the target sites were PCR amplified, Sanger sequenced, and compared to the same sequence in unedited cells. (**i**) Indel spectrum representing the frequency of different types*

*of mutations and their position relative to the expected cut site. The efficiency of each edit is shown in the top left of the indel spectrum, as well as the R^2 value in the top right. Statistically significant indels (p<0.001) are shown in red, while insignificant ones are black. (**ii**) Visualisation of the aberrant sequence signal of unedited control (black) and edited (green) sequences, as well as the expected cut site (vertical blue dashed line) and the decomposition window (grey bar). (**iii**) Prediction of inserted base for +1 insertions. The percentage of inserted thymine (T, red), guanine (G, black), cytosine (C, blue), and adenine (A, green) predicted is illustrated by the stacked bar graph shown, as well as the percentages underneath said graph. Note that the upstream enhancer sgRNA didn't cause insertions, so no predictions were made.*

5.3.1.2 Testing different combinations of sgRNAs

To further test CD33 KO efficiency in THP-1s, the level of CD33 expression 3 days after editing was assessed using flow cytometry. This approach gives different information to TIDE analysis, as it assesses the quantity of a surface protein on edited cells. As a result, more complex systems, such as those utilising multiple sgRNAs, can be assessed accurately using this method. These multiple sgRNA systems have been shown to be effective, either at targeting a single site with multiple sgRNAs (Campa et al., 2019), or at targeting multiple sites in different genes (Cong et al., 2013). Conditions in which various combinations of sgRNAs were used were included at this stage to investigate if they had an additive effect on CD33 protein level on the cells' surfaces. A non-electroporated control and a MOCK control, in which the cells were electroporated without RNPs present, were included in addition (see **Figure 5.6**).

These initial results suggested that the exon 2 sgRNA caused the most significant decrease in CD33 expression, and that combining sgRNAs had a synergistic effect (Campa et al., 2019). It was possible that all three sgRNAs cause some degree of CD33 KO, as suggested by the previous TIDE data (see **Figure 5.5**), but that the level of KO was low when exon 3 and the +21 enhancer were targeted. However, when multiple sgRNAs were included, a level of redundancy may have been created, leading to a higher level of overall CD33 KO. Notably, even with the cocktail of all three sgRNAs, total knock out wasn't observed, as expression wasn't as low as unstained controls.

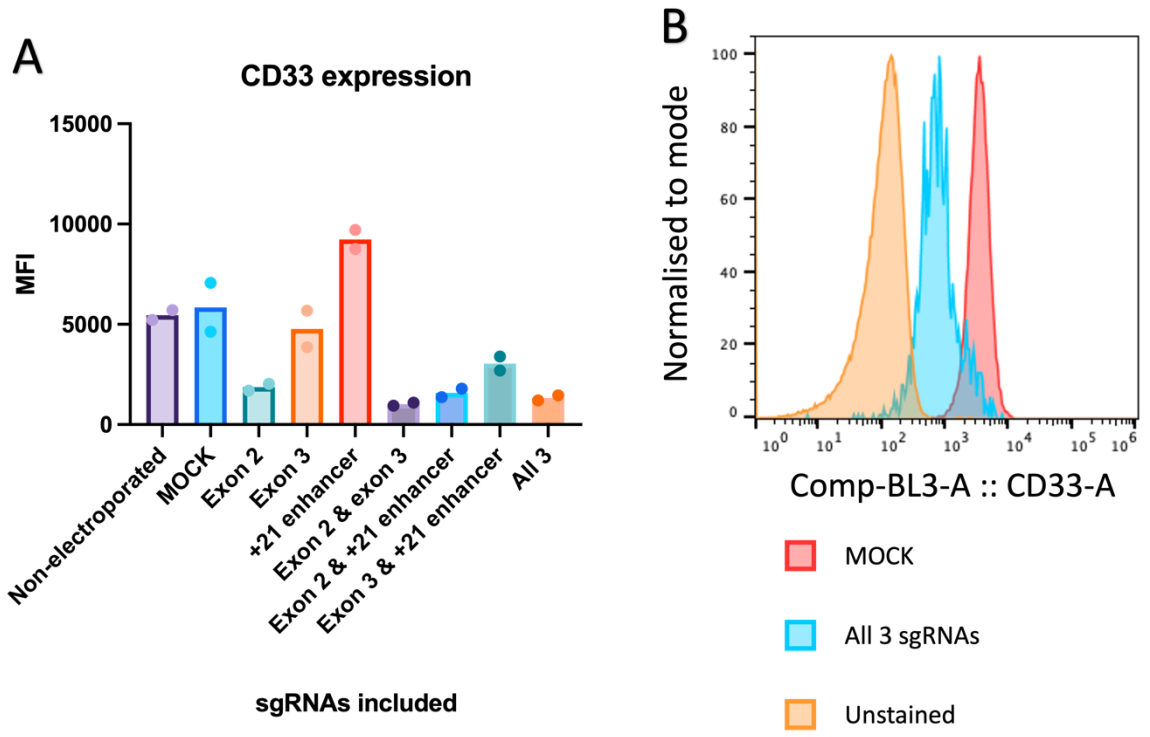

Figure 5.6 Different combinations of sgRNAs' effect on CD33 KO efficiency in THP-1s assessed by flow cytometry. *An anti-HIM3-4 CD33 antibody was used to detect CD33 expression in THP-1s 3 days after electroporation using flow cytometry. (**A**) Graph of measured MFI. Graph shows mean. N=2 experimental replicates. (**B**) Representative histogram of BL3-A fluorescence, corresponding to CD33 expression. The MOCK control (pink), cocktail of all 3 sgRNAs (blue), and unstained control (orange) conditions are shown.*

It was possible that in samples with low measured levels of CD33, the mutant protein was still formed, but it either didn't translocate to the cells' surfaces, or the sites targeted by the antibodies used to assess CD33 expression were changed by missense mutations that were otherwise tolerated. A lack of translocation would still result in increased CD33-redirected CAR T-cell resistance, but missense mutations wouldn't necessarily, as the site recognised by the CAR T-cells was different from that recognised by the antibody used for flow cytometry. However, missense mutations would only result in false positive data if they appeared in exon 3, the target of the antibody used for CD33 detection in this instance. To increase the reliability of the flow cytometry results, qPCR and western blot could be performed to assess CD33 transcription and translation. Regardless, the exon 2 sgRNA, as well as the cocktail of all three sgRNAs, were carried forwards and compared rigorously (see **Figure 5.7**).

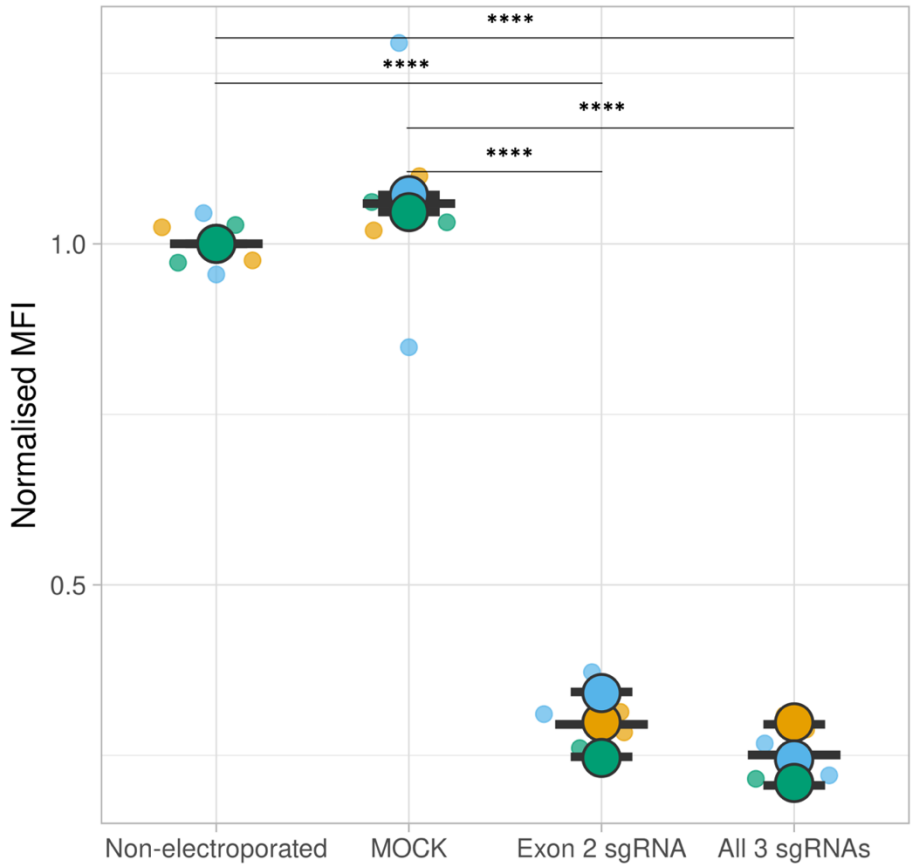

Figure 5.7 Flow cytometry analysis of candidate sgRNA combinations' abilities to KO CD33 in THP-1s. *An anti-HIM3-4 CD33 or an anti-WM53 antibody was used to detect CD33 expression in THP-1s 3 days after electroporation using flow cytometry. Exon 2 sgRNA, as well as a cocktail of all 3 sgRNAs, non-electroporated and MOCK controls were tested. CD33 expression was normalised against a non-electroporated control. Large dots represent the mean of all MFI values for each replicate. Smaller dots represent individual technical repeat values. All dots with the same colour are from the same biological replicate. Graphs show mean ± SD. Statistics by one-way ANOVA followed by Tukey multiple comparison test. ****p < 0.0001. Non-significant not shown. N=3 experimental replicates with unique THP-1 samples, each consisting of n=2 technical replicates.*

Taken together, the flow cytometry data demonstrates that both the sgRNA targeting exon 2 alone and the cocktail of all three sgRNAs caused highly efficient CD33 KO in THP-1s.

5.3.1.3 CD33 KO stability over time

The clinical approach this system was working towards required the stable KO of CD33, as the purpose of the edited cells was to form the foundation for a CD33- haematopoietic system that would resist the long-term surveillance of implanted

CD33-redirected CAR T-cells. Therefore, the expression of CD33 in edited THP-1 cells over 30 days was assessed using flow cytometry (see **Figure 5.8**).

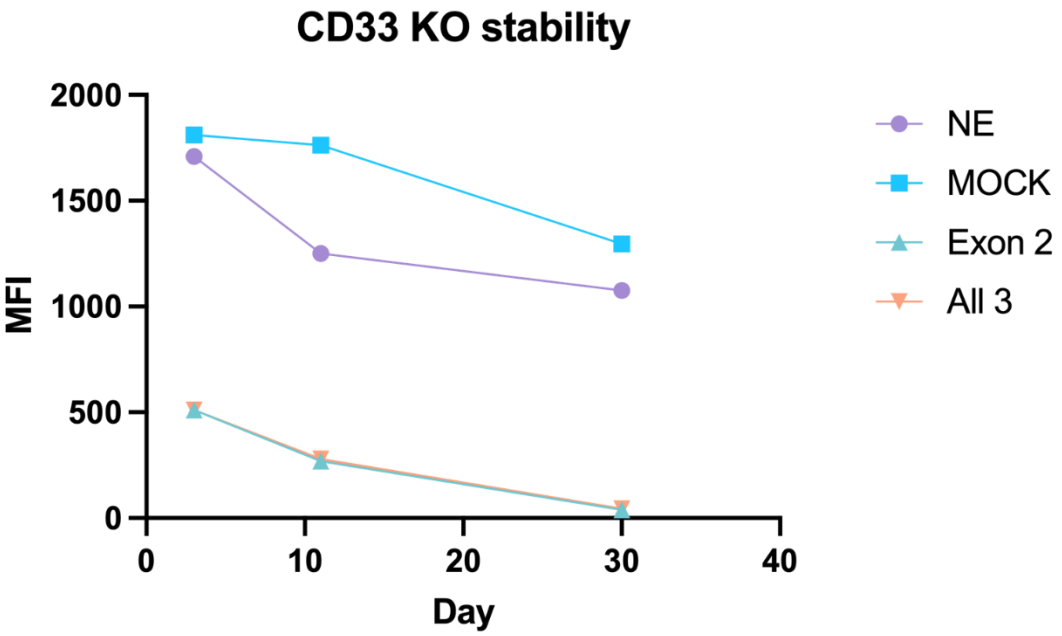

***Figure 5.8 Stability of CD33 KO over 30 days**. A HIM3-4 anti-CD33 antibody was used to detect CD33 expression in THP-1s using flow cytometry. This was done 3-, 11- and 30-days following electroporation. Exon 2 sgRNA, as well as a cocktail of all 3 sgRNAs, non-electroporated and MOCK controls were tested. Graph shows mean. n=2 technical replicates.*

The CD33 KO generated by the sgRNA cocktail and the exon 2 sgRNA alone appeared to be stable over 30 days. Notably, there was a downward trend in CD33 expression across all conditions, indicating a potential decay in CD33 expression in later passage THP-1s.

5.3.1.4 Edited and unedited cells grow similarly

It was important to assess the growth rate of edited and unedited THP-1s to confirm that the previous results were due to efficient KO of CD33, rather than edited cells outgrowing unedited ones. Therefore, THP-1s were edited with a cocktail of all three sgRNAs then processed with FACS, isolating a population of exclusively CD33- THP-1s. These cells were then grown alongside an equivalent starting number of unedited cells for 14 days, and the number of live cells assessed by trypan blue staining and automated counting daily (see **Figure 5.9**).

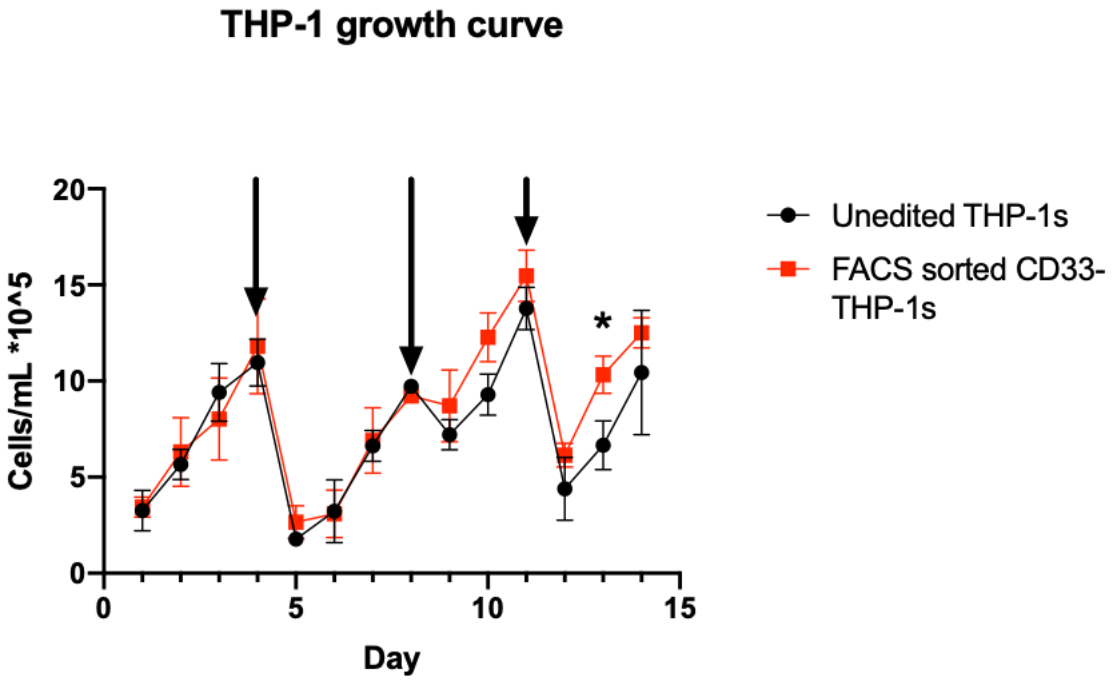

***Figure 5.9 Edited and unedited THP-1 growth rate**. THP-1s edited with a cocktail of all 3 sgRNAs targeting CD33 were FACS sorted to isolate CD33- cells. These cells were grown in parallel to unedited CD33+ THP-1s for 14 days and counted every day with trypan blue. The live cell counts are shown. The arrows indicate the days on which the wells had some of their media replaced, resulting in a drop in the number of non-adherent THP-1s. The significance of any difference between edited and unedited cell counts was measured using a t-test to compare data points taken on the same day. Graphs show mean ± SD. *p < 0.05. Non-significant not shown. n=3 technical replicates.*

The growth rates of the edited and unedited cells were very similar, suggesting that the edit had little to no effect on proliferation, and the previous results, which were obtained three days after electroporation, were in fact due to efficient CD33 KO.

5.3.2 Knocking out CD33 in HSCs

5.3.2.1 Electroporation protocol optimisation

Once the efficiency of the CD33 KO in THP-1s was established, the next step was applying this system to both bought and isolated human HSCs. The electroporation protocol used for THP-1s was compared to a well-established HSC electroporation protocol (1700 V/20 ms/1 pulse) (Donnelly et al., 2024; Gundry et al., 2016; Shiroshita et al., 2022) (see **Figure 5.10**).

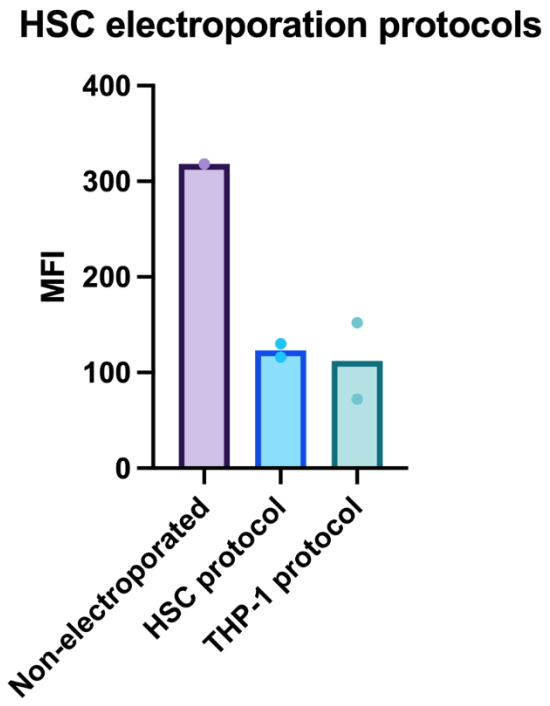

Figure 5.10 Different electroporation protocols' effect on CD33 expression in HSCs. *The protocol previously shown to be effective on THP-1s (1600V/10 ms/3 pulses) (THP-1 protocol) was compared to a well-established HSC electroporation protocol (1700 V/20 ms/1 pulse) (HSC protocol) in patient derived HSCs. Three days after electroporation the cells were collected and analysed using flow cytometry with an anti-HIM3-4 CD33 antibody. Graph shows mean. Non-electroporated n=1 technical replicate, other conditions n=2 technical replicates.*

Despite HSCs typically not expressing CD33 until they differentiate into myeloid cells, a drop in CD33 expression was observed in both editing conditions compared to the negative non-electroporated control. This was likely due to partial differentiation of the patient-derived HSCs used for this experiment prior to editing, resulting in high initial CD33 expression that was subsequently lost in edited cells. As there was no significant difference in CD33 expression between the protocols tested, the more established protocol (1700 V/20 ms/1 pulse) was carried forwards. Ideally all possible electroporation protocols would have been trialled to ensure the selected protocol was best, however this was impossible due to limitations in the number of available HSCs.

5.3.2.2 Knockout efficiency

A principle aim of this project was the production of genetically modified HSCs that produce CD33- progeny. This was initially assessed using TIDE analysis. The effect of the cocktail of all three sgRNAs was compared to the individual sgRNAs mutagenesis efficiency, as well as MOCK controls (see **Figure 5.11**, **Figure 5.12**, and **Figure 5.13**).

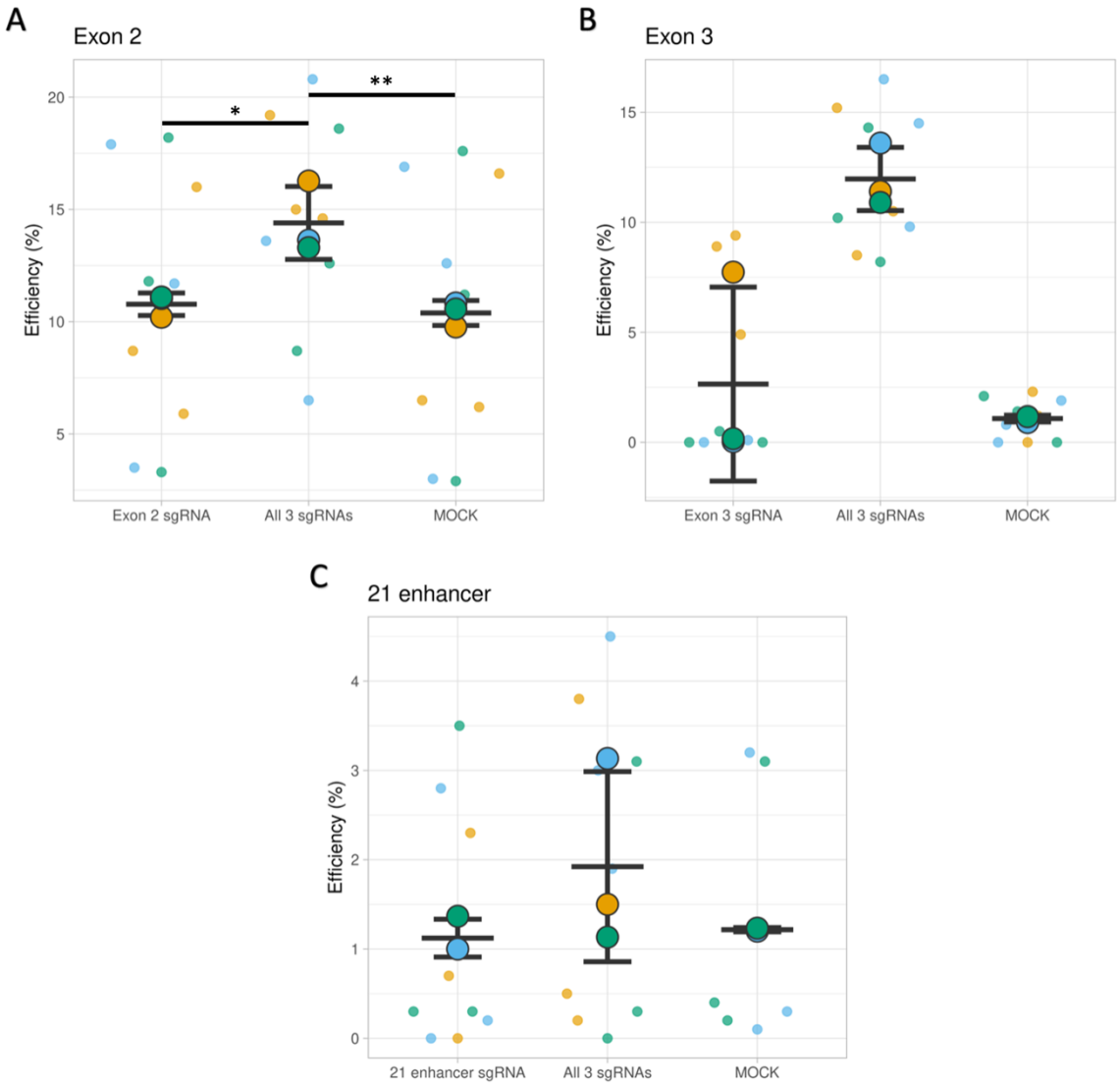

Figure 5.11 HSC CD33 KO efficiency. *Patient derived HSCs were edited with the optimised HSC protocol. Three days after electroporation, the target sites were PCR amplified, Sanger sequenced and compared to the same sequence in unedited cells. TIDE analysis was used to determine editing efficiency, i.e. percentage of cells containing INDELs at each site, at sgRNA target sites in (**A**) exon 2, (**B**) exon 3, and (**C**) +21 enhancer. Each sample's sequence was compared to three different non-electroporated control samples, giving the individual data points represented by the small dots. The mean efficiency for each sample was then calculated and is shown by the large dots. Statistics for (**A**) by one-way ANOVA followed by Tukey multiple comparison test. *p < 0.05 and **p < 0.01. Non-significant not shown. Graphs show mean of means ± SD. n=3 technical replicates.*

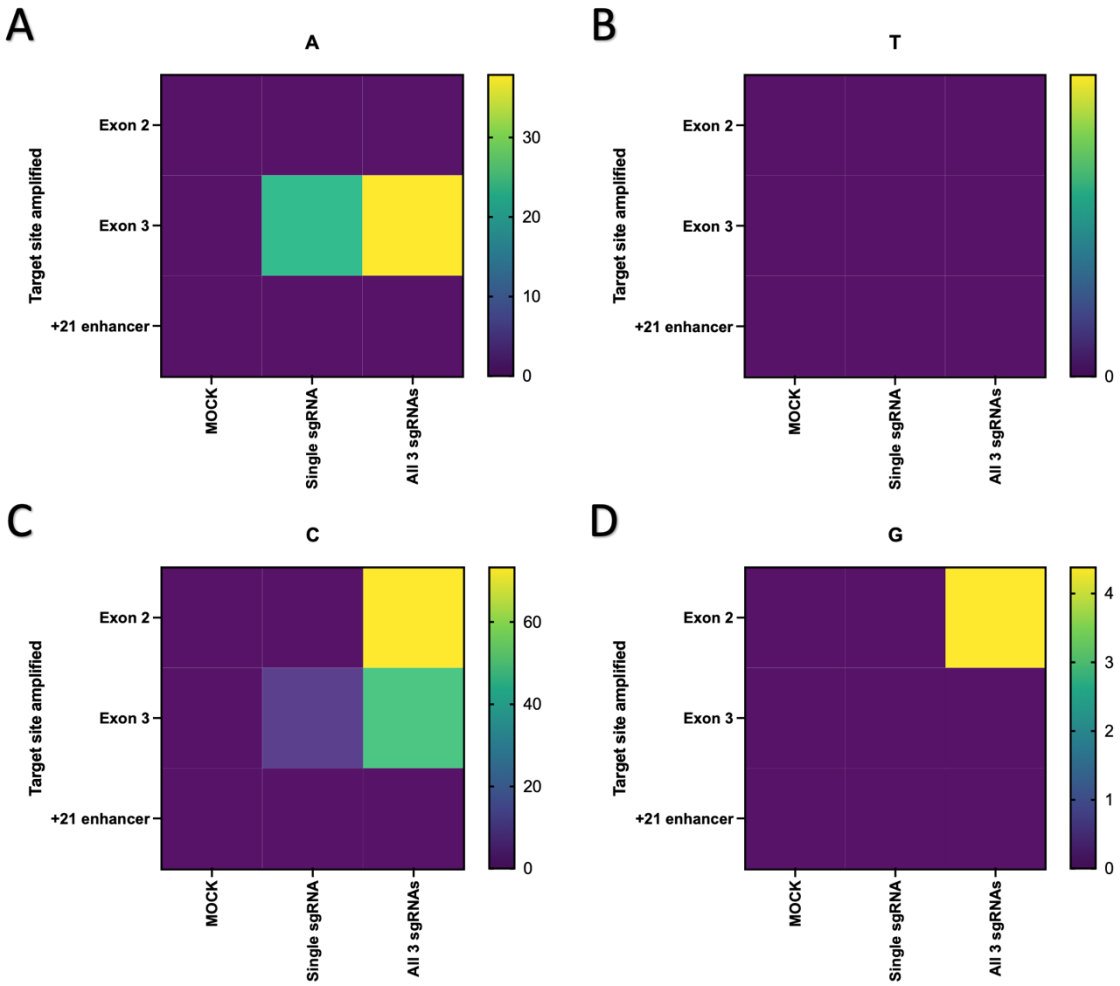

Figure 5.12 Insertion characterisation following HSC CD33 KO. *TIDE analysis was used as in* ***Figure 5.11*** *to determine the average percentage of +1 insertions for each condition that are a specific nucleotide base following CD33 KO in patient derived HSCs. Each possible base is represented by a dedicated heat map: (**A**) adenine, (**B**) thymine, (**C**) cytosine, (**D**) guanine. Note that the scale used for height is different for each heatmap to allow for clear visualisation. Heatmaps show mean. n=3 technical replicates.*

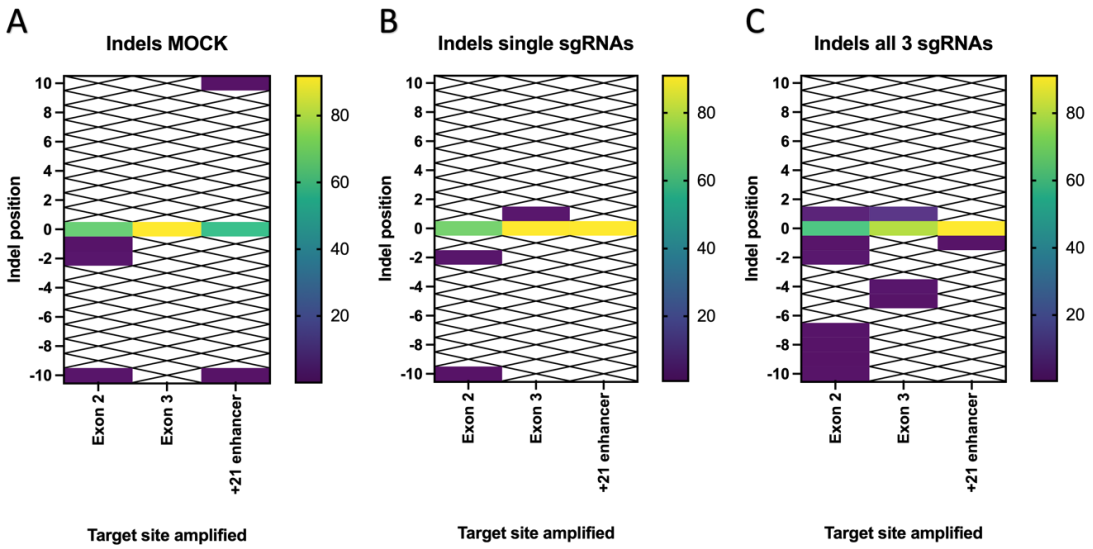

Figure 5.13 INDEL characterisation following HSC CD33 KO*. TIDE analysis was used as in* ***Figure 5.11*** *to determine the types of mutations present following CD33 KO in patient derived HSCs. These mutations were characterised by the percentage of nucleotide insertions (positive values) or deletions (negative values) around the cut site (represented by 0). (**A**) MOCK control samples, (**B**) samples edited with a single sgRNA, and (**C**) samples edited with a cocktail of all 3 sgRNAs are shown. A higher percentage of 0 values indicates greater alignment of the control and test sequences, implying lower mutagenesis. White boxes with a black cross indicate that no statistically significant indels were detected at the corresponding site for the corresponding condition. Heatmaps show mean. n=3 technical replicates.*

The TIDE analysis results suggested that HSCs responded differently to THP-1s, causing different patterns and degrees of mutagenesis (see **Figure 5.11**). Firstly, KO efficiency was lower in the lone sgRNA conditions, with minimal difference observed between these and the MOCK negative controls with any of the sgRNAs tested. This was potentially caused by unexpectedly high mutagenesis measured in the MOCK negative controls, especially at the exon 2 target site. This anomalous data may have been due to poor sequencing, either of the MOCK or non-electroporated controls which all samples were compared to. Alternatively, it is possible, though highly unlikely, that the act of electroporation itself caused mutations. However, there was a large increase in mutagenesis efficiency in the sgRNA cocktail conditions when investigating the exon 2 and exon 3 target sites. This was unexpected, as initially it was assumed that the lower levels of each sgRNA, and therefore reduced amount of Cas9 activity at each site, would result in lower mutagenesis, but still produce a greater level of CD33 KO cumulatively. However, these results suggest that the opposite is true, and that the sgRNA cocktail is the ideal condition for promoting indel formation at the exon 2 and exon 3 target sites. This may have been due to the introduction of DSBs at multiple sites, increasing both the strain on the cells' DNA repair pathways, and competition for repair resources between cut sites (Mali et al., 2013).

While the efficiency of KO was increased in HSCs edited with the sgRNA cocktail, using multiple sgRNAs also increases the risk of off-target activity, which is a concern for cells that would be transplanted into patients due to potentially harmful mutations being introduced (Becker et al., 2023; Q. Cheng et al., 2020). To still produce the same competition, efficiency sgRNAs (esgRNAs) which are highly specific to non-coding regions of DNA in a cell could be used alongside individual sgRNAs. While the sgRNAs used were designed to minimise off-target

effects, future work could look to assess this experimentally using assays such as whole genome sequencing. Nevertheless, the three sgRNA cocktail was selected as the most promising of the conditions tested and used in further experiments.

Another difference between THP-1 and HSC mutagenesis was the types of mutations observed (see **Figure 5.12** and **Figure 5.13**); the exon 2 target site primarily experienced deletions across all conditions, despite most mutations at this site in THP-1 cells treated with the exon 2 sgRNA alone being +1 insertions. The exon 3 target site also exclusively had insertions in HSCs mutated with a single sgRNA, unlike THP-1s, in which a mix of insertions and deletions was observed. This mix was however replicated in the sgRNA cocktail condition for HSCs, albeit with different nucleotides inserted and the deletions recorded at different positions. The +21 enhancer target site also experienced higher mean mutagenesis when subjected to the sgRNA cocktail condition, though this change was not significant. The mutations seen at this site in the cocktail condition were like those observed in THP-1s. However, no statistically significant indels were observed in the lone +21 enhancer sgRNA condition, indirectly implying that the cocktail caused more efficient editing at this site. One MOCK sample also showed a range of non-specific indels at various points around the +21 enhancer sgRNA target site, suggesting poor sequencing led to misalignment in this sample's TIDE analysis, leading to the only statistically significant INDELs in the MOCK control for the +21 enhancer target site.

The differences observed between edited HSCs and THP-1s have various potential explanations. Firstly, disparities in the INDEL spectrum may have been due to small differences around the cut sites (Hsu et al., 2013). Despite the sites chosen having no common SNPs present, the genetic instability of cancerous THP-1 cells makes this a possibility. In addition, HDR was likely active in a large subset of the highly proliferative THP-1s, while NHEJ would dominate the mostly quiescent HSC population, altering the editing dynamics (Mohrin et al., 2010). Finally, differences in the availability of target sites due to differential chromatin structure and cell cycle phase may have played a part as well (Jansen et al., 2015).

The efficiency of knockout with the sgRNA cocktail was subsequently assessed using flow cytometry. This presented a challenge as naïve HSCs do not express CD33 until they differentiate into myeloid cells, regardless of whether they have

been edited successfully or not (Laszlo et al., 2014). Therefore, the level of CD33 expression was tracked over time with flow cytometry, with the expectation that the HSCs would rapidly differentiate under standard tissue culture conditions (Jaroscak et al., 2003), producing CD33+ myeloid progeny if the CD33 gene was intact, and vice versa (see **Figure 5.14**).

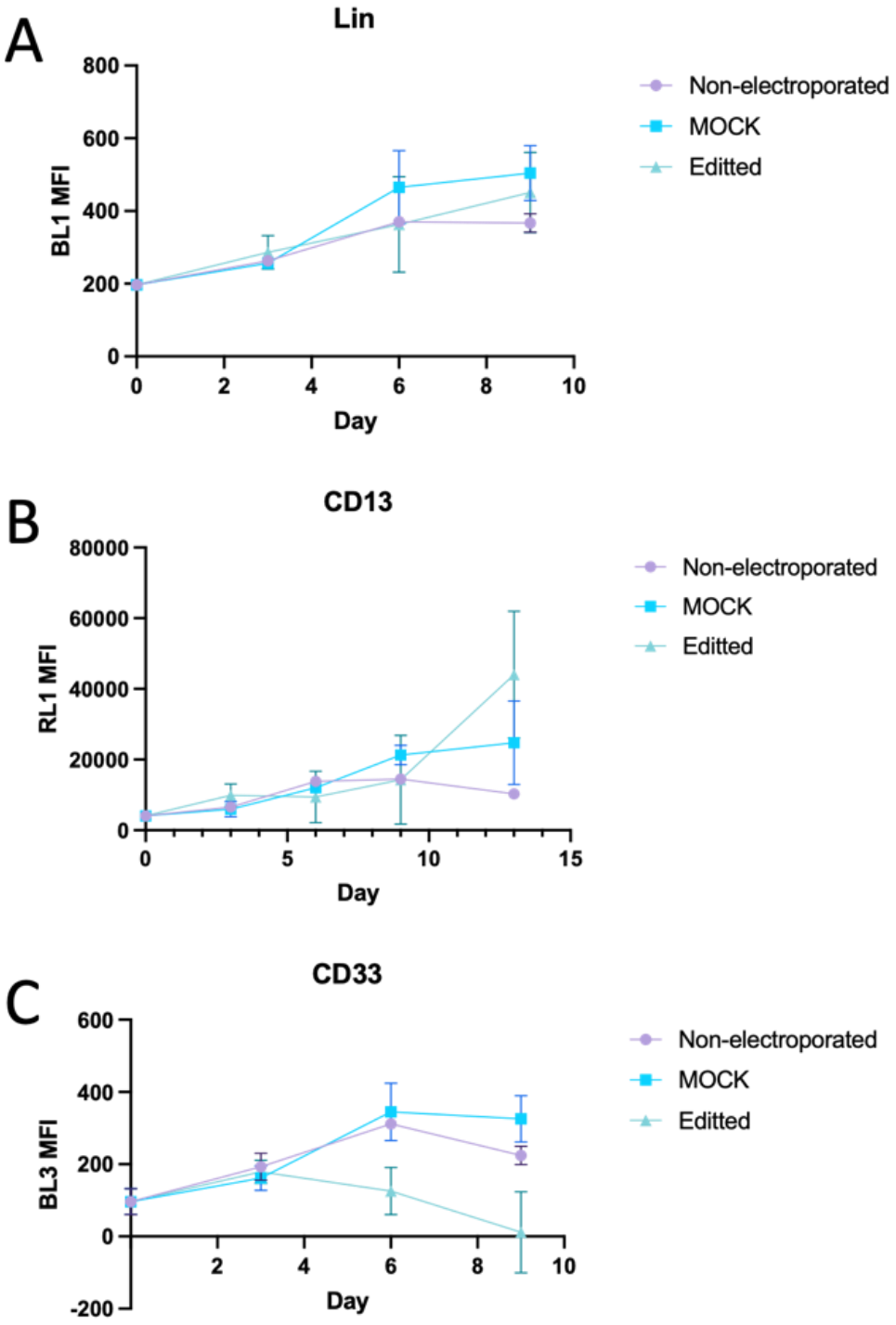

***Figure 5.14 Effect of gene editing on HSCs over time**. Flow cytometry was used to measure changes to expression of (**A**) various lineage-associated surface markers surface markers, (**B**) CD13, or (**C**) CD33 on patient derived HSCs over 9 days. Graphs show mean ± SD. n=3 technical*

The level of the myeloid marker CD13 and a cocktail of lineage cell surface markers' staining intensity increased over nine days across conditions, suggesting that the HSCs began to differentiate and produce myeloid cells over this time. CD33 expression also followed this trend in the non-electroporated and MOCK conditions. However, in edited HSCs CD33 initially increased in line with other conditions, before rapidly dropping on days 6 and 9. When measured with a Kruskal-Wallis test followed by Dunn's multiple comparisons test, the difference between the MOCK control and the edited sample was found to be significant ($p=0.0211$). These results suggested that the edit was at least partially successful at reducing detectable CD33 levels on HSCs' surfaces. The initial increase could have been caused by CD33 precursors that were already present in edited cells that had begun to undergo myeloid differentiation but had yet to migrate to the cell surface. On subsequent days the HSCs may have continued to divide but experienced a gradual dilution of CD33 with successive mitotic events, having lost the ability to produce CD33 or it's precursors due to the edit. This would also explain the much more rapid drop seen on THP-1s, which proliferate much faster than healthy HSCs. Future work could test this hypothesis by utilising qPCR and western to assess CD33 expression and protein levels respectively following editing.

As day 9 demonstrated a large difference in CD33 expression, subsequent experiments sought to verify these findings by investigating this time point or later (see **Figure 5.15**).

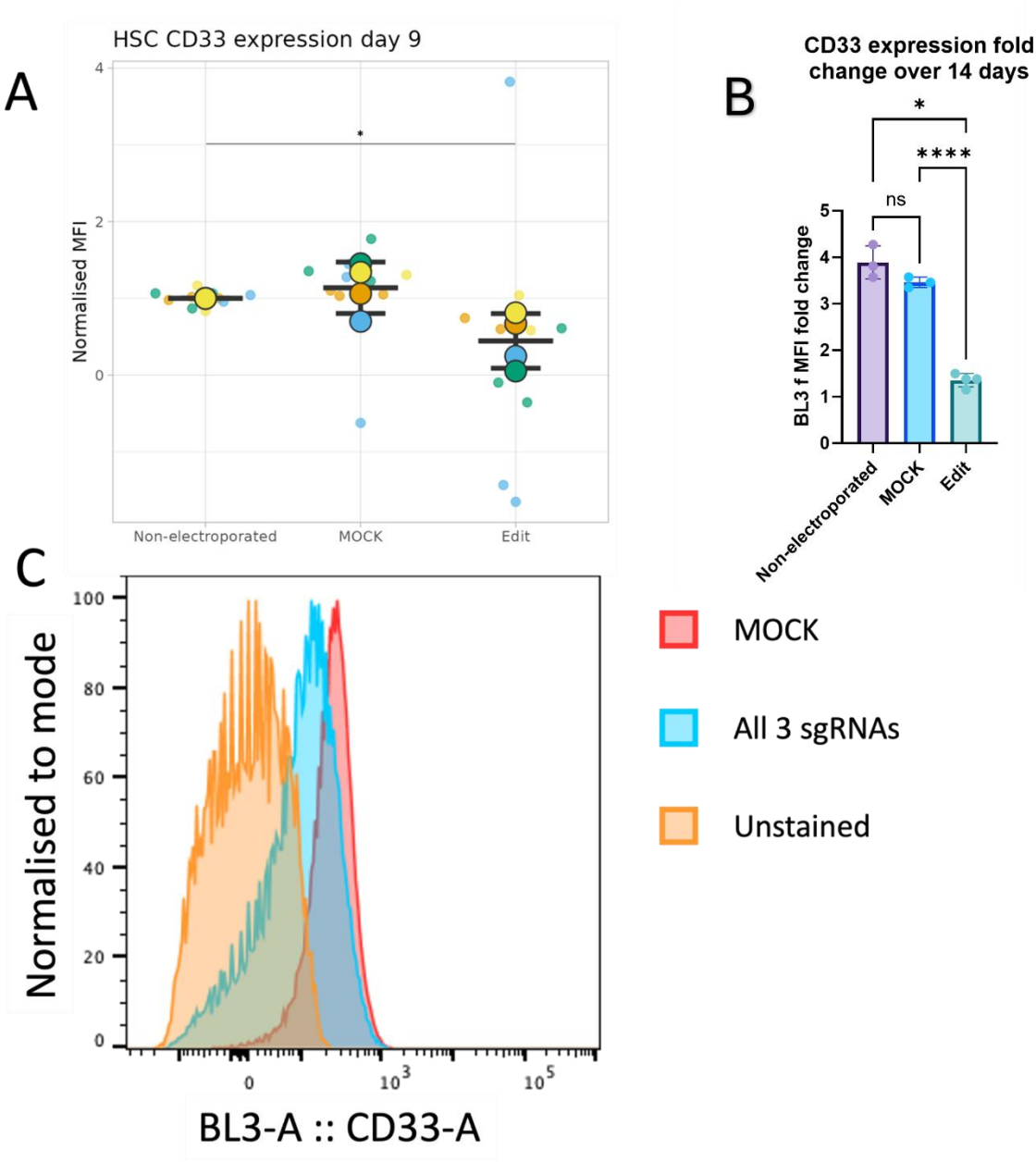

***Figure 5.15 CD33 KO efficiency in HSCs**. The level of CD33 expression in patient derived HSCs after (**A**) 9 days, (N=4 experimental replicates, each consisting of n=2 or 3 technical replicates) illustrated by a super plot, or (**B**) 14 days (Non-electroporated and MOCK both had n=3 technical replicates performed, Edit had n=4 technical replicates performed) was assessed by flow cytometry using an anti-HIM3-4 CD33 antibody. Statistics for (**A**) by one-way ANOVA followed by Tukey multiple comparisons test. Statistics for (**B**) by Brown-Forsyth and Welch one-way ANOVA followed by Dunnett T3 multiple comparisons test. Graphs show mean ± SD. *p < 0.05 and ****p < 0.0001. Non-significant not shown in (**A**). (**C**) Representative histogram of BL3-A fluorescence measured in samples cultured for 14 days, corresponding to CD33 expression. The MOCK control (pink), cocktail of all 3 sgRNAs (blue), and unstained control (orange) conditions are shown.*

CD33 expression was significantly lower in edited HSCs compared to unedited HSCs after 9 days, settling at ~45% of non-electroporated CD33 expression on average.

Most samples' cell numbers dropped too low to reliably characterise after 9 days due to the well-established difficulties associated with culturing HSCs *in vitro* (Jaroscak et al., 2003). However, for one sample the cell number was high enough that CD33 expression could be quantified after 14 days in culture. In this sample, the level of CD33 expression was ~35% of the equivalent value for the non-electroporated control. In addition, when comparing day 0 and day 14 samples, CD33 expression only increased by an average of ~35% in edited HSCs, compared to ~246% in MOCK control cells, and ~289% in non-electroporated cells. This system is comparable to similar systems, which reportedly caused the percentage of HSPCs which are CD33+ to drop from 85% to 10% (Borot et al., 2019) and from 92% to 27% (Kim et al., 2018). The further decrease after 14 days was likely due to a continuation of the downward trend in CD33 expression observed over the first 9 days (see **Figure 5.14**). It was also likely that not all HSCs' CD33 genes were knocked out, and that these unedited cells contributed to the small increase in CD33 expression seen after 14 days. This result confirmed that editing HSCs with the optimised protocol discussed caused a significant drop in CD33 expression that became increasingly apparent as the cells differentiated.

5.3.2.3 HSC viability following electroporation

Low viability in edited cells would be an issue for translating this approach to clinic; at least $8x10^6$ CD34+ cells are recommended for a typical autologous HSCT operation (Siena et al., 2000), and an equivalent number would likely be necessary for this approach as well. Therefore, the viability of HSCs following CRISPR gene editing was assessed (see **Figure 5.16**).

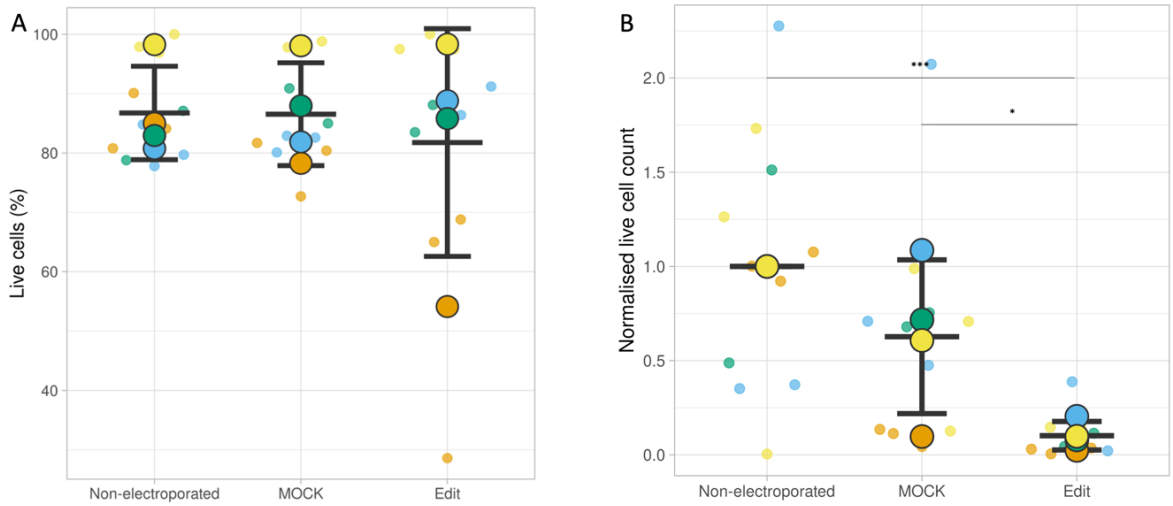

Figure 5.16 Viability of HSCs following editing. ***(A)*** *The viability of patient derived HSCs after 9 days in culture was assessed using flow cytometry. In addition, (**B**) the number of live HSCs, normalised against the number of live HSCs in the non-electroporated control, was calculated. Statistics by one-way ANOVA with Dunnett multiple comparisons. Graphs show mean ± SD. *p < 0.05 and ***p < 0.001. Non-significant not shown. N=4 biological replicates, each consisting of n=2 or 3 technical replicates.*

The viability of edited HSCs was remarkably high, with no significant differences observed between conditions, all of which had an average viability over 80%. However, the number of live edited cells after 9 days was significantly lower than the non-electroporated and MOCK control, the latter of which was also lower on average than the unedited control. This suggested that the process of electroporation caused a drop in cell number (Polajžer & Miklavčič, 2023). Other transfection methods, such as transduction or lipofection, are known cause lower levels of cell death (Chong et al., 2021) and could be explored in future. The CD33- edit itself also caused a drop in cell number. One explanation is that the introduction of RNPs into the cells decreased viability (Q. Cheng et al., 2022). Alternatively, the loss of CD33 could have led to increased phagocytotic activity. Increased phagocytosis has been observed in CD33- microglia (Bhattacherjee et al., 2019), which are specialised CNS macrophages (J. Yang et al., 2014). If the same phenomenon occurred in other types of macrophages, this could result in those produced by differentiating HSCs *in vitro* indiscriminately phagocytosing other cells, potentially explaining the drop in cell number observed. This was contrary to previous reports that CD33- haematopoietic cells were phenotypically

normal (Kim et al., 2018), and could be tested with bioparticle internalisation assay or similar phagocytosis assay.

While CD33 was efficiently knocked out in HSCs, future work could look into the effect of the edit on differentiation capacity using flow cytometry or a long-term culture initiation cell (LTC-IC) assay followed by a colony forming unit (CFU) assay (Donnelly et al., 2024). The edited HSCs could also have their transcription and translation profiles assessed using RNA-seq, proteomic, and metabolomic analyses.

5.4 Summary

A combined CRISPR-CAR T-cell system targeting CD33 while simultaneously maintaining the haematopoietic system with CD33- HSCs has proven effective at treating AML in mouse and macaque models (Borot et al., 2019; Kim et al., 2018). *In vitro* models offer a safe, facile way of testing this system on human cells. To accomplish this, a protocol for efficient CD33 KO in HSCs was optimised.

First, various sgRNAs, alone or in combination, were tested on THP-1s, an AML cell line (see **Figure 5.5** and **Figure 5.6**). The sgRNA targeting exon 2 and a cocktail of all three sgRNAs were identified as the best conditions, and further validated (see **Figure 5.7, Figure 5.8,** and **Figure 5.9**). Next, these conditions were trialled in HSCs. Despite lower efficiency of the individual sgRNAs measured by TIDE analysis compared to the equivalent data for THP-1s (see **Figure 5.11**), the cocktail of all three sgRNAs was shown to cause DSBs efficiently. This was confirmed with flow cytometry analysis following a short period of differentiation (see **Figure 5.14** and **Figure 5.15**). A caveat to the success of this system was the low number of edited HSCs that survived long-term, suggesting that CD33 KO negatively affects HSC maintenance (see **Figure 5.16**). Despite this, the successful KO of CD33 in HSCs allowed progression of the project to CAR T-cell and HSC co-culture. In theory, the CD33- HSCs produced and their progeny would also be resistant to CD33-targetted immunotherapy. Implanting CD33- HSCs into patients to allow establishment of a CD33- haematopoietic system prior to treatment could therefore ameliorate some of the safety concerns around drugs such as CD33-redirected CAR T-cells and GO (Humbert et al., 2019).

Chapter 6 Testing a combined CRISPR-CAR T-cell therapy for AML

6.1 Introduction

After developing a method for efficiently knocking out CD33 in THP-1s and HSCs, the next step was to test the effect of CD33-redirected CAR T-cells on CD33+ and CD33- cells. This was first done using THP-1s, allowing the optimum target to effector (T:E) ratio to be determined. The CAR T-cells were then applied to differentiated haematopoietic cells before finally being tested on a mix of THP-1s and HSCs in the BM niche model. If the CAR T-cells were able to selectively eliminate unedited cells while sparing edited ones, even in a complex environment such as that created in the BM niche model, then the reliability of this therapeutic approach would be demonstrated in an *in vitro* human model, complimenting previous animal model research (Borot et al., 2019; Kim et al., 2018).

6.1.1 Testing CAR T-cell therapy in a model BM niche

As previously discussed, CAR T-cell therapy holds great promise for the curative treatment of AML (Kim et al., 2018). CD33 KO has previously been used to make healthy HSCs and their progeny resistant to CD33-redirected CAR T-cells, allowing them to eliminate CD33+ AML cells and endogenous CD33+ HSCs while the edited cells establish a parallel CD33- haematopoietic system (Borot et al., 2019; Kim et al., 2018). However, this system has yet to be tested in human models, with the closest approximation being immunodeficient mice engrafted with human cells (Borot et al., 2019; Kim et al., 2018). A principal application of the BM niche model developed was to facilitate testing of novel treatments for BM associated diseases and disorders, removing ethical and safety concerns associated with clinical trials, as well as poor translatability of animal trials into the clinic (Ingber, 2020). This model was therefore ideally situated to assess the CRISPR-CAR T-cell BM replacement therapy developed.

6.1.2 Aims

The aims of this chapter were first to test whether the CD33 KO system devised in chapter 5 provided resistance to CD33-redirected CAR T-cells in THP-1s and HSCs, and secondly to test the efficacy of this therapy in the model BM niche developed in chapters 3 and 4.

6.2 Materials and methods

6.2.1 CAR T-cell thawing and preparation

CD33-redirected (CD33 scFv-Beam 2-TM-CD28-CD3z) CAR T-cells were purchased (AMSbio, AMS.PM-CAR1056-1M). On receipt the cells were stored at -150°C. Before use, CAR T-cells were thawed for 3 minutes at 37°C in a water bath, then added dropwise to 10 ml prewarmed 10% RPMI media. The resultant cell suspension was centrifuged at 300 x g for 5 minutes. Next, the supernatant was discarded, and the cell pellet resuspended in 1 mL 10% RPMI. The CAR T-cells were then stained with cell trace far red (CTFR) (Invitrogen, C34572). To do this, the CTFR was first diluted to 1 µM with DMSO. 1 µL was then added to the CAR T-cells before incubation at 37°C for 20 minutes. 15 mL of 10% RPMI was then added, and the suspension incubated for a further 5 minutes at 37°C. Afterwards, the suspension was centrifuged at 300 x g, then resuspended in 1 mL of media used in the experiment the CAR T-cells were being added to and incubated for 10 minutes at 37°C. Finally, the CAR T-cells were diluted to the desired cell density and added to the experiment.

6.2.2 Co-culture and assembling the model leukaemic niche

When co-culturing THP-1s with CAR T-cells, 10% RPMI was used. When co-culturing HSCs with CAR T-cells, IMDM + cytokines was used. When assembling the model leukaemic niche, a similar set-up to the model BM niche was performed, with identical plates, coating, MSC seeding, and gel deposition steps utilised (see **2.2.2.7**). Polymer cover slip (PCS) controls were also made in which no FN or BMP2

coatings or MSCs were used; PBS was used in place of the coatings and 2% DMEM in place of the MSC suspension. On day 7, THP-1s and/or HSCs were edited where appropriate as previously described (see **2.2.5.2** and **2.2.5.3**). The media in the model systems was then replaced with cell suspension containing a 1:1 ratio of THP-1s and HSCs in IMDM + cytokines if both cell types were included. The model was left for 5 days before CARTs were added where appropriate, making the cell ratio 1:1:1 for CAR T-cells, HSCs and THP-1s if all three cell types were included. 2 days later, the liquid phase was removed and the cells in it analysed with flow cytometry to assess the number of live cells and their phenotypes.

6.2.3 CAR T-cell flow cytometry

Flow cytometry was carried out as described previously (see **2.2.4**). Gating strategies used for each experiment are shown in figures. The stains used were sytox blue (ThermoFisher Scientific, S34857), CTFR (Invitrogen, C34572), and two anti-CD33 antibodies; HIM3-4 (Invitrogen, 15-0339-42), WM53 (BioLegend, 303421).

6.3 Results and discussion

6.3.1 CAR T-cells selectively eliminate unedited CD33+ THP-1s

CAR T-cells were used to challenge THP-1 cells at various T:E ratios to determine the optimum conditions for subsequent CAR T-cell experiments. THP-1s were fist edited using the optimised THP-1 system with all three sgRNAs described in **Chapter 5**. The resultant edited cells were then grown for ten days before their CD33 expression was checked with flow cytometry. The following day CAR T-cells were thawed and stained with CTFR, facilitating separation of CAR T-cell and THP-1 populations by flow cytometry. Edited and unedited THP-1s were then seeded alongside stained CAR T-cells at various ratios, with the number of THP-1s in each repeat kept consistent. Flow cytometry was used to identify and count the number of live THP-1s after 1, 2 and 3 days of co-culture (see **Figure 6.1**).

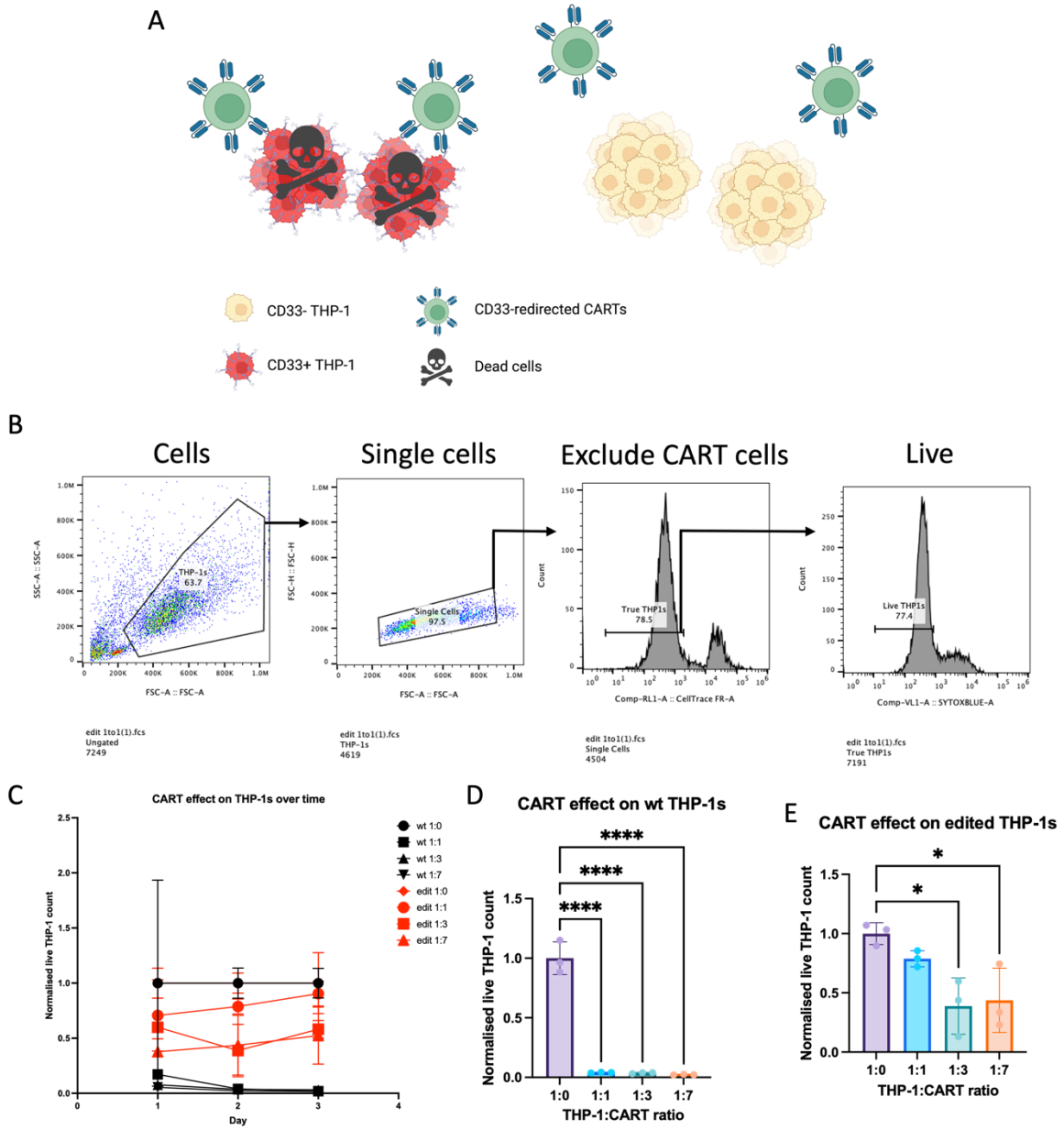

Figure 6.1 Effect of CAR T-cells on THP-1s. *Edited and unedited THP-1s were challenged with various T:E ratios of CAR T-cells, and the number of live THP-1s over a 3 day co-culture assessed daily by flow cytometry. (**A**) Schematic of the coculture system with CAR T-cells and unedited CD33+ THP-1, or edited, CD33- THP-1s. Created with BioRender.com. Flow cytometry was used to assess live THP-1 cell count. (B) Flow gating strategy. FSC-A and SSC-A were used to identify cells. FSC-A and FSC-H were used to identify single cells. A CTFR gate was used to omit stained CAR T-cells, and a sytox blue gate was used to omit dead cells. The normalised live THP-1 cell count (**C**) over time is shown, as well as (**D**) the unedited wild-type (wt) and (**E**) edited live THP-1 count on day 2. These values were calculated by dividing the cell count of each repeat by the corresponding 1:0 cell count on the same day for edited or unedited cells. Graphs show mean ± SD. Statistics by one-way ANOVA followed by Tukey multiple comparisons test. *p < 0.05 and ****p < 0.0001. Non-significant not shown. n=3 technical replicates.*

The normalised live THP-1 cell count dropped dramatically in all unedited THP-1 conditions tested, with a statistically significant difference between the no CAR T-cell condition (T:E of 1:0) emerging after two days of co-culture. A smaller drop in live THP-1 count was seen in edited conditions, though this difference was insignificant in all conditions on day 1, the 1:1 T:E ratio on day 2, and all except the 1:7 T:E condition on day 3. These results demonstrated the efficient elimination of CD33+ cells by the CAR T-cells used at all T:E ratios tested, allowing future experiments to use the 1:1 T:E ratio and therefore maximise the number of repeats possible with the highly expensive CAR T-cells used. This ratio was also ideal as it produced the lowest level of edited cell death, with no significant difference in live THP-1 cell count observed between this condition and the 1:0 no CAR T-cell controls observed at any of the time points investigated.

The CAR T-cells causing a reduction in edited live THP-1 cell number suggested that the edit was not 100% efficient, as previously hypothesised (see **Chapter 5**). This inefficiency likely led to a small number of unedited THP-1s that were eliminated by the CAR T-cells. The increased cell death seen with higher T:E ratios also implied that some edited THP-1s were able to tolerate the lower T:E ratios tested but perished at higher ones. This was probably caused by CD33 knock down (KD), where only one allele of a target gene is rendered non-functional (Shapiro et al., 2020), causing reduced levels of CD33 expression but not complete KO. This suggested that some of the inefficiency in the CD33 KO was caused by inefficient gene editing once the RNPs were already in the cells and capable of editing, rather than being solely caused by poor RNP delivery. This could have been caused by an incomplete cocktail of sgRNAs entering some cells, resulting in the lower level of efficiency seen when single sgRNA edits were tested, or by imperfect editing efficiency of RNPs within the cells. Alternatively, a heterogenous population of cells was produced by the edit, some of which contained hypomorphic CD33 mutations that resulted in CD33 proteins that were still recognised by the CAR T-cells (Doench et al., 2014). A combination of these causes was probably responsible. The reduced difference at the day 3 timepoint in the edited THP-1 conditions could have been caused by the cells in the no CAR T-cell control conditions reaching confluency, stymieing their growth while cells in the other conditions grew quickly. Despite these considerations, the normalised THP-1 count in the edited controls was statistically significantly higher than in the unedited

conditions across T:E ratios, barring the 1:0 controls, demonstrating that the edited THP-1s on average were more resistant to CAR T-cell induced cell death than unedited THP-1s.

6.3.2 CAR T-cells selectively eliminate unedited CD33+ HSCs

To test if CAR T-cells selectively target CD33+ haematopoietic cells, HSCs were edited alongside relevant controls and analysed with flow cytometry. They were then cultured for 14 days to allow for differentiation and an increase in CD33 expression, as observed in **Chapter 5**. The resultant cells were then challenged with a 1:1 T:E ratio of CTFR stained CAR T-cells, alongside 1:0 controls. After a further two days of culture, the final number of live HSCs was determined by flow cytometry, as well as their CD33 expression (see **Figure 6.2**).

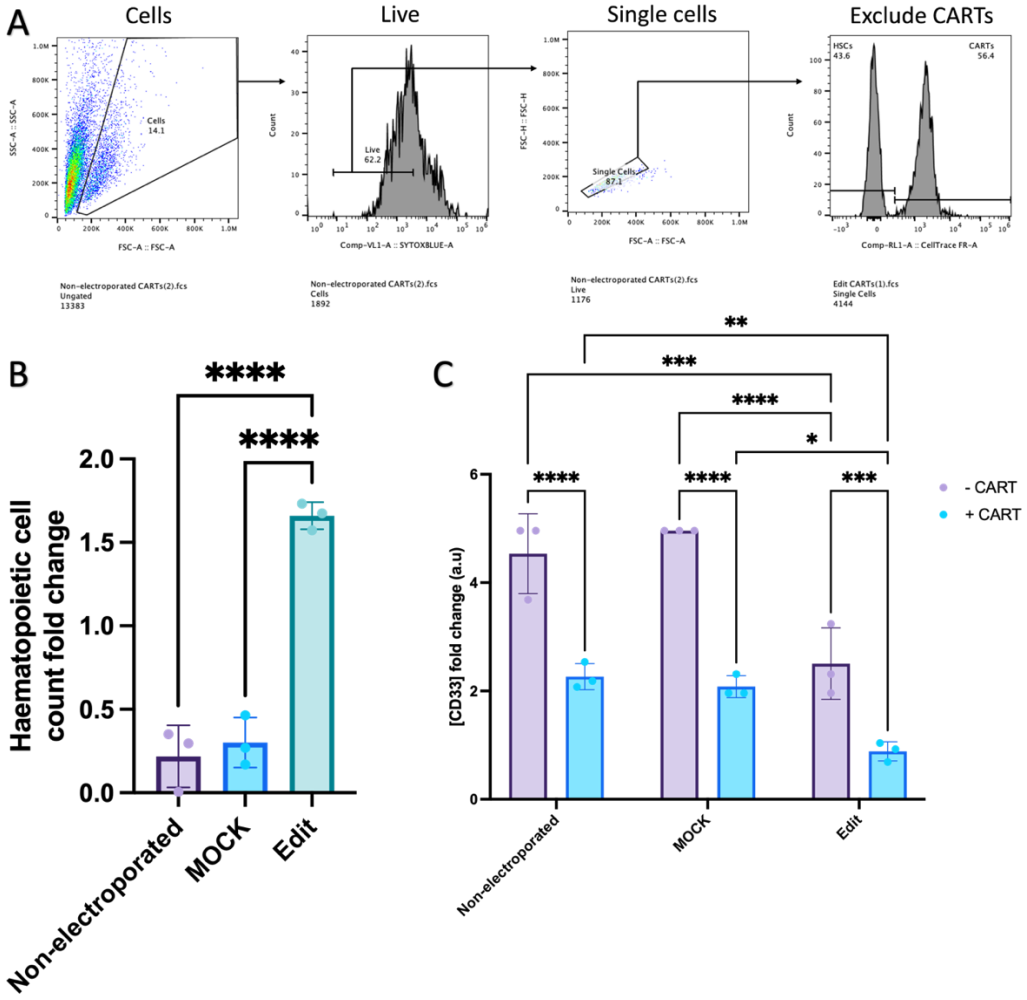

***Figure 6.2 Effect of CAR T-cells on differentiated HSCs**. STEMCELL technologies HSCs were cultured for 14 days then co-cultured with CAR T-cells at a 1:1 T:E ratio for a further 2 days alongside 1:0 controls. Flow cytometry was used to determine the number of live haematopoietic cells and their CD33 expression. (**A**) Flow gating strategy. FSC-A and SSC-A were used to identify cells. Sytox blue was used to exclude dead cells. FSC-A and FSC-H were used to identify single cells. A CTFR gate was used to omit stained CAR T-cells. (**B**) Haematopoietic cell count fold change when CAR T-cells were present was calculated. (**C**) CD33 expression after CAR T-cell co-culture measured using an anti-HIM3-4 CD33 antibody. MFI was normalised against day 0 measurements to calculate fold change. Graphs show mean ± SD. Statistics for (**A**) by one-way ANOVA followed by Tukey multiple comparisons test. Statistics for (**B**) by two-way ANOVA followed by Šídák multiple comparison test. *p < 0.05, **p < 0.01, ***p < 0.001 and ****p < 0.0001. Non-significant not shown. n=3 technical replicates.*

Inclusion of the CAR T-cells caused a similar drop in non-electroporated and MOCK haematopoietic cells' numbers, evidenced by the fold change in this value being consistently below 1, with an average of 0.22 and 0.30 respectively. This demonstrated efficient, CAR T-cell mediated ablation of these cells. The edited cells on the other hand had a high degree of CAR T-cell resistance, with significantly higher fold change values averaging around 1.66. These values were likely inflated due to an aberrant value in one of the 1:0 control samples used to normalise this data. When this value was excluded from analysis, the average fold change of edited HSCs was 0.96, and the difference between this group and the controls maintained a p value of <0.05. This demonstrated that edited HSCs' numbers were virtually unaffected by the CAR T-cells, implying that the edit itself conferred resistance, as previously hypothesised.

However, changes in CD33 expression when CAR T-cells were included suggested additional complexity. Firstly, CD33 expression dropped in non-electroporated and MOCK conditions with CAR T-cells, suggesting that CD33-/low cells, likely more naïve or lymphoblastic lineage cells (Laszlo et al., 2014), made up the majority of the surviving cells, while CD33+ myeloid cells were killed. CD33 expression was also reduced in edited conditions, as seen in **Chapter 5.** However, CD33 expression was reduced further in edited conditions which included CAR T-cells. As no measurable loss in cell count was observed, ablation of unedited or CD33 KD cells cannot be the sole explanation of these results. The HSCs may have proliferated more in the presence of CAR T-cells, making up for lost CD33+ cells, though the likelihood of this resulting in almost identical cell numbers to no CAR T-cell controls is low. Alternatively, the presence of CAR T-cells may have altered

the haematopoietic cells' expression of CD33, similar to antigen loss that has been observed in cancer cells targeted with CAR T-cell therapy (Mishra et al., 2024). Similar results have been observed in healthy B cells exposed to CD19-redirected CAR T-cells, and found to be due to reversible epigenetic changes (Fioretti et al., 2023), which could be a possible explanation. The fact that antigen loss did not come with a corresponding drop in HSCs' count, as well as the non-cancerous, genetically stable nature of these cells, rules out clonal selection (Rotolo et al., 2019) and supports this hypothesis. However, other possibilities, including lineage switching (Gardner et al., 2016; Mishra et al., 2024), antigen shedding (Sun et al., 2021), or undiscovered mechanisms are also possible.

Future work must investigate the effect of CD33-redirected CAR T-cell exposure on HSCs' differentiation capacity. If this is found to be affected, even reversibly, it could have serious implications for this and other CD33-targeting AML treatments' usability.

6.3.3 BM replacement therapy in the model BM niche

The effect of CAR T-cells on the delta 1 model BM niche was tested. Here, the model was used to mimic the BM niche of an AML patient. THP-1s are AML cells (Chanput et al., 2014), and were used to represent cancerous cells. HSCs were thawed the day before addition to the model and electroporated immediately prior to addition. Five days after THP-1 and HSC addition, CAR T-cells were thawed and stained with CTFR. Two days after addition of CAR T-cells, the liquid phase of the model niche was extracted and analysed with flow cytometry, allowing the number of live THP-1s and HSCs to be determined (see **Figure 6.3**).

Across the conditions that included CAR T-cells, a significant drop in normalised, live THP-1 cell count was observed, suggesting that the CAR Tcells were able to kill unedited THP-1s in all conditions, including the complex, multicellular, BM-mimetic environment of the model BM niche. This demonstrated the possibility of testing novel therapies for BM-associated disorders and diseases using the model BM niche developed.

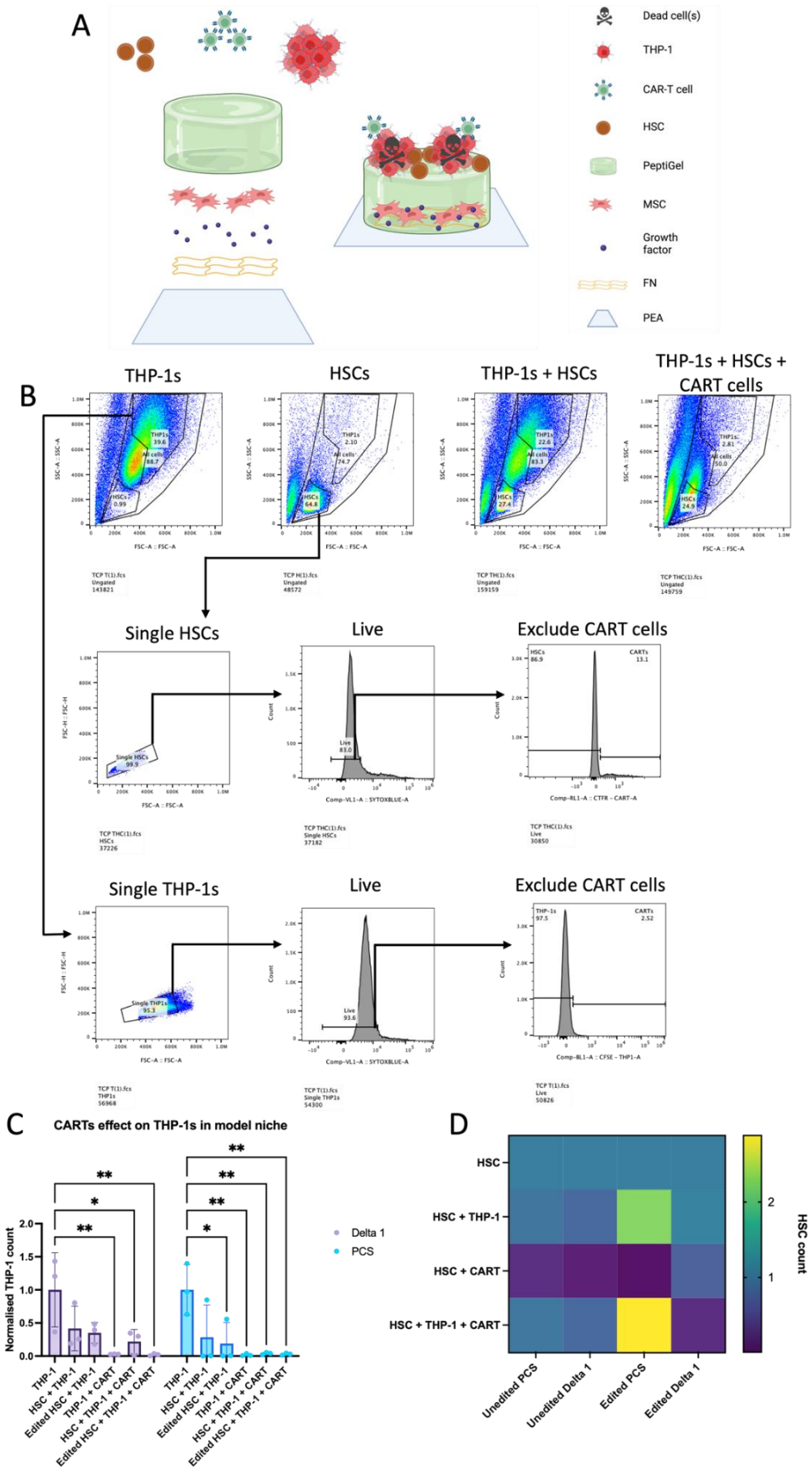
A
Dead cell(s)
THP-1
CAR-T cell
HSC
PeptiGel
MSC
Growth factor
FN
PEA
B
THP-1s
HSCs
THP-1s + HSCs
THP-1s + HSCs + CART cells
Single HSCs
Live
Exclude CART cells
Single THP-1s
Live
Exclude CART cells
C
CARTs effect on THP-1s in model niche
Normalised THP-1 count
Delta 1
PCS
THP-1
HSC + THP-1
Edited HSC + THP-1
THP-1 + CART
HSC + THP-1 + CART
Edited HSC + THP-1 + CART
D
HSC
HSC + THP-1
HSC + CART
HSC + THP-1 + CART
Unedited PCS
Unedited Delta 1
Edited PCS
Edited Delta 1
HSC count

***Figure 6.3 Effect of CAR T-cells on a model BM niche**. A BM niche model was assembled as shown in (**A**). The HSCs used were all from STEMCELL technologies. Created with BioRender.com. Various iterations of the niche were tested, namely polymer cover slip (PCS) controls with no ECM or GF coatings or MSCs, and delta 1 niches, which included FN, BMP2, MSCs and delta 1 PeptiGel. THP-1s, CAR-T cells, unedited CD33+, and edited CD33- HSCs were also added to these systems, either alone or in combination with other cell types. The liquid phase of the model niche was extracted and the cells within analysed with flow cytometry. (**B**) Flow gating strategy. FSC-A and SSC-A were used to identify HSCs and THP-1s. The first row of dot plots shows examples of different cell combinations with this gating strategy. FSC-A and FSC-H were used to identify single HSCs and THP-1s. A sytox blue gate was used to omit dead cells, and a CTFR gate was used to omit stained CAR T-cells. (**C**) THP-1 cell count normalised against the THP-1 only control in the delta 1 and PCS niches. (**D**) HSC count normalised against the HSC only control with corresponding niche and edit status. Graphs show mean ± SD. Statistics by two-way ANOVA followed by Tukey multiple comparisons test. *p < 0.05 and **p < 0.01. Non-significant not shown. n=3 technical replicates.*

Unexpectedly, a drop in the number of live normalised THP-1s was also seen in conditions in which THP-1s and HSCs were cultured together, though the difference between these conditions and the THP-1 only controls was only significant in the PCS condition with edited HSCs and THP-1s. This trend could be indicative of a GvL effect, with the HSCs competing with the THP-1s for resources and producing immune cells to target them (Dickinson et al., 2017). This could also explain the high variability in the conditions which only included THP-1s and HSCs, as the GvL effect itself is known to produce variable results (Dickinson et al., 2017). Interestingly, this effect was seen in both delta 1 and PCS conditions, despite the reduced immune cell population seen in the delta 1 niche, as discussed in **Chapter 4**. Future work could verify this finding and determine whether the presence of leukaemic cells causes an increase in lymphocyte differentiation in the HSCs when co-cultured. In addition, the model developed could be used to further investigate the GvL and GvHD effects by looking at how the inclusion of HSCs and cancerous cells from the same or HLA-matched donors effects this GvL effect, and if non-cancerous unmatched myeloid cells are also eliminated by HSCs.

Interestingly, when THP-1s were included in PCS BM models alongside HSCs with or without CAR T-cells, the number of HSCs increased. This anomalous result could be explained by THP-1s incorrectly being identified as HSCs during flow cytometry, or the THP-1s protecting the HSCs from the CAR T-cells. This protection could be due to remodelling of the niche by the THP-1s (Ishikawa et al., 2007; Tabe & Konopleva, 2015) or overwhelming the CAR T-cells with the number of CD33

antigens present, resulting in CAR T-cell exhaustion (Kouro et al., 2022; Vigano et al., 2020). Further investigation is required to confirm that this result is genuine, and then to determine its cause. Future work could also investigate the long-term surveillance of the model BM niche by the CAR T-cells by testing longer timepoints.

The live normalised HSC count was affected by the addition of CAR T-cells, with a drop seen in most conditions with both cell types, though no significance was observed. The initial hypothesis was that HSCs would be unaffected by the addition of CAR T-cells, as they were only in culture for 7 days and likely experienced limited differentiation. This would have resulted in low levels of CD33 expression, limiting targeting by CAR T-cells. While no significance was observed, it is possible that a small amount of differentiation occurred, resulting in some CD33 expression in edited and unedited HSCs. Expression in edited cells could be attributable to maturing CD33 translocating to the HSCs' membrane, as postulated in **Chapter 5,** as well as incomplete CD33 KO and KD. This potentially resulted in elimination of CD33+ HSC myeloid progeny, which comprised a small proportion of the haematopoietic cells present, though this would contradict results presented in **Figure 6.2**, possibly due to patient sample variability. To investigate this further, CD33 expression in the different cell populations was examined (see **Figure 6.4**).

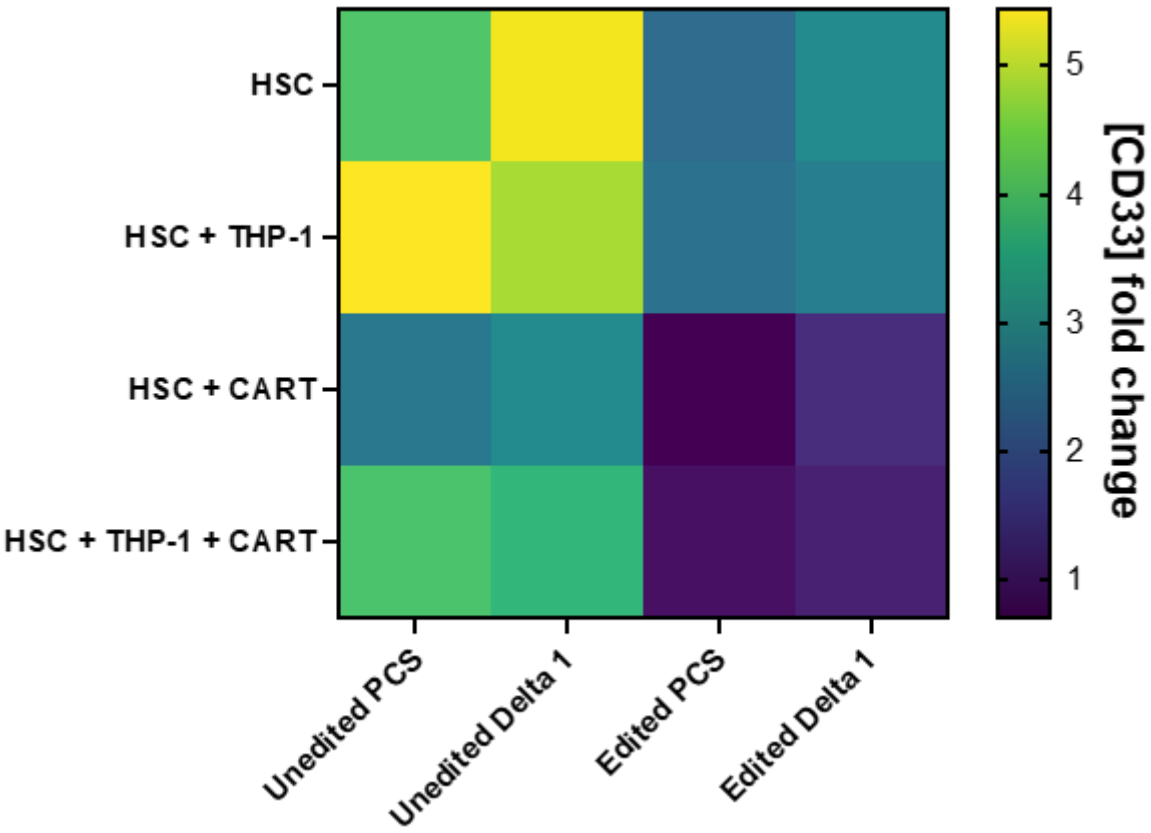

***Figure 6.4 CD33 expression fold change in HSCs in BM models**. The level of CD33 expression by cells in various BM niche models with or without CRISPR editing was assessed using flow cytometry. An identical gating strategy to that described in **Figure 6.3** was used to identify HSCs before an anti-HIM3-4 CD33 antibody was used to assess CD33 expression. Graph shows mean MFI for each condition normalised against day 0 samples' mean MFI. n=3 technical replicates.*

CD33 expression was shown to drop when HSCs were edited, suggesting that some differentiation occurred, allowing a difference to be seen. In addition, CD33 expression dropped when CAR T-cells were included in the model system, presumably due to CD33+ cells being eliminated by the CAR T-cells. A cumulative effect was seen when edited cells were co-cultured with CAR T-cells, suggesting that CAR T-cells still targeted edited HSCs, despite them producing lower levels of CD33.

The reduction in AML cell count demonstrated the feasibility of using a combined CRISPR-CAR T-cell BM replacement strategy to treat leukaemia, as well as the utility of the model BM niche for investigating therapies for BM-associated disorders and diseases. In addition, these results showed that the model BM niche developed could mimic some of the complex interactions that occur within the native leukaemic niche, such as GvL and AML remodelling. The unexpected

adverse effects on HSCs' count across conditions highlights the complexity of this therapy. The cause of this requires further investigation.

6.4 Summary

CD33-redirected CAR T-cells were shown to be able to efficiently ablate CD33+ THP-1 cells at different T:E ratios. In addition, the CD33 KO gene edit developed in **Chapter 4** was shown to reduce cell death in edited THP-1s, most notably at a 1:1 T:E ratio, at which the cell count was not significantly different from no CAR T-cell controls at any of the timepoints tested (see **Figure 6.1**).

HSCs were also edited and then differentiated alongside unedited controls. The resultant cells were then challenged with CAR T-cells (see **Figure 6.2**). The edited HSCs were found to have a high degree of resistance to CAR T-cells, while the unedited cells experienced a significant drop in cell number. In addition, across conditions, CD33 expression dropped in the presence of CAR T-cells. This implied that CD33+ cells were being eliminated, but that HSCs were also responding to the presence of CAR T-cells by downregulating CD33 expression.

This system was then tested in the complex environment of the model BM niche developed in **Chapter 3** and **Chapter 4** (see **Figure 6.3**). The addition of CAR T-cells caused cell death for CD33+ THP-1s, demonstrating the efficacy of this system, while also demonstrating the possibility of testing therapies for BM-associated disorders and diseases on the model BM niche. A possible GvL effect was also observed, demonstrating the usefulness of the model BM niche for investigating complex interactions within the BM niche. Additionally, HSC count dropped in the presence of CAR T-cells, despite CD33 expression being reduced (see **Figure 6.4**). This was attributed to HSC donor variability, though further investigation is required to elucidate the cause fully.

Chapter 7 Discussion

7.1 Project summary

The BM niche is a highly complex organ that acts as a reservoir for the clinically relevant mesenchymal and haematopoietic stem cell populations (Mendelson & Frenette, 2014; Wei & Frenette, 2018; Xiao, McGuinness, et al., 2022). While MSCs can be cultured under standard conditions, HSCs rapidly differentiate, losing their clinical usefulness. This has led to a concerted effort to model the BM niche *in vitro*, and create a system which can maintain or expand HSCs for treatments (Chatterjee et al., 2021; Fares et al., 2022). Rapid developments in this field have led to greater insights on how elements of the BM and BM models affect resident cells (see **Table 1.1, Table 1.2,** and **Table 1.3**). This has allowed models with varied objectives to be developed, including modelling BM-associated disorders and diseases, such as AML (Frenz-Wiessner et al., 2024; Khan et al., 2023). These models have increased similarity to human physiology compared to gold standard animal models, and incorporate the complexity of cells' microenvironment, unlike simple suspension cultures (Dozzo et al., 2023). Furthermore, their relatively low cost and ability to be produced at scale (Haddrick & Simpson, 2019) raises *in vitro* models' potential as platforms for testing novel treatments for BM-associated disorders and diseases.

This project aimed to develop a synthetic BM niche model for testing a novel AML therapy. This entailed characterising the chemical and mechanical properties of materials used for the model and assessing the impact of various model elements on BM cells to determine the optimal model constituents. In parallel, a system for effectively knocking out the CD33 myeloid marker to make HSCs and their progeny resistant to CD33-redirected CAR T-cells was developed. These separate research areas then converged when the effectiveness of the combined CRISPR-CAR T-cell system in a BM-mimetic environment was tested using the model BM niche developed (see **Figure 7.1**).

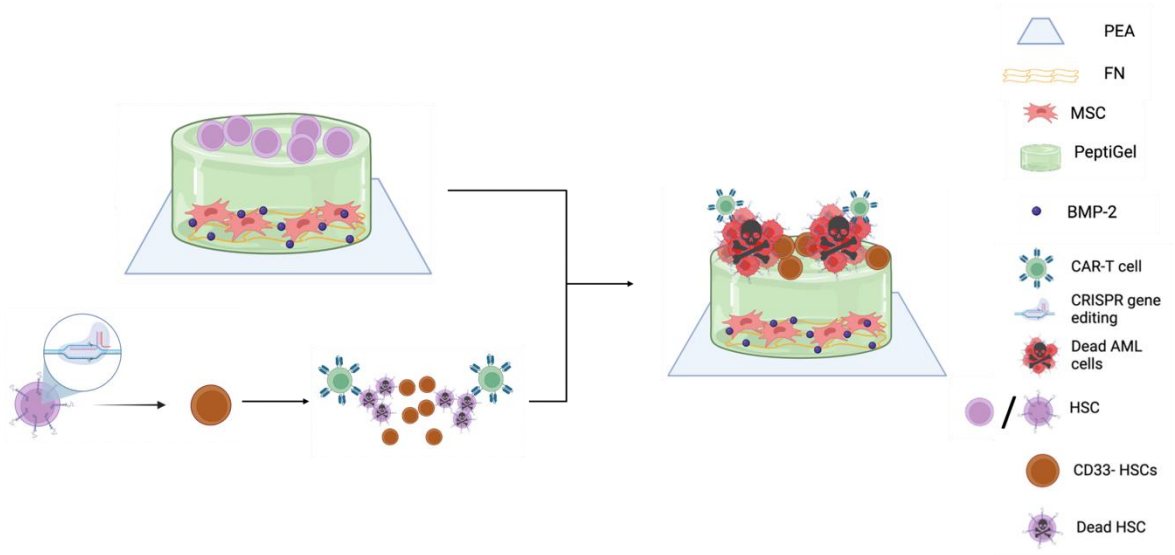

***Figure 7.1 Project summary**. A model* in vitro *BM niche was developed following rigorous investigation of included substrates material and chemical properties. This system was shown to induce a niche-like phenotype in included MSCs, which acted as a feeder layer, supporting included HSCs. In parallel, a system for efficiently knocking out CD33 in HSCs was devised and shown to provide resistance to CD33-redirected CAR T-cells. The model niche was then used to test the efficiency of a combined CRISPR-CAR T-cell therapy for AML. Ultimately, the CRISPR-CAR T-cell system was shown to effectively ablate THP-1 cells, which were used as a model for AML cells, though the included HSCs were also affected, even when they were edited and had reduced CD33 expression. Created with BioRender.com.*

Key achievements are highlighted below:

- Synthetic PeptiGels, despite low biocompatibility, were shown to effectively promote a niche-like phenotype in MSCs in combination with other BM niche model elements, with these cells producing higher levels of the niche-like markers nestin and SCF than a well-established collagen system (Donnelly et al., 2024).
- This model system was capable of maintaining populations of AML cells and haematopoietic cells, and may have encouraged a megakaryopoiesis-favouring differentiation pattern in HSCs, which was similar to undisturbed haematopoiesis (Rodriguez-Fraticelli et al., 2018).
- An efficient, reliable method for knocking out CD33 in THP-1s and HSCs was developed and shown to effectively provide resistance to CD33-redirected CAR T-cells.
- The combined CRISPR-CAR T-cell therapy was tested in the model BM niche and shown to effectively eliminate AML cells, though HSCs' number and

CD33 expression were also affected. This demonstrated the usefulness of the BM niche model for testing novel therapies for BM-associated disorders and diseases.

The model BM niche developed was simple and biomimetic. It promoted a niche-like phenotype in MSCs (Donnelly et al., 2024), and physically separating the MSCs from suspension cells made them easy to analyse. Furthermore, the synthetic nature of the PeptiGel used allowed for the system to be optimised, and could fascilitate further improvements (King et al., 2016). As a result, this model worked well as an approximation of the BM niche for the purposes of testing novel leukaemia therapies, and may also have been capable of modelling other BM interactions, such as GvL.

In addition, the development of the combined CRISPR-CAR T-cell system and subsequent demonstration of its effectiveness in the complex, biomimetic environment of the model BM niche represents the first time this approach has been tested in a fully human system (Borot et al., 2019; Kim et al., 2018). This highlights the potential of this therapy, as well as the niche's usefulness as a drug testing platform.

These successes were highly promising, however some improvements to the model niche and the combined CRISPR-CAR T-cell therapy are possible.

7.2 Recommendations for future work

7.2.1 Alternative approaches to BM modelling

The biggest limitation with the finalised BM niche model was the low biocompatibility of the PeptiGels, which was deemed responsible for reducing the viability of MSCs and HSCs. PeptiGels can be readily functionalised (King et al., 2016), which could offer a solution; the inclusion of native ECM elements or appropriate substitutes could provide cell adhesion points, GF retention, and other benefits that would allow cells to interact with the PeptiGel scaffold in a similar fashion to the native ECM. In addition, as SAPHs continue to develop and the cause of this low biocompatibility is investigated further, this issue could be

overcome. This has been seen already with the identification of charged peptides as a potential cause of cell death, which has begun to be addressed by the production of neutrally charged SAPHs (Clough et al., 2021). The method for conditioning the PeptiGels with media could also be improved to prevents cells from experiencing the gels' supraphysiological pH, which may be a factor in the high cellular mortality observed (Treacy et al., 2022).

Another consideration for the use of PeptiGels is their incompatibility with standard analysis techniques such as qPCR and western blot. This is primarily due to difficulties separating the gel from cell components. The development of optimised strategies for dealing with PeptiGels in this context could improve ease of data acquisition (Burgess et al., 2017, 2018).

The system developed also only investigated MSC phenotype in the absence of HSCs and CAR T-cells, even though these cell types and their progeny are known to interact reciprocally (Doherty-Boyd et al., 2024). Investigations into changes in MSC phenotype when HSCs and/or CAR T-cells are included in model BM niche systems could further elucidate these cell types' interactions.

More complex BM models could also be developed. These could include systems in which the MSCs and/or the HSCs are suspended in 3D in the PeptiGel, more accurately replicating the 3D BM niche and allowing for juxtracrine signalling between HSCs and MSCs (Isern et al., 2013; Pinho et al., 2013) that was absent in the model described. Models could also be developed which use both collagen and PeptiGel, with the former modelling the sinusoidal niche and the latter the arteriolar niche (Doherty-Boyd et al., 2024; Pinho & Frenette, 2019). These sub-niches could be connected using microfluidic channels to allow fluid exchange (Nelson et al., 2021), or intertwined in a more BM-mimetic fashion, with a disc of collagen surrounded by a layer of PeptiGel. Increasing complexity could be added by incorporating differential oxygen tension (Donnelly et al., 2024), perfusion (Bourgine et al., 2018), more BM cell types, or even connecting this model to other tissue models (Novak et al., 2021) to replicate the native BM niche more accurately. This could provide greater insight into the efficacy of therapies tested in these models, as well as other information such as off-target effects. While these extra elements may improve the model's similarity to endogenous BM, they

could also ameliorate some of its benefits, such as its simplicity and ease of cell type separation.

7.2.2 Improvements to gene editing

The gene editing approach developed was highly efficient, outcompeting traditional single sgRNA systems (Borot et al., 2019; Humbert et al., 2019; Kim et al., 2018) and providing robust protection against CD33-redirected CAR T-cells. However, some shortcomings were present. The delivery method for the RNPs is a prime example; electroporation places a large amount of stress on cells, which causes cell death and may influence long-term engraftment capacity (Polajžer & Miklavčič, 2023). Viral and lipid-based transfection techniques induce less stress (Chong et al., 2021). Viral transfection has been used effectively for editing HSCs in the past (Dever et al., 2016), though its use in the clinic is limited due to possible immunogenic responses (C. L. Xu et al., 2019). More recently, lipofection has shown promise for effective delivery of CRISPR reagents, and has been engineered to allow targeting of specific cell types (Q. Cheng et al., 2020; Wang et al., 2023). Lipofection has also been proposed as a safe method for *in vivo* gene editing, bypassing the need for complex *in vitro* cell therapy processes to make the combined CRIPR-CAR T-cell therapy viable. This would also facilitate continuous, high throughput, cheap therapy manufacture, as opposed to batch production of edited cells harvested from patients or donors. However, lipofection typically results in comparatively lower editing efficiency compared to other methods (Lino et al., 2018), and there is a risk of eliciting an immune response (Y. Lee et al., 2023). In addition, for the process to work, HSCs must be specifically targeted without any AML cells also being affected, to prevent the creation of CD33-, CAR T-cell resistant AML cells.

In addition, the CD33 edit itself was hypothesised to affect HSC viability due to increased phagocytosis (Bhattacherjee et al., 2019), though this phenomenon could be due to the introduction of RNPs in general as well. To avoid this issue, and any others arising from CD33 KO, the target site of the CD33-redirected cells could be genetically scrambled, potentially preventing CAR T-cell targeting without losing CD33 activity. An obstacle to this approach is the need to find a method for inserting the scrambled sequence despite HSCs' tendency for NHEJ

(Mohrin et al., 2010). Prime editing offers a promising avenue for this (Anzalone et al., 2019), as does base editing (Rees & Liu, 2018).

7.2.3 Improvements to combined CRISPR-CAR T-cell therapy

A potential issue with this therapeutic approach is phenotypic escape of AML cells (Duy et al., 2021; Farge et al., 2017; Passaro et al., 2017). CD33+ AML cells would likely be eliminated by CAR T-cell therapy, as shown in **Chapter 5**. However, any CD33- AML cells, which could include cancer initiating LSCs or LRCs (Bonnet, 2005), could survive and propagate to re-establish the cancer with CD33- progeny. Therefore, it is essential to eliminate all AML cells when using this method, possibly by combining it with established chemotherapy regimens. This would need to be assessed in future work.

The combined CRISPR-CAR T-cell therapy is also not repeatable. If a patient were to experience another instance of AML after the treatment, which has an increased likelihood due to the remodelling of the BM niche by AML (Pinho & Frenette, 2019), other options would have to be explored even if the patient responded well to the initial treatment, as all their HSCs, as well as any derived leukaemic cells, would be CD33-. A potential solution to this could be to introduce a unique marker alongside the CD33 knock out. This would result in the edited cells expressing the new marker, which could in turn be used as a CAR T-cell target to eliminate any leukaemic cells derived from the edited cells in a similar fashion to how CD33 was used in the system described.

7.2.4 Further applications of BM model

As previously discussed, other applications of BM niche models beyond screening novel therapies exist. These include expanding HSCs (Chatterjee et al., 2021; Fares et al., 2022), investigating BM components impacts on resident cells in greater detail (Eaves, 2015), modelling disease states (Pak et al., 2015), and producing personalised medicine models that incorporate a patient's cells and

could be used to test therapeutic responses *in vitro* prior to treatment. Future work could test the applicability of the model presented in these scenarios.

7.3 Conclusion

Recent, rapid developments in BM niche model research (Doherty-Boyd et al., 2024; Xiao, McGuinness, et al., 2022), have paved the way for increasingly mimetic models. As the field continues to advance, this progress promises to elucidate the precise mechanisms of healthy and diseased haematopoiesis, and facilitate the development of effective, curative treatments for BM-associated disorders and diseases. This project represents an early step in this process, demonstrating the usability of a synthetic BM niche for testing a novel leukaemia therapy.

Appendices

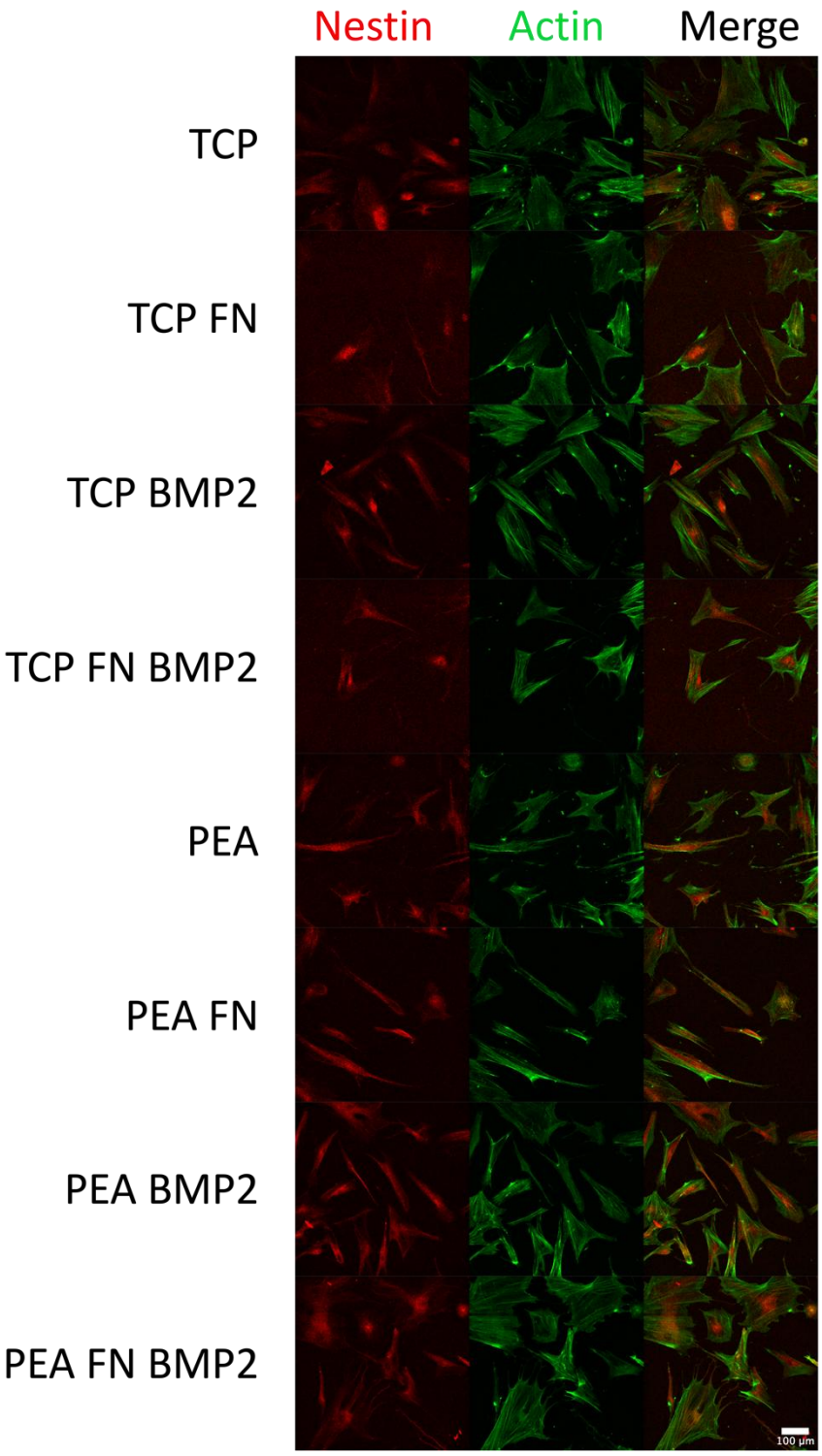

Supplementary Figure 1 MSCs' nestin expression in no gel conditions. *Representative confocal microscopy images of MSCs with stained actin and nestin cultured on various surfaces in no gel conditions. Scale bar is 100 µm.*

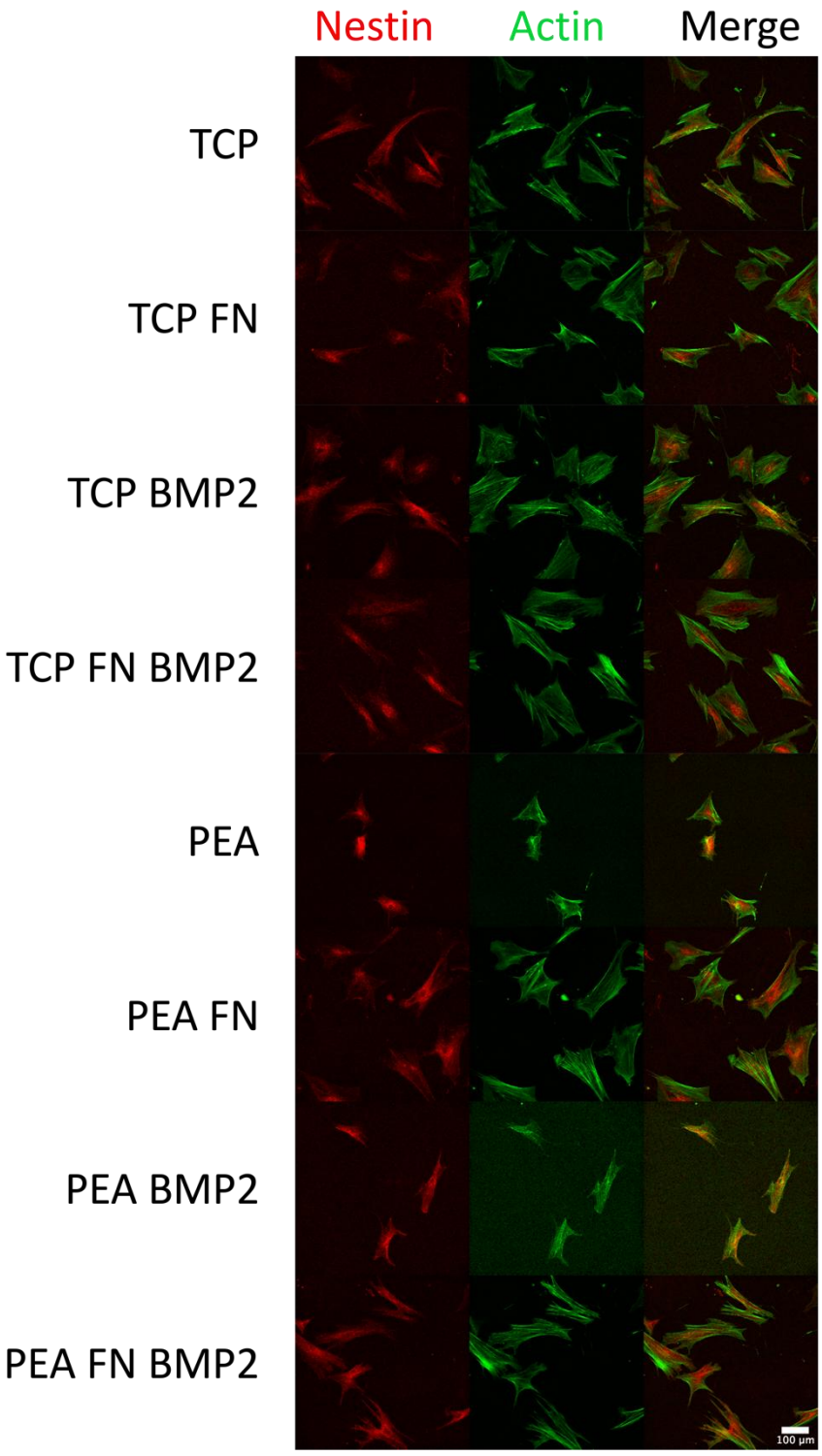

Supplementary Figure 2 MSCs' nestin expression in collagen conditions. *Representative confocal microscopy images of MSCs with stained actin and nestin cultured on various surfaces in collagen conditions. Scale bar is 100 µm.*

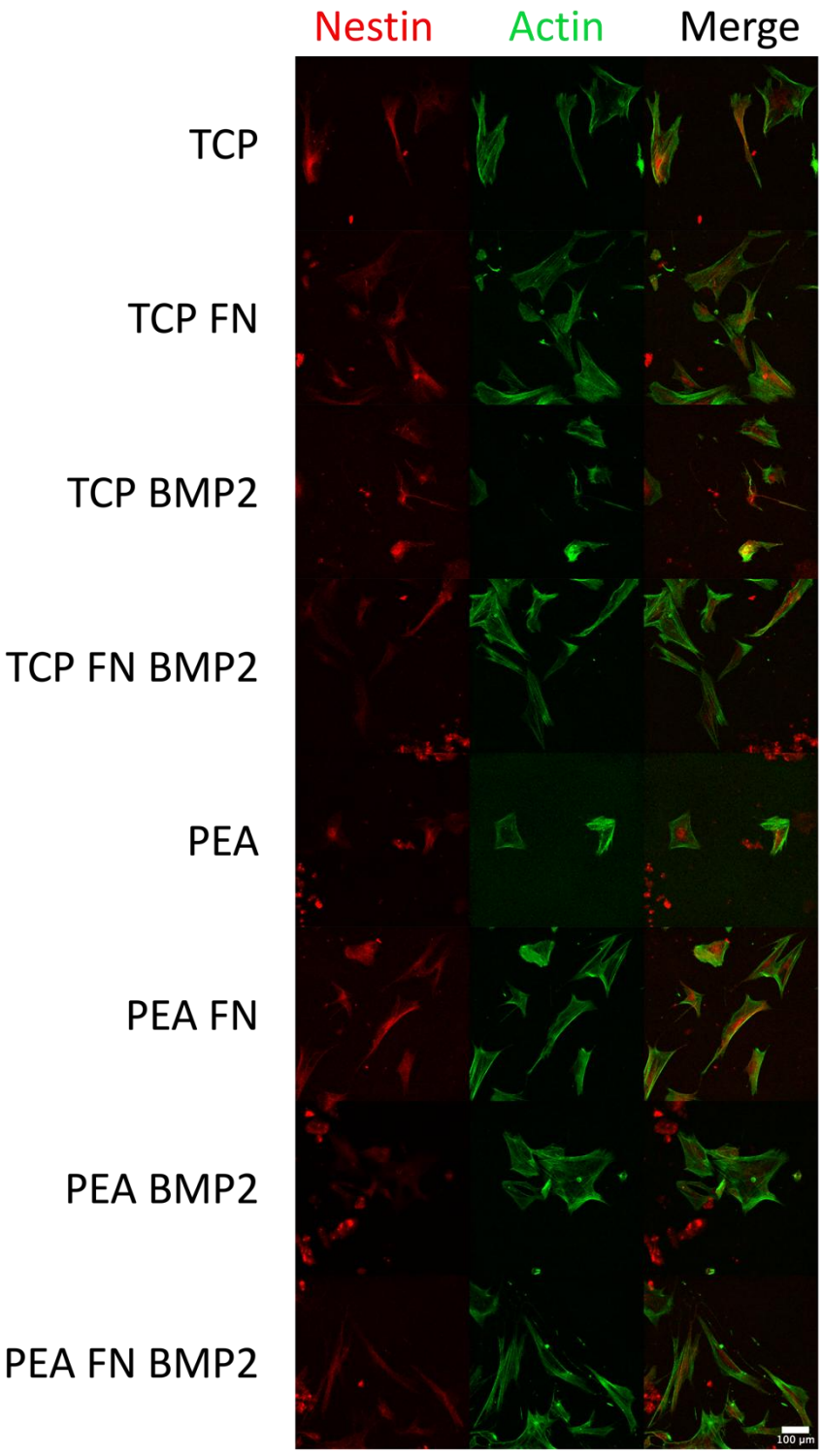

Supplementary Figure 3 MSCs' nestin expression in delta 1 conditions. *Representative confocal microscopy images of MSCs with stained actin and nestin cultured on various surfaces in delta 1 conditions. Scale bar is 100 µm.*

List of references

Abbott, R. D., & Kaplan, D. L. (2015). Strategies for improving the physiological relevance of human engineered tissues. *Trends in Biotechnology*, *33*(7), 401–407. https://doi.org/10.1016/j.tibtech.2015.04.003

Abkowitz, J. L., Catlin, S. N., McCallie, M. T., & Guttorp, P. (2002). Evidence that the number of hematopoietic stem cells per animal is conserved in mammals. *Blood*, *100*(7), 2665–2667. https://doi.org/10.1182/blood-2002-03-0822

Acar, M., Kocherlakota, K. S., Murphy, M. M., Peyer, J. G., Oguro, H., Inra, C. N., Jaiyeola, C., Zhao, Z., Luby-Phelps, K., & Morrison, S. J. (2015). Deep imaging of bone marrow shows non-dividing stem cells are mainly perisinusoidal. *Nature*, *526*(7571), 126–130. https://doi.org/10.1038/nature15250

Adams, J. M., & Cory, S. (2007). The Bcl-2 apoptotic switch in cancer development and therapy. *Oncogene*, *26*(9), 1324–1337. https://doi.org/10.1038/sj.onc.1210220

Ailles, L. E., & Weissman, I. L. (2007). Cancer stem cells in solid tumors. *Current Opinion in Biotechnology*, *18*(5), 460–466. https://doi.org/10.1016/j.copbio.2007.10.007

Akhtar, A. (2015). The Flaws and Human Harms of Animal Experimentation. *Cambridge Quarterly of Healthcare Ethics*, *24*(4), 407–419. https://doi.org/10.1017/S0963180115000079

Alba-Perez, A., Jayawarna, V., Childs, P. G., Dalby, M. J., & Salmeron-Sanchez, M. (2020). Plasma polymerised nanoscale coatings of controlled thickness for efficient solid-phase presentation of growth factors. *Materials Science and Engineering C*, *113*(April). https://doi.org/10.1016/j.msec.2020.110966

Aleman, J., George, S. K., Herberg, S., Devarasetty, M., Porada, C. D., Skardal, A., & Almeida-Porada, G. (2019). Deconstructed Microfluidic Bone Marrow On-A-Chip to Study Normal and Malignant Hemopoietic Cell–Niche Interactions. *Small*, *15*(43), 1–13. https://doi.org/10.1002/smll.201902971

Anzalone, A. V., Randolph, P. B., Davis, J. R., Sousa, A. A., Koblan, L. W., Levy, J. M., Chen, P. J., Wilson, C., Newby, G. A., Raguram, A., & Liu, D. R. (2019).

Search-and-replace genome editing without double-strand breaks or donor DNA. *Nature*, *576*(7785), 149–157. https://doi.org/10.1038/s41586-019-1711-4

Appelbaum, F. R., Gundacker, H., Head, D. R., Slovak, M. L., Willman, C. L., Godwin, J. E., Anderson, J. E., & Petersdorf, S. H. (2006). Age and acute myeloid leukemia. *Blood*, *107*(9), 3481–3485. https://doi.org/10.1182/blood-2005-09-3724

Arai, F., Hirao, A., Ohmura, M., Sato, H., Matsuoka, S., Takubo, K., Ito, K., Koh, G. Y., & Suda, T. (2004). Tie2/angiopoietin-1 signaling regulates hematopoietic stem cell quiescence in the bone marrow niche. *Cell*, *118*(2), 149–161. https://doi.org/10.1016/j.cell.2004.07.004

Asada, N., Kunisaki, Y., Pierce, H., Wang, Z., Fernandez, N. F., Birbrair, A., Ma'ayan, A., & Frenette, P. S. (2017). Differential cytokine contributions of perivascular haematopoietic stem cell niches. *Nature Cell Biology*, *19*(3), 214–223. https://doi.org/10.1038/ncb3475

Ayad, N. M. E., Kaushik, S., & Weaver, V. M. (2019). Tissue mechanics, an important regulator of development and disease. *Philosophical Transactions of the Royal Society B: Biological Sciences*, *374*(1779). https://doi.org/10.1098/rstb.2018.0215

Bai, T., Li, J., Sinclair, A., Imren, S., Merriam, F., Sun, F., O'Kelly, M. B., Nourigat, C., Jain, P., Delrow, J. J., Basom, R. S., Hung, H.-C., Zhang, P., Li, B., Heimfeld, S., Jiang, S., & Delaney, C. (2019). Expansion of primitive human hematopoietic stem cells by culture in a zwitterionic hydrogel. *Nature Medicine*, *25*(10), 1566–1575. https://doi.org/10.1038/s41591-019-0601-5

Bak, R. O., Dever, D. P., & Porteus, M. H. (2018). CRISPR/Cas9 genome editing in human hematopoietic stem cells. *Nature Protocols*, *13*(2), 358–376. https://doi.org/10.1038/nprot.2017.143

Baker, E. A. G., Schapiro, D., Dumitrascu, B., Vickovic, S., & Regev, A. (2023). In silico tissue generation and power analysis for spatial omics. *Nature Methods*, *20*(3), 424–431. https://doi.org/10.1038/s41592-023-01766-6

Banfi, A., Muraglia, A., Dozin, B., Mastrogiacomo, M., Cancedda, R., & Quarto, R. (2000). Proliferation kinetics and differentiation potential of ex vivo

expanded human bone marrow stromal cells: Implications for their use in cell therapy. *Experimental Hematology*, *28*(6), 707–715. https://doi.org/10.1016/S0301-472X(00)00160-0

Barrangou, R., & Doudna, J. A. (2016). Applications of CRISPR technologies in research and beyond. *Nature Biotechnology*, *34*(9), 933–941. https://doi.org/10.1038/nbt.3659

Batlle, E., & Clevers, H. (2017). Cancer stem cells revisited. *Nature Medicine*, *23*(10), 1124–1134. https://doi.org/10.1038/nm.4409

Beamson, G., & Briggs, D. (1993). High Resolution XPS of Organic Polymers: The Scienta ESCA300 Database. *Journal of Chemical Education*, *70*(1), A25. https://doi.org/10.1021/ed070pA25.5

Becker, H. J., Ishida, R., Wilkinson, A. C., Kimura, T., Lee, M. S. J., Coban, C., Ota, Y., Tanaka, Y., Roskamp, M., Sano, T., Tojo, A., Kent, D. G., & Yamazaki, S. (2023). Controlling genetic heterogeneity in gene-edited hematopoietic stem cells by single-cell expansion. *Cell Stem Cell*, *30*(7), 987-1000.e8. https://doi.org/10.1016/j.stem.2023.06.002

Bello, A. B., Park, H., & Lee, S. H. (2018). Current approaches in biomaterial-based hematopoietic stem cell niches. *Acta Biomaterialia*, *72*, 1–15. https://doi.org/10.1016/j.actbio.2018.03.028

Bender, A., Scheiber, J., Glick, M., Davies, J. W., Azzaoui, K., Hamon, J., Urban, L., Whitebread, S., & Jenkins, J. L. (2007). Analysis of pharmacology data and the prediction of adverse drug reactions and off-target effects from chemical structure. *ChemMedChem*, *2*(6), 861–873. https://doi.org/10.1002/cmdc.200700026

Bennett, M., Cantini, M., Reboud, J., Cooper, J. M., Roca-Cusachs, P., & Salmeron-Sanchez, M. (2018). Molecular clutch drives cell response to surface viscosity. *Proceedings of the National Academy of Sciences of the United States of America*, *115*(6), 1192–1197. https://doi.org/10.1073/pnas.1710653115

Bernasconi, P., & Borsani, O. (2019). Targeting Leukemia Stem Cell-Niche Dynamics: A New Challenge in AML Treatment. *Journal of Oncology*, *2019*. https://doi.org/10.1155/2019/8323592

Bertrand, J. Y., Chi, N. C., Santoso, B., Teng, S., Stainier, D. Y. R., & Traver, D. (2010). Haematopoietic stem cells derive directly from aortic endothelium during development. *Nature*, *464*(7285), 108–111. https://doi.org/10.1038/nature08738

Bhat, S., Viswanathan, P., Chandanala, S., Prasanna, S. J., & Seetharam, R. N. (2021). Expansion and characterization of bone marrow derived human mesenchymal stromal cells in serum-free conditions. *Scientific Reports*, *11*(1), 1–18. https://doi.org/10.1038/s41598-021-83088-1

Bhattacherjee, A., Rodrigues, E., Jung, J., Luzentales-Simpson, M., Enterina, J. R., Galleguillos, D., St. Laurent, C. D., Nakhaei-Nejad, M., Fuchsberger, F. F., Streith, L., Wang, Q., Kawasaki, N., Duan, S., Bains, A., Paulson, J. C., Rademacher, C., Giuliani, F., Sipione, S., & Macauley, M. S. (2019). Repression of phagocytosis by human CD33 is not conserved with mouse CD33. *Communications Biology*, *2*(1), 1–13. https://doi.org/10.1038/s42003-019-0698-6

Bi, Y., Stuelten, C. H., Kilts, T., Wadhwa, S., Iozzo, R. V., Robey, P. G., Chen, X.-D., & Young, M. F. (2005). Extracellular Matrix Proteoglycans Control the Fate of Bone Marrow Stromal Cells. *Journal of Biological Chemistry*, *280*(34), 30481–30489. https://doi.org/10.1074/jbc.M500573200

Bianco, J. E. R., Rosa, R. G., Congrains-Castillo, A., Joazeiro, P. P., Waldman, S. D., Weber, J. F., & Saad, S. T. O. (2019). Characterization of a novel decellularized bone marrow scaffold as an inductive environment for hematopoietic stem cells. *Biomaterials Science*, *7*(4), 1516–1528. https://doi.org/10.1039/c8bm01503a

Blank, U., & Karlsson, S. (2015). TGF-ß signaling in the control of hematopoietic stem cells. *Blood*, *125*(23), 3542–3550. https://doi.org/10.1182/blood-2014-12-618090

Boitano, A. E., Wang, J., Romeo, R., Bouchez, L. C., Parker, A. E., Sutton, S. E., Walker, J. R., Flaveny, C. A., Perdew, G. H., Denison, M. S., Schultz, P. G., & Cooke, M. P. (2010). Aryl Hydrocarbon Receptor Antagonists Promote the Expansion of Human Hematopoietic Stem Cells. *Science*, *329*(5997), 1345–1348. https://doi.org/10.1126/science.1191536

Bonnet, D. (2005). Cancer stem cells: lessons from leukaemia. *Cell Proliferation*, *38*(6), 357–361. https://doi.org/10.1111/j.1365-2184.2005.00353.x

Borot, F., Wang, H., Ma, Y., Jafarov, T., Raza, A., Ali, A. M., & Mukherjee, S. (2019). Gene-edited stem cells enable CD33-directed immune therapy for myeloid malignancies. *Proceedings of the National Academy of Sciences of the United States of America*, *116*(24), 11978–11987. https://doi.org/10.1073/pnas.1819992116

Bourgine, P. E., Klein, T., Paczulla, A. M., Shimizu, T., Kunz, L., Kokkaliaris, K. D., Coutu, D. L., Lengerke, C., Skoda, R., Schroeder, T., & Martin, I. (2018). In vitro biomimetic engineering of a human hematopoietic niche with functional properties. *Proceedings of the National Academy of Sciences of the United States of America*, *115*(25), E5688–E5695. https://doi.org/10.1073/pnas.1805440115

Bowerman, C. J., & Nilsson, B. L. (2012). Self-assembly of amphipathic β-sheet peptides: insights and applications. *Biopolymers*, *98*(3), 169–184. https://doi.org/10.1002/bip.22058

Boyd, A. L., Aslostovar, L., Reid, J., Ye, W., Tanasijevic, B., Porras, D. P., Shapovalova, Z., Almakadi, M., Foley, R., Leber, B., Xenocostas, A., & Bhatia, M. (2018). Identification of Chemotherapy-Induced Leukemic-Regenerating Cells Reveals a Transient Vulnerability of Human AML Recurrence. *Cancer Cell*, *34*(3), 483-498.e5. https://doi.org/10.1016/j.ccell.2018.08.007

Braham, M. V. J., Li Yim, A. S. P., Garcia Mateos, J., Minnema, M. C., Dhert, W. J. A., Öner, F. C., Robin, C., & Alblas, J. (2019). A Human Hematopoietic Niche Model Supporting Hematopoietic Stem and Progenitor Cells In Vitro. *Advanced Healthcare Materials*, *8*(10), 1–14. https://doi.org/10.1002/adhm.201801444

Bray, L. J., Binner, M., Körner, Y., Von Bonin, M., Bornhäuser, M., & Werner, C. (2017). A three-dimensional ex vivo tri-culture model mimics cell-cell interactions between acute myeloid leukemia and the vascular niche. *Haematologica*, *102*(7), 1215–1226. https://doi.org/10.3324/haematol.2016.157883

Brazil, D. P., Church, R. H., Surae, S., Godson, C., & Martin, F. (2015). BMP signalling: Agony and antagony in the family. *Trends in Cell Biology*, *25*(5), 249–264. https://doi.org/10.1016/j.tcb.2014.12.004

Brinkman, E. K., Chen, T., Amendola, M., & Van Steensel, B. (2014). Easy quantitative assessment of genome editing by sequence trace decomposition. *Nucleic Acids Research*, *42*(22), 1–8. https://doi.org/10.1093/nar/gku936

Broome, C. S., & Miyan, J. A. (2000). Neuropeptide control of bone marrow neutrophil production: A key axis for neuroimmunomodulation. *Annals of the New York Academy of Sciences*, *917*, 424–434. https://doi.org/10.1111/j.1749-6632.2000.tb05407.x

Bruns, I., Lucas, D., Pinho, S., Ahmed, J., Lambert, M. P., Kunisaki, Y., Scheiermann, C., Schiff, L., Poncz, M., Bergman, A., & Frenette, P. S. (2014). Megakaryocytes regulate hematopoietic stem cell quiescence through CXCL4 secretion. *Nature Medicine*, *20*(11), 1315–1320. https://doi.org/10.1038/nm.3707

Buchner, T., Berdel, W. E., Haferlach, C., Schnittger, S., Haferlach, T., Serve, H., Müller-Tidow, C., Braess, J., Spiekermann, K., Kienast, J., Mesters, R., Volpert, S., Staib, P., Grüneisen, A., Kern, W., Reichle, A., Ludwig, W.-D., Maschmeyer, G., Balleisen, L., … Hiddemann, W. (2008). Older Age Is An Independent Risk Factor in AML. *Blood*, *112*(11), 555–555. https://doi.org/10.1182/blood.v112.11.555.555

Buijs, A., Poddighe, P., Van Wijk, R., Van Solinge, W., Borst, E., Verdonck, L., Hagenbeek, A., Pearson, P., & Lokhorst, H. (2001). A novel CBFA2 single-nucleotide mutation in familial platelet disorder with propensity to develop myeloid malignancies. *Blood*, *98*(9), 2856–2858. https://doi.org/10.1182/blood.V98.9.2856

Burgess, K. A., Miller, A. F., Oceandy, D., & Saiani, A. (2017). Western Blot Analysis of Cells Encapsulated in Self-Assembling Peptide Hydrogels. *BioTechniques*, *63*(6), 253–260. https://doi.org/10.2144/000114617

Burgess, K. A., Workman, V. L., Elsawy, M. A., Miller, A. F., Oceandy, D., & Saiani, A. (2018). RNA extraction from self-assembling peptide hydrogels to allow

qPCR analysis of encapsulated cells. *PLOS ONE*, *13*(6), e0197517. https://doi.org/10.1371/journal.pone.0197517

Busch, K., Klapproth, K., Barile, M., Flossdorf, M., Holland-Letz, T., Schlenner, S. M., Reth, M., Höfer, T., & Rodewald, H.-R. (2015). Fundamental properties of unperturbed haematopoiesis from stem cells in vivo. *Nature*, *518*(7540), 542–546. https://doi.org/10.1038/nature14242

Butler, J. M., Nolan, D. J., Vertes, E. L., Varnum-Finney, B., Kobayashi, H., Hooper, A. T., Seandel, M., Shido, K., White, I. A., Kobayashi, M., Witte, L., May, C., Shawber, C., Kimura, Y., Kitajewski, J., Rosenwaks, Z., Bernstein, I. D., & Rafii, S. (2010). Endothelial Cells Are Essential for the Self-Renewal and Repopulation of Notch-Dependent Hematopoietic Stem Cells. *Cell Stem Cell*, *6*(3), 251–264. https://doi.org/10.1016/j.stem.2010.02.001

Calvi, L. M., Adams, G. B., Weibrecht, K. W., Weber, J. M., Olson, D. P., Knight, M. C., Martin, R. P., Schipani, E., Divieti, P., Bringhurst, F. R., Milner, L. A., Kronenberg, H. M., & Scadden, D. T. (2003). Osteoblastic cells regulate the haematopoietic stem cell niche. *Nature*, *425*(6960), 841–846. https://doi.org/10.1038/nature02040

Campa, C. C., Weisbach, N. R., Santinha, A. J., Incarnato, D., & Platt, R. J. (2019). Multiplexed genome engineering by Cas12a and CRISPR arrays encoded on single transcripts. *Nature Methods*, *16*(9), 887–893. https://doi.org/10.1038/s41592-019-0508-6

Canaani, J. (2019). Management of AML Beyond "3 + 7" in 2019. *Clinical Hematology International*, *1*(1), 10. https://doi.org/10.2991/chi.d.190316.001

Cantini, M., Donnelly, H., Dalby, M. J., & Salmeron-Sanchez, M. (2020). The Plot Thickens: The Emerging Role of Matrix Viscosity in Cell Mechanotransduction. *Advanced Healthcare Materials*, *9*(8). https://doi.org/10.1002/adhm.201901259

Cantini, M., Rico, P., Moratal, D., & Salmerón-Sánchez, M. (2012). Controlled wettability, same chemistry: Biological activity of plasma-polymerized coatings. *Soft Matter*, *8*(20), 5575–5584. https://doi.org/10.1039/c2sm25413a

Castillo Diaz, L. A., Elsawy, M., Saiani, A., Gough, J. E., & Miller, A. F. (2016). Osteogenic differentiation of human mesenchymal stem cells promotes mineralization within a biodegradable peptide hydrogel. *Journal of Tissue Engineering*, *7*. https://doi.org/10.1177/2041731416649789

Ceredig, R., Rolink, A., & Brown, G. (2009). Models of haematopoiesis. *Nature Reviews Immunology*, *9*(Aprll), 293–300.

Chang, R. L., Xie, L., Xie, L., Bourne, P. E., & Palsson, B. (2010). Drug off-target effects predicted using structural analysis in the context of a metabolic network model. *PLoS Computational Biology*, *6*(9). https://doi.org/10.1371/journal.pcbi.1000938

Chanput, W., Mes, J. J., & Wichers, H. J. (2014). THP-1 cell line: An in vitro cell model for immune modulation approach. *International Immunopharmacology*, *23*(1), 37–45. https://doi.org/10.1016/j.intimp.2014.08.002

Chatterjee, C., Schertl, P., Frommer, M., Ludwig-husemann, A., Mohra, A., Dilger, N., Naolou, T., Meermeyer, S., Bergmann, T. C., Calleja, A. A., & Lee-thedieck, C. (2021). Rebuilding the hematopoietic stem cell niche: recent developments and future prospects. *Acta Biomaterialia*. https://doi.org/10.1016/j.actbio.2021.03.061

Chaudhuri, O., Cooper-White, J., Janmey, P. A., Mooney, D. J., & Shenoy, V. B. (2020). Effects of extracellular matrix viscoelasticity on cellular behaviour. *Nature*, *584*(7822), 535–546. https://doi.org/10.1038/s41586-020-2612-2

Chen, B., Lee, J. B., Kang, H., Minden, M. D., & Zhang, L. (2018). Targeting chemotherapy-resistant leukemia by combining DNT cellular therapy with conventional chemotherapy. *Journal of Experimental and Clinical Cancer Research*, *37*(1), 1–11. https://doi.org/10.1186/s13046-018-0756-9

Chen, C. S., Mrksich, M., Huang, S., Whitesides, G. M., & Ingber, D. E. (1997). Geometric control of cell life and death. *Science*, *276*(5317), 1425–1428. https://doi.org/10.1126/science.276.5317.1425

Chen, D., Zhao, M., & Mundy, G. R. (2004). Bone morphogenetic proteins. *Growth Factors*, *22*(4), 233–241. https://doi.org/10.1080/08977190412331279890

Chen, J., Li, Y., Yu, T.-S., McKay, R. M., Burns, D. K., Kernie, S. G., & Parada, L. F. (2012). A restricted cell population propagates glioblastoma growth after chemotherapy. *Nature*, *488*(7412), 522–526. https://doi.org/10.1038/nature11287

Chen, X., Hughes, R., Mullin, N., Hawkins, R. J., Holen, I., Brown, N. J., & Hobbs, J. K. (2020). Mechanical Heterogeneity in the Bone Microenvironment as Characterized by Atomic Force Microscopy. *Biophysical Journal*, *119*(3), 502–513. https://doi.org/10.1016/j.bpj.2020.06.026

Cheng, Q., Wei, T., Farbiak, L., Johnson, L. T., Dilliard, S. A., & Siegwart, D. J. (2020). Selective organ targeting (SORT) nanoparticles for tissue-specific mRNA delivery and CRISPR–Cas gene editing. *Nature Nanotechnology*, *15*(4), 313–320. https://doi.org/10.1038/s41565-020-0669-6

Cheng, Q., Xia, J., Wang, K., Zhang, Y., Chen, Y., Zhong, Q., Wang, X., & Wu, Q. (2022). CRISPR/Cas9 ribonucleoprotein (RNP) complex enables higher viability of transfected cells in genome editing of acute myeloid cells. *Annals of Translational Medicine*, *10*(16), 862–862. https://doi.org/10.21037/atm-22-3279

Cheng, Z. A., Alba-Perez, A., Gonzalez-Garcia, C., Donnelly, H., Llopis-Hernandez, V., Jayawarna, V., Childs, P., Shields, D. W., Cantini, M., Ruiz-Cantu, L., Reid, A., Windmill, J. F. C., Addison, E. S., Corr, S., Marshall, W. G., Dalby, M. J., & Salmeron-Sanchez, M. (2019). Nanoscale Coatings for Ultralow Dose BMP-2-Driven Regeneration of Critical-Sized Bone Defects. *Advanced Science*, *6*(2). https://doi.org/10.1002/advs.201800361

Cheshier, S. H., Morrison, S. J., Liao, X., & Weissman, I. L. (1999). In vivo proliferation and cell cycle kinetics of long-term self-renewing hematopoietic stem cells. *Proceedings of the National Academy of Sciences of the United States of America*, *96*(6), 3120–3125. https://doi.org/10.1073/pnas.96.6.3120

Choi, J. S., & Harley, B. A. C. (2017). Marrow-inspired matrix cues rapidly affect early fate decisions of hematopoietic stem and progenitor cells. *Science Advances*, *3*(1), 1–10. https://doi.org/10.1126/sciadv.1600455

Chong, Z. X., Yeap, S. K., & Ho, W. Y. (2021). Transfection types, methods and strategies: A technical review. *PeerJ*, *9*, 1–37. https://doi.org/10.7717/peerj.11165

Chou, D. B., Frismantas, V., Milton, Y., David, R., Pop-Damkov, P., Ferguson, D., MacDonald, A., Vargel Bölükbaşı, Ö., Joyce, C. E., Moreira Teixeira, L. S., Rech, A., Jiang, A., Calamari, E., Jalili-Firoozinezhad, S., Furlong, B. A., O'Sullivan, L. R., Ng, C. F., Choe, Y., Marquez, S., … Ingber, D. E. (2020). On-chip recapitulation of clinical bone marrow toxicities and patient-specific pathophysiology. *Nature Biomedical Engineering*, *4*(4), 394–406. https://doi.org/10.1038/s41551-019-0495-z

Clarke, B. (2008). Normal Bone Anatomy and Physiology. *Clinical Journal of the American Society of Nephrology*, *3*(Supplement_3), S131–S139. https://doi.org/10.2215/CJN.04151206

Clough, H. C. (2021). *Engineering the tumour microenvironment in vitro using self-assembling peptide hydrogels*.

Clough, H. C., O'Brien, M., Zhu, X., Miller, A. F., Saiani, A., & Tsigkou, O. (2021). Neutrally charged self-assembling peptide hydrogel recapitulates in vitro mechanisms of breast cancer progression. *Materials Science and Engineering: C*, *127*(February), 112200. https://doi.org/10.1016/j.msec.2021.112200

Cohen, S., Bambace, N., Ahmad, I., Roy, J., Tang, X., Zhang, M. J., Burns, L., Barabé, F., Bernard, L., Delisle, J. S., Kiss, T., Lachance, S., Roy, D. C., Veilleux, O., & Sauvageau, G. (2023). Improved outcomes of UM171–expanded cord blood transplantation compared with other graft sources: real-world evidence. *Blood Advances*, *7*(19), 5717–5726. https://doi.org/10.1182/bloodadvances.2023010599

Cong, L., Ran, F. A., Cox, D., Lin, S., Barretto, R., Hsu, P. D., Wu, X., Jiang, W., & Marraffini, L. a. (2013). Multiplex Genome Engineering Using CRISPR/Cas Systems Le. *Science (New York, N.Y.)*, *339*(6121), 819–823. https://doi.org/10.1126/science.1231143.Multiplex

Cornelissen, J. J., & Blaise, D. (2016). Hematopoietic stem cell transplantation for patients with AML in first complete remission. *Blood*, *127*(1), 62–70. https://doi.org/10.1182/blood-2015-07-604546

Corselli, M., Chin, C. J., Parekh, C., Sahaghian, A., Wang, W., Ge, S., Evseenko, D., Wang, X., Montelatici, E., Lazzari, L., Crooks, G. M., & Péault, B. (2013). Perivascular support of human hematopoietic stem/progenitor cells. *Blood*, *121*(15), 2891–2901. https://doi.org/10.1182/blood-2012-08-451864

Coutu, D. L., Kokkaliaris, K. D., Kunz, L., & Schroeder, T. (2017). Three-dimensional map of nonhematopoietic bone and bone-marrow cells and molecules. *Nature Biotechnology*, *35*(12), 1202–1210. https://doi.org/10.1038/nbt.4006

Crisan, M., Yap, S., Casteilla, L., Chen, C. W., Corselli, M., Park, T. S., Andriolo, G., Sun, B., Zheng, B., Zhang, L., Norotte, C., Teng, P. N., Traas, J., Schugar, R., Deasy, B. M., Badylak, S., Buhring, H. J., Giacobino, J. P., Lazzari, L., … Péault, B. (2008). A Perivascular Origin for Mesenchymal Stem Cells in Multiple Human Organs. *Cell Stem Cell*, *3*(3), 301–313. https://doi.org/10.1016/j.stem.2008.07.003

Curtis, A., & Wilkinson, C. (1997). Topographical control of cells. *Biomaterials*, *18*(24), 1573–1583. https://doi.org/10.1016/S0142-9612(97)00144-0

Dalby, M. J., Gadegaard, N., Tare, R., Andar, A., Riehle, M. O., Herzyk, P., Wilkinson, C. D. W., & Oreffo, R. O. C. (2007). The control of human mesenchymal cell differentiation using nanoscale symmetry and disorder. *Nature Materials*, *6*(12), 997–1003. https://doi.org/10.1038/nmat2013

Daver, N., Schlenk, R. F., Russell, N. H., & Levis, M. J. (2019). Targeting FLT3 mutations in AML: review of current knowledge and evidence. *Leukemia*, *33*(2), 299–312. https://doi.org/10.1038/s41375-018-0357-9

De Barros, A. P. D. N., Takiya, C. M., Garzoni, L. R., Leal-Ferreira, M. L., Dutra, H. S., Chiarini, L. B., Meirelles, M. N., Borojevic, R., & Rossi, M. I. D. (2010). Osteoblasts and bone marrow mesenchymal stromal cells control hematopoietic stem cell migration and proliferation in 3D in vitro model. *PLoS ONE*, *5*(2). https://doi.org/10.1371/journal.pone.0009093

de Haan, G., Weersing, E., Dontje, B., van Os, R., Bystrykh, L. V., Vellenga, E., & Miller, G. (2003). In vitro generation of long-term repopulating hematopoietic stem cells by fibroblast growth factor-1. *Developmental Cell*, *4*(2), 241–251. https://doi.org/10.1016/S1534-5807(03)00018-2

De La Garza, A., Sinha, A., & Bowman, T. V. (2017). Concise Review: Hematopoietic Stem Cell Origins: Lessons from Embryogenesis for Improving Regenerative Medicine. *Stem Cells Translational Medicine*, *6*(1), 60–67. https://doi.org/10.5966/sctm.2016-0110

Decker, M., Leslie, J., Liu, Q., & Ding, L. (2018). Hepatic thrombopoietin is required for bone marrow hematopoietic stem cell maintenance. *Science*, *360*(6384), 106–110. https://doi.org/10.1126/science.aap8861

Delaney, C., Heimfeld, S., Brashem-Stein, C., Voorhies, H., Manger, R. L., & Bernstein, I. D. (2010). Notch-mediated expansion of human cord blood progenitor cells capable of rapid myeloid reconstitution. *Nature Medicine*, *16*(2), 232–236. https://doi.org/10.1038/nm.2080

Denu, R. A., Nemcek, S., Bloom, D. D., Goodrich, A. D., Kim, J., Mosher, D. F., & Hematti, P. (2016). Fibroblasts and Mesenchymal Stromal/Stem Cells Are Phenotypically Indistinguishable. *Acta Haematologica*, *136*(2), 85–97. https://doi.org/10.1159/000445096

Dever, D. P., Bak, R. O., Reinisch, A., Camarena, J., Washington, G., Nicolas, C. E., Pavel-Dinu, M., Saxena, N., Wilkens, A. B., Mantri, S., Uchida, N., Hendel, A., Narla, A., Majeti, R., Weinberg, K. I., & Porteus, M. H. (2016). CRISPR/Cas9 β-globin gene targeting in human haematopoietic stem cells. *Nature*, *539*(7629), 384–389. https://doi.org/10.1038/nature20134

Dexter, T. M., Allen, T. D., & Lajtha, L. G. (1977). Conditions controlling the proliferation of haemopoietic stem cells in vitro. *Journal of Cellular Physiology*, *91*(3), 335–344. https://doi.org/10.1002/jcp.1040910303

Dickinson, A. M., Norden, J., Li, S., Hromadnikova, I., Schmid, C., Schmetzer, H., & Jochem-Kolb, H. (2017). Graft-versus-Leukemia Effect Following Hematopoietic Stem Cell Transplantation for Leukemia. *Frontiers in Immunology*, *8*(JUN). https://doi.org/10.3389/fimmu.2017.00496

Ding, L., Ley, T. J., Larson, D. E., Miller, C. A., Koboldt, D. C., Welch, J. S., Ritchey, J. K., Young, M. A., Lamprecht, T., McLellan, M. D., McMichael, J. F., Wallis, J. W., Lu, C., Shen, D., Harris, C. C., Dooling, D. J., Fulton, R. S., Fulton, L. L., Chen, K., … Dipersio, J. F. (2012). Clonal evolution in relapsed

acute myeloid leukaemia revealed by whole-genome sequencing. *Nature*, *481*(7382), 506–510. https://doi.org/10.1038/nature10738

Ding, L., Saunders, T. L., Enikolopov, G., & Morrison, S. J. (2012). Endothelial and perivascular cells maintain haematopoietic stem cells. *Nature*, *481*(7382), 457–462. https://doi.org/10.1038/nature10783

Doench, J. G., Hartenian, E., Graham, D. B., Tothova, Z., Hegde, M., Smith, I., Sullender, M., Ebert, B. L., Xavier, R. J., & Root, D. E. (2014). Rational design of highly active sgRNAs for CRISPR-Cas9-mediated gene inactivation. *Nature Biotechnology*, *32*(12), 1262–1267. https://doi.org/10.1038/nbt.3026

Doherty-Boyd, W. S., Donnelly, H., Tsimbouri, M. P., & Dalby, M. J. (2024). Building bones for blood and beyond: the growing field of bone marrow niche model development. *Experimental Hematology*, *135*, 104232. https://doi.org/10.1016/j.exphem.2024.104232

Döhner, H., Weisdorf, D. J., & Bloomfield, C. D. (2015). Acute Myeloid Leukemia. *New England Journal of Medicine*, *373*(12), 1136–1152. https://doi.org/10.1056/NEJMra1406184

Dombret, H., & Itzykson, R. (2017). How and when to decide between epigenetic therapy and chemotherapy in patients with AML. *Hematology*, *2017*(1), 45–53. https://doi.org/10.1182/asheducation-2017.1.45

Donnelly, H., Ross, E., Xiao, Y., Hermantara, R., Taqi, A. F., Doherty-Boyd, W. S., Cassels, J., Tsimbouri, P. M., Dunn, K. M., Hay, J., Cheng, A., Meek, R. M. D., Jain, N., West, C., Wheadon, H., Michie, A. M., Peault, B., West, A. G., Salmeron-Sanchez, M., & Dalby, M. J. (2024). Bioengineered niches that recreate physiological extracellular matrix organisation to support long-term haematopoietic stem cells. *Nature Communications*, *15*(1). https://doi.org/10.1038/s41467-024-50054-0

Donnelly, H., Salmeron-Sanchez, M., & Dalby, M. J. (2018). Designing stem cell niches for differentiation and self-renewal. *Journal of the Royal Society Interface*, *15*(145). https://doi.org/10.1098/rsif.2018.0388

Dorrell, C., Gan, O. I., Pereira, D. S., Hawley, R. G., & Dick, J. E. (2000). Expansion of human cord blood CD34+CD38−cells in ex vivo culture during retroviral transduction without a corresponding increase in SCID repopulating

cell (SRC) frequency: dissociation of SRC phenotype and function. *Blood*, *95*(1), 102–110. https://doi.org/10.1182/blood.V95.1.102

Doudna, J. A., & Charpentier, E. (2014). The new frontier of genome engineering with CRISPR-Cas9. *Science*, *346*(6213). https://doi.org/10.1126/science.1258096

Dozzo, A., Galvin, A., Shin, J. W., Scalia, S., O'Driscoll, C. M., & Ryan, K. B. (2023). Modelling acute myeloid leukemia (AML): What's new? A transition from the classical to the modern. *Drug Delivery and Translational Research*, *13*(8), 2110–2141. https://doi.org/10.1007/s13346-022-01189-4

Du, M., Chen, W., Liu, K., Wang, L., Hu, Y., Mao, Y., Sun, X., Luo, Y., Shi, J., Shao, K., Huang, H., & Ye, D. (2022). The Global Burden of Leukemia and Its Attributable Factors in 204 Countries and Territories: Findings from the Global Burden of Disease 2019 Study and Projections to 2030. *Journal of Oncology*, *2022*. https://doi.org/10.1155/2022/1612702

Dunn, K. W., Kamocka, M. M., & McDonald, J. H. (2011). A practical guide to evaluating colocalization in biological microscopy. In *American Journal of Physiology - Cell Physiology* (Vol. 300, Issue 4). https://doi.org/10.1152/ajpcell.00462.2010

Dupuis, V., & Oltra, E. (2021). Methods to produce induced pluripotent stem cell-derived mesenchymal stem cells: Mesenchymal stem cells from induced pluripotent stem cells. *World Journal of Stem Cells*, *13*(8), 1094–1111. https://doi.org/10.4252/wjsc.v13.i8.1094

Duy, C., Li, M., Teater, M., Meydan, C., Garrett-Bakelman, F. E., Lee, T. C., Chin, C. R., Durmaz, C., Kawabata, K. C., Dhimolea, E., Mitsiades, C. S., Doehner, H., D'Andrea, R. J., Becker, M. W., Paietta, E. M., Mason, C. E., Carroll, M., & Melnick, A. M. (2021). Chemotherapy Induces Senescence-Like Resilient Cells Capable of Initiating AML Recurrence. *Cancer Discovery*, *11*(6), 1542–1561. https://doi.org/10.1158/2159-8290.CD-20-1375

Dykstra, B., Kent, D., Bowie, M., McCaffrey, L., Hamilton, M., Lyons, K., Lee, S. J., Brinkman, R., & Eaves, C. (2007). Long-Term Propagation of Distinct Hematopoietic Differentiation Programs In Vivo. *Cell Stem Cell*, *1*(2), 218–229. https://doi.org/10.1016/j.stem.2007.05.015

Eaves, C. J. (2015). Hematopoietic stem cells: Concepts, definitions, and the new reality. *Blood*, *125*(17), 2605–2613. https://doi.org/10.1182/blood-2014-12-570200

Edelman, L. B., Eddy, J. A., & Price, N. D. (2010). In silico models of cancer. *WIREs Systems Biology and Medicine*, *2*(4), 438–459. https://doi.org/10.1002/wsbm.75

Elosegui-Artola, A., Oria, R., Chen, Y., Kosmalska, A., Pérez-González, C., Castro, N., Zhu, C., Trepat, X., & Roca-Cusachs, P. (2016). Mechanical regulation of a molecular clutch defines force transmission and transduction in response to matrix rigidity. *Nature Cell Biology*, *18*(5), 540–548. https://doi.org/10.1038/ncb3336

Elosegui-Artola, A., Trepat, X., & Roca-Cusachs, P. (2018). Control of Mechanotransduction by Molecular Clutch Dynamics. *Trends in Cell Biology*, *28*(5), 356–367. https://doi.org/10.1016/j.tcb.2018.01.008

Engler, A. J., Sen, S., Sweeney, H. L., & Discher, D. E. (2006). Matrix Elasticity Directs Stem Cell Lineage Specification. *Cell*, *126*(4), 677–689. https://doi.org/10.1016/j.cell.2006.06.044

Eshraghi, M., Adlimoghaddam, A., Mahmoodzadeh, A., Sharifzad, F., Yasavoli-sharahi, H., Lorzadeh, S., Albensi, B. C., & Ghavami, S. (2021). Alzheimer's disease pathogenesis: Role of autophagy and mitophagy focusing in microglia. *International Journal of Molecular Sciences*, *22*(7), 1–36. https://doi.org/10.3390/ijms22073330

Fares, I., Calvanese, V., & Mikkola, H. K. A. (2022). Decoding Human Hematopoietic Stem Cell Self-Renewal. *Current Stem Cell Reports*, 93–106. https://doi.org/10.1007/s40778-022-00209-w

Farge, T., Saland, E., de Toni, F., Aroua, N., Hosseini, M., Perry, R., Bosc, C., Sugita, M., Stuani, L., Fraisse, M., Scotland, S., Larrue, C., Boutzen, H., Féliu, V., Nicolau-Travers, M.-L., Cassant-Sourdy, S., Broin, N., David, M., Serhan, N., … Sarry, J.-E. (2017). Chemotherapy-Resistant Human Acute Myeloid Leukemia Cells Are Not Enriched for Leukemic Stem Cells but Require Oxidative Metabolism. *Cancer Discovery*, *7*(7), 716–735. https://doi.org/10.1158/2159-8290.CD-16-0441

Faroni, A., Workman, V. L., Saiani, A., & Reid, A. J. (2019). Self-Assembling Peptide Hydrogel Matrices Improve the Neurotrophic Potential of Human Adipose-Derived Stem Cells. *Advanced Healthcare Materials*, *8*(17). https://doi.org/10.1002/adhm.201900410

Ferreira, M. S. V., & Mousavi, S. H. (2018). Nanofiber technology in the ex vivo expansion of cord blood-derived hematopoietic stem cells. *Nanomedicine: Nanotechnology, Biology, and Medicine*, *14*(5), 1707–1718. https://doi.org/10.1016/j.nano.2018.04.017

Fioretti, S., Matson, C. A., Rosenberg, K. M., & Singh, N. J. (2023). Host B cells escape CAR-T immunotherapy by reversible downregulation of CD19. *Cancer Immunology, Immunotherapy*, *72*(1), 257–264. https://doi.org/10.1007/s00262-022-03231-3

Fliefel, R., Popov, C., Tröltzsch, M., Kühnisch, J., Ehrenfeld, M., & Otto, S. (2016). Mesenchymal stem cell proliferation and mineralization but not osteogenic differentiation are strongly affected by extracellular pH. *Journal of Cranio-Maxillofacial Surgery*, *44*(6), 715–724. https://doi.org/10.1016/j.jcms.2016.03.003

Frangoul, H., Altshuler, D., Cappellini, M. D., Chen, Y.-S., Domm, J., Eustace, B. K., Foell, J., de la Fuente, J., Grupp, S., Handgretinger, R., Ho, T. W., Kattamis, A., Kernytsky, A., Lekstrom-Himes, J., Li, A. M., Locatelli, F., Mapara, M. Y., de Montalembert, M., Rondelli, D., … Corbacioglu, S. (2021). CRISPR-Cas9 Gene Editing for Sickle Cell Disease and β-Thalassemia. *New England Journal of Medicine*, *384*(3), 252–260. https://doi.org/10.1056/nejmoa2031054

Frenz-Wiessner, S., Fairley, S. D., Buser, M., Goek, I., Salewskij, K., Jonsson, G., Illig, D., zu Putlitz, B., Petersheim, D., Li, Y., Chen, P. H., Kalauz, M., Conca, R., Sterr, M., Geuder, J., Mizoguchi, Y., Megens, R. T. A., Linder, M. I., Kotlarz, D., … Klein, C. (2024). Generation of complex bone marrow organoids from human induced pluripotent stem cells. *Nature Methods*. https://doi.org/10.1038/s41592-024-02172-2

Fry, T. J., & Mackall, C. L. (2013). T-cell adoptive immunotherapy for acute lymphoblastic leukemia. *Hematology / the Education Program of the*

American Society of Hematology. American Society of Hematology. Education Program, *2013*, 348–353. https://doi.org/10.1182/asheducation-2013.1.348

Futrega, K., Atkinson, K., Lott, W. B., & Doran, M. R. (2017). Spheroid Coculture of Hematopoietic Stem/Progenitor Cells and Monolayer Expanded Mesenchymal Stem/Stromal Cells in Polydimethylsiloxane Microwells Modestly Improves in Vitro Hematopoietic Stem/Progenitor Cell Expansion. *Tissue Engineering - Part C: Methods*, *23*(4), 200–218. https://doi.org/10.1089/ten.tec.2016.0329

Gabbianelli, M., Pelosi, E., Montesoro, E., Valtieri, M., Luchetti, L., Samoggia, P., Vitelli, L., Barberi, T., Testa, U., Lyman, S., & Peschle, C. (1995). Multi-level effects of flt3 ligand on human hematopoiesis: Expansion of putative stem cells and proliferation of granulomonocytic progenitors/monocytic precursors. *Blood*, *86*(5), 1661–1670. https://doi.org/10.1182/blood.v86.5.1661.bloodjournal8651661

Gaj, T., Staahl, B. T., Rodrigues, G. M. C., Limsirichai, P., Ekman, F. K., Doudna, J. A., & Schaffer, D. V. (2017). Targeted gene knock-in by homology-directed genome editing using Cas9 ribonucleoprotein and AAV donor delivery. *Nucleic Acids Research*, *45*(11), 1–11. https://doi.org/10.1093/nar/gkx154

Galán-Díez, M., & Kousteni, S. (2017). The Osteoblastic Niche in Hematopoiesis and Hematological Myeloid Malignancies. *Current Molecular Biology Reports*, *3*(2), 53–62. https://doi.org/10.1007/s40610-017-0055-9

Galarza Torre, A., Shaw, J. E., Wood, A., Gilbert, H. T. J., Dobre, O., Genever, P., Brennan, K., Richardson, S. M., & Swift, J. (2018). An immortalised mesenchymal stem cell line maintains mechano-responsive behaviour and can be used as a reporter of substrate stiffness. *Scientific Reports*, *8*(1), 1–13. https://doi.org/10.1038/s41598-018-27346-9

Gao, J., Tang, C., Elsawy, M. A., Smith, A. M., Miller, A. F., & Saiani, A. (2017). Controlling Self-Assembling Peptide Hydrogel Properties through Network Topology. *Biomacromolecules*, *18*(3), 826–834. https://doi.org/10.1021/acs.biomac.6b01693

Gardner, R., Wu, D., Cherian, S., Fang, M., Hanafi, L. A., Finney, O., Smithers, H., Jensen, M. C., Riddell, S. R., Maloney, D. G., & Turtle, C. J. (2016).

Acquisition of a CD19-negative myeloid phenotype allows immune escape of MLL-rearranged B-ALL from CD19 CAR-T-cell therapy. *Blood*, *127*(20), 2406–2410. https://doi.org/10.1182/blood-2015-08-665547

Geris, L., Lambrechts, T., Carlier, A., & Papantoniou, I. (2018). The future is digital: In silico tissue engineering. *Current Opinion in Biomedical Engineering*, *6*, 92–98. https://doi.org/10.1016/j.cobme.2018.04.001

Gewirtz, D. (1999). A critical evaluation of the mechanisms of action proposed for the antitumor effects of the anthracycline antibiotics adriamycin and daunorubicin. *Biochemical Pharmacology*, *57*(7), 727–741. https://doi.org/10.1016/S0006-2952(98)00307-4

Gilchrist, A. E., Lee, S., Hu, Y., & Harley, B. A. C. (2019). Soluble Signals and Remodeling in a Synthetic Gelatin-Based Hematopoietic Stem Cell Niche. *Advanced Healthcare Materials*, *8*(20), 1–11. https://doi.org/10.1002/adhm.201900751

Gill, S., Tasian, S. K., Ruella, M., Shestova, O., Li, Y., Porter, D. L., Carroll, M., Danet-Desnoyers, G., Scholler, J., Grupp, S. A., June, C. H., & Kalos, M. (2014). Preclinical targeting of human acute myeloid leukemia and myeloablation using chimeric antigen receptor–modified T cells. *Blood*, *123*(15), 2343–2354. https://doi.org/10.1182/blood-2013-09-529537

Glaser, D. E., Curtis, M. B., Sariano, P. A., Rollins, Z. A., Shergill, B. S., Anand, A., Deely, A. M., Shirure, V. S., Anderson, L., Lowen, J. M., Ng, N. R., Weilbaecher, K., Link, D. C., & George, S. C. (2022). Organ-on-a-chip model of vascularized human bone marrow niches. *Biomaterials*, *280*(June 2021), 121245. https://doi.org/10.1016/j.biomaterials.2021.121245

Glass, J. L., Hassane, D., Wouters, B. J., Kunimoto, H., Avellino, R., Garrett-Bakelman, F. E., Guryanova, O. A., Bowman, R., Redlich, S., Intlekofer, A. M., Meydan, C., Qin, T., Fall, M., Alonso, A., Guzman, M. L., Valk, P. J. M., Thompson, C. B., Levine, R., Elemento, O., … Figueroa, M. E. (2017). Epigenetic identity in AML depends on disruption of nonpromoter regulatory elements and is affected by antagonistic effects of mutations in epigenetic modifiers. *Cancer Discovery*, *7*(8), 868–883. https://doi.org/10.1158/2159-8290.CD-16-1032

Goranov, V., Shelyakova, T., De Santis, R., Haranava, Y., Makhaniok, A., Gloria, A., Tampieri, A., Russo, A., Kon, E., Marcacci, M., Ambrosio, L., & Dediu, V. A. (2020). 3D Patterning of cells in Magnetic Scaffolds for Tissue Engineering. *Scientific Reports*, *10*(1), 1–8. https://doi.org/10.1038/s41598-020-58738-5

Greenbaum, A., Hsu, Y. M. S., Day, R. B., Schuettpelz, L. G., Christopher, M. J., Borgerding, J. N., Nagasawa, T., & Link, D. C. (2013). CXCL12 in early mesenchymal progenitors is required for haematopoietic stem-cell maintenance. *Nature*, *495*(7440), 227–230. https://doi.org/10.1038/nature11926

Gross, G., Waks, T., & Eshhar, Z. (1989). Expression of immunoglobulin-T-cell receptor chimeric molecules as functional receptors with antibody-type specificity. *Proceedings of the National Academy of Sciences of the United States of America*, *86*(24), 10024–10028. https://doi.org/10.1073/pnas.86.24.10024

Gugutkov, D., Altankov, G., Rodríguez Hernández, J. C., Monleón Pradas, M., & Salmerón Sánchez, M. (2010). Fibronectin activity on substrates with controlled - OH density. *Journal of Biomedical Materials Research - Part A*, *92*(1), 322–331. https://doi.org/10.1002/jbm.a.32374

Gundry, M. C., Brunetti, L., Lin, A., Mayle, A. E., Kitano, A., Wagner, D., Hsu, J. I., Hoegenauer, K. A., Rooney, C. M., Goodell, M. A., & Nakada, D. (2016). Highly Efficient Genome Editing of Murine and Human Hematopoietic Progenitor Cells by CRISPR/Cas9. *Cell Reports*, *17*(5), 1453–1461. https://doi.org/10.1016/j.celrep.2016.09.092

Guo, B., Huang, X., Lee, M. R., Lee, S. A., & Broxmeyer, H. E. (2018). Antagonism of PPAR-γ 3 signaling expands human hematopoietic stem and progenitor cells by enhancing glycolysis. *Nature Medicine*, *24*(3), 360–367. https://doi.org/10.1038/nm.4477

Guvendiren, M., Lu, H. D., & Burdick, J. A. (2012). Shear-thinning hydrogels for biomedical applications. *Soft Matter*, *8*(2), 260–272. https://doi.org/10.1039/c1sm06513k

Haas, S., Trumpp, A., & Milsom, M. D. (2018). Causes and Consequences of Hematopoietic Stem Cell Heterogeneity. *Cell Stem Cell*, *22*(5), 627–638. https://doi.org/10.1016/j.stem.2018.04.003

Habbel, J., Arnold, L., Chen, Y., Ollmann, M. M., Bruderek, K., Brandau, S., Uhrsen, U. D., & Hanoun, M. (2020). Inflammation-driven activation of JAK/STAT signaling reversibly accelerates acute myeloid leukemia in vitro. *Blood Advances*, *4*(13), 3000–3010. https://doi.org/10.1182/bloodadvances.2019001292

Haddrick, M., & Simpson, P. B. (2019). Organ-on-a-chip technology: turning its potential for clinical benefit into reality. *Drug Discovery Today*, *24*(5), 1217–1223. https://doi.org/10.1016/j.drudis.2019.03.011

Hamada, A., Kawaguchi, T., & Nakano, M. (2002). Clinical Pharmacokinetics of Cytarabine Formulations. *Clinical Pharmacokinetics*, *41*(10), 705–718. https://doi.org/10.2165/00003088-200241100-00002

Hass, R., Kasper, C., Böhm, S., & Jacobs, R. (2011). Different populations and sources of human mesenchymal stem cells (MSC): A comparison of adult and neonatal tissue-derived MSC. *Cell Communication and Signaling*, *9*(1), 12. https://doi.org/10.1186/1478-811X-9-12

He, L., Yao, Y., Wang, N., & Nan, G. (2022). Effects of electric charge on fracture healing. *Scientific Reports*, *12*(1), 15839. https://doi.org/10.1038/s41598-022-20153-3

Heath, E. M., Chan, S. M., Minden, M. D., Murphy, T., Shlush, L. I., & Schimmer, A. D. (2017). Biological and clinical consequences of NPM1 mutations in AML. *Leukemia*, *31*(4), 798–807. https://doi.org/10.1038/leu.2017.30

Hebbar, N., Epperly, R., Vaidya, A., Thanekar, U., Moore, S. E., Umeda, M., Ma, J., Patil, S. L., Langfitt, D., Huang, S., Cheng, C., Klco, J. M., Gottschalk, S., & Velasquez, M. P. (2022). CAR T cells redirected to cell surface GRP78 display robust anti-acute myeloid leukemia activity and do not target hematopoietic progenitor cells. *Nature Communications*, *13*(1), 1–14. https://doi.org/10.1038/s41467-022-28243-6

Heil, J., Olsavszky, V., Busch, K., Klapproth, K., de la Torre, C., Sticht, C., Sandorski, K., Hoffmann, J., Schönhaber, H., Zierow, J., Winkler, M., Schmid,

C. D., Staniczek, T., Daniels, D. E., Frayne, J., Metzgeroth, G., Nowak, D., Schneider, S., Neumaier, M., … Koch, P. S. (2021). Bone marrow sinusoidal endothelium controls terminal erythroid differentiation and reticulocyte maturation. *Nature Communications*, *12*(1), 1–14. https://doi.org/10.1038/s41467-021-27161-3

Hernández-Caselles, T., Martínez-Esparza, M., Pérez-Oliva, A. B., Quintanilla-Cecconi, A. M., García-Alonso, A., Alvarez-López, D. M. R., & García-Peñarrubia, P. (2006). A study of CD33 (SIGLEC-3) antigen expression and function on activated human T and NK cells: two isoforms of CD33 are generated by alternative splicing. *Journal of Leukocyte Biology*, *79*(1), 46–58. https://doi.org/10.1189/jlb.0205096

Himburg, H. A., Harris, J. R., Ito, T., Daher, P., Russell, J. L., Quarmyne, M., Doan, P. L., Helms, K., Nakamura, M., Fixsen, E., Herradon, G., Reya, T., Chao, N. J., Harroch, S., & Chute, J. P. (2012). Pleiotrophin Regulates the Retention and Self-Renewal of Hematopoietic Stem Cells in the Bone Marrow Vascular Niche. *Cell Reports*, *2*(4), 964–975. https://doi.org/10.1016/j.celrep.2012.09.002

Himburg, H. A., Muramoto, G. G., Daher, P., Meadows, S. K., Russell, J. L., Doan, P., Chi, J.-T., Salter, A. B., Lento, W. E., Reya, T., Chao, N. J., & Chute, J. P. (2010). Pleiotrophin regulates the expansion and regeneration of hematopoietic stem cells. *Nature Medicine*, *16*(4), 475–482. https://doi.org/10.1038/nm.2119

Homeyer, A., Geißler, C., Schwen, L. O., Zakrzewski, F., Evans, T., Strohmenger, K., Westphal, M., Bülow, R. D., Kargl, M., Karjauv, A., Munné-Bertran, I., Retzlaff, C. O., Romero-López, A., Sołtysiński, T., Plass, M., Carvalho, R., Steinbach, P., Lan, Y. C., Bouteldja, N., … Zerbe, N. (2022). Recommendations on compiling test datasets for evaluating artificial intelligence solutions in pathology. *Modern Pathology*, *35*(12), 1759–1769. https://doi.org/10.1038/s41379-022-01147-y

Hope, K. J., Jin, L., & Dick, J. E. (2004). Acute myeloid leukemia originates from a hierarchy of leukemic stem cell classes that differ in self-renewal capacity. *Nature Immunology*, *5*(7), 738–743. https://doi.org/10.1038/ni1080

Horwitz, M. E., Chao, N. J., Rizzieri, D. A., Long, G. D., Sullivan, K. M., Gasparetto, C., Chute, J. P., Morris, A., McDonald, C., Waters-Pick, B., Stiff, P., Wease, S., Peled, A., Snyder, D., Cohen, E. G., Shoham, H., Landau, E., Friend, E., Peleg, I., … Peled, T. (2014). Umbilical cord blood expansion with nicotinamide provides long-term multilineage engraftment. *Journal of Clinical Investigation*, *124*(7), 3121–3128. https://doi.org/10.1172/JCI74556

Hsu, P. D., Scott, D. A., Weinstein, J. A., Ran, F. A., Konermann, S., Agarwala, V., Li, Y., Fine, E. J., Wu, X., Shalem, O., Cradick, T. J., Marraffini, L. A., Bao, G., & Zhang, F. (2013). DNA targeting specificity of RNA-guided Cas9 nucleases. *Nature Biotechnology*, *31*(9), 827–832. https://doi.org/10.1038/nbt.2647

Hulbert, M. L., & Shenoy, S. (2018). Hematopoietic stem cell transplantation for sickle cell disease: Progress and challenges. *Pediatric Blood & Cancer*, *65*(9), 1–10. https://doi.org/10.1002/pbc.27263

Humbert, O., Laszlo, G. S., Sichel, S., Ironside, C., Haworth, K. G., Bates, O. M., Beddoe, M. E., Carrillo, R. R., Kiem, H. P., & Walter, R. B. (2019). Engineering resistance to CD33-targeted immunotherapy in normal hematopoiesis by CRISPR/Cas9-deletion of CD33 exon 2. *Leukemia*, *33*(3), 762–808. https://doi.org/10.1038/s41375-018-0277-8

Hur, J., Choi, J. Il, Lee, H., Nham, P., Kim, T. W., Chae, C. W., Yun, J. Y., Kang, J. A., Kang, J., Lee, S. E., Yoon, C. H., Boo, K., Ham, S., Roh, T. Y., Jun, J. K., Lee, H., Baek, S. H., & Kim, H. S. (2016). CD82/KAI1 Maintains the Dormancy of Long-Term Hematopoietic Stem Cells through Interaction with DARC-Expressing Macrophages. *Cell Stem Cell*, *18*(4), 508–521. https://doi.org/10.1016/j.stem.2016.01.013

Hynes, R. O. (1992). Integrins: Versatility, modulation, and signaling in cell adhesion. *Cell*, *69*(1), 11–25. https://doi.org/10.1016/0092-8674(92)90115-S

Hynes, R. O. (2009). The Extracellular Matrix: Not Just Pretty Fibrils. *Science*, *326*(5957), 1216–1219. https://doi.org/10.1126/science.1176009

Ingber, D. E. (2020). Is it Time for Reviewer 3 to Request Human Organ Chip Experiments Instead of Animal Validation Studies? *Advanced Science*, *2002030*, 1–15. https://doi.org/10.1002/advs.202002030

Isern, J., Martín-Antonio, B., Ghazanfari, R., Martín, A. M., López, J. A., delToro, R., Sánchez-Aguilera, A., Arranz, L., Martín-Pérez, D., Suárez-Lledó, M., Marín, P., VanPel, M., Fibbe, W. E., Vázquez, J., Scheding, S., Urbano-Ispizúa, Á., & Méndez-Ferrer, S. (2013). Self-Renewing Human Bone Marrow Mesenspheres Promote Hematopoietic Stem Cell Expansion. *Cell Reports*, *3*(5), 1714–1724. https://doi.org/10.1016/j.celrep.2013.03.041

Ishikawa, F., Yoshida, S., Saito, Y., Hijikata, A., Kitamura, H., Tanaka, S., Nakamura, R., Tanaka, T., Tomiyama, H., Saito, N., Fukata, M., Miyamoto, T., Lyons, B., Ohshima, K., Uchida, N., Taniguchi, S., Ohara, O., Akashi, K., Harada, M., & Shultz, L. D. (2007). Chemotherapy-resistant human AML stem cells home to and engraft within the bone-marrow endosteal region. *Nature Biotechnology*, *25*(11), 1315–1321. https://doi.org/10.1038/nbt1350

Issa, J.-P. J., Roboz, G., Rizzieri, D., Jabbour, E., Stock, W., O'Connell, C., Yee, K., Tibes, R., Griffiths, E. A., Walsh, K., Daver, N., Chung, W., Naim, S., Taverna, P., Oganesian, A., Hao, Y., Lowder, J. N., Azab, M., & Kantarjian, H. (2015). Safety and tolerability of guadecitabine (SGI-110) in patients with myelodysplastic syndrome and acute myeloid leukaemia: a multicentre, randomised, dose-escalation phase 1 study. *The Lancet Oncology*, *16*(9), 1099–1110. https://doi.org/10.1016/S1470-2045(15)00038-8

Jagannathan-Bogdan, M., & Zon, L. I. (2013). Hematopoiesis. *Development*, *140*(12), 2463–2467. https://doi.org/10.1242/dev.083147

James, S., Fox, J., Afsari, F., Lee, J., Clough, S., Knight, C., Ashmore, J., Ashton, P., Preham, O., Hoogduijn, M., Ponzoni, R. D. A. R., Hancock, Y., Coles, M., & Genever, P. (2015). Multiparameter Analysis of Human Bone Marrow Stromal Cells Identifies Distinct Immunomodulatory and Differentiation-Competent Subtypes. *Stem Cell Reports*, *4*(6), 1004–1015. https://doi.org/10.1016/j.stemcr.2015.05.005

Jan, Y. N., & Jan, L. Y. (1998). Asymmetric cell division. *Nature*, *392*(6678), 775–778. https://doi.org/10.1038/33854

Jang, Y. Y., & Sharkis, S. J. (2007). A low level of reactive oxygen species selects for primitive hematopoietic stem cells that may reside in the low-oxygenic niche. *Blood*, *110*(8), 3056–3063. https://doi.org/10.1182/blood-2007-05-087759

Janmey, P. A., Fletcher, D. A., & Reinhart-King, C. A. (2020). Stiffness sensing by cells. *Physiological Reviews*, *100*(2), 695–724. https://doi.org/10.1152/physrev.00013.2019

Jansen, L. E., Birch, N. P., Schiffman, J. D., Crosby, A. J., & Peyton, S. R. (2015). Mechanics of intact bone marrow. *Journal of the Mechanical Behavior of Biomedical Materials*, *50*, 299–307. https://doi.org/10.1016/j.jmbbm.2015.06.023

Jaroscak, J., Goltry, K., Smith, A., Waters-Pick, B., Martin, P. L., Driscoll, T. A., Howrey, R., Chao, N., Douville, J., Burhop, S., Fu, P., & Kurtzberg, J. (2003). Augmentation of umbilical cord blood (UCB) transplantation with ex vivo-expanded UCB cells: Results of a phase 1 trial using the AastromReplicell system. *Blood*, *101*(12), 5061–5067. https://doi.org/10.1182/blood-2001-12-0290

Jawad, M., Seedhouse, C., Mony, U., Grundy, M., Russell, N. H., & Pallis, M. (2010). Analysis of factors that affect in vitro chemosensitivity of leukaemic stem and progenitor cells to gemtuzumab ozogamicin (Mylotarg) in acute myeloid leukaemia. *Leukemia*, *24*(1), 74–80. https://doi.org/10.1038/leu.2009.199

Kantarjian, H. (2016). Acute myeloid leukemia-Major progress over four decades and glimpses into the future. *American Journal of Hematology*, *91*(1), 131–145. https://doi.org/10.1002/ajh.24246

Kantarjian, H., Kadia, T., DiNardo, C., Daver, N., Borthakur, G., Jabbour, E., Garcia-Manero, G., Konopleva, M., & Ravandi, F. (2021). Acute myeloid leukemia: current progress and future directions. *Blood Cancer Journal*, *11*(2). https://doi.org/10.1038/s41408-021-00425-3

Kaplan, F. S., Xu, M., Seemann, P., Connor, J. M., Glaser, D. L., Carroll, L., Delai, P., Fastnacht-Urban, E., Forman, S. J., Gillessen-Kaesbach, G., Hoover-Fong, J., Köster, B., Pauli, R. M., Reardon, W., Zaidi, S. A., Zasloff, M., Morhart, R., Mundlos, S., Groppe, J., & Shore, E. M. (2009). Classic and atypical fibrodysplasia ossificans progressiva (FOP) phenotypes are caused by mutations in the bone morphogenetic protein (BMP) type I receptor ACVR1. *Human Mutation*, *30*(3), 379–390. https://doi.org/10.1002/humu.20868

Karamitros, D., Stoilova, B., Aboukhalil, Z., Hamey, F., Reinisch, A., Samitsch, M., Quek, L., Otto, G., Repapi, E., Doondeea, J., Usukhbayar, B., Calvo, J., Taylor, S., Goardon, N., Six, E., Pflumio, F., Porcher, C., Majeti, R., Göttgens, B., & Vyas, P. (2018). Single-cell analysis reveals the continuum of human lympho-myeloid progenitor cells. *Nature Immunology*, *19*(1), 85–97. https://doi.org/10.1038/s41590-017-0001-2

Karimpoor, M., Yebra-Fernandez, E., Parhizkar, M., Orlu, M., Craig, D., Khorashad, J. S., & Edirisinghe, M. (2018). Alginate foam-based three-dimensional culture to investigate drug sensitivity in primary leukaemia cells. *Journal of the Royal Society Interface*, *15*(141). https://doi.org/10.1098/rsif.2017.0928

Katayama, Y., Battista, M., Kao, W. M., Hidalgo, A., Peired, A. J., Thomas, S. A., & Frenette, P. S. (2006). Signals from the sympathetic nervous system regulate hematopoietic stem cell egress from bone marrow. *Cell*, *124*(2), 407–421. https://doi.org/10.1016/j.cell.2005.10.041

Kaushansky, K. (2006). Lineage-Specific Hematopoietic Growth Factors. *New England Journal of Medicine*, *354*(19), 2034–2045. https://doi.org/10.1056/NEJMra052706

Kechagia, J. Z., Ivaska, J., & Roca-Cusachs, P. (2019). Integrins as biomechanical sensors of the microenvironment. *Nature Reviews Molecular Cell Biology*, *20*(8), 457–473. https://doi.org/10.1038/s41580-019-0134-2

Kenderian, S. S., Ruella, M., Shestova, O., Klichinsky, M., Aikawa, V., Morrissette, J. J. D., Scholler, J., Song, D., Porter, D. L., Carroll, M., June, C. H., & Gill, S. (2015). CD33-specific chimeric antigen receptor T cells exhibit potent preclinical activity against human acute myeloid leukemia. *Leukemia*, *29*(8), 1637–1647. https://doi.org/10.1038/leu.2015.52

Keselowsky, B. G., Collard, D. M., & García, A. J. (2005). Integrin binding specificity regulates biomaterial surface chemistry effects on cell differentiation. *Proceedings of the National Academy of Sciences of the United States of America*, *102*(17), 5953–5957. https://doi.org/10.1073/pnas.0407356102

Khan, A. O., Rodriguez-Romera, A., Reyat, J. S., Olijnik, A. A., Colombo, M., Wang, G., Wen, W. X., Sousos, N., Murphy, L. C., Grygielska, B., Perrella, G., Mahony, C. B., Ling, R. E., Elliott, N. E., Karali, C. S., Stone, A. P., Kemble, S., Cutler, E. A., Fielding, A. K., … Psaila, B. (2023). Human Bone Marrow Organoids for Disease Modeling, Discovery, and Validation of Therapeutic Targets in Hematologic Malignancies. *Cancer Discovery*, *13*(2), 364–385. https://doi.org/10.1158/2159-8290.CD-22-0199

Kiel, M. J., Yilmaz, Ö. H., Iwashita, T., Yilmaz, O. H., Terhorst, C., & Morrison, S. J. (2005). SLAM family receptors distinguish hematopoietic stem and progenitor cells and reveal endothelial niches for stem cells. *Cell*, *121*(7), 1109–1121. https://doi.org/10.1016/j.cell.2005.05.026

Kierans, S. J., & Taylor, C. T. (2021). Regulation of glycolysis by the hypoxia-inducible factor (HIF): implications for cellular physiology. *Journal of Physiology*, *599*(1), 23–37. https://doi.org/10.1113/JP280572

Kilian, K. A., Bugarija, B., Lahn, B. T., & Mrksich, M. (2010). Geometric cues for directing the differentiation of mesenchymal stem cells. *Proceedings of the National Academy of Sciences of the United States of America*, *107*(11), 4872–4877. https://doi.org/10.1073/pnas.0903269107

Kim, M. Y. (2023). Making normal hematopoiesis invisible to CAR T cells. *Trends in Cancer*, *9*(12), 983–984. https://doi.org/10.1016/j.trecan.2023.10.001

Kim, M. Y., Yu, K. R., Kenderian, S. S., Ruella, M., Chen, S., Shin, T. H., Aljanahi, A. A., Schreeder, D., Klichinsky, M., Shestova, O., Kozlowski, M. S., Cummins, K. D., Shan, X., Shestov, M., Bagg, A., Morrissette, J. J. D., Sekhri, P., Lazzarotto, C. R., Calvo, K. R., … Gill, S. (2018). Genetic Inactivation of CD33 in Hematopoietic Stem Cells to Enable CAR T Cell Immunotherapy for Acute Myeloid Leukemia. *Cell*, *173*(6), 1439-1453.e19. https://doi.org/10.1016/j.cell.2018.05.013

King, P. J. S., Giovanna Lizio, M., Booth, A., Collins, R. F., Gough, J. E., Miller, A. F., & Webb, S. J. (2016). A modular self-assembly approach to functionalised ß-sheet peptide hydrogel biomaterials. *Soft Matter*, *12*(6), 1915–1923. https://doi.org/10.1039/c5sm02039e

Klamer, S., & Voermans, C. (2014). The role of novel and known extracellular matrix and adhesion molecules in the homeostatic and regenerative bone marrow microenvironment http://www.tandfonline.com/doi/pdf/10.4161/19336918.2014.968501. In *Cell Adhesion and Migration* (Vol. 8, Issue 6, pp. 563–577). Landes Bioscience. https://doi.org/10.4161/19336918.2014.968501

Klco, J. M., Spencer, D. H., Lamprecht, T. L., Sarkaria, S. M., Wylie, T., Magrini, V., Hundal, J., Walker, J., Varghese, N., Erdmann-Gilmore, P., Lichti, C. F., Meyer, M. R., Townsend, R. R., Wilson, R. K., Mardis, E. R., & Ley, T. J. (2013). Genomic impact of transient low-dose decitabine treatment on primary AML cells. *Blood*, *121*(9), 1633–1643. https://doi.org/10.1182/blood-2012-09-459313

Kobayashi, C. I., & Suda, T. (2012). Regulation of reactive oxygen species in stem cells and cancer stem cells. *Journal of Cellular Physiology*, *227*(2), 421–430. https://doi.org/10.1002/jcp.22764

Kode, A., Mosialou, I., Manavalan, S. J., Rathinam, C. V, Friedman, R. A., Teruya-Feldstein, J., Bhagat, G., Berman, E., & Kousteni, S. (2016). FoxO1-dependent induction of acute myeloid leukemia by osteoblasts in mice. *Leukemia*, *30*(1), 1–13. https://doi.org/10.1038/leu.2015.161

Kojima, K., McQueen, T., Chen, Y., Jacamo, R., Konopleva, M., Shinojima, N., Shpall, E., Huang, X., & Andreeff, M. (2011). p53 activation of mesenchymal stromal cells partially abrogates microenvironment-mediated resistance to FLT3 inhibition in AML through HIF-1α-mediated down-regulation of CXCL12. *Blood*, *118*(16), 4431–4439. https://doi.org/10.1182/blood-2011-02-334136

Konig, H., & Levis, M. (2015). Targeting FLT3 to treat leukemia. *Expert Opinion on Therapeutic Targets*, *19*(1), 37–54. https://doi.org/10.1517/14728222.2014.960843

Konopleva, M., Pollyea, D. A., Potluri, J., Chyla, B., Hogdal, L., Busman, T., McKeegan, E., Salem, A. H., Zhu, M., Ricker, J. L., Blum, W., DiNardo, C. D., Kadia, T., Dunbar, M., Kirby, R., Falotico, N., Leverson, J., Humerickhouse, R., Mabry, M., … Letai, A. (2016). Efficacy and Biological Correlates of Response in a Phase II Study of Venetoclax Monotherapy in Patients with Acute

Myelogenous Leukemia. *Cancer Discovery*, *6*(10), 1106–1117. https://doi.org/10.1158/2159-8290.CD-16-0313

Kouro, T., Himuro, H., & Sasada, T. (2022). Exhaustion of CAR T cells: potential causes and solutions. *Journal of Translational Medicine*, *20*(1), 1–10. https://doi.org/10.1186/s12967-022-03442-3

Kreso, A., O'Brien, C. A., van Galen, P., Gan, O. I., Notta, F., Brown, A. M. K., Ng, K., Ma, J., Wienholds, E., Dunant, C., Pollett, A., Gallinger, S., McPherson, J., Mullighan, C. G., Shibata, D., & Dick, J. E. (2013). Variable Clonal Repopulation Dynamics Influence Chemotherapy Response in Colorectal Cancer. *Science*, *339*(6119), 543–548. https://doi.org/10.1126/science.1227670

Kumar, B., Garcia, M., Weng, L., Jung, X., Murakami, J. L., Hu, X., McDonald, T., Lin, A., Kumar, A. R., Digiusto, D. L., Stein, A. S., Pullarkat, V. A., Hui, S. K., Carlesso, N., Kuo, Y. H., Bhatia, R., Marcucci, G., & Chen, C. C. (2018). Acute myeloid leukemia transforms the bone marrow niche into a leukemia-permissive microenvironment through exosome secretion. *Leukemia*, *32*(3), 575–587. https://doi.org/10.1038/leu.2017.259

Kunisaki, Y., Bruns, I., Scheiermann, C., Ahmed, J., Pinho, S., Zhang, D., Mizoguchi, T., Wei, Q., Lucas, D., Ito, K., Mar, J. C., Bergman, A., & Frenette, P. S. (2013). Arteriolar niches maintain haematopoietic stem cell quiescence. *Nature*, *502*(7473), 637–643. https://doi.org/10.1038/nature12612

Kurth, I., Franke, K., Pompe, T., Bornhäuser, M., & Werner, C. (2009). Hematopoietic stem and progenitor cells in adhesive microcavities. *Integrative Biology*, *1*(5–6), 427–434. https://doi.org/10.1039/b903711j

Lai, W. Y., Li, Y. Y., Mak, S. K., Ho, F. C., Chow, S. T., Chooi, W. H., Chow, C. H., Leung, A. Y., & Chan, B. P. (2013). Reconstitution of bone-like matrix in osteogenically differentiated mesenchymal stem cell-collagen constructs: A three-dimensional in vitro model to study hematopoietic stem cell niche. *Journal of Tissue Engineering*, *4*(1), 1–14. https://doi.org/10.1177/2041731413508668

Lampreia, F. P., Carmelo, J. G., & Anjos-Afonso, F. (2017). Notch Signaling in the Regulation of Hematopoietic Stem Cell. *Current Stem Cell Reports*, *3*(3), 202–209. https://doi.org/10.1007/s40778-017-0090-8

Lapidot, T., & Petit, I. (2002). Current understanding of stem cell mobilization: The roles of chemokines, proteolytic enzymes, adhesion molecules, cytokines, and stromal cells. *Experimental Hematology*, *30*(9), 973–981. https://doi.org/10.1016/S0301-472X(02)00883-4

Laszlo, G. S., Estey, E. H., & Walter, R. B. (2014). The past and future of CD33 as therapeutic target in acute myeloid leukemia. *Blood Reviews*, *28*(4), 143–153. https://doi.org/10.1016/j.blre.2014.04.001

Laszlo, G. S., Harrington, K. H., Gudgeon, C. J., Beddoe, M. E., Fitzgibbon, M. P., Ries, R. E., Lamba, J. K., McIntosh, M. W., Meshinchi, S., & Walter, R. B. (2016). Expression and functional characterization of CD33 transcript variants in human acute myeloid leukemia. *Oncotarget*, *7*(28), 43281–43294. https://doi.org/10.18632/oncotarget.9674

LeBleu, V. S., & Neilson, E. G. (2020). Origin and functional heterogeneity of fibroblasts. *The FASEB Journal*, *34*(3), 3519–3536. https://doi.org/10.1096/fj.201903188R

Lee, H., Li, N., Evans, S., Diaz, M., & Wenzel, P. (2005). Biomechanical force in blood development: extrinsic physical cues drive pro-hematopoietic signaling. *Bone*, *23*(1), 1–7. https://doi.org/10.1016/j.diff.2013.06.004.Biomechanical

Lee, Y., Jeong, M., Park, J., Jung, H., & Lee, H. (2023). Immunogenicity of lipid nanoparticles and its impact on the efficacy of mRNA vaccines and therapeutics. *Experimental and Molecular Medicine*, *55*(10), 2085–2096. https://doi.org/10.1038/s12276-023-01086-x

Lee-Thedieck, C., Schertl, P., & Klein, G. (2022). The extracellular matrix of hematopoietic stem cell niches. *Advanced Drug Delivery Reviews*, *181*, 114069. https://doi.org/10.1016/j.addr.2021.114069

Leisten, I., Kramann, R., Ventura Ferreira, M. S., Bovi, M., Neuss, S., Ziegler, P., Wagner, W., Knüchel, R., & Schneider, R. K. (2012). 3D co-culture of hematopoietic stem and progenitor cells and mesenchymal stem cells in

collagen scaffolds as a model of the hematopoietic niche. *Biomaterials*, *33*(6), 1736–1747. https://doi.org/10.1016/j.biomaterials.2011.11.034

Lendahl, U., Zimmerman, L. B., & McKay, R. D. G. (1990). CNS stem cells express a new class of intermediate filament protein. *Cell*, *60*(4), 585–595. https://doi.org/10.1016/0092-8674(90)90662-X

Lerman, M. J., Lembong, J., Muramoto, S., Gillen, G., & Fisher, J. P. (2018). The Evolution of Polystyrene as a Cell Culture Material. *Tissue Engineering - Part B: Reviews*, *24*(5), 359–372. https://doi.org/10.1089/ten.teb.2018.0056

Lewis, N. S., Lewis, E. E. L., Mullin, M., Wheadon, H., Dalby, M. J., & Berry, C. C. (2017). Magnetically levitated mesenchymal stem cell spheroids cultured with a collagen gel maintain phenotype and quiescence. *Journal of Tissue Engineering*, *8*, 204173141770442. https://doi.org/10.1177/2041731417704428

Li, D., Lin, T. L., Lipe, B., Hopkins, R. A., Shinogle, H., & Aljitawi, O. S. (2018). A novel extracellular matrix-based leukemia model supports leukemia cells with stem cell-like characteristics. *Leukemia Research*, *72*(August), 105–112. https://doi.org/10.1016/j.leukres.2018.08.012

Li, D., Xue, W., Li, M., Dong, M., Wang, J., Wang, X., Li, X., Chen, K., Zhang, W., Wu, S., Zhang, Y., Gao, L., Chen, Y., Chen, J., Zhou, B. O., Zhou, Y., Yao, X., Li, L., Wu, D., & Pan, W. (2018). VCAM-1+ macrophages guide the homing of HSPCs to a vascular niche. *Nature*, *564*(7734), 119–124. https://doi.org/10.1038/s41586-018-0709-7

Li, H., Ghazanfari, R., Zacharaki, D., Lim, H. C., & Scheding, S. (2016). Isolation and characterization of primary bone marrow mesenchymal stromal cells. *Annals of the New York Academy of Sciences*, *1370*(1), 109–118. https://doi.org/10.1111/nyas.13102

Li, J., Wang, X., Ding, J., Zhu, Y., Min, W., Kuang, W., Yuan, K., Sun, C., & Yang, P. (2022). Development and clinical advancement of small molecules for ex vivo expansion of hematopoietic stem cell. *Acta Pharmaceutica Sinica B*, *12*(6), 2808–2831. https://doi.org/10.1016/j.apsb.2021.12.006

Lienemann, P. S., Vallmajo-Martin, Q., Papageorgiou, P., Blache, U., Metzger, S., Kiveliö, A. S., Milleret, V., Sala, A., Hoehnel, S., Roch, A., Reuten, R., Koch,

M., Naveiras, O., Weber, F. E., Weber, W., Lutolf, M. P., & Ehrbar, M. (2020). Smart Hydrogels for the Augmentation of Bone Regeneration by Endogenous Mesenchymal Progenitor Cell Recruitment. *Advanced Science*, *7*(7). https://doi.org/10.1002/advs.201903395

Ligorio, C., Zhou, M., Wychowaniec, J. K., Zhu, X., Bartlam, C., Miller, A. F., Vijayaraghavan, A., Hoyland, J. A., & Saiani, A. (2019). Graphene oxide containing self-assembling peptide hybrid hydrogels as a potential 3D injectable cell delivery platform for intervertebral disc repair applications. *Acta Biomaterialia*, *92*, 92–103. https://doi.org/10.1016/j.actbio.2019.05.004

Lima, M. De, Mcniece, I., Robinson, S. N., Munsell, M., Eapen, M., Horowitz, M., Alousi, A., Saliba, R., John, D., Kaur, I., Kebriaei, P., Parmar, S., Molldrem, J., Jones, R. B., Nieto, Y., & Andersson, B. S. (2013). *Cord-Blood Engraftment with Ex Vivo Mesenchymal-Cell Coculture Marcos*. *367*(24), 2305–2315. https://doi.org/10.1056/NEJMoa1207285.Cord-Blood

Lino, C. A., Harper, J. C., Carney, J. P., & Timlin, J. A. (2018). Delivering CRISPR: a review of the challenges and approaches. *Drug Delivery*, *25*(1), 1234–1257. https://doi.org/10.1080/10717544.2018.1474964

Llopis-Hernández, V., Cantini, M., González-García, C., Cheng, Z. A., Yang, J., Tsimbouri, P. M., García, A. J., Dalby, M. J., & Salmerón-Sánchez, M. (2016). Material-driven fibronectin assembly for high-efficiency presentation of growth factors. *Science Advances*, *2*(8), 1–11. https://doi.org/10.1126/sciadv.1600188

Locatelli, F. (2005). Hematopoietic stem cell transplantation (HSCT) in children with juvenile myelomonocytic leukemia (JMML): results of the EWOG-MDS/EBMT trial. *Blood*, *105*(1), 410–419. https://doi.org/10.1182/blood-2004-05-1944

Lucas, D., Scheiermann, C., Chow, A., Kunisaki, Y., Bruns, I., Barrick, C., Tessarollo, L., & Frenette, P. S. (2013). Chemotherapy-induced bone marrow nerve injury impairs hematopoietic regeneration. *Nature Medicine*, *19*(6), 695–703. https://doi.org/10.1038/nm.3155

Luens, K. M., Travis, M. A., Chen, B. P., Hill, B. L., Scollay, R., & Murray, L. J. (1998). Thrombopoietin, kit ligand, and flk2/flt3 ligand together induce increased numbers of primitive hematopoietic progenitors from human CD34+Thy-1+Lin- cells with preserved ability to engraft SCID-hu bone. *Blood*, *91*(4), 1206–1215. https://doi.org/10.1182/blood.v91.4.1206

Ma, C., Witkowski, M. T., Harris, J., Dolgalev, I., Sreeram, S., Qian, W., Tong, J., Chen, X., Aifantis, I., & Chen, W. (2020). Leukemia-on-a-chip: Dissecting the chemoresistance mechanisms in B cell acute lymphoblastic leukemia bone marrow niche. *Science Advances*, *6*(44). https://doi.org/10.1126/sciadv.aba5536

Mahadik, B. P., Bharadwaj, N. A. K., Ewoldt, R. H., & Harley, B. A. C. (2017). Regulating dynamic signaling between hematopoietic stem cells and niche cells via a hydrogel matrix. *Biomaterials*, *125*, 54–64. https://doi.org/10.1016/j.biomaterials.2017.02.013

Mali, P., Yang, L., Esvelt, K. M., Aach, J., Guell, M., DiCarlo, J. E., Norville, J. E., & Church, G. M. (2013). RNA-guided human genome engineering via Cas9. *Science*, *339*(6121), 823–826. https://doi.org/10.1126/science.1232033

Mansour, A., Abou-Ezzi, G., Sitnicka, E., Jacobsen, S. E. W., Wakkach, A., & Blin-Wakkach, C. (2012). Osteoclasts promote the formation of hematopoietic stem cell niches in the bone marrow. *Journal of Experimental Medicine*, *209*(3), 537–549. https://doi.org/10.1084/jem.20110994

Mardiana, S., & Gill, S. (2020). CAR T Cells for Acute Myeloid Leukemia: State of the Art and Future Directions. *Frontiers in Oncology*, *10*(May), 1–12. https://doi.org/10.3389/fonc.2020.00697

Martino, M. M., Briquez, P. S., Maruyama, K., & Hubbell, J. A. (2015). Extracellular matrix-inspired growth factor delivery systems for bone regeneration. *Advanced Drug Delivery Reviews*, *94*, 41–52. https://doi.org/10.1016/j.addr.2015.04.007

Martino, M. M., & Hubbell, J. A. (2010). The 12th–14th type III repeats of fibronectin function as a highly promiscuous growth factor-binding domain. *The FASEB Journal*, *24*(12), 4711–4721. https://doi.org/10.1096/fj.09.151282

Maryanovich, M., Zahalka, A. H., Pierce, H., Pinho, S., Nakahara, F., Asada, N., Wei, Q., Wang, X., Ciero, P., Xu, J., Leftin, A., & Frenette, P. S. (2018). Adrenergic nerve degeneration in bone marrow drives aging of the hematopoietic stem cell niche. *Nature Medicine*, *24*(6), 782–791. https://doi.org/10.1038/s41591-018-0030-x

Meaker, G. A., & Wilkinson, A. C. (2024). Ex vivo hematopoietic stem cell expansion technologies: recent progress, applications, and open questions. *Experimental Hematology*, *130*, 104136. https://doi.org/10.1016/j.exphem.2023.12.001

Melkov, A., & Abdu, U. (2018). Regulation of long-distance transport of mitochondria along microtubules. In *Cellular and Molecular Life Sciences* (Vol. 75, Issue 2, pp. 163–176). Birkhauser Verlag AG. https://doi.org/10.1007/s00018-017-2590-1

Mendelson, A., & Frenette, P. S. (2014). Hematopoietic stem cell niche maintenance during homeostasis and regeneration. *Nature Medicine*, *20*(8), 833–846. https://doi.org/10.1038/nm.3647

Méndez-Ferrer, S., Bonnet, D., Steensma, D. P., Hasserjian, R. P., Ghobrial, I. M., Gribben, J. G., Andreeff, M., & Krause, D. S. (2020). Bone marrow niches in haematological malignancies. *Nature Reviews Cancer*, *20*(5), 285–298. https://doi.org/10.1038/s41568-020-0245-2

Méndez-Ferrer, S., Michurina, T. V., Ferraro, F., Mazloom, A. R., MacArthur, B. D., Lira, S. A., Scadden, D. T., Ma'ayan, A., Enikolopov, G. N., & Frenette, P. S. (2010). Mesenchymal and haematopoietic stem cells form a unique bone marrow niche. *Nature*, *466*(7308), 829–834. https://doi.org/10.1038/nature09262

Menendez, P., Catalina, P., Rodríguez, R., Melen, G. J., Bueno, C., Arriero, M., García-Sánchez, F., Lassaletta, A., García-Sanz, R., & García-Castro, J. (2009). Bone marrow mesenchymal stem cells from infants with MLL-AF4+ acute leukemia harbor and express the MLL-AF4 fusion gene. *Journal of Experimental Medicine*, *206*(13), 3131–3141. https://doi.org/10.1084/jem.20091050

Mikkola, H. K. A., & Orkin, S. H. (2006). The journey of developing hematopoietic stem cells. *Development*, *133*(19), 3733–3744. https://doi.org/10.1242/dev.02568

Mishra, A., Maiti, R., Mohan, P., & Gupta, P. (2024). Antigen loss following CAR-T cell therapy: Mechanisms, implications, and potential solutions. *European Journal of Haematology*, *112*(2), 211–222. https://doi.org/10.1111/ejh.14101

Mohammed, A., Miller, A. F., & Saiani, A. (2007). 3D networks from self-assembling ionic-complementary octa-peptides. *Macromolecular Symposia*, *251*, 88–95. https://doi.org/10.1002/masy.200750512

Mohrin, M., Bourke, E., Alexander, D., Warr, M. R., Barry-Holson, K., Le Beau, M. M., Morrison, C. G., & Passegué, E. (2010). Hematopoietic stem cell quiescence promotes error-prone DNA repair and mutagenesis. *Cell Stem Cell*, *7*(2), 174–185. https://doi.org/10.1016/j.stem.2010.06.014

Molica, M., Perrone, S., Mazzone, C., Niscola, P., Cesini, L., Abruzzese, E., & de Fabritiis, P. (2021). Cd33 expression and gentuzumab ozogamicin in acute myeloid leukemia: Two sides of the same coin. *Cancers*, *13*(13), 1–20. https://doi.org/10.3390/cancers13133214

Morrison, S. J., & Scadden, D. T. (2014). The bone marrow niche for haematopoietic stem cells. *Nature*, *505*(7483), 327–334. https://doi.org/10.1038/nature12984

Morrison, S. J., & Weissman, I. L. (1994). The long-term repopulating subset of hematopoietic stem cells is deterministic and isolatable by phenotype. *Immunity*, *1*(8), 661–673. https://doi.org/10.1016/1074-7613(94)90037-X

Naveiras, O., Nardi, V., Wenzel, P. L., Hauschka, P. V., Fahey, F., & Daley, G. Q. (2009). Bone-marrow adipocytes as negative regulators of the haematopoietic microenvironment. *Nature*, *460*(7252), 259–263. https://doi.org/10.1038/nature08099

Negi, N., & Griffin, M. D. (2020). Effects of mesenchymal stromal cells on regulatory T cells: Current understanding and clinical relevance. *Stem Cells*, *38*(5), 596–605. https://doi.org/10.1002/stem.3151

Nelson, M. R., Ghoshal, D., Mejías, J. C., Rubio, D. F., Keith, E., & Roy, K. (2021). A multi-niche microvascularized human bone marrow (hBM) on-a-chip elucidates key roles of the endosteal niche in hBM physiology. *Biomaterials*, *270*(January), 120683. https://doi.org/10.1016/j.biomaterials.2021.120683

Nelson, M. R., & Roy, K. (2016). Bone-marrow mimicking biomaterial niches for studying hematopoietic stem and progenitor cells. *Journal of Materials Chemistry B*, *4*(20), 3490–3503. https://doi.org/10.1039/c5tb02644j

Ng, A. P., & Alexander, W. S. (2017). Haematopoietic stem cells: Past, present and future. *Cell Death Discovery*, *3*(December 2016), 2–5. https://doi.org/10.1038/cddiscovery.2017.2

Ngandu Mpoyi, E., Cantini, M., Reynolds, P. M., Gadegaard, N., Dalby, M. J., & Salmerón-Sánchez, M. (2016). Protein Adsorption as a Key Mediator in the Nanotopographical Control of Cell Behavior. *ACS Nano*, *10*(7), 6638–6647. https://doi.org/10.1021/acsnano.6b01649

Nichols, J. E., Cortiella, J., Lee, J., Niles, J. A., Cuddihy, M., Wang, S., Bielitzki, J., Cantu, A., Mlcak, R., Valdivia, E., Yancy, R., McClure, M. L., & Kotov, N. A. (2009). In vitro analog of human bone marrow from 3D scaffolds with biomimetic inverted colloidal crystal geometry. *Biomaterials*, *30*(6), 1071–1079. https://doi.org/10.1016/j.biomaterials.2008.10.041

Nilsson, S. K., Debatis, M. E., Dooner, M. S., Madri, J. A., Quesenberry, P. J., & Becker, P. S. (1998). Immunofluorescence characterization of key extracellular matrix proteins in murine bone marrow in situ. *Journal of Histochemistry and Cytochemistry*, *46*(3), 371–377. https://doi.org/10.1177/002215549804600311

Nilsson, S. K., Johnston, H. M., Whitty, G. A., Williams, B., Webb, R. J., Denhardt, D. T., Bertoncello, I., Bendall, L. J., Simmons, P. J., & Haylock, D. N. (2005). Osteopontin, a key component of the hematopoietic stem cell niche and regulator of primitive hematopoietic progenitor cells. *Blood*, *106*(4), 1232–1239. https://doi.org/10.1182/blood-2004-11-4422

Noetzli, L. J., French, S. L., & Machlus, K. R. (2019). New Insights Into the Differentiation of Megakaryocytes From Hematopoietic Progenitors.

Arteriosclerosis, Thrombosis, and Vascular Biology, *39*(7), 1288–1300. https://doi.org/10.1161/ATVBAHA.119.312129

Nombela-Arrieta, C., Pivarnik, G., Winkel, B., Canty, K. J., Harley, B., Mahoney, J. E., Park, S. Y., Lu, J., Protopopov, A., & Silberstein, L. E. (2013). Quantitative imaging of haematopoietic stem and progenitor cell localization and hypoxic status in the bone marrow microenvironment. *Nature Cell Biology*, *15*(5), 533–543. https://doi.org/10.1038/ncb2730

Novak, R., Ingram, M., Clauson, S., Das, D., Delahanty, A., Herland, A., Maoz, B., Jeanty, S., & Ingber, D. (2021). A robotic platform for fluidically-linked human body-on-chips experimentation. In *Physiology & behavior*. https://doi.org/10.1038/s41551-019-0497-x.A

Omatsu, Y., Sugiyama, T., Kohara, H., Kondoh, G., Fujii, N., Kohno, K., & Nagasawa, T. (2010). The Essential Functions of Adipo-osteogenic Progenitors as the Hematopoietic Stem and Progenitor Cell Niche. *Immunity*, *33*(3), 387–399. https://doi.org/10.1016/j.immuni.2010.08.017

Oria, R., Wiegand, T., Escribano, J., Elosegui-Artola, A., Uriarte, J. J., Moreno-Pulido, C., Platzman, I., Delcanale, P., Albertazzi, L., Navajas, D., Trepat, X., García-Aznar, J. M., Cavalcanti-Adam, E. A., & Roca-Cusachs, P. (2017). Force loading explains spatial sensing of ligands by cells. *Nature*, *552*(7684), 219–224. https://doi.org/10.1038/nature24662

Oshimori, N., Oristian, D., & Fuchs, E. (2015). TGF-β Promotes Heterogeneity and Drug Resistance in Squamous Cell Carcinoma. *Cell*, *160*(5), 963–976. https://doi.org/10.1016/j.cell.2015.01.043

Ottensmeier, C. (2001). The classification of lymphomas and leukemias. *Chemico-Biological Interactions*, *135–136*, 653–664. https://doi.org/10.1016/S0009-2797(01)00201-0

Pak, C., Callander, N. S., Young, E. W. K., Titz, B., Kim, K. M., Saha, S., Chng, K., Asimakopoulos, F., Beebe, D. J., & Miyamoto, S. (2015). MicroC3: an ex vivo microfluidic cis-coculture assay to test chemosensitivity and resistance of patient multiple myeloma cells. *Integrative Biology (United Kingdom)*, *7*(6), 643–654. https://doi.org/10.1039/c5ib00071h

Pankov, R., & Yamada, K. M. (2002). Fibronectin at a glance. *Journal of Cell Science*, *115*(20), 3861–3863. https://doi.org/10.1242/jcs.00059

Passaro, D., Di Tullio, A., Abarrategi, A., Rouault-Pierre, K., Foster, K., Ariza-McNaughton, L., Montaner, B., Chakravarty, P., Bhaw, L., Diana, G., Lassailly, F., Gribben, J., & Bonnet, D. (2017). Increased Vascular Permeability in the Bone Marrow Microenvironment Contributes to Disease Progression and Drug Response in Acute Myeloid Leukemia. *Cancer Cell*, *32*(3), 324-341.e6. https://doi.org/10.1016/j.ccell.2017.08.001

Patra, A. K. (2021). New aspects of HSC mobilization for better therapeutic outcomes. *Cellular and Molecular Immunology*, *18*(12), 2583–2585. https://doi.org/10.1038/s41423-021-00723-7

Peled, T., Shoham, H., Aschengrau, D., Yackoubov, D., Frei, G., Rosenheimer G, N., Lerrer, B., Cohen, H. Y., Nagler, A., Fibach, E., & Peled, A. (2012). Nicotinamide, a SIRT1 inhibitor, inhibits differentiation and facilitates expansion of hematopoietic progenitor cells with enhanced bone marrow homing and engraftment. *Experimental Hematology*, *40*(4), 342-355.e1. https://doi.org/10.1016/j.exphem.2011.12.005

Pérez-Oliva, A. B., Martínez-Esparza, M., Vicente-Fernández, J. J., Corral-San Miguel, R., García-Peñarrubia, P., & Hernández-Caselles, T. (2011). Epitope mapping, expression and post-translational modifications of two isoforms of CD33 (CD33M and CD33m) on lymphoid and myeloid human cells. *Glycobiology*, *21*(6), 757–770. https://doi.org/10.1093/glycob/cwq220

Perlin, J. R., Sporrij, A., & Zon, L. I. (2017). Blood on the tracks: hematopoietic stem cell-endothelial cell interactions in homing and engraftment. *Journal of Molecular Medicine*, *95*(8), 809–819. https://doi.org/10.1007/s00109-017-1559-8

Pietras, E. M., Reynaud, D., Kang, Y. A., Carlin, D., Calero-Nieto, F. J., Leavitt, A. D., Stuart, J. A., Göttgens, B., & Passegué, E. (2015). Functionally Distinct Subsets of Lineage-Biased Multipotent Progenitors Control Blood Production in Normal and Regenerative Conditions. *Cell Stem Cell*, *17*(1), 35–46. https://doi.org/10.1016/j.stem.2015.05.003

Pinho, S., & Frenette, P. S. (2019). Haematopoietic stem cell activity and interactions with the niche. *Nature Reviews Molecular Cell Biology*, *20*(5), 303–320. https://doi.org/10.1038/s41580-019-0103-9

Pinho, S., Lacombe, J., Hanoun, M., Mizoguchi, T., Bruns, I., Kunisaki, Y., & Frenette, P. S. (2013). PDGFRα and CD51 mark human Nestin+ sphere-forming mesenchymal stem cells capable of hematopoietic progenitor cell expansion. *Journal of Experimental Medicine*, *210*(7), 1351–1367. https://doi.org/10.1084/jem.20122252

Pittenger, M. F., Mackay, A. M., Beck, S. C., Jaiswal, R. K., Douglas, R., Mosca, J. D., Moorman, M. A., Simonetti, D. W., Craig, S., & Marshak, D. R. (1999). Multilineage potential of adult human mesenchymal stem cells. *Science*, *284*(5411), 143–147. https://doi.org/10.1126/science.284.5411.143

Polajžer, T., & Miklavčič, D. (2023). Immunogenic Cell Death in Electroporation-Based Therapies Depends on Pulse Waveform Characteristics. *Vaccines*, *11*(6), 1036. https://doi.org/10.3390/vaccines11061036

Poulos, M. G., Guo, P., Kofler, N. M., Pinho, S., Gutkin, M. C., Tikhonova, A., Aifantis, I., Frenette, P. S., Kitajewski, J., Rafii, S., & Butler, J. M. (2013). Endothelial Jagged-1 Is necessary for homeostatic and regenerative hematopoiesis. *Cell Reports*, *4*(5), 1022–1034. https://doi.org/10.1016/j.celrep.2013.07.048

Qian, H., Buza-Vidas, N., Hyland, C. D., Jensen, C. T., Antonchuk, J., Månsson, R., Thoren, L. A., Ekblom, M., Alexander, W. S., & Jacobsen, S. E. W. (2007). Critical Role of Thrombopoietin in Maintaining Adult Quiescent Hematopoietic Stem Cells. *Cell Stem Cell*, *1*(6), 671–684. https://doi.org/10.1016/j.stem.2007.10.008

Qin, H., Cho, M., Haso, W., Zhang, L., Tasian, S. K., Oo, H. Z., Negri, G. L., Lin, Y., Zou, J., Mallon, B. S., Maude, S., Teachey, D. T., Barrett, D. M., Orentas, R. J., Daugaard, M., Sorensen, P. H. B., Grupp, S. A., & Fry, T. J. (2015). Eradication of B-ALL using chimeric antigen receptor-expressing T cells targeting the TSLPR oncoprotein. *Blood*, *126*(5), 629–639. https://doi.org/10.1182/blood-2014-11-612903

Qin, Z. (2012). The use of THP-1 cells as a model for mimicking the function and regulation of monocytes and macrophages in the vasculature. *Atherosclerosis*, *221*(1), 2–11. https://doi.org/10.1016/j.atherosclerosis.2011.09.003

Raic, A., Rödling, L., Kalbacher, H., & Lee-Thedieck, C. (2014). Biomimetic macroporous PEG hydrogels as 3D scaffolds for the multiplication of human hematopoietic stem and progenitor cells. *Biomaterials*, *35*(3), 929–940. https://doi.org/10.1016/j.biomaterials.2013.10.038

Raitman, I., Huang, M. L., Williams, S. A., Friedman, B., Godula, K., & Schwarzbauer, J. E. (2018). Heparin-fibronectin interactions in the development of extracellular matrix insolubility. *Matrix Biology*, *67*, 107–122. https://doi.org/10.1016/j.matbio.2017.11.012

Ramalingam, P., Gutkin, M. C., Poulos, M. G., Tillery, T., Doughty, C., Winiarski, A., Freire, A. G., Rafii, S., Redmond, D., & Butler, J. M. (2023). Restoring bone marrow niche function rejuvenates aged hematopoietic stem cells by reactivating the DNA Damage Response. *Nature Communications*, *14*(1). https://doi.org/10.1038/s41467-023-37783-4

Rameshwar, P., & Gascon, P. (1995). Substance P (SP) mediates production of stem cell factor and interleukin-1 in bone marrow stroma: potential autoregulatory role for these cytokines in SP receptor expression and induction. *Blood*, *86*(2), 482–490. https://doi.org/10.1182/blood.V86.2.482.bloodjournal862482

Rees, H. A., & Liu, D. R. (2018). Base editing: precision chemistry on the genome and transcriptome of living cells. *Nature Reviews Genetics*, *19*(12), 770–788. https://doi.org/10.1038/s41576-018-0059-1

Reinisch, A., Hernandez, D. C., Schallmoser, K., & Majeti, R. (2017). Generation and use of a humanized bone-marrow-ossicle niche for hematopoietic xenotransplantation into mice. *Nature Protocols*, *12*(10), 2169–2178. https://doi.org/10.1038/nprot.2017.088

Reinisch, A., Thomas, D., Corces, M. R., Zhang, X., Gratzinger, D., Hong, W. J., Schallmoser, K., Strunk, D., & Majeti, R. (2016). A humanized bone marrow ossicle xenotransplantation model enables improved engraftment of healthy

and leukemic human hematopoietic cells. *Nature Medicine*, *22*(7), 812–821. https://doi.org/10.1038/nm.4103

Renders, S., Svendsen, A. F., Panten, J., Rama, N., Maryanovich, M., Sommerkamp, P., Ladel, L., Redavid, A. R., Gibert, B., Lazare, S., Ducarouge, B., Schönberger, K., Narr, A., Tourbez, M., Dethmers-Ausema, B., Zwart, E., Hotz-Wagenblatt, A., Zhang, D., Korn, C., … Trumpp, A. (2021). Niche derived netrin-1 regulates hematopoietic stem cell dormancy via its receptor neogenin-1. *Nature Communications*, *12*(1), 608. https://doi.org/10.1038/s41467-020-20801-0

Reya, T., Duncan, A. W., Ailles, L., Domen, J., Scherer, D. C., Willert, K., Hintz, L., Nusse, R., & Weissman, I. L. (2003). A role for Wnt signalling in self-renewal of haematopoietic stem cells. *Nature*, *423*(6938), 409–414. https://doi.org/10.1038/nature01593

Richter, J., Traver, D., & Willert, K. (2017). The role of Wnt signaling in hematopoietic stem cell development. *Critical Reviews in Biochemistry and Molecular Biology*, *52*(4), 414–424. https://doi.org/10.1080/10409238.2017.1325828

Rivlin, N., Brosh, R., Oren, M., & Rotter, V. (2011). Mutations in the p53 tumor suppressor gene: Important milestones at the various steps of tumorigenesis. *Genes and Cancer*, *2*(4), 466–474. https://doi.org/10.1177/1947601911408889

Rödling, L., Schwedhelm, I., Kraus, S., Bieback, K., Hansmann, J., & Lee-Thedieck, C. (2017). 3D models of the hematopoietic stem cell niche under steady-state and active conditions. *Scientific Reports*, *7*(1), 1–15. https://doi.org/10.1038/s41598-017-04808-0

Rodriguez-Fraticelli, A. E., Wolock, S. L., Weinreb, C. S., Panero, R., Patel, S. H., Jankovic, M., Sun, J., Calogero, R. A., Klein, A. M., & Camargo, F. D. (2018). Clonal analysis of lineage fate in native haematopoiesis. *Nature*, *553*(7687), 212–216. https://doi.org/10.1038/nature25168

Romani, P., Valcarcel-Jimenez, L., Frezza, C., & Dupont, S. (2021). Crosstalk between mechanotransduction and metabolism. *Nature Reviews Molecular Cell Biology*, *22*(1), 22–38. https://doi.org/10.1038/s41580-020-00306-w

Rosen, V. (2009). BMP2 signaling in bone development and repair. *Cytokine & Growth Factor Reviews*, *20*(5–6), 475–480. https://doi.org/10.1016/j.cytogfr.2009.10.018

Ross, E. A., Turner, L. A., Donnelly, H., Saeed, A., Tsimbouri, M. P., Burgess, K. V., Blackburn, G., Jayawarna, V., Xiao, Y., Oliva, M. A. G., Willis, J., Bansal, J., Reynolds, P., Wells, J. A., Mountford, J., Vassalli, M., Gadegaard, N., Oreffo, R. O. C., Salmeron-Sanchez, M., & Dalby, M. J. (2023). Nanotopography reveals metabolites that maintain the immunomodulatory phenotype of mesenchymal stromal cells. *Nature Communications*, *14*(1). https://doi.org/10.1038/s41467-023-36293-7

Ross, E. A., Turner, L., Saeed, A., Burgess, K. V, Blackburn, G., Wells, J. A., Mountford, J., Gadegaard, N., Salmeron-, M., Oreffo, R. O. C., & Dalby, M. J. (2019). *Nanotopography reveals metabolites that maintain the immunosuppressive phenotype of mesenchymal stem cells*. 1–22.

Rossi, G., Manfrin, A., & Lutolf, M. P. (2018). Progress and potential in organoid research. *Nature Reviews Genetics*, *19*(11), 671–687. https://doi.org/10.1038/s41576-018-0051-9

Rossi, L., Challen, G., Sirin, O., Lin, K., & Goodel, M. (2011). HSC Characterisation and Isolation. *Bone*, *23*(1), 1–7. https://doi.org/10.1007/978-1-61779-145-1

Rotolo, R., Leuci, V., Donini, C., Cykowska, A., Gammaitoni, L., Medico, G., Valabrega, G., Aglietta, M., & Sangiolo, D. (2019). Car-based strategies beyond t lymphocytes: Integrative opportunities for cancer adoptive immunotherapy. *International Journal of Molecular Sciences*, *20*(11). https://doi.org/10.3390/ijms20112839

Sakurai, M., Ishitsuka, K., Ito, R., Wilkinson, A. C., Kimura, T., Mizutani, E., Nishikii, H., Sudo, K., Becker, H. J., Takemoto, H., Sano, T., Kataoka, K., Takahashi, S., Nakamura, Y., Kent, D. G., Iwama, A., Chiba, S., Okamoto, S., Nakauchi, H., & Yamazaki, S. (2023). Chemically defined cytokine-free expansion of human haematopoietic stem cells. *Nature*, *615*(7950), 127–133. https://doi.org/10.1038/s41586-023-05739-9

Salmerón-Sánchez, M., & Dalby, M. J. (2016). Synergistic growth factor microenvironments. *Chemical Communications*, *52*(91), 13327–13336. https://doi.org/10.1039/C6CC06888J

Salmerón-Sánchez, M., Rico, P., Moratal, D., Lee, T. T., Schwarzbauer, J. E., & García, A. J. (2011). Role of material-driven fibronectin fibrillogenesis in cell differentiation. *Biomaterials*, *32*(8), 2099–2105. https://doi.org/10.1016/j.biomaterials.2010.11.057

Sánchez-Lanzas, R., Kalampalika, F., & Ganuza, M. (2022). Diversity in the bone marrow niche: Classic and novel strategies to uncover niche composition. *British Journal of Haematology*, *199*(5), 647–664. https://doi.org/10.1111/bjh.18355

Sarker, I. H. (2022). AI-Based Modeling: Techniques, Applications and Research Issues Towards Automation, Intelligent and Smart Systems. *SN Computer Science*, *3*(2), 158. https://doi.org/10.1007/s42979-022-01043-x

Sarrazin, S., Lamanna, W. C., & Esko, J. D. (2011). Heparan sulfate proteoglycans. *Cold Spring Harbor Perspectives in Biology*, *3*(7), 1–33. https://doi.org/10.1101/cshperspect.a004952

Sayama, C., Willsey, M., Chintagumpala, M., Brayton, A., Briceño, V., Ryan, S. L., Luerssen, T. G., Hwang, S. W., & Jea, A. (2015). Routine use of recombinant human bone morphogenetic protein–2 in posterior fusions of the pediatric spine and incidence of cancer. *Journal of Neurosurgery: Pediatrics*, *16*(1), 4–13. https://doi.org/10.3171/2014.10.PEDS14199

Scelsi, A., Bochicchio, B., Smith, A., Workman, V. L., Castillo Diaz, L. A., Saiani, A., & Pepe, A. (2019). Tuning of hydrogel stiffness using a two-component peptide system for mammalian cell culture. *Journal of Biomedical Materials Research Part A*, *107*(3), 535–544. https://doi.org/10.1002/jbm.a.36568

Schmid, C., Labopin, M., Nagler, A., Niederwieser, D., Castagna, L., Tabrizi, R., Stadler, M., Kuball, J., Cornelissen, J., Vorlicek, J., Socié, G., Falda, M., Vindeløv, L., Ljungman, P., Jackson, G., Kröger, N., Rank, A., Polge, E., Rocha, V., & Mohty, M. (2012). Treatment, risk factors, and outcome of adults with relapsed AML after reduced intensity conditioning for allogeneic stem

cell transplantation. *Blood*, *119*(6), 1599–1606. https://doi.org/10.1182/blood-2011-08-375840

Schmitz, N., Pfistner, B., Sextro, M., Sieber, M., Carella, A. M., Haenel, M., Boissevain, F., Zschaber, R., Müller, P., Kirchner, H., Lohri, A., Decker, S., Koch, B., Hasenclever, D., Goldstone, A. H., & Diehl, V. (2002). Aggressive conventional chemotherapy compared with high-dose chemotherapy with autologous haemopoietic stem-cell transplantation for relapsed chemosensitive Hodgkin's disease: a randomised trial. *The Lancet*, *359*(9323), 2065–2071. https://doi.org/10.1016/S0140-6736(02)08938-9

Schoedel, K. B., Morcos, M. N. F., Zerjatke, T., Roeder, I., Grinenko, T., Voehringer, D., Göthert, J. R., Waskow, C., Roers, A., & Gerbaulet, A. (2016). The bulk of the hematopoietic stem cell population is dispensable for murine steady-state and stress hematopoiesis. *Blood*, *128*(19), 2285–2296. https://doi.org/10.1182/blood-2016-03-706010

Schuettpelz, L. G., Borgerding, J. N., Christopher, M. J., Gopalan, P. K., Romine, M. P., Herman, A. C., Woloszynek, J. R., Greenbaum, A. M., & Link, D. C. (2014). G-CSF regulates hematopoietic stem cell activity, in part, through activation of Toll-like receptor signaling. *Leukemia*, *28*(9), 1851–1860. https://doi.org/10.1038/leu.2014.68

Schuh, A. C., Döhner, H., Pleyer, L., Seymour, J. F., Fenaux, P., & Dombret, H. (2017). Azacitidine in adult patients with acute myeloid leukemia. *Critical Reviews in Oncology/Hematology*, *116*, 159–177. https://doi.org/10.1016/j.critrevonc.2017.05.010

Segers, V. F. M., & Lee, R. T. (2008). Stem-cell therapy for cardiac disease. *Nature*, *451*(7181), 937–942. https://doi.org/10.1038/nature06800

Seita, J., & Weissman, I. L. (2010). Hematopoietic stem cell: self-renewal versus differentiation. *WIREs Systems Biology and Medicine*, *2*(6), 640–653. https://doi.org/10.1002/wsbm.86

Shang, Y., Guan, H., & Zhou, F. (2021). Biological Characteristics of Umbilical Cord Mesenchymal Stem Cells and Its Therapeutic Potential for Hematological Disorders. *Frontiers in Cell and Developmental Biology*, *9*(May), 1–11. https://doi.org/10.3389/fcell.2021.570179

Shapiro, J., Iancu, O., Jacobi, A. M., McNeill, M. S., Turk, R., Rettig, G. R., Amit, I., Tovin-Recht, A., Yakhini, Z., Behlke, M. A., & Hendel, A. (2020). Increasing CRISPR Efficiency and Measuring Its Specificity in HSPCs Using a Clinically Relevant System. *Molecular Therapy - Methods and Clinical Development*, *17*(June), 1097–1107. https://doi.org/10.1016/j.omtm.2020.04.027

Sharma, P., Chauhan, U., Kumar, S., & Kamal Sharma, D. (2018). A Review on Dynamic Rheology for Polymers. *International Journal of Applied Engineering Research*, *13*(6), 363–368. http://www.ripublication.com

Shin, J. J., Schröder, M. S., Caiado, F., Wyman, S. K., Bray, N. L., Bordi, M., Dewitt, M. A., Vu, J. T., Kim, W. T., Hockemeyer, D., Manz, M. G., & Corn, J. E. (2020). Controlled Cycling and Quiescence Enables Efficient HDR in Engraftment-Enriched Adult Hematopoietic Stem and Progenitor Cells. *Cell Reports*, *32*(9). https://doi.org/10.1016/j.celrep.2020.108093

Shiroshita, K., Kobayashi, H., Watanuki, S., Karigane, D., Sorimachi, Y., Fujita, S., Tamaki, S., Haraguchi, M., Itokawa, N., Aoyoama, K., Koide, S., Masamoto, Y., Kobayashi, K., Nakamura-Ishizu, A., Kurokawa, M., Iwama, A., Okamoto, S., Kataoka, K., & Takubo, K. (2022). A culture platform to study quiescent hematopoietic stem cells following genome editing. *Cell Reports Methods*, *2*(12), 100354. https://doi.org/10.1016/j.crmeth.2022.100354

Siena, S., Schiavo, R., Pedrazzoli, P., & Carlo-Stella, C. (2000). Therapeutic Relevance of CD34 Cell Dose in Blood Cell Transplantation for Cancer Therapy. *Journal of Clinical Oncology*, *18*(6), 1360–1377. https://doi.org/10.1200/JCO.2000.18.6.1360

Simonson, T., & Brooks, C. L. (1996). Charge screening and the dieletric constant of proteins: Insights from molecular dynamics. *Journal of the American Chemical Society*, *118*(35), 8452–8458. https://doi.org/10.1021/ja960884f

Singh, P., Carraher, C., & Schwarzbauer, J. E. (2010). Assembly of fibronectin extracellular matrix. *Annual Review of Cell and Developmental Biology*, *26*, 397–419. https://doi.org/10.1146/annurev-cellbio-100109-104020

Sitnicka, E., Bryder, D., Theilgaard-Mönch, K., Buza-Vidas, N., Adolfsson, J., & Jacobsen, S. E. W. (2002). Key role of flt3 ligand in regulation of the common lymphoid progenitor but not in maintenance of the hematopoietic stem cell

pool. *Immunity*, *17*(4), 463–472. https://doi.org/10.1016/S1074-7613(02)00419-3

Smith, R. A. A., Murali, S., Rai, B., Lu, X., Lim, Z. X. H., Lee, J. J. L., Nurcombe, V., & Cool, S. M. (2018). Minimum structural requirements for BMP-2-binding of heparin oligosaccharides. *Biomaterials*, *184*(August), 41–55. https://doi.org/10.1016/j.biomaterials.2018.08.056

Song, N., Scholtemeijer, M., & Shah, K. (2020). Mesenchymal Stem Cell Immunomodulation: Mechanisms and Therapeutic Potential. *Trends in Pharmacological Sciences*, *41*(9), 653–664. https://doi.org/10.1016/j.tips.2020.06.009

Song, W. J., Sullivan, M. G., Legare, R. D., Hutchings, S., Tan, X., Kufrin, D., Ratajczak, J., Resende, I. C., Haworth, C., Hock, R., Loh, M., Felix, C., Roy, D. C., Busque, L., Kurnit, D., Willman, C., Gewirtz, A. M., Speck, N. A., Bushweller, J. H., … Gilliland, D. G. (1999). Haploinsufficiency of CBFA2 causes familial thrombocytopenia with propensity to develop acute myelogenous leukaemia. *Nature Genetics*, *23*(2), 166–175. https://doi.org/10.1038/13793

Sonoda, Y. (2021). Human CD34-negative hematopoietic stem cells: The current understanding of their biological nature. *Experimental Hematology*, *96*, 13–26. https://doi.org/10.1016/j.exphem.2021.02.004

Spencer, D. H., Russler-Germain, D. A., Ketkar, S., Helton, N. M., Lamprecht, T. L., Fulton, R. S., Fronick, C. C., O'Laughlin, M., Heath, S. E., Shinawi, M., Westervelt, P., Payton, J. E., Wartman, L. D., Welch, J. S., Wilson, R. K., Walter, M. J., Link, D. C., DiPersio, J. F., & Ley, T. J. (2017). CpG Island Hypermethylation Mediated by DNMT3A Is a Consequence of AML Progression. *Cell*, *168*(5), 801-816.e13. https://doi.org/10.1016/j.cell.2017.01.021

Spencer, J. A., Ferraro, F., Roussakis, E., Klein, A., Runnels, J. M., Zaher, W., Mortensen, L. J., Alt, C., Yusuf, R., Côté, D., Vinogradov, S. A., David, T., & Lin, C. P. (2014). *Direct measurement of local oxygen concentration in the bone marrow of live animals*. *508*(7495), 269–273. https://doi.org/10.1038/nature13034.Direct

Stengel, A., Kern, W., Haferlach, T., Meggendorfer, M., Fasan, A., & Haferlach, C. (2017). The impact of TP53 mutations and TP53 deletions on survival varies between AML, ALL, MDS and CLL: An analysis of 3307 cases. *Leukemia*, *31*(3), 705–711. https://doi.org/10.1038/leu.2016.263

Stier, S., Ko, Y., Forkert, R., Lutz, C., Neuhaus, T., Grünewald, E., Cheng, T., Dombkowski, D., Calvi, L. M., Rittling, S. R., & Scadden, D. T. (2005). Osteopontin is a hematopoietic stem cell niche component that negatively regulates stem cell pool size. *Journal of Experimental Medicine*, *201*(11), 1781–1791. https://doi.org/10.1084/jem.20041992

Stone, A. P., Nascimento, T. F., & Barrachina, M. N. (2022). The bone marrow niche from the inside out: how megakaryocytes are shaped by and shape hematopoiesis. *Blood*, *139*(4), 483–491. https://doi.org/10.1182/blood.2021012827

Stone, R. M., Mandrekar, S. J., Sanford, B. L., Laumann, K., Geyer, S., Bloomfield, C. D., Thiede, C., Prior, T. W., Döhner, K., Marcucci, G., Lo-Coco, F., Klisovic, R. B., Wei, A., Sierra, J., Sanz, M. A., Brandwein, J. M., de Witte, T., Niederwieser, D., Appelbaum, F. R., … Döhner, H. (2017). Midostaurin plus Chemotherapy for Acute Myeloid Leukemia with a FLT3 Mutation . *New England Journal of Medicine*, *377*(5), 454–464. https://doi.org/10.1056/nejmoa1614359

Stratmann, A. T., Fecher, D., Wangorsch, G., Göttlich, C., Walles, T., Walles, H., Dandekar, T., Dandekar, G., & Nietzer, S. L. (2014). Establishment of a human 3D lung cancer model based on a biological tissue matrix combined with a Boolean in silico model. *Molecular Oncology*, *8*(2), 351–365. https://doi.org/10.1016/j.molonc.2013.11.009

Sugimura, R., He, X. C., Venkatraman, A., Arai, F., Box, A., Semerad, C., Haug, J. S., Peng, L., Zhong, X., Suda, T., & Li, L. (2012). Noncanonical Wnt Signaling Maintains Hematopoietic Stem Cells in the Niche. *Cell*, *150*(2), 351–365. https://doi.org/10.1016/j.cell.2012.05.041

Sugiyama, T., Kohara, H., Noda, M., & Nagasawa, T. (2006). Maintenance of the Hematopoietic Stem Cell Pool by CXCL12-CXCR4 Chemokine Signaling in Bone Marrow Stromal Cell Niches. *Immunity*, *25*(6), 977–988. https://doi.org/10.1016/j.immuni.2006.10.016

Sugiyama, T., & Nagasawa, T. (2012). Bone Marrow Niches for Hematopoietic Stem Cells and Immune Cells. *Inflamm Allergy Drug Targets*, *11*(3), 201–206. internal-pdf://87.203.121.227/IADT-11-201.pdf%0Ahttps://www.ncbi.nlm.nih.gov/pubmed/22452607

Sun, L., Gao, F., Gao, Z., Ao, L., Li, N., Ma, S., Jia, M., Li, N., Lu, P., Sun, B., Ho, M., Jia, S., Ding, T., & Gao, W. (2021). Shed antigen-induced blocking effect on CAR-T cells targeting Glypican-3 in Hepatocellular Carcinoma. *Journal for ImmunoTherapy of Cancer*, *9*(4), 1–14. https://doi.org/10.1136/jitc-2020-001875

Sung, J. H., Wang, Y. I., Sriram, N. N., Jackson, M., Long, C., Hickman, J. J., & Shuler, M. L. (2019). *Recent advances in body-on-a-chip systems*. *91*(1), 330–351. https://doi.org/10.1021/acs.analchem.8b05293.Recent

Sweeten, P. (2019). *Modelling an in vitro haematopoietic stem cell niche using poly (ethyl acrylate) surfaces*.

Tabe, Y., & Konopleva, M. (2015). Role of Microenvironment in Resistance to Therapy in AML. *Current Hematologic Malignancy Reports*, *10*(2), 96–103. https://doi.org/10.1007/s11899-015-0253-6

Taichman, R. S., & Emerson, S. G. (1994). Human osteoblasts support hematopoiesis through the production of granulocyte colony-stimulating factor. *The Journal of Experimental Medicine*, *179*(5), 1677–1682. https://doi.org/10.1084/jem.179.5.1677

Takahashi, K., Tanabe, K., Ohnuki, M., Narita, M., Ichisaka, T., Tomoda, K., & Yamanaka, S. (2007). Induction of Pluripotent Stem Cells from Adult Human Fibroblasts by Defined Factors. *Cell*, *131*(5), 861–872. https://doi.org/10.1016/j.cell.2007.11.019

Takubo, K., Goda, N., Yamada, W., Iriuchishima, H., Ikeda, E., Kubota, Y., Shima, H., Johnson, R. S., Hirao, A., Suematsu, M., & Suda, T. (2010). Regulation of the HIF-1α level is essential for hematopoietic stem cells. *Cell Stem Cell*, *7*(3), 391–402. https://doi.org/10.1016/j.stem.2010.06.020

Takubo, K., Nagamatsu, G., Kobayashi, C. I., Nakamura-Ishizu, A., Kobayashi, H., Ikeda, E., Goda, N., Rahimi, Y., Johnson, R. S., Soga, T., Hirao, A., Suematsu, M., & Suda, T. (2013). Regulation of glycolysis by Pdk functions as a metabolic

checkpoint for cell cycle quiescence in hematopoietic stem cells. *Cell Stem Cell*, *12*(1), 49–61. https://doi.org/10.1016/j.stem.2012.10.011

Tefferi, A., & Letendre, L. (2012). Going beyond 7 + 3 regimens in the treatment of adult acute myeloid leukemia. *Journal of Clinical Oncology*, *30*(20), 2425–2428. https://doi.org/10.1200/JCO.2011.38.9601

Thanaskody, K., Jusop, A. S., Tye, G. J., Wan Kamarul Zaman, W. S., Dass, S. A., & Nordin, F. (2022). MSCs vs. iPSCs: Potential in therapeutic applications. *Frontiers in Cell and Developmental Biology*, *10*(November), 1–31. https://doi.org/10.3389/fcell.2022.1005926

Till, J. E., & McCulloch, E. A. (2011). A direct measurement of the radiation sensitivity of normal mouse bone marrow cells. 1961. *Radiation Research*, *175*(2), 145–149. https://doi.org/10.1667/RRXX28.1

Tiwari, A., Tursky, M., Mushahary, D., Wasnik, S., Collier, F., Suma, K., Kirkland, M., & Pande, G. (2012). Ex vivo expansion of haematopoietic stem/progenitor cells from human umbilical cord blood on acellular scaffolds prepared from MS-5 stromal cell line. *Annals of the American Thoracic Society*. https://doi.org/10.1002/term

Treacy, N. J., Clerkin, S., Davis, J. L., Kennedy, C., Miller, A. F., Saiani, A., Wychowaniec, J. K., Brougham, D. F., & Crean, J. (2022). Growth and differentiation of human induced pluripotent stem cell (hiPSC)-derived kidney organoids using fully synthetic peptide hydrogels. *Bioactive Materials*, *21*(June 2022), 142–156. https://doi.org/10.1016/j.bioactmat.2022.08.003

Trounson, A., & DeWitt, N. D. (2016). Pluripotent stem cells progressing to the clinic. *Nature Reviews Molecular Cell Biology*, *17*(3), 194–200. https://doi.org/10.1038/nrm.2016.10

Tsapogas, P., Mooney, C., Brown, G., & Rolink, A. (2017). The Cytokine Flt3-Ligand in Normal and Malignant Hematopoiesis. *International Journal of Molecular Sciences*, *18*(6), 1115. https://doi.org/10.3390/ijms18061115

Tsimbouri, P. M., McMurray, R. J., Burgess, K. V., Alakpa, E. V., Reynolds, P. M., Murawski, K., Kingham, E., Oreffo, R. O. C., Gadegaard, N., & Dalby, M. J. (2012). Using nanotopography and metabolomics to identify biochemical

effectors of multipotency. *ACS Nano*, *6*(11), 10239–10249. https://doi.org/10.1021/nn304046m

Tsuji, W. (2014). Adipose-derived stem cells: Implications in tissue regeneration. *World Journal of Stem Cells*, *6*(3), 312. https://doi.org/10.4252/wjsc.v6.i3.312

Tusi, B. K., Wolock, S. L., Weinreb, C., Hwang, Y., Hidalgo, D., Zilionis, R., Waisman, A., Huh, J. R., Klein, A. M., & Socolovsky, M. (2018). Population snapshots predict early haematopoietic and erythroid hierarchies. *Nature*, *555*(7694), 54–60. https://doi.org/10.1038/nature25741

Ugurlu, B., & Karaoz, E. (2020). Comparison of similar cells: Mesenchymal stromal cells and fibroblasts. *Acta Histochemica*, *122*(8), 151634. https://doi.org/10.1016/j.acthis.2020.151634

Urist, M. R. (1965). Bone: Formation by Autoinduction. *Science*, *150*(3698), 893–899. https://doi.org/10.1126/science.150.3698.893

Van Der Velden, V. H. J., Te Marvelde, J. G., Hoogeveen, P. G., Bernstein, I. D., Houtsmuller, A. B., Berger, M. S., & Van Dongen, J. J. M. (2001). Targeting of the CD33-calicheamicin immunoconjugate Mylotarg (CMA-676) in acute myeloid leukemia: In vivo and in vitro saturation and internalization by leukemic and normal myeloid cells. *Blood*, *97*(10), 3197–3204. https://doi.org/10.1182/blood.V97.10.3197

Vashisth, V., Nigam, K. D. P., & Kumar, V. (2021). Design and development of high shear mixers: Fundamentals, applications and recent progress. *Chemical Engineering Science*, *232*, 116296. https://doi.org/10.1016/j.ces.2020.116296

Vigano, S., Bobisse, S., Coukos, G., Perreau, M., & Harari, A. (2020). Cancer and HIV-1 Infection: Patterns of Chronic Antigen Exposure. *Frontiers in Immunology*, *11*(June), 1–18. https://doi.org/10.3389/fimmu.2020.01350

Vignjevic, R., Djordjevic, N., Vuyst, T. De, & Gemkow, S. (2018). Modelling of strain softening materials based on equivalent damage force. *Computer Methods in Applied Mechanics and Engineering*, *335*, 52–68. https://doi.org/10.1016/j.cma.2018.01.049

Vining, K. H., & Mooney, D. J. (2017). Mechanical forces direct stem cell behaviour in development and regeneration. *Nature Reviews Molecular Cell Biology*, *18*(12), 728–742. https://doi.org/10.1038/nrm.2017.108

Vodyanik, M. A., Yu, J., Zhang, X., Tian, S., Stewart, R., Thomson, J. A., & Slukvin, I. I. (2010). A Mesoderm-Derived Precursor for Mesenchymal Stem and Endothelial Cells. *Cell Stem Cell*, *7*(6), 718–729. https://doi.org/10.1016/j.stem.2010.11.011

Wagner, D. O., Sieber, C., Bhushan, R., Börgermann, J. H., Graf, D., & Knaus, P. (2010). BMPs: From bone to body morphogenetic proteins. *Science Signaling*, *3*(107), 1–6. https://doi.org/10.1126/scisignal.3107mr1

Wagner, J. E., Brunstein, C. G., Boitano, A. E., Defor, T. E., McKenna, D., Sumstad, D., Blazar, B. R., Tolar, J., Le, C., Jones, J., Cooke, M. P., & Bleul, C. C. (2016). Phase I/II Trial of StemRegenin-1 Expanded Umbilical Cord Blood Hematopoietic Stem Cells Supports Testing as a Stand-Alone Graft. *Cell Stem Cell*, *18*(1), 144–155. https://doi.org/10.1016/j.stem.2015.10.004

Wang, X., Liu, S., Sun, Y., Yu, X., Lee, S. M., Cheng, Q., Wei, T., Gong, J., Robinson, J., Zhang, D., Lian, X., Basak, P., & Siegwart, D. J. (2023). Preparation of selective organ-targeting (SORT) lipid nanoparticles (LNPs) using multiple technical methods for tissue-specific mRNA delivery. *Nature Protocols*, *18*(1), 265–291. https://doi.org/10.1038/s41596-022-00755-x

Wang, X., Shen, X., Yan, Y., & Li, H. (2021). Pyruvate dehydrogenase kinases (PDKs): an overview toward clinical applications. *Bioscience Reports*, *41*(4), 1–15. https://doi.org/10.1042/BSR20204402

Warburg Berlin-Dahlem, O. (1925). The Metabolism of Carcinoma Cells. *The Journal of Cancer Research*, *9*(1), 148–163.

Watcham, S., Kucinski, I., & Gottgens, B. (2019). New insights into hematopoietic differentiation landscapes from single-cell RNA sequencing. *Blood*, *133*(13), 1415–1426. https://doi.org/10.1182/blood-2018-08-835355

Wei, Q., & Frenette, P. S. (2018). Niches for Hematopoietic Stem Cells and Their Progeny. *Immunity*, *48*(4), 632–648. https://doi.org/10.1016/j.immuni.2018.03.024

Wellbrock, J., Latuske, E., Kohler, J., Wagner, K., Stamm, H., Vettorazzi, E., Vohwinkel, G., Klokow, M., Uibeleisen, R., Ehm, P., Riecken, K., Loges, S., Thol, F., Schubert, C., Amling, M., Jucker, M., Bokemeyer, C., Heuser, M., Krauter, J., & Fiedler, W. (2015). Expression of hedgehog pathway mediator GLI represents a negative prognostic marker in human acute myeloid leukemia and its inhibition exerts Antileukemic effects. *Clinical Cancer Research*, *21*(10), 2388–2398. https://doi.org/10.1158/1078-0432.CCR-14-1059

Wheadon, H., Wheadon, H., Tsimbouri, M. P., Donnelly, H., & Dalby, M. J. (2024). *Complexities of modelling the bone marrow microenvironment to facilitate haematopoietic research*.

Whiteley, A. E., Price, T. T., Cantelli, G., & Sipkins, D. A. (2021). Leukaemia: a model metastatic disease. *Nature Reviews Cancer*, *21*(7), 461–475. https://doi.org/10.1038/s41568-021-00355-z

Wilkinson, A. C., Igarashi, K. J., & Nakauchi, H. (2020). Haematopoietic stem cell self-renewal in vivo and ex vivo. *Nature Reviews Genetics*, *21*(9), 541–554. https://doi.org/10.1038/s41576-020-0241-0

Wilkinson, A. C., Ishida, R., Kikuchi, M., Sudo, K., Morita, M., Crisostomo, R. V., Yamamoto, R., Loh, K. M., Nakamura, Y., Watanabe, M., Nakauchi, H., & Yamazaki, S. (2019). Long-term ex vivo haematopoietic-stem-cell expansion allows nonconditioned transplantation. *Nature*, *571*(7763), 117–121. https://doi.org/10.1038/s41586-019-1244-x

Willasch, A. M., Peters, C., Sedláček, P., Dalle, J.-H., Kitra-Roussou, V., Yesilipek, A., Wachowiak, J., Lankester, A., Prete, A., Hamidieh, A. A., Ifversen, M., Buechner, J., Kriván, G., Hamladji, R.-M., Diaz-de-Heredia, C., Skorobogatova, E., Michel, G., Locatelli, F., Bertaina, A., … Bader, P. (2020). Myeloablative conditioning for allo-HSCT in pediatric ALL: FTBI or chemotherapy?—A multicenter EBMT-PDWP study. *Bone Marrow Transplantation*, *55*(8), 1540–1551. https://doi.org/10.1038/s41409-020-0854-0

Wilson, A., Laurenti, E., Oser, G., van der Wath, R. C., Blanco-Bose, W., Jaworski, M., Offner, S., Dunant, C. F., Eshkind, L., Bockamp, E., Lió, P., MacDonald, H. R., & Trumpp, A. (2008). Hematopoietic Stem Cells Reversibly Switch from

Dormancy to Self-Renewal during Homeostasis and Repair. *Cell*, *135*(6), 1118–1129. https://doi.org/10.1016/j.cell.2008.10.048

Wimmer, R. A., Leopoldi, A., Aichinger, M., Kerjaschki, D., & Penninger, J. M. (2019). Generation of blood vessel organoids from human pluripotent stem cells. *Nature Protocols*, *14*(11), 3082–3100. https://doi.org/10.1038/s41596-019-0213-z

Winkler, A. L., Koenig, M., Welle, A., Trouillet, V., Kratzer, D., Hussal, C., Lahann, J., & Lee-Thedieck, C. (2017). Bioinstructive Coatings for Hematopoietic Stem Cell Expansion Based on Chemical Vapor Deposition Copolymerization. *Biomacromolecules*, *18*(10), 3089–3098. https://doi.org/10.1021/acs.biomac.7b00743

Winkler, A. L., von Wulffen, J., Rödling, L., Raic, A., Reinartz, I., Schug, A., Gralla-Koser, R., Geckle, U., Welle, A., & Lee-Thedieck, C. (2017). Significance of Nanopatterned and Clustered DLL1 for Hematopoietic Stem Cell Proliferation. *Advanced Functional Materials*, *27*(21), 1–13. https://doi.org/10.1002/adfm.201606495

Wisniewski, D., Affer, M., Willshire, J., & Clarkson, B. (2011). Further phenotypic characterization of the primitive lineage− CD34+CD38−CD90+CD45RA− hematopoietic stem cell/progenitor cell sub-population isolated from cord blood, mobilized peripheral blood and patients with chronic myelogenous leukemia. *Blood Cancer Journal*, *1*(9), e36–e36. https://doi.org/10.1038/bcj.2011.35

Wouters, B. J., & Delwel, R. (2016). Epigenetics and approaches to targeted epigenetic therapy in acute myeloid leukemia. *Blood*, *127*(1), 42–52. https://doi.org/10.1182/blood-2015-07-604512

Wright, D. E., Wagers, A. J., Pathak Gulati, A., Johnson, F. L., & Weissman, I. L. (2001). Physiological migration of hematopoietic stem and progenitor cells. *Science*, *294*(5548), 1933–1936. https://doi.org/10.1126/science.1064081

Xiao, Y., Donnelly, H., Sprott, M., Luo, J., Jayawarna, V., Lemgruber, L., Tsimbouri, P. M., Meek, R. M. D., Salmeron-Sanchez, M., & Dalby, M. J. (2022). Material-driven fibronectin and vitronectin assembly enhances BMP-2

presentation and osteogenesis. *Materials Today Bio*, *16*, 100367. https://doi.org/10.1016/j.mtbio.2022.100367

Xiao, Y., McGuinness, ChanelleA. S., Doherty-Boyd, W. S., Salmeron-Sanchez, M., Donnelly, H., & Dalby, M. J. (2022). Current insights into the bone marrow niche: From biology in vivo to bioengineering ex vivo. *Biomaterials*, *286*(April), 121568. https://doi.org/10.1016/j.biomaterials.2022.121568

Xu, C., Gao, X., Wei, Q., Nakahara, F., Zimmerman, S. E., Mar, J., & Frenette, P. S. (2018). Stem cell factor is selectively secreted by arterial endothelial cells in bone marrow. *Nature Communications*, *9*(1), 1–13. https://doi.org/10.1038/s41467-018-04726-3

Xu, C. L., Ruan, M. Z. C., Mahajan, V. B., & Tsang, S. H. (2019). Viral Delivery Systems for CRISPR. *Viruses*, *11*(1), 28. https://doi.org/10.3390/v11010028

Yamamoto, R., Morita, Y., Ooehara, J., Hamanaka, S., Onodera, M., Rudolph, K. L., Ema, H., & Nakauchi, H. (2013). Clonal analysis unveils self-renewing lineage-restricted progenitors generated directly from hematopoietic stem cells. *Cell*, *154*(5), 1112–1126. https://doi.org/10.1016/j.cell.2013.08.007

Yamazaki, S., Ema, H., Karlsson, G., Yamaguchi, T., Miyoshi, H., Shioda, S., Taketo, M. M., Karlsson, S., Iwama, A., & Nakauchi, H. (2011). Nonmyelinating schwann cells maintain hematopoietic stem cell hibernation in the bone marrow niche. *Cell*, *147*(5), 1146–1158. https://doi.org/10.1016/j.cell.2011.09.053

Yan, C., Altunbas, A., Yucel, T., Nagarkar, R. P., Schneider, J. P., & Pochan, D. J. (2010). Injectable solid hydrogel: Mechanism of shear-thinning and immediate recovery of injectable β-hairpin peptide hydrogels. *Soft Matter*, *6*(20), 5143–5156. https://doi.org/10.1039/c0sm00642d

Yang, J., Zhang, L., Yu, C., Yang, X.-F., & Wang, H. (2014). Monocyte and macrophage differentiation: circulation inflammatory monocyte as biomarker for inflammatory diseases. *Biomarker Research*, *2*(1), 1. https://doi.org/10.1186/2050-7771-2-1

Yang, Y., McCloskey, J. E., Yang, H., Puc, J., Alcaina, Y., Vedvyas, Y., Gomez Gallegos, A. A., Ortiz-Sánchez, E., de Stanchina, E., Min, I. M., von Hofe, E., & Jin, M. M. (2021). Bispecific CAR T cells against EpCAM and inducible ICAM-

1 overcome antigen heterogeneity and generate superior antitumor responses. *Cancer Immunology Research*, *9*(10), 1158–1174. https://doi.org/10.1158/2326-6066.CIR-21-0062

Yates, J., Glidewell, O., Wiernik, P., Cooper, M. R., Steinberg, D., Dosik, H., Levy, R., Hoagland, C., Henry, P., Gottlieb, A., Cornell, C., Berenberg, J., Hutchison, J. L., Raich, P., Nissen, N., Ellison, R. R., Frelick, R., James, G. W., Falkson, G., … Holland, J. F. (1982). Cytosine arabinoside with daunorubicin or adriamycin for therapy of acute myelocytic leukemia: A CALGB study. *Blood*, *60*(2), 454–462. https://doi.org/10.1182/blood.v60.2.454.454

Yeh, S.-C. A., Hou, J., Wu, J. W., Yu, S., Zhang, Y., Belfield, K. D., Camargo, F. D., & Lin, C. P. (2022). Quantification of bone marrow interstitial pH and calcium concentration by intravital ratiometric imaging. *Nature Communications*, *13*(1), 393. https://doi.org/10.1038/s41467-022-27973-x

Yonemura, Y., Ku, H., Lyman, S. D., & Ogawa, M. (1997). In Vitro Expansion of Hematopoietic Progenitors and Maintenance of Stem Cells: Comparison Between FLT3/FLK-2 Ligand and KIT Ligand. *Blood*, *89*(6), 1915–1921. https://doi.org/10.1182/blood.V89.6.1915

Yoshihara, H., Arai, F., Hosokawa, K., Hagiwara, T., Takubo, K., Nakamura, Y., Gomei, Y., Iwasaki, H., Matsuoka, S., Miyamoto, K., Miyazaki, H., Takahashi, T., & Suda, T. (2007). Thrombopoietin/MPL Signaling Regulates Hematopoietic Stem Cell Quiescence and Interaction with the Osteoblastic Niche. *Cell Stem Cell*, *1*(6), 685–697. https://doi.org/10.1016/j.stem.2007.10.020

Yoshino, S., Yokoyama, T., Sunami, Y., Takahara, T., Nakamura, A., Yamazaki, Y., Tsutsumi, S., Aburatani, H., & Nakamura, T. (2021). Trib1 promotes acute myeloid leukemia progression by modulating the transcriptional programs of Hoxa9. *Blood*, *137*(1), 75–88. https://doi.org/10.1182/blood.2019004586

Young, R. A. (2011). Control of the Embryonic Stem Cell State. *Cell*, *144*(6), 940–954. https://doi.org/10.1016/j.cell.2011.01.032

Zeng, Y., He, J., Bai, Z., Li, Z., Gong, Y., Liu, C., Ni, Y., Du, J., Ma, C., Bian, L., Lan, Y., & Liu, B. (2019). Tracing the first hematopoietic stem cell generation

in human embryo by single-cell RNA sequencing. *Cell Research*, *29*(11), 881–894. https://doi.org/10.1038/s41422-019-0228-6

Zeng, Z., Liu, W., Tsao, T., Qiu, Y. H., Zhao, Y., Samudio, I., Sarbassov, D. D., Kornblau, S. M., Baggerly, K. A., Kantarjian, H. M., Konopleva, M., & Andreeff, M. (2017). High-throughput profiling of signaling networks identifies mechanism-based combination therapy to eliminate microenvironmental resistance in acute myeloid leukemia. *Haematologica*, *102*(9), 1537–1548. https://doi.org/10.3324/haematol.2016.162230

Zeytin, I. C., Alkan, B., Ozdemir, C., Cetinkaya, D. U., & Okur, F. V. (2022). Alterations in Hematopoietic and Mesenchymal Stromal Cell Components of the Osteopetrotic Bone Marrow Niche. *Stem Cells Translational Medicine*, *11*(3), 310–321. https://doi.org/10.1093/stcltm/szab019

Zhang, D., & Kilian, K. A. (2013). The effect of mesenchymal stem cell shape on the maintenance of multipotency. *Biomaterials*, *34*(16), 3962–3969. https://doi.org/10.1016/j.biomaterials.2013.02.029

Zhang, G. L., Zhu, Z. H., & Wang, Y. Z. (2019). Neural stem cell transplantation therapy for brain ischemic stroke: Review and perspectives. *World Journal of Stem Cells*, *11*(10), 817–830. https://doi.org/10.4252/wjsc.v11.i10.817

Zhang, P., Li, X., Pan, C., Zheng, X., Hu, B., Xie, R., Hu, J., Shang, X., & Yang, H. (2022). Single-cell RNA sequencing to track novel perspectives in HSC heterogeneity. *Stem Cell Research and Therapy*, *13*(1), 1–15. https://doi.org/10.1186/s13287-022-02718-1

Zhang, P., Zhang, C., Li, J., Han, J., Liu, X., & Yang, H. (2019). The physical microenvironment of hematopoietic stem cells and its emerging roles in engineering applications. *Stem Cell Research and Therapy*, *10*(1), 1–13. https://doi.org/10.1186/s13287-019-1422-7

Zhao, L. (2019). CD33 in Alzheimer's disease - Biology, pathogenesis, and therapeutics: A mini-review. *Gerontology*, *65*(4), 323–331. https://doi.org/10.1159/000492596

Zhao, M., Perry, J. M., Marshall, H., Venkatraman, A., Qian, P., He, X. C., Ahamed, J., & Li, L. (2014). Megakaryocytes maintain homeostatic

quiescence and promote post-injury regeneration of hematopoietic stem cells. *Nature Medicine*, *20*(11), 1321–1326. https://doi.org/10.1038/nm.3706

Zhao, M., Ross, J. T., Itkin, T., Perry, J. M., Venkatraman, A., Haug, J. S., Hembree, M. J., Deng, C. X., Lapidot, T., He, X. C., & Li, L. (2012). FGF signaling facilitates postinjury recovery of mouse hematopoietic system. *Blood*, *120*(9), 1831–1842. https://doi.org/10.1182/blood-2011-11-393991

Zhou, B. O., Ding, L., & Morrison, S. J. (2015). Hematopoietic stem and progenitor cells regulate the regeneration of their niche by secreting Angiopoietin-1. *ELife*, *2015*(4), 1–25. https://doi.org/10.7554/eLife.05521

Zhou, B. O., Yue, R., Murphy, M. M., Peyer, J. G., & Morrison, S. J. (2014). Leptin-Receptor-Expressing Mesenchymal Stromal Cells Represent the Main Source of Bone Formed by Adult Bone Marrow. *Cell Stem Cell*, *15*(2), 154–168. https://doi.org/10.1016/j.stem.2014.06.008

Zhou, H. S., Carter, B. Z., & Andreeff, M. (2016). Bone marrow niche-mediated survival of leukemia stem cells in acute myeloid leukemia: Yin and Yang. *Cancer Biology and Medicine*, *13*(2), 248–259. https://doi.org/10.20892/j.issn.2095-3941.2016.0023

Zhu, Q., Gao, P., Tober, J., Bennett, L., Chen, C., Uzun, Y., Li, Y., Howell, E. D., Mumau, M., Yu, W., He, B., Speck, N. A., & Tan, K. (2020). Developmental trajectory of prehematopoietic stem cell formation from endothelium. *Blood*, *136*(7), 845–856. https://doi.org/10.1182/blood.2020004801

Zon, L. I. (2008). Intrinsic and extrinsic control of haematopoietic stem-cell self-renewal. *Nature*, *453*(7193), 306–313. https://doi.org/10.1038/nature07038